Development and optimisation of a zinc oxide nanowire nanogenerator

Thomas Stanley van den Heever

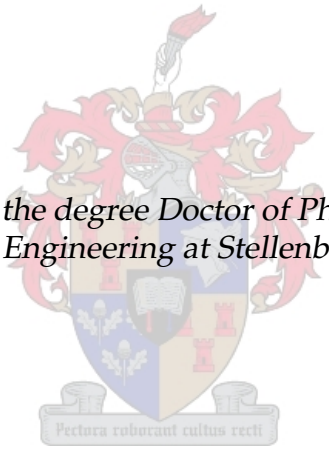

Dissertation presented for the degree Doctor of Philosophy in Engineering in the Faculty of Engineering at Stellenbosch University

Supervisor: Prof. W.J. Perold
Department of Electrical and Electronic Engineering

December 2013

The financial assistance of the National Research Foundation (NRF) towards this research is hereby acknowledged. Opinions expressed and conclusions arrived at are however those of the author and are not necessarily to be attributed to the NRF.

Declaration

By submitting this thesis electronically, I declare that the entirety of the work contained therein is my own, original work, that I am the sole author thereof (save to the extent explicitly otherwise stated), that reproduction and publication thereof by Stellenbosch University will not infringe any third party rights and that I have not previously in its entirety or in part submitted it for obtaining any qualification.

Date: December 2013

Abstract

This study developed and optimised zinc oxide (ZnO) nanowire-based nanogenerator. The nanogenerator works on the piezoelectric effect that is, a mechanical force is converted to an electrical voltage. The ZnO nanowires are piezoelectric and when any force is applied to the nanowires an output voltage is generated. This ZnO nanowire-based nanogenerator can be used to power small electronic devices, such as pacemakers. The nanogenerator can also be incorporated into clothes and shoes to generate electricity to charge a cell phone for example. The problem experienced currently is that the nanogenerator does not generate enough electricity to be of practical use and needs to be further optimised. Simulations and mathematical models were used to identify areas where the nanogenerator could be optimised in order to increase the output voltage. It is shown that the morphology of the nanowires can have a considerable effect on the output voltage. For this reason the growth of the nanowires was investigated first. Different methods were used to propagate the nanowires in order to select the method that, on average, has the highest output voltage. Accordingly, one parameter at a time and design of experiments were used to optimise the nanowire growth. Consequently, these two methods were used to optimise the growth parameters with the respect to the output voltage. The aqueous solution method was found to yield nanowires that give the highest generated output voltage. After growing over 600 nanowire samples, optimal growth parameters for this method were found. These optimal growth parameters were subsequently used to grow nanowires that were used to manufacture the nanogenerator. The nanowires were grown on a solid substrate and hence the nanogenerator was also manufactured on the solid substrate. Through various optimisations of the manufacturing process the maximum output voltage achieved was about 500 mV. However, this output voltage is too low to be of practical use, even though the output has been raised considerably. The main problem was found to be the fact that the contact between the nanowires and the electrode was weak due to contamination. A new method was therefore required where the electrode and the nanowires would be in proper contact to ensure that higher output voltages were achieved. Subsequently, a flexible nanogenerator was manufactured in

order to solve this problem. Accordingly, the nanowires were grown on the flexible polyimide film and a buffer layer was then spun onto the flexible substrate, leaving only the nanowire tips exposed. The electrode was then sputtered on top of this buffer layer, covering the nanowire tips. This ensured proper contact between the nanowires and the electrode. The nanogenerator, which was manufactured with non-optimal growth parameters, gives a maximum voltage output of 1 V, double the maximum achieved with the solid nanogenerator. When the optimal growth parameters were used the output voltage was raised to 2 V. Various optimisation techniques were performed on the nanogenerator, including plasma treatment and annealing and the use of various materials in the buffer layer. Combining these optimisation methods subsequently led to an optimised nanogenerator that can generate an output voltage of over 5 V. This was achieved after over 1200 nanogenerators had been manufactured. However, the output voltage was not in a usable form. Circuitry was therefore developed to transform the voltage generated by the nanogenerator to a useable form. The best circuit, the LTC3588, was used to power an LED for 10 seconds. The completed device was found to achieve a power output of 0.3 mW, enough for small electronic devices.

Opsomming

'n Sink-oksied (ZnO) nanodraad gebaseerde nanogenerator is ontwikkeld en geöptimeer. Die nanogenerator werk met behulp van die piezoelektriese effek - meganiese krag work omgesit in 'n elektriese spanning. Die ZnO nanodrade is piezoelektries en wanneer 'n krag op die drade aangewend word, word 'n uittree spanning gegenereer. Die nanogenerator kan gebruik word om klein elektroniese toestelle, soos 'n pasaangeër, van krag te voorsien. Die nanogenerator kan in klere en skoene geïnkorporeer word om elektrisiteit op te wek vir die laai van 'n selfoon. Die probleem is egter dat die nanogenerator tans nie genoeg krag opwek om prakties van nut te wees nie en verdere optimasie word benodig. Simulasies en wikundige modelle work gebruik om areas te identifiseer waar die nanogenerator geöptimeer kan word, met die doel om die uittreespanning te verhoog. Dit word bewys dat die morfologie van die nanodrade 'n groot effek het op die uittreespanning. Dus word die groei van die nanodrade eerste ondersoek. Verskillende metodes word gebruik om die nanodrade te groei en die beste metode, wat die hoogste uittreespanning op gemiddeld verskaf, word gekies. Een parameter op 'n slag en ontwerp van eksperimente word gebruik om die nanodraad groei te optimeer. Die groei parameters word geöptimeer deur van die twee metodes gebruik te maak, en die optimeering word gedoen in terme van die uittreespanning. Die oplossing groei metode lei tot nanodrade wat die hoogste uittreespanning verskaf. Na oor die 600 nanodraad monsters gegroei is, is die optimale parameters gevind. Hierdie optimale parameters word uitsluitlik gebruik om die nanogenerator te vervaardig. Die nanodrade word op 'n soliede substraat gegroei en dus word die nanogenerator op dieselfde soliede substraat vervaardig. Verskeie metodes is gebruik om die vervaardiging te optimeer en die hoogste uittreespanning wat bereik is, is 500 mV. Die uittreespanning is te laag om van praktiese nut te wees alhoewel dit heelwat verhoog is. Die grootste probleem is die swak kontak tussen die nanodrade en die elektrode, wat veroorsaak word deur kontaminasie. 'n Nuwe metode word verlang wat beter kontak tussen die nanodrade en elektrode sal verseker. 'n Buigbare nanogenerator is vervaardig om die probleem op te los. Die nanodrade word nou op 'n buigbare film gegroei. 'n Bufferlaag word tussen die nanodrade in gedraai, tot net die

punte van die nanodrade nog sigbaar is. Die elektrode word bo-op die bufferlaag gedeponeer, wat behoorlike kontak tussen die nanodrade en elektrode verseker. Die nanogenerator wat met nie-optimale groei parameters vervaardig is, bereik ‘n uittreespanning van 1 V, dubbel die soliede nanogenerator. Met optimale groei parameters word die uittreespanning tot 2 V verhoog. Verskeie optimasie tegnieke word op die nanogenerator toegepas. Die metodes sluit in suurstof plasma behandeling, verhitting en die inkorporasie van verskillende materiale in die bufferlaag. ‘n Kombinasie van die metodes geïnkorporeer in een nanogenerator lei tot ‘n uittreespanning van 5 V. Die uittreespanning is bereik na oor die 1200 nanogenerators vervaardig is. The uittreespanning is nog nie in ‘n bruikbare vorm nie. Spesiale stroombane is ontwikkel wat die nanogenerator spanning omskakel na ‘n bruikbare vorm. Die beste stroombaan, die LTC3588, kan ‘n LED aanskakel vir 10 sekondes. The toestel kan ook 0.3 mW uittreekrag voorsien, genoeg vir klein elektroniese toestelle om te werk.

Acknowledgements

Firstly, I would like to thank my supervisor, Prof Willem Perold, for all his help throughout the project. His guidance and support are acknowledged and greatly appreciated.

I would like to thank our previous lab manager, Ulrich Büttner. Although he left during the course of my PhD, he gave me good advice whenever he could. To our new lab manager, Graham Hardie, thanks for all the help and hard work getting all the equipment up and running.

To all my colleagues in room E210, Carlo Schenke, Arnoux Roussow, Hercules du Plessis, Frederic Isingizwe, Goran Kitic and, again, Graham Hardie, thanks for all the good times. We worked hard at times, but played even harder. The last three years would not have been the same without all of you. You guys made it extra special and I will always remember all the fun times in the lab and the office.

I would also like to thank all the support personnel. Firstly, to the personnel of SED, Mr Lincoln Saunders and Mr Wessel Croukamp, thank you for all your hard work, without you this project would not have been successful. Mr Johan Booysen, Ms Petro Basson, Ms Alna Bougas and Ms Anita van der Spuy, thank you all for all the work behind the scenes. Other people always get the credit, but I appreciate all the hard work you did for me.

To all my friends, thanks for the support. It is not easy being a student while all of you are hard at work. Thanks for listening to me when things did not go according to plan. I would not have made it if it were not for your support.

Special thanks go to my family. My father and mother who supported me throughout my studies, financially and emotionally as well as to my two brothers for their support. I love you all. Lastly, a special thanks to my fiancée, Janine, for all your love and support.

Contents

Nomenclature

ϵ_0	Permittivity of free space
e	Electron charge
h	Plank's constant
ADC	Analog to digital converter
AFM	Atomic force microscopy
CBD	Chemical bath deposition
CNT	Carbon nanotubes
DC	Direct current
DI	Deionised
DoE	Design of experiments
EE	Estimate effect
FEM	Finite element method
HMTA	Hexamethylenetetramine
IBM	International Business Machines Corporation
IC	Integrated circuit
ICM	Inverted cylindrical magnetron
ISO	International Organization for Standardization
LCD	Liquid crystal display
MEMS	Microelectromechanical systems
MIT	Massachusetts Institute of Technology

MWCNT	Multi walled carbon nanotube
nm	Nanometre
PC	Personal computer
PMMA	Poly(methyl methacrylate)
PVDF	Polyvinylidene fluoride
PZT	Lead zirconate titanate
QCM	Quartz crystal microbalance
SEM	Scanning electron microscope
SS	Sum of squares
SSHI	Synchronized switch harvesting on inductor
SWCNT	Single walled carbon nanotube
TEM	Transmission electron microscopy
UV	Ultraviolet
UVLO	Undervoltage lockout
UWC	University of the Western Cape
VLS	Vapour liquid solid
VS	Vapour solid
ZnO	Zinc oxide

List of Figures

List of Tables

Chapter 1

Introduction

1.1 Motivation and problem statement

> Nanotechnology will let us build computers that are incredibly powerful. We will have more power in the volume of a sugar cube than exists in the entire world today.
>
> (*Ralph Merkle*, creator of encryption software)
>
> Nanotechnology is probably, as a phenomenon, the single most important new emerging force in technology.
>
> (*Charlie Harris*, CEO, Harris and Harris Group)

These two quotes highlight the fact that nanotechnology has the potential to change the world we live in today. It will eventually have an impact on every industry as we know it [1]. Most new technologies evolve in experimental laboratories and, in this environment, nanotechnology is gaining popularity. Publications related to nanotechnology increased from less than 10 000 in 1990 to almost 500 000 in 2006 [2]. Moreover, patents on nanotechnology increased from less than 60 in 1990 to over 900 in 2004 [3].

Nanotechnology, which started in 1959, is still a relatively new scientific field [1]. This means that nanotechnology has been researched for only 50 years, much less time than most of today's scientific fields. The big bang theory was developed in the 1920s [4], Einstein published his theories in 1905 and Newton developed his theories three hundred years earlier. These theories have been around for a long time and much research and experimentation has been done to verify and prove them. In contrast, nanotechnology is a new scientific field, with less available literature. This means there is still a lot being discovered in the field of nanotechnology. However, owing to its infancy, there is a lot of room for improvement and new developments.

Although nanotechnology is a new scientific field, various commercial products

have been developed. Figure 1.1 shows the worldwide spending on nanotechnology-related products from 1997 to 2005 [5]. Nanotechnology is increasingly impacting on our daily lives and it is predicted that it will affect nearly every industry we know today and even create completely new industries [1].

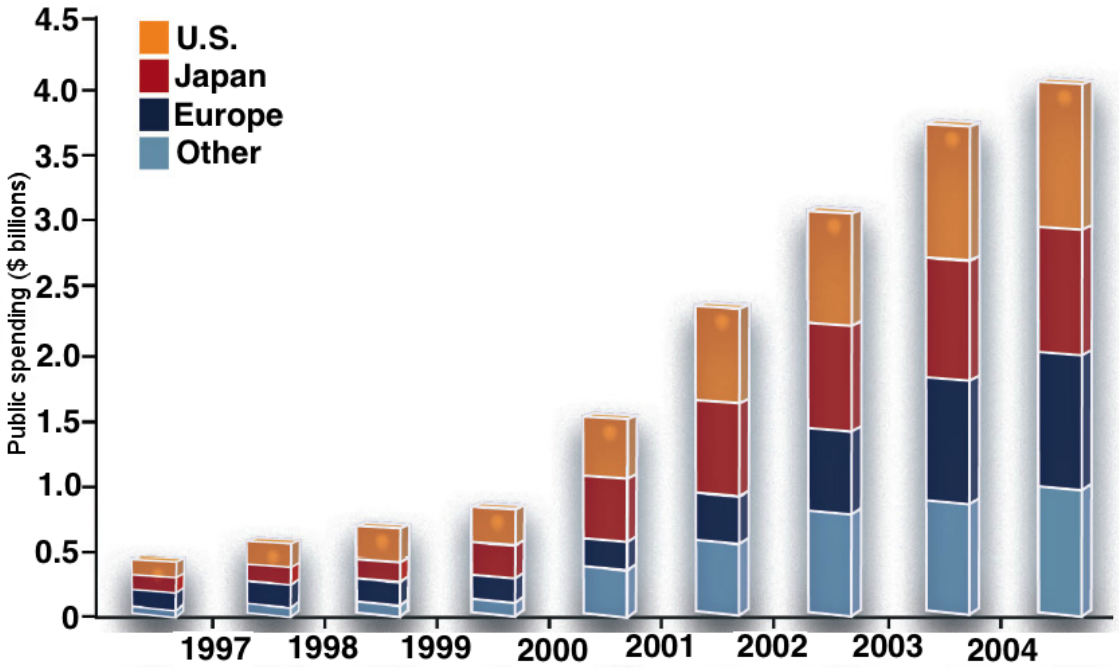

Figure 1.1: Graph showing the worldwide increase in spending on nanotechnology related products from 1997 to 2005 [5].

The world is increasingly becoming dependant on batteries as the power source for electronic devices. Battery sales were estimated at $73.6 billion in 2010, making it one of the biggest markets in the world [6]. With mobile devices becoming increasingly popular the need for longer lasting batteries is increasing . Devices such as mobile phones, laptops and camcorders require batteries that can last longer while still being lightweight and compact [7].

One of the major drawbacks to batteries is that they need replacing or recharging after a certain amount of time. This replacement or recharging of batteries in remote or hard to reach places, for devices such as pacemakers or early detection tsunami sensors, is difficult and in some cases impossible. However, the failure of a device, such as a pacemaker, can be fatal and must be prevented at all costs. For this reason it is necessary to find an alternative power source for specific applications.

Figure 1.2 shows various energy sources that can be used to power electronic devices. The conversion of energy is done by a nanogenerator –a nanodevice that

converts one type of energy to electrical energy. Using the different energy sources on the left, the devices on the right can be powered. Subsequently, these devices will not be dependent on batteries but be self-powering, scavenging power from the environment.

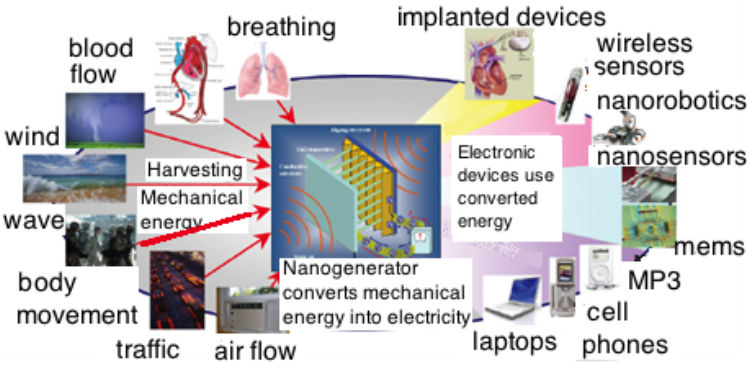

Figure 1.2: Diagram showing different energy sources that can be converted by the nanogenerator to power various devices [8].

This project will investigated the nanodevice depicted in the centre of Figure 1.2. This device converts mechanical force to an electrical signal through the piezoelectric effect. Zinc oxide (ZnO) nanowires are used as the piezoelectric material, accordingly, when an external force is applied to the nanowires an electrical signal will be generated. The completed device, consisting of ZnO nanowires, that converts any mechanical strain to an electrical signal is called a nanogenerator.

1.2 Aims and objectives

The project is divided into four main objectives: first, a thorough literature study; second, simulating the nanogenerator; third, investigating the nanowire growth; and fourth, optimising the nanogenerator.

The first objective is to complete a comprehensive literature study, which provided a better understanding of the piezoelectric effect. Both a physical and a mathematical model of the piezoelectric effect is developed. These models are used to identify parameters that can be optimised to ensure that a higher output voltage is generated by the nanogenerator. The literature study is also used to develop both a physical and mathematical model of the nanogenerator. These models are also used to optimise the nanogenerator, in order to achieve a higher voltage output. The literature study is also used to identify areas where further research is

required on the nanogenerator. Because the nanogenerator is a new field that was only discovered in 2005 [8], there is still a great deal of room for improvement.

After the literature study, simulations were performed to verify the literature. The ZnO nanowires were simulated using a software package. The aim of the simulations was to verify the physical model developed from the literature study. The simulations were also used to change specific parameters of the nanowires in order to optimise the voltage output. The aim here was to identify parameters that can be changed during the various stages of nanogenerator manufacturing in order to achieve a higher output voltage. The simulations were also used to verify that ZnO is one of the best materials to use. This was done by simulating nanowires of various materials and recording the output voltage when the same force is applied to all of them. Accordingly, the material that results in the highest output voltage was considered the best material. The material also needs to be easily synthesised in order to be considered suitable.

The nanowires are crucial to the success of this project. Hence, it was important to find a synthesis method that produced nanowires of perfect quality on a regular basis. Therefore, different growth methods were investigated to see which method achieved the best results. Optimisation techniques were applied to these growth methods with the aim of increasing the output voltage.

In order to increase the output voltage, reliable output voltage measurements must be taken. A new method was thus developed to measure the output voltage. This method does not require expensive equipment, but it still ensured accurate measurements. This method was used to measure the generated voltage from the ZnO nanowire nanogenerator throughout the project.

Once reliable measurements can be taken, the various growth methods can be compared. The best method was then further optimised using the design of experiments (DoE) optimisation method. The DoE method uses statistics to find the optimal growth parameters for the specific growth method. Once an optimal set of growth parameters were found, they were used exclusively to manufacture the ZnO nanowire-based nanogenerator.

The main aim and objective of this project is the optimisation of the nanogenerator, which needs to supply a higher output voltage in order to be of practical use. The output voltage needs to be increased to around 5 V, the same voltage as the USB slot of a PC supplies. This means most of the devices that can work from the USB slot of a computer will function off the nanogenerator. Table 1.1 shows a number of small electronic devices and the amount of power they consume.

The optimisation of the nanogenerator was completely new, as no previous work has been done on the optimisation of a ZnO nanogenerator. Various ap-

Table 1.1: Power consumption of various electronic devices [9].

Device	Power consumption (W)
iPhone charger	2
iPod nano charger	1
iPad charger	2
External hard drive	9
Camcorder charger	3

proaches were implemented in this study. There are various techniques for increasing the performance of ZnO thin film devices. These techniques were changed and implemented on the ZnO nanowires to see if any change is witnessed. Furthermore, during the manufacturing of the nanogenerator various approaches were taken to optimise the manufacturing. The manufacturing must ensure that maximum bending of the ZnO nanowires is possible as to achieve the highest output voltage.

The last objective of the optimisation of the nanogenerator was the output circuitry. Special electronic hardware was required to convert the electrical signal generated by the nanogenerator to a usable form. The generated voltage was not useable in its current form and requires hardware to convert it. The hardware must ensure optimal functioning, which means it should have low loss, should function under different magnitude loads and should achieve optimal power transfer.

1.3 Research Topic

The research topic for this project is: The utilisation of various growth and optimisation techniques to increase the output voltage of a zinc oxide nanowire nanogenerator.

The research topic can be broken down into various facets. The first part of the project comprises the growth of the ZnO nanowires. As mentioned, various techniques exist to synthesise the nanowires. For this project, however, only two growth techniques are investigated: vapour liquid solid (VLS) and an aqueous solution method. These two methods were chosen because they function at different spectrums of the temperature scale. The VLS method works at temperatures as high as 1000°C and the aqueous solution method, in contrast, works below 100°C. These two methods were used to grow the nanowires that were used to manufacture the nanogenerator.

The first optimisation was performed on nanowire growth. Each of the two growth methods has different growth parameters that can be altered and will have

an effect on the nanowire quality. The growth parameters were optimised with respect to the output voltage and the set of growth parameters that led to the highest measured output voltage were the optimal parameters. In achieving this goal two optimisation methods were used: one parameter at a time and design of experiment (DoE). The one parameter at a time method was performed first to find a range within which good growth is ensured and this range was then refined using the DoE method.

After optimal growth parameters were found, they were used exclusively to manufacture the nanogenerator. The nanogenerator was manufactured using different techniques, the aim of which was, once again, to achieve higher voltage output. This was achieved by perusing literature, developing both a physical and a mathematical model for the nanogenerator and identifying areas where optimisation can help to improve the output voltage. Simulations were also used to help in the identification of parameters that can be optimised.

The manufacturing of the nanogenerator was focused on achieving maximum bending of the nanowires. A higher degree of bending in the nanowires should lead to an increase in the measured output voltage. Hence, the aim of the manufacturing optimisation was to construct the top electrode in such a fashion that maximum bending can be achieved. Different methods were applied in order to achieve this goal.

Nanotechnology can help to improve the sensitivity of devices. This is due to the increase in the surface-to-volume ratio of the device. Bulk piezoelectric devices have been around for a long time, but the use of nanotechnology can improve the sensitivity and functionality of piezoelectric devices. Consequently, this could ensure that existing applications of piezoelectric devices will improve and new applications, such as the nanogenerator, will be developed. The nanogenerator, if optimised sufficiently, could help to alleviate our dependency on batteries. Nanogenerators could be incorporated into clothes, shoes, roads, sidewalks and much more in order to generated electricity as we walk, jog or drive. This electricity could then be used to charge our mobile phones or even pacemakers. The possibilities are endless.

1.4 Scope

This project focuses on a very small field within the broader field of nanotechnology. This project combines electronic engineering with nanotechnology in order to overcome certain obstacles. Other approaches and solutions exist, but did not form part of this project.

Firstly, only ZnO nanowires were investigated as the piezoelectric material. Other nanowires, such as InN, exist that can achieve higher output voltages compared to ZnO, but the synthesis of these nanowires is more complicated [10]. Various bulk materials that have the piezoelectric properties, also exist, but were also not investigated [11]. ZnO nanowires are easy to synthesise and many methods are found in the literature to synthesise the nanowires. These methods include electrospinning [12], pulsed laser deposition [13] and chemical etching [14], to name but a few. None of these methods were investigated because they require specialised equipment that was not readily available for this project. The two methods that are investigated in this project are the two most commonly used growth methods for ZnO nanowires.

The growth of the nanowires was also not investigated in full. The growth methods are found in literature and were adapted to work in our laboratory. However, they were not studied in full due to a lack of the chemistry background required to fully understand the mechanics behind nanowire growth. The methods used were taken as is and used for this particular application.

The second big limitation was the investigation of the grown nanowires. Much equipment exists that can be used to investigate the properties of nanowires. These properties include the crystal structure, material composition, lattice spacing, contamination percentage, luminance properties and many more. Unfortunately this equipment is very expensive and beyond the scope of our laboratory. Although some of this equipment was available in other departments or other universities the operation is complicated and expensive. Therefore, the equipment used throughout this project was sufficient but a more in-depth analysis could have added another dimension to the project.

Thirdly, the manufacturing of the nanogenerator was limited because a nano-manipulator was not used. A nano-manipulator can move an object around on the nanoscale which would have been very useful for moving the electrode to the correct position above the nanowires. The manipulator can also be used to test various electrodes by placing them in the correct position and applying an equal force to all of them.

This project has a number of limitations and certain aspects were not even considered owing to a number of factors. These limitations and delineations do not influence the outcome of this project however. Alternative instruments and methods were used to overcome these obstacles and the success of the project was guaranteed.

1.5 Definitions, terms and assumptions

Throughout this dissertation scientific terms are explained before use. Nanotechnology crosses over most scientific fields and not everybody knows all the terms and definitions. For that reason the terms and definitions are explained throughout the dissertation.

The two most commonly used terms in the dissertation is ”zinc oxide nanowires” and ”nanogenerator”. The ZnO nanowires are small, hexagonal structures that are made up of periodically arranged zinc and oxygen atoms. The atoms stack to form the structure and when the diameter is less than 100 nm and the length is orders of magnitude larger, then the structure is defined as a nanowire. The nanowire is a solid structure with carbon nanotubes that are defined in the same way, but which are hollow structures. Nanowires are two-dimensional structures, having both length and diameter. One-dimensional structures, like nanoparticles, only have diameters and ignorable lengths (like the gold nanoparticles introduced in Chapter 6).

The nanogenerator is manufactured from the nanowires. The nanogenerator consists of multiple nanowires grown on a pre-coated substrate. An electrode is placed on top of the nanowires to complete the nanogenerator manufacturing.

A couple of assumptions have been made at the beginning of this project. Firstly, it was assumed that all the instrumentation used was calibrated and the measured values were correct. This assumption is valid because most instruments have been calibrated within the last couple of years and, prior to the first measurement, a calibrated sample is measured. Set values for the calibrated sample are given and software parameters can be adjusted to ensure that the measurements are correct. This was done at the beginning of this project and it is assumed that the calibration did not change considerably throughout the project.

Voltage measurements are influenced equally by environmental noise. Although care was taken to minimise the effect of environmental noise, it is difficult to get rid of it completely. All the measurements were taken in the same environment and hence it is assumed that the noise had an equal effect on all measurements.

The above-mentioned assumptions do not significantly influence the output of this project. The first assumption has been tested with calibration standards and seems to hold true. Measurements taken weeks apart did not differ substantially but the difference is attributed to measurement noise. The second assumption is harder to test, but measurements in a Faraday cage did lead to less noisy measurements, although the effect was not great enough to take all measurements in the same setup. The noise is ever present and all measurements will be affected in the same manner.

1.6 Significance

The main objective of this project, as mentioned, was to increase the output voltage of the nanogenerator. Everything that was done throughout the project was done to ultimately increase the output voltage of the nanogenerator. The project started with a literature study that helped to identify areas where optimisation can be done. If any techniques exist, these techniques were implemented, but the intention of this project was to develop new, novel methods and techniques to optimise the output voltage of the nanogenerator. Techniques and methods used for thin films and other nanowire applications were adapted and used for the nanogenerator.

The methods and techniques used for the optimisation of the nanogenerator were novel. After an initial literature study it was found that very little information is available on the optimisation of ZnO nanowire devices. This means that there is still a lot for room of improvement. Optimisation of nanowire growth can also be done, with optimisation being done with respect to the output voltage.

In order to optimise the output voltage, reliable measurements must be made. This work will develop a new method to measure the output voltage of a nanogenerator accurately using inexpensive equipment.

The project will also help to develop an alternative power source for electronic devices. As already mentioned, electronic devices are dependent on batteries for power and these batteries need replacing or recharging on a regular basis. Replacing batteries with an alternative source can ensure continuous operation. The devices could then be self-powered by a clean energy source that scavenges energy from the environment.

This project aims to combine electronic engineering principles with nanotechnology to optimise and design a nanogenerator. The project will require a wide range of knowledge in order to solve all the obstacles that it will face.

1.7 Dissertation flow

The flow of the dissertation is discussed in the remaining part of this chapter. Each chapter will be discussed briefly.

The literature study is given in Chapter 2. The chapter begins with a discussion of the most common energy harvesting technologies that are available today. A brief description of each technology is given together with a few advantages and disadvantages of each.

This is followed by a brief discussion on nanotechnology. Although a definition of nanotechnology is still up for debate a few definitions are given. A brief look at

the history of nanotechnology is also presented. This section concludes with a look at the properties that make nanotechnology such a promising technology.

After the discussion on nanotechnology, piezoelectricity is introduced. A definition of piezoelectricity is given together with a brief look at its history. This is followed by a physical and mathematical description of the piezoelectric effect. The nanogenerator is just one application of the piezoelectric effect and this section concludes by discussing a couple of extra applications.

The ZnO nanowires are introduced next. An in-depth look at the crystal structure is presented. This is followed by an explanation of the unique mechanical and electrical properties of the nanowires, as well as a discussion on the two different growth methods that are used for this project. Both methods are discussed in detail, giving the chemical reactions that happen in order to form the ZnO nanowires.

The nanogenerator is discussed next. The discussion begins by giving a complete physical description of the nanogenerator. This is followed by deriving a mathematical description of the output voltage of the nanogenerator. The contact between the nanowires and electrode is discussed in the next two sections. Firstly, the role of the Schottky contact is discussed followed by a discussion of the contact resistance between the nanowires and electrode.

Chapter 3 contains a discussion on the methodology used throughout the project. The chapter starts with a discussion on the ZnO nanowire growth. Both methods, the VLS and the aqueous solution, are discussed with more detail. Both methods require pretreatment of the substrate and this is also discussed.

The ZnO nanowire optimisation is introduced by discussing the two methods used namely, the one parameter at a time and the design of experiments optimisation methods. These are discussed in terms of their specific application in optimising the growth parameters of the ZnO nanowires.

The nanowires must be characterised after growth, and methods such as scanning electron microscopy (SEM), tunneling electron micropscopy (TEM), atomic force microscopy (AFM) and Hall measurements are discussed in the next section. Two different characterisation techniques are used: optical and electrical. Optical methods, like SEM and TEM are discussed in detail as are the electrical methods.

Lastly, the limitations are discussed. Owing to a number of restrictions, it was not possible to do all the tests. Although these limitations are discussed, they did not have a significant influence on the output of the project.

The simulations of the nanogenerator are introduced in Chapter 4. These simulations commenced by simulating a single ZnO nanowire with various parameters and properties being simulated in order to investigate the influence on the output voltage. Subsequently, more nanowires are introduced to ascertain the effect of

multiple nanowires on the total output of voltage and current.

Chapter 5 discussess the commencement of the bulk of the work done for this project. This chapter contains a discussion about the optimisation of the ZnO nanowire growth. The optimisation starts with the one parameter at a time approach. This technique is carried out on both growth methods to see which method, on average, results in the larger output voltage. During this step it was observed that the seed layer used in the substrate has a substantial influence on nanowire growth. This is followed by a discussion on the optimisation of the nanowires done by carrier concentration and resistance. This section concludes with a discussion on the optimisation of the growth parameters by the design of experiments (DoE) method. This method is used to find optimal growth parameters within the range identified by the one parameter at a time method.

Chapter 6 explains the optimisation of the nanogenerator, the most important and novel part of the project. The discussion starts with the manufacture of the solid nanogenerator. The discussion then continues by following the progress of the solid nanogenerator to the point where the flexible nanogenerator is introduced. The manufacture of the flexible nanogenerator is then discussed in detail. This is followed by a discussion on the optimisation of the nanogenerator. Various approaches to optimisation are discussed, with certain methods producing better results. Finally current measurements are introduced.

Chapter 7 explains the output circuitry used for the nanogenerator. This section was not initially planned for, but its importance became clear as the project continued. The output circuitry is discussed by introducing various circuits. These circuits are simulated using software in order to optimise the circuits. Subsequently, practical tests are performed with the optimised nanogenerator to see which circuit gives the best practical results.

Chapter 9 concludes the dissertation. The chapter commences with a review of the aims and objectives of this research. Comments are made on the success or otherwise of each of these aims and objectives.

The main findings are discussed next. Firstly, the measurements made on the nanowires are discussed. The electrical measurements are unique to this project and both this uniqueness and the results are discussed. The growth and optimisation of the nanowires are also unique and conclusions in this regard are drawn in this section. Secondly, conclusions regarding the optimisation of the nanogenerator are discussed.

This chapter concludes with a discussion on the significance of this work in the bigger field of nanotechnology and its practical implications for industry. This work has resulted in the publication of articles in a number of peer-reviewed jour-

nals, which are also discussed in this section. Lastly, the limitations of this project are presented, as well as a brief look at future work that could be conducted in this field.

Chapter 2

Literature Study

Scientific research often builds on research that has been done in the past. For this reason it is very important to conduct a comprehensive literature study to find out what has already been done. The aim of a literature study is to collect all the data that is available on a specific subject, and then build on and improve the research. The aim of this project is not to repeat experiments and research that have been carried out in the past, but rather to conduct new research and fill in the gaps that currently exist.

The project is divided into four main sections: energy harvesting, nanotechnology, piezoelectricity and zinc oxide nanogenerator. Each section is investigated by finding appropriate literature that is freely available and easily accessible. This chapter is divided into these main sections, which are further subdivided. The literature study starts by looking at energy harvesting and the related technologies that currently exist. This is done in order to identify an energy harvesting method that requires more research in order to reach its full potential. This is followed by a brief introduction to nanotechnology and then a more comprehensive look at piezoelectricity. A mathematical description of the piezoelectric effect is derived to highlight parameters that are important to the output voltage. Subsequently, zinc oxide nanowires are introduced through a discussion of their various properties. This is followed by a section covering the synthesis of these nanowires. Next, the nanogenerator is introduced and discussed in detail. Both a physical and mathematical description of the nanogenerator is given, as this is the main focus of this study.

2.1 Energy harvesting

Energy harvesting is the process by which energy is scavenged from the environment using different technologies including solar, thermal, wind and vibrations.

The energy is captured and then stored for use by small, and often wireless, electronic devices [15, 16]. The application of energy harvesting modules in wireless sensor networks is endless. However, energy is the factor that limits the achievement of long lifetimes for these systems [17]. Nevertheless, scavenging energy from the immediate environment of these sensors increases the possibility of infinite operation.

A number of new devices and technologies have emerged from this new field of energy harvesting [18, 19, 20, 21]. The major benefit of these devices is that energy harvesting systems are clean technologies in the sense that they emit no greenhouse gases. In a world that is becoming increasingly aware of the amount of air pollution that is generated by the burning of fossil fuels, self-powered devices will help decrease our dependency on these polluting energy sources [22].

In the following section, the four most popular alternative energy sources, solar, wind, thermal and vibrations, are discussed. A brief description of each source is given and a few advantages and disadvantages are then discussed.

2.1.1 Solar power

Solar power is one of the most commonly used forms of alternative energy. That is due to the fact that the amount of power delivered to the earth from the sun is about 1.5 ZWh per annum (Zeta is 10^{21}) [23]. Currently 13 TW of energy is needed to sustain the 6.5 billion inhabitants of earth and most of this energy is generated by the burning of fossil fuels [24]. These fossil fuels are in limited supply and are also one of the biggest contributors to air pollution.

Although the sun supplies the earth with enough energy the main problem is the conversion methods. In 1873 the first photovoltaic cell was produced from selenium, although its efficiency was below 1% [24]. Since then steady progress has been made; in 1972 the efficiency was raised to 17% using GaAs cells [25]. By reducing the losses of these cells and combining various technologies the overall efficiency has subsequently been raised to almost 25% [26]. This means that we are able to convert less than a quarter of the energy from the sun. Nevertheless, this is still enough to supply the earth with sufficient power.

The main advantages of solar energy is that the technology has been well studied, the source is abundant, it is relatively inexpensive to manufacture solar cells, and the cells have no moving parts and can last for decades. The main disadvantages are that the solar cells must be placed in the right locations and have to be correctly orientated and they must be kept clean. Moreover, the energy is only available for a part of the day and solar cells do not scale down particularly well (not feasible on the nanoscale).

2.1.2 Wind power

Wind power is currently the fastest growing source of clean energy [27]. Atmospheric winds are caused by the sun heating different parts of the atmosphere, meaning that wind power can indirectly be viewed as a different form of energy from sun power. There are also other forms of wind flow, such as the air flow in air-conditioning units and ducts, moving vehicles and moving objects.

Wind power is more feasible on the nanoscale compared to solar power, because it can easily be scaled down. For example, the opening of an air-conditioning duct can be reduced, accelerating the air flow through a smaller opening. A wind harvesting device can then be placed at this opening, harvesting the faster flow [28]. Most wind-powered devices, on a small scale, make use of the piezoelectric effect, where mechanical force is converted to an electrical signal. Accordingly, wind is used to produce a mechanical force that bends or vibrates a piezoelectric device, thus generating an electrical signal [29].

The advantages of wind power are that efficiency is a lot higher compared to solar power and certain areas in the world have almost constant air flow. On the other hand, the main disadvantages are that there are many moving parts, frictional forces reduce the efficiency and consequently these forces increase as size decreases.

2.1.3 Thermal power

Thermal power is generated from the energy that dissipates from an object as it cools down [30]. For example, the human body loses about 320 W of heat energy during a one-hour hike [31, 32]. This means there is an abundance of power sources available for thermal powered devices.

Certain thermal power devices use pyro-electric materials, that is, materials that convert the change in temperature into an electric signal. These materials can be synthesised on small scale to supply power to small devices.

The advantages of thermal power are that there are no moving parts, the construction of thermal power generators is simple and can easily be scaled down. The disadvantages include the low efficiency of devices and the technology is expensive.

2.1.4 Vibration energy

The last energy source that is investigated is vibration. Vibrations are present in most situations, be it the wind blowing the leaves or branches of a tree, a person typing on a keyboard or walking around, loudspeakers, airplane wings, different

types of machines and any form of road. It has been shown that 6.9 mW of energy can be generated by a typist typing at a rate of 40 words per minute and up to 67 W by a person walking at just over 5 km/h [33]. Utilising vibrational forces for power generation is a new field and a great deal of research is necessary to optimise the method.

Vibrational energy is usually converted to an electrical signal with the use of piezoelectric materials [34]. The efficiency of these devices greatly depends on the source and the frequency of the vibration. Most devices can be designed to function optimally at a desired frequency [34].

The advantages of vibration power are that it is abundant, devices can be designed to work optimally for different types of vibration and the materials needed are cheap. The disadvantages are low efficiencies and the vibrations are low in energy to start with.

Of the four alternative energy sources mentioned above, vibrational power looks the most promising as vibrations are always present in some form. Both thermal and wind are limited in terms of the locations in which they can be used, while solar is limited to the time of day it can be used. Although solar power can provide more power, the applications are limited. Using vibrations as energy source looks like the most promising as it is easily down scaled with piezoelectric materials, it is freely available and the efficiencies are adequate.

Nanotechnology is leading to improved designs and manufacturing techniques for all the alternative energy sources. This is because of the new properties and characteristics being discovered as a result of the small scale of nanotechnology materials. New piezoelectric materials are also being discovered that have mechanical to electrical conversion properties with order of magnitude greater than conventional materials. The combination of vibrational forces and piezoelectric materials on the nanoscale can lead to improved energy scavenging devices.

2.2 Nanotechnology

2.2.1 Definition and history

A nanometre is defined as one thousand-millionth of a metre, or 10^{-9} metre. Nano is derived from the Greek word *nânos*, meaning "dwarf" [35]. To put the size in perspective, the average width of a human hair is 75 000 to 100 000 nm [36]. Figure 2.1 shows a number of objects with their corresponding size, starting with a human being, that is 1 metre in height and ending with an atom, that is 0.1 nm in diameter [37].

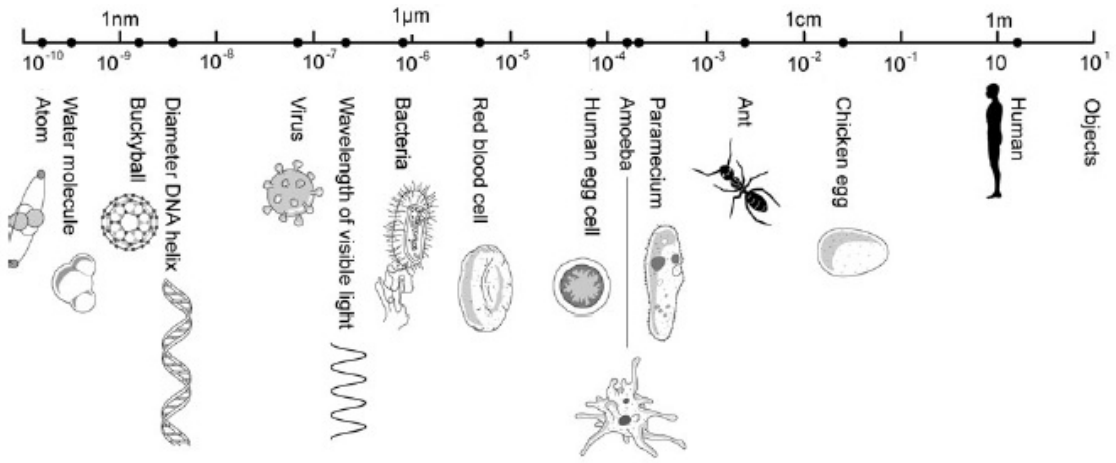

Figure 2.1: Objects on a length scale to put nanoscale objects in perspective [37]

To date, no officially recognised definition of nanotechnology exists. The International Organization for Standardization (ISO) has provisionally defined nanotechnology as follows [38]:

- Understanding and control of matter and processes at the nanoscale, typically, but not exclusively, below 100 nanometres, in one or more dimensions where the onset of size-dependent phenomena usually enables novel applications.

- Utilising the properties of nanoscale materials that differ from the properties of individual atoms, molecules, and bulk matter to create improved materials, devices and systems that exploit these new properties.

Nanotechnology was used as far back as the Middle Ages when gold nanoparticles were used to make red pigments in stained glass [39]. The term "nanotechnology" was coined by Professor Norio Taniguchi at the Tokyo Science University in 1974. Professor Taniguchi described the method of machining down silicon into regions smaller than one micron, or one millionth of a metre [40]. However, Richard Feynman is widely recognised as the father of modern nanotechnology due to his speech "There's plenty of room at the bottom" in 1959. In his speech he discussed the possibility of manipulating objects on the molecular scale and combining chemistry, physics and mathematics to realise this dream [41].

Eric Drexler carried out theoretical work on molecular nanotechnology in 1977 at Massachusetts Institute of Technology (MIT), but no practical work could be done, because it was impossible to observe down to a nanometre. In 1981 the scanning tunnelling microscope (SEM) was invented by Gerd Binnig and Heinrich Ro-

her at IBM and this made it possible to see objects that are only a few nanometers in size. Later that year the first publication relating to nanotechnology appeared [42]. The nanotechnology revolution had begun and major breakthroughs occurred over the next few years, including the synthesis of carbon nanotubes (CNT) in 1991 [42].

Nanotechnology is often compared to the computer revolution and it is said that it will have an even bigger impact on the world. Computers are found in a number of different products, ranging from cell phones, children's toys, cars and many more. Computers, and integrated circuits in particular, have changed the world and have had a huge impact on nearly every industry. The impact has not always been a positive one, as many people who have lost their jobs to computers will testify. Nanotechnology will have an even larger impact on the world and all the different industries [43].

In the Middle Ages the people did not realise that the physical properties of gold changed when gold nanoparticles were used to stain glass. Changes in material properties are attracting a lot of attention and new properties are being discovered.

2.2.2 Nanotechnology properties

What the people in the Middle Ages did not realise is that gold nanoparticles have properties that are distinct from those of bulk gold material. Gold nanoparticles caused the stained glass to appear ruby red or green, depending on the size of the nanoparticles [44].

The properties of materials are size dependant. The physical, chemical and biological properties of materials differ from the bulk material when used at the nanoscale. This is due to the difference in surface area per unit volume of the nanomaterial compared to the bulk material [36].

A cube with three equal sides of one millimetre in length has a volume of one cubic millimeter. The cube has six square sides; each side has an area of one square millimetre, so the whole cube has an area of six square millimetres. The ratio of area to volume of the cube is 6:1. A bigger cube, with sides of two millimetres in length will have a volume of eight cubic millimetres. The area of each of the six sides is four square millimetres, and the area of the cube is 24 square millimetres. The ratio of area to volume is now 24:8, or divided by eight, 3:1. Thus, a smaller object has a bigger area to volume ratio than bigger objects [36].

With the increase in area compared to volume, the number of atoms on the surface of an object also increases compared to the number of atoms in the volume of the object. The atoms in the interior of the object have a higher energy state, which means that these atoms are more likely to react with particles of neighbouring sub-

stances. This means that the more surface area there is, the quicker the reaction will be when compared to bulk materials [36].

Material properties on the nanoscale are unique, because the familiar material properties, such as conductivity, hardness or melting point, meet the more exotic properties of atomic and molecular properties, like wave-particle duality and quantum effects. A nanowire does not always obey Ohm's law, because if the wire is too small, the atoms cannot flow transversely to one another [43].

It is these unique properties of materials at the nanoscale that is attracting so much attention. New uses for existing materials are found, because materials exhibit such drastic changes in properties at the nanoscale. Sunscreen manufacturers use silver nanoparticles to improve the effectiveness of the sunscreen, which leads to better protection against the harmful ultraviolet (UV) rays. More and more everyday products are beginning to incorporate nanotechnology in one way or another.

As mentioned, nanotechnology has the potential to enhance the properties of certain materials due to the increase in surface area. Providing more surface area for the vibrational forces to act on can increase the efficiency of piezoelectric devices.

2.3 Piezoelectricity

2.3.1 Definition and history

The formal definition of the direct piezoelectric effect is the electric polarization produced by mechanical strain in crystals belonging to certain classes, the polarization being proportional to the strain and changing sign with it. Closely related to it is the converse effect, whereby a piezoelectric crystal becomes strained, when electrically polarized, by an amount proportional to the polarizing field [45].

Piezoelectricity, defined in a simpler manner, is the conversion of mechanical force applied to a certain material to an electric potential across that material. Piezoelectricity occurs only in specific crystalline materials. When the material is subjected to a mechanical force, the crystal becomes electrically polarised. Accordingly, tension and compression generate voltages of opposite polarity in proportion to the applied force. The converse effect is also observed, where an applied voltage causes the material to lengthen or shorten, depending on the polarity of the applied potential [46].

Piezoelectricity is derived from the Greek word *piezein*, which means "to press" or "to squeeze". Piezoelectric materials are either crystalline or ceramics. The most well-known and most-used piezoelectric material is quartz. Other materials that

possess the piezoelectric characteristic include berlinite, gallium orthophosphate and tourmaline, which are all crystals, and barium titanate and lead zirconate titanate (PZT), which are ceramics. New piezoelectric materials are constantly being found and some of the new materials include zinc oxide, aluminium nitrate and polyvinylidene fluoride (PVDF) [46].

Jacques and Pierre Curie discovered the piezoelectric effect in 1880. Between 1881 and 1910 more than twenty naturally occurring crystals were found that possessed the piezoelectric effect. In 1910, a book by Viogt, with the title *Lerbuch der Kristallphysik*, was published and it became the standard reference for piezoelectric materials [46].

2.3.2 Piezoelectric effect

The piezoelectric effect occurs as a result of the relative displacement of atoms with respect to each other. These atoms also have an electrostatic force of attraction or repulsion between them, as defined by Coulomb's Law. The electrostatic force, F, between two point charges is given by

$$F = \frac{1}{(4\pi\epsilon_0)} \frac{|q_1||q_2|}{r^2}, \tag{2.3.1}$$

where ϵ_0 is the permittivity of free space, q_1 and q_2 are the two point charges and r is the distance between the two charges [47]. Each point charge exerts an equal force, but in an opposite direction to its neighbouring charges. The magnitude of the electric field vector at a point charge is given by

$$E = \frac{F}{q} = \frac{1}{(4\pi\epsilon_0)} \frac{|q_1|}{r^2}. \tag{2.3.2}$$

The direction of the electric field coincides with the direction of the force. The piezoelectric effect relies on the creation of an electric dipole between anions and cations in the crystal structure [47, 48].

An electric dipole is defined as a pair of point charges, with a fixed distance between them, with equal magnitude, but opposite sign [47]. Figure 2.2 shows that an electric dipole creates an electric field at a fixed distance, z, from the centre of the dipole.

The magnitude of the electric field is calculated by applying the superposition principle as follows [47]:

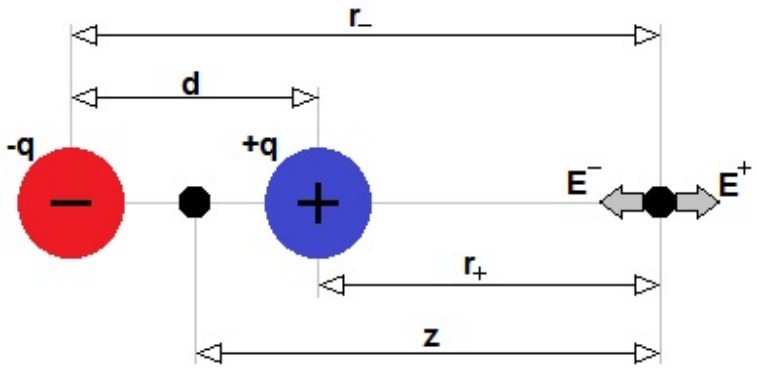

Figure 2.2: Graphical representation of an electric dipole, which creates an electric field at a fixed distance from the centre of the dipole.

$$\begin{aligned} E &= E^{+} - E^{-} \\ &= \frac{1}{(4\pi\epsilon_0)}\frac{q}{r_{+}^2} - \frac{1}{(4\pi\epsilon_0)}\frac{q}{r_{-}^2} \\ &= \frac{q}{(4\pi\epsilon_0)}[\frac{1}{r_{+}^2} - \frac{1}{r_{-}^2}] \\ &= \frac{q}{(4\pi\epsilon_0)}[\frac{1}{(z-0.5d)^2} - \frac{1}{(z+0.5d)^2}] \\ &= \frac{q}{(4\pi\epsilon_0)}[\frac{1}{(1-\frac{d}{2z})^{-2}} - \frac{1}{(1+\frac{d}{2z})^{-2}}]. \end{aligned} \tag{2.3.3}$$

Assuming that the distance, d, between the charges is much smaller than the distance, z, the term in the brackets can be expanded with the binominal theorem, and only the first two terms will be needed, because $\frac{d}{2z}$ is smaller than one. The above equation can then be simplified [47] to

$$
\begin{aligned}
E &= \frac{q}{(4\pi\epsilon_0 z^2)}[(1+\frac{2d}{2z(1!)}+...)-(1-\frac{2d}{2z(1!)}-...)] \\
&= \frac{q}{(4\pi\epsilon_0 z^2)}[(1+\frac{d}{z}+...)-(1-\frac{d}{z}-...)] \\
&= \frac{q}{(4\pi\epsilon_0 z^2)}[(1+\frac{d}{z})-(1-\frac{d}{z})] \\
&= \frac{q}{(4\pi\epsilon_0 z^2)}[\frac{z+d}{z}-\frac{z-d}{z}] \\
&= \frac{q}{(4\pi\epsilon_0 z^2)}\frac{2d}{z} \\
&= \frac{q}{(2\pi\epsilon_0)}\frac{qd}{z^3} \\
&= \frac{q}{(2\pi\epsilon_0)}\frac{p}{z^3},
\end{aligned}
\tag{2.3.4}
$$

with $p = qd$ being defined as the dipole moment. From (2.3.4) it is clear that any change in the dipole moment will correspond to a change in the electric field. This is the origin of the piezoelectric effect [49]. The anions and cations are displaced with respect to one another due to an external applied force, which causes a change in the dipole moment. The accumulation of dipole moments within the crystal causes the polarisation of surface charges and this results in an electric field [46].

Piezoelectricity couples the mechanical properties and electrical properties of crystals via the polarisation vector. To describe the piezoelectric effect in full, the mechanical and electrical properties must be viewed separately and then combined.

The mechanical properties are described by Hooke's Law in three dimensions, with

$$T_I = c_{IJ} S_J, \tag{2.3.5}$$

$$S_I = s_{IJ} T_J, \tag{2.3.6}$$

where T is stress, S is strain, c is the elasticity coefficient and s is the elastic compliance coefficient and also the inverse of c. When (2.3.5) is written in expanded matrix form, both T and S consist of nine terms and c and s are nine by nine matrices. There are, however, symmetrical stress and strain conditions which reduce T and S to six terms and c and s to six by six matrices [48]. In terms of the notation used in (2.3.7), indices 1, 2, 3 correspond to Cartesian directions x, y, z and indices 4, 5, 6 represent shear directions yz, zx, xy. The equation in its expanded form is as

follows [48]:

$$\begin{bmatrix} T_1 \\ T_2 \\ T_3 \\ T_4 \\ T_5 \\ T_6 \end{bmatrix} = \left[\begin{array}{ccc|ccc} c_{11} & c_{12} & c_{13} & c_{14} & c_{15} & c_{16} \\ c_{21} & c_{22} & c_{23} & c_{24} & c_{25} & c_{26} \\ c_{31} & c_{32} & c_{33} & c_{34} & c_{35} & c_{36} \\ \hline c_{41} & c_{42} & c_{43} & c_{44} & c_{45} & c_{46} \\ c_{51} & c_{52} & c_{53} & c_{54} & c_{55} & c_{56} \\ c_{61} & c_{62} & c_{63} & c_{64} & c_{65} & c_{66} \end{array}\right] \times \begin{bmatrix} S_1 \\ S_2 \\ S_3 \\ S_4 \\ S_5 \\ S_6 \end{bmatrix}. \tag{2.3.7}$$

The electric properties are a result of electric polarisation which is proportional to the electric field and is given by [50]

$$P_i = \epsilon_0 \kappa_{ij} E_j \text{ , } i = 1, 2, 3, \tag{2.3.8}$$

where P is the polarisation vector, ϵ_0 is the permittivity of free space, κ_{ij} is the electric susceptibility and E_j is the electric field. Polarisation is not always in the same direction as the induced electric field and therefore it may couple to other directions. Polarisation is replaced by electric displacement, D, for convention purposes [50]

$$\begin{aligned} D_i &= \epsilon_0 E_j + P_i, \\ D_i &= \epsilon_0 E_j + \epsilon_0 \kappa_{ij} E_j, \\ D_i &= \epsilon_0 E_j (1 + \kappa_{ij}), \\ D_i &= \epsilon_{ij} E_j \text{ for } i = 1, 2, 3 \text{ and} \\ \epsilon_{ij} &= \epsilon_0 (1 + \kappa_{ij}). \end{aligned} \tag{2.3.9}$$

Piezoelectric materials polarise when an external electric field is present; consequently, the lattice of the crystal will also deform, as shown in Figure 2.3. The lattice shape is shown in yellow and it undergoes deformation as the crystal is deformed, becomes shorter and broader when a force is applied and becomes larger, but narrower when the crystal is pulled. The coupling of stress and polarisation is what make piezoelectric materials unique and is described as [48]

$$Direct : P_i = d_{iJ} T_J, \; i = 1 \text{ to } 3 \text{ and } \; J = 1 \text{ to } 6, \tag{2.3.10}$$

$$Converse : S_J = d'_{Ji} E_i \; J = 1 \text{ to } 6 \text{ and } \; i = 1 \text{ to } 3, \tag{2.3.11}$$

where d is the piezoelectric coupling coefficient in the strain-charge form and d' is the transpose matrix of d. Index i represents polarisation and index J represents stress components [48].

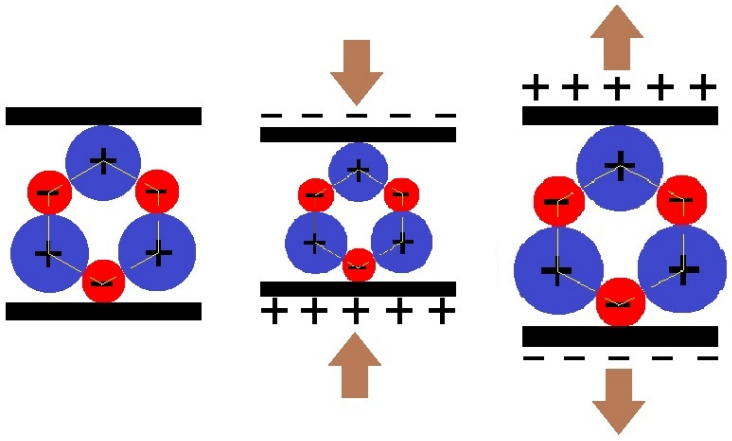

Figure 2.3: Deformation of the lattice of the crystal when the crystal is subjected to an external force.

Piezoelectricity has to do with the coupling of mechanical and electrical properties. A piezoelectric material that is present in a constant electric field will adhere to the following [51]:

$$S_I = S_I^E + S_J, \tag{2.3.12}$$

$$S_I = s_{IJ}^E T_J + d_{kJ} E_K. \tag{2.3.13}$$

The strain of the material is equal to the original strain plus a new strain induced as a result of the piezoelectric effect. When under constant strain, the piezoelectric material will also adhere to the following [51]:

$$D_i = P_i + D_i^T, \tag{2.3.14}$$

$$D_i = d_{iJ} T_J + \epsilon_{ik}^T E_k. \tag{2.3.15}$$

The electric displacement is equal to the electric displacement plus polarisation due to the force applied to the material.

Equations (2.3.13) and (2.3.15) are the standard equations that describe the piezoelectric effect in materials. These equations are in strain-charge form; there are three other forms, but the strain-charge form is the most popular.

Piezoelectric materials have been around since the Curies discovered them back in 1880 [46]. Since then, the mathematics that describes the phenomenon has been developed, together with new and unique applications.

2.3.3 Piezoelectric uses

Piezoelectric materials are used in a number of different applications. Uses for piezoelectric materials include generators, sensors, actuators and transducers [46].

The voltages generated by piezoelectric materials can create a spark across an electrode gap. This spark can then be used to ignite a flame. Piezoelectric ignition systems are used in lighters, gas stoves and welding equipment [46].

Piezoelectric actuators convert electric signals into a physical displacement. Manipulation on the nanoscale has seen an increase in piezoelectric actuators, because of their precise control and small range [46].

Research in nanotechnology is finding new applications for old materials and material characteristics. ZnO is widely used as an additive in a number of different products, such as paint and plastic. It is also a piezoelectric material and nanoscale ZnO structures enhance the piezoelectric effect. This has led to a new field, nanopiezotronics.

2.4 Zinc oxide nanowire properties

ZnO has been studied since 1935 and over the years has attracted the attention of scientists owing to its unique properties at the nanoscale [52]. It has a number of unique characteristics that makes it an ideal candidate for a nanogenerator. These unique characteristics include, but are not limited to, the following:

- It has extremely high elasticity that allows for large degrees of bending without damage to the nanowire [53, 54].
- The nanowires will not break after continuous vibration [55].
- The power density of ZnO is estimated at 2.7 mW/cm^3 which is ten times higher than for other piezoelectric materials [56].
- The piezoelectric effect of ZnO nanostructures are about 14 times higher than that of the bulk material [55].
- Low temperature growth via the hydrothermal method [57] allows for growth on various substrates.
- ZnO is biocompatible [58] and environmental friendly [59].

Other properties that make ZnO such an attractive material include mechanical and electrical properties that arise from the crystal structure of ZnO. The crystal structure will now be discussed, as well as some of the unique mechanical and electrical properties.

2.4.1 Crystal structure

Crystals grow in a constant environment by continuously adding identical building blocks. The building blocks for crystals are atoms or a group of atoms so that the crystal is a three-dimensional periodic array of atoms [60]. Each individual ZnO nanowire is a single crystal, with a periodic array of Zn and O atoms arranged in a specific pattern.

Appendix A gives the background to crystallography. During the course of this study, the author attended a six week course on crystallography in order to better understand the significance of the crystal structure of the ZnO nanowires.

At ambient pressure and temperature, ZnO has a wurtzite structure. The wurtzite structure is a hexagonal lattice and is characterised by two interconnecting sub-lattices of Zn^{2+} and O^{2-}. Each Zn-ion is surrounded by a tetrahedra of O-ions, or vice versa [52], as shown in Figure 2.4.

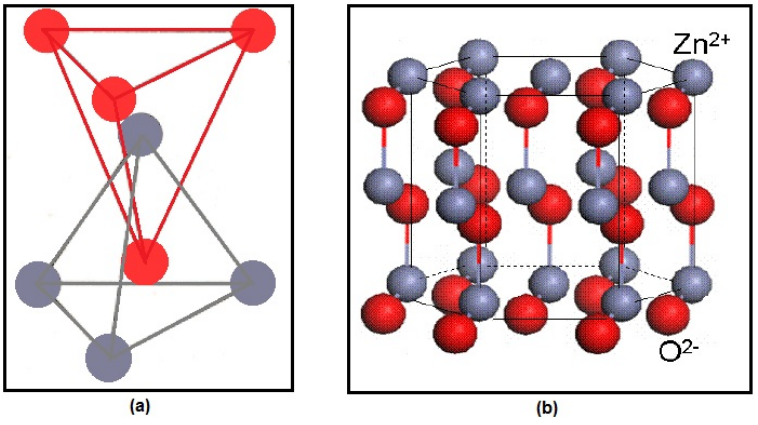

Figure 2.4: (a) Tetrahedral coordination of Zn and O atoms, (b) hexagonal packing of Zn and O planes.

The lattice parameters of the hexagonal crystal system are $a = 0.32495$ nm and $c = 0.52069$ nm, with a density of 5.605 g/cm^3 [52, 61]. The crystal structure also has 6 mm symmetry, meaning there are six mirror planes present in the structure, which result in high symmetry within the structure [62].

The tetrahedral configuration of the ions gives rise to polar symmetry along the hexagonal axis. The polar symmetry is responsible for most of the properties of ZnO, such as the piezoelectric effect. The polar symmetry also plays an important role in the growth of different nanostructures of ZnO [52].

The four most common face terminations of wurtzite ZnO are the polar Zn-terminated (0001) and O-terminated $(000\bar{1})$ faces, as well as the non-polar $(11\bar{2}0)$ and $(10\bar{1}0)$ faces, both containing an equal number of Zn and O atoms. A polar face is an ionised surface that increases the magnetic attraction between the polarised surface and another arbitrary surface. Polar surfaces possess different chemical and physical properties from the rest of the material [52, 61, 62, 63].

The tetrahedral configuration of the ZnO atoms indicates a covalent bond between the Zn and the O atoms. However, the Zn-O bond also possesses ionic bonding characteristics and, thus, ZnO is borderline classified as a covalent and ionic compound [64]. ZnO possesses unique mechanical and electrical properties that arise from the unique crystal structure. These properties are what makes ZnO such a unique material and why it is being widely studied in the scientific community.

2.4.2 Mechanical properties

The crystal structure of ZnO determines the mechanical properties of ZnO. The mechanical properties relating to the piezoelectric effect, such as the elasticity coefficient and piezoelectric coupling coefficient, are simplified because of the crystal structure [50, 52, 65, 66].

The elasticity coefficient, c_{IJ}, is simplified from (2.3.5) to [50, 52, 65, 66]

$$\begin{bmatrix} c_{11} & c_{12} & c_{13} & 0 & 0 & 0 \\ c_{12} & c_{11} & c_{13} & 0 & 0 & 0 \\ c_{13} & c_{13} & c_{33} & 0 & 0 & 0 \\ 0 & 0 & 0 & c_{44} & 0 & 0 \\ 0 & 0 & 0 & 0 & c_{44} & 0 \\ 0 & 0 & 0 & 0 & 0 & c_{66} \end{bmatrix}, \text{with } c_{66} = \frac{(c_{11} - c_{12})}{2}. \tag{2.4.1}$$

The piezoelectric coefficient, d_{iJ}, is simplified to [50, 52, 65, 66]

$$\begin{bmatrix} 0 & 0 & 0 & 0 & d_{15} & 0 \\ 0 & 0 & 0 & d_{15} & 0 & 0 \\ d_{31} & d_{31} & d_{33} & 0 & 0 & 0 \end{bmatrix}, \tag{2.4.2}$$

and the dielectric coefficient, ϵ_{ik}, to [50, 52, 65, 66]

$$\begin{bmatrix} \epsilon_{11} & 0 & 0 \\ 0 & \epsilon_{22} & 0 \\ 0 & 0 & \epsilon_{33} \end{bmatrix}. \tag{2.4.3}$$

Table 2.1 shows the values of the independent parameters of the above equations, as well as other important parameters of ZnO [50, 52, 65, 66].

Table 2.1: Mechanical parameters of ZnO bulk material [50, 52, 65, 66]

Parameter	Value
Young's modolus, E	111.2 GPa
Hardness, H	5.0 GPa
$\frac{\epsilon_{11}}{\epsilon_0}$	1.32
$\frac{\epsilon_{22}}{\epsilon_0}$	-0.57
$\frac{\epsilon_{33}}{\epsilon_0}$	-0.48
d_{33}	12.4×10^{-12} C/N
d_{31}	-5×10^{-12} C/N
d_{15}	-8.3×10^{-12} C/N
c_{11}	210×10^{9} N/m^2
c_{12}	121×10^{9} N/m^2
c_{13}	105×10^{9} N/m^2
c_{33}	211×10^{9} N/m^2
c_{44}	43×10^{9} N/m^2

Table 2.1 shows that ZnO is a relatively soft material, with a hardness of only 5 GPa, but it is still one of the hardest semiconductors. The relative softness of ZnO means it will indent easily [65]. The indentation causes long-term damage to ZnO and hampers the propagation of light or current through the material [65, 66].

The piezoelectric coefficient of ZnO is also higher than the coefficient of other, similar materials, such as GaN and AlN. This means that the conversion of mechanical force to an electric potential will be more efficient for ZnO when compared to other materials [52].

2.4.3 Electrical properties

ZnO is a semiconductor compound with a wide band gap of 3.37 eV [67]. It is an energy range where no electron can exist. The band gap falls in between the valance band and the conduction band of an electron energy state. Electrons can only exist in the valance band, and once they acquire enough energy, they can jump to the conduction band. In other words, the electron can never exist in the band gap. Accordingly, the larger the band gap, the more insulating the material is,

because the electrons never acquire enough energy to jump over the band gap to the conduction band [47].

ZnO also has a large excitation binding energy of 60 meV [67]. The excitation binding energy is the energy that is present owing to the attraction of an electron to an electron hole. The energy is electrically neutral and exists mainly in semiconductors [47]. The large excitation binding energy of ZnO means that the electrons and electron holes are highly attracted to each other and a great deal of energy is needed to break that bond.

ZnO is generally an n-type semiconductor, which means electrons are the main carriers of charge. N-type conductivity is attributed to oxygen vacancies. One oxygen vacancy is accompanied by two electrons in order to keep the charge balance [68].

The contact between ZnO and a metal electrode plays a vital role in the electrical properties of ZnO. This metal semiconductor contact can form two different types of contact, namely ohmic or Schottky. An ohmic contact has a linear relationship between current and voltage, while in a Schottky contact the current voltage behaviour will be non-linear [68, 69].

The characteristics of the contact are determined by the difference in work function of the semiconductor and the metal [68, 69]. The work function is the minimum energy required to remove an electron from one material to a region just outside that material [47]. Electron affinity is the amount of energy released when an atom acquires an electron [47]. The electron affinity of ZnO is 4.53 eV. Gold, with a work function of 5.1 eV, and platinum, with a work function of 6.1 eV, will form a Schottky contact with ZnO. This is because the electron affinity of the semiconducting ZnO is lower than the work function of the metal. The semiconducting ZnO will lose an electron to the metal and, thus, an electron flow will develop between the semiconductor and the metal. Silver, with a work function of 4.2 eV, and titanium, with a work function of 3.9 eV, will form an ohmic contact with ZnO. In this case the semiconductor has a higher electron affinity than the work function of the metal. Hence, the metal will lose an electron to the semiconductor and an electron flow from the metal to the semiconductor will develop [68, 69].

The electric transport of ZnO is heavily dependent on the number of oxygen vacancies in the material. During the synthesis of ZnO structures, this can be controlled by adding either more or less oxygen vacancies. The crystal structure of ZnO also plays an important role in the types of nanostructures that can be synthesised.

2.5 Zinc oxide nanowire growth

One-dimensional nanostructures have attracted a lot of attention since L. V. Radushkevich discovered carbon nanotubes in 1952 [70]. There are two categories in the synthesis of one dimentional nanostructures: bottom-up and top-down. Bottom-up is the growing of structures from raw material, methods such as chemical vapour deposition or physical vapour deposition. Top-down is the method by means of which bulk materials are manipulated down to nanoscale structures; such methods include lithography or etching [71].

Different ZnO nanostructures can be achieved by means of these methods. Nanostructures, including nanoarrays [72], nanorods [73], nanowires [74], nanobelts [75], nanorings [76], nanohelices [77] and nanosprings [78] of ZnO have been successfully synthesised.

There are a number of different methods for growing ZnO nanowires. However, only two methods were considered for this project and these are vapour liquid solid and chemical bath deposition. These methods were chosen, because they are easy to implement with the equipment at hand. Only these two methods were used and the syntheses of nanowires were investigated.

2.5.1 Vapour Liquid Solid

Vapour liquid solid (VLS) is one of the most used methods to synthesise ZnO nanowires, although the exact working of the method is still not fully understood. The basic mechanism that drives the growth is understood, but what exactly drives the growth is not [71, 79, 80, 81, 82, 83, 84].

The VLS method consists of a open-ended furnace that can heat up to 1200°C and a quartz tube that fits inside the furnace and is longer than the furnace. Source materials are then loaded into the quartz tube and placed in the hottest region of the furnace. Substrates, where the growth will take place, are then placed a fixed distance from the source materials. A carrier gas is connected to the quartz tube, as is a vacuum system, as shown in Figure 2.5 [71].

For ZnO nanowire growth the samples/substrates are covered with a thin layer of gold, 2 - 20 nm thick. The gold is annealed before the growth starts to form small gold droplets [83]. The gold acts as catalyst and initiates and guides the growth [81, 82]. The source materials, that is either Zn powder, ZnO powder or a 1 : 1 mixture of ZnO and graphite, are heated up to temperatures ranging from 850°C to 1200°C. This causes the source materials to evaporate and the carrier gas, argon in most cases, carries the source material vapour to the samples, which are a fixed distance away and also in a lower temperature region than the source materials. The vapour

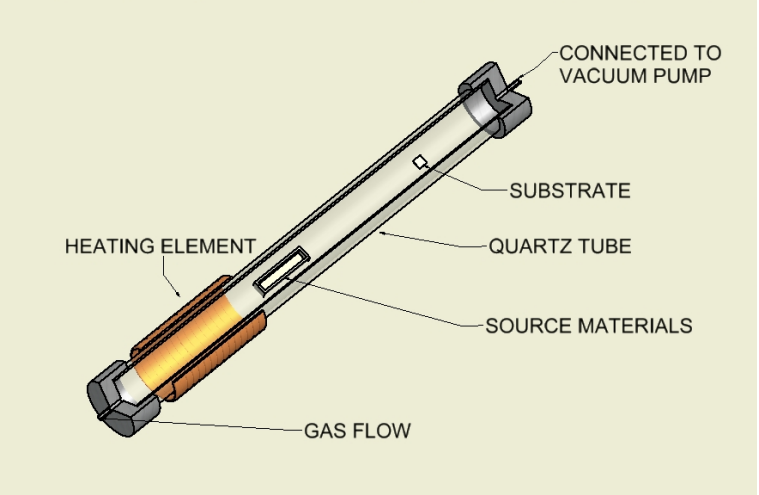

Figure 2.5: Schematic of vapour liquid solid growth setup.

then reacts with the gold droplet and the growth is initiated. The phenomenon that occurs when the vapour reaches and reacts with the gold droplet is still not fully understood and is still being investigated [71, 79, 80, 81, 82, 83, 84].

There are two different proposed mechanisms that drive the growth of the nanowires. The first is the vapour liquid solid (VLS) method and the second is the vapour solid (VS) method. The difference between the two methods, only present at the time when the source vapour reaches the catalyst droplet, is in the interaction of the vapour and the catalyst [71, 79, 80, 81, 82, 83, 84].

For the VLS method, when the vaporised source material, Zn, reaches the catalyst droplet, Au, it is absorbed by and diffused in the droplet, forming a liquid alloy, Au-Zn. The Au-Zn alloy droplets will gradually reach supersaturation, because the concentration of source materials will exceed the solubility of the catalyst droplet. The Zn atoms separates and oxidises, forming ZnO, and with time this grows into nanowires, as shown in Figure 2.6 [81, 82, 84]. The presence of the catalyst droplet at the tip of the nanowire is a characteristic feature of the VLS method [81].

The VS method also uses a metal catalyst, but the growth sites are determined by surface defects, dislocations or metal patterns on the substrate, which provide energetic favoured nucleation sites. The Zn solidifies to ZnO by means of oxygen that is present in the system and creates ZnO nanowires. The Au droplet should be present at the root of the nanowire. The VS method is much slower, 10 to 100 times, than the VLS method. The VS method is also not studied as much as the VLS method [81].

The chemical formula that is present at the start of the growth is the same for both the VLS and the VS methods.

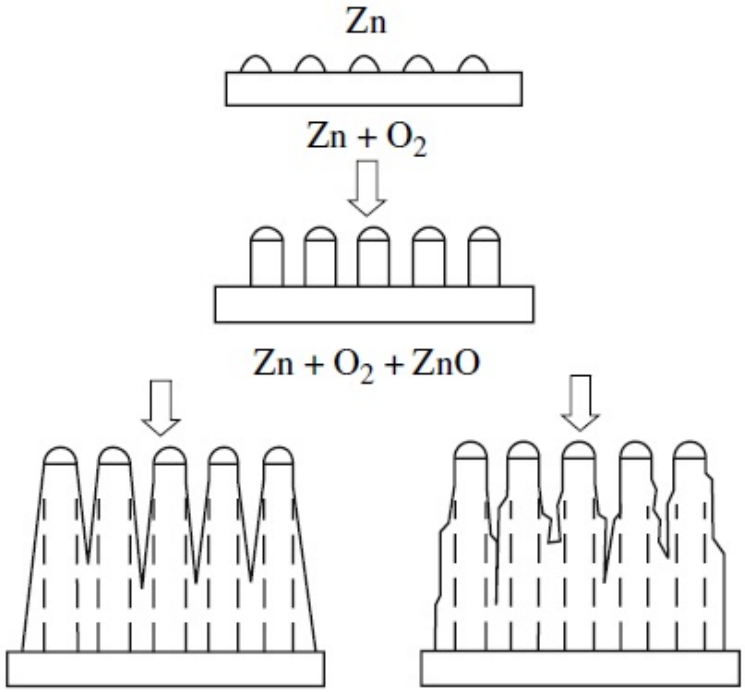

Figure 2.6: Schematic representation of the vapour liquid solid growth mechanism. The diagram shows the formation of seed layers during the growth of the nanowires [84].

$$ZnO(S) + C(S) \rightarrow Zn(g) + CO(g). \tag{2.5.1}$$

This creates the Zn source material for the growth. The equation can also be driven in reverse, but due to the high temperatures it is not done. For both the VLS and the VS methods the ZnO forms via the oxidation reaction.

$$2Zn(g) + O_2(g) \rightarrow 2ZnO(S). \tag{2.5.2}$$

Using the VLS method, the Zn reacts with the Au droplet and forms an alloy. The oxygen attaches to the Zn atoms afterwards and the growth starts. Using the VS method Au merely acts as a preferential defect site for the growth to take place. In both cases the oxygen is provided along with the Ar carrier gas. The Zn oxidation could also result from a reaction with CO and CO_2, but the above equation would be dominant [81].

The problem with both the VLS and the VS methods is the high temperatures that are required for growth and this limits the types of substrate that can be used. Therefore, growing the nanowires at lower temperatures is critical, because nanowires can then be grown on almost any substrate.

2.5.2 Chemical bath deposition

Chemical bath deposition (CBD) is the deposition of metal oxide structures from an aqueous solution. The growth originates from the control of the precipitation on a substrate via hydrolysis and condensation reactions of metal ions and complexes from the aqueous solution [85]. The main advantage that the CBD method has over the VLS is that it is less expensive and growth takes place at lower temperatures [86].

The growth is done by mixing zinc nitrate hexahydrate [$Zn(NO_3)_2$ $6H_2O$] and HMTA [$C_6H_{12}N_4$] in deionised (DI) water. The solution is transparent with some white particles, $Zn(OH)_2$ dispersed throughout the volume. The reactions in the solution are described by the following [86]

$$C_6H_{12}N_4 + 6H_20 \leftrightarrow 6CH_2O + 4NH_3, \tag{2.5.3}$$

$$NH_3 + H_2O \rightarrow NH_4^+ + OH^-, \tag{2.5.4}$$

$$Zn(NO_3)_2 \rightarrow Zn^{2+} + 2{NO_3}^-, \tag{2.5.5}$$

$$Zn^{2+} + 4NH_3 \rightarrow {Zn(NH_3)_4}^{2+}, \tag{2.5.6}$$

$$Zn^{2+} + 4OH^- \rightarrow {Zn(OH)_4}^{2-}, \tag{2.5.7}$$

$${Zn(NH_3)_4}^{2+} + 2OH^- \rightarrow ZnO + 4NH_3 + H_2O, \text{ and} \tag{2.5.8}$$

$${Zn(OH)_4}^{2-} \rightarrow ZnO + H_2O + 2OH^-. \tag{2.5.9}$$

The zinc oxide for the growth originates from zinc salts that are dissolved in the deionised water. Zinc metal, Zn^{2+}, is soluble in water and forms aqueous ions in the form of hydroxyl species $ZnOH^+$, $Zn(OH)_2$, $Zn(OH)_3^-$ and $Zn(OH)_4^{2-}$. ZnO nuclei are formed as a result of the dehydration of these hydroxyl species. The ZnO crystals continue to grow due to the condensation of the surface hydroxyl groups with the zinc hydroxyl species [57, 85, 87].

The pH of the aqueous solution plays a critical role in the growth of the nanowires. Additives, such as HMTA, are added to alter the pH of the solution. The exact function of the HMTA during growth is still under investigation. HMTA acts

as a base and is known to hydrolyse, producing ammonia, which alters the pH value [85, 87, 88].

The growth of the nanowires takes place in two steps. First, nucleation sites are formed when the zinc salts are first dissolved in water. Nucleation sites form where the nanowires will start to grow, and these sites thus determine the diameter of the nanowires. The molar mass of the zinc solution determines the size of the nucleation sites; the lower the molar mass, the smaller the diameter of the nanowires. The second step is the growth of the nanowires from the nucleation sites. The zinc metals in the solution and oxygen from the water are attracted to the nucleation sites and form layers which stack up to form the ZnO nanowires [57, 86, 88].

The CBD method has another big advantage over other methods. The substrate on which the nanowires grow does not influence the growth in any considerable manner. This fact, together with the low temperature associated with CBD, makes it possible to grow the nanowires on plastic substrates [88].

The nanowires are used in a variety of applications. In this study the use of the nanowires as an electricity generating device (nanogenerator) is investigated.

2.6 Nanogenerator

Small implantable electronics, like pacemakers, still require batteries for operation. These batteries have a limited lifetime and must consequently be replaced once they are depleted. Futhermore, sensors that are placed in remote and hard to reach areas, that function with batteries, are non-sustainable, because the batteries will need replacement, which is not an easy task. These two examples illustrate the need for devices to be self-powered.

This need for devices to be self-powered becomes even more apparent when devices are shrunk to nanosize. Attaching a battery to a nanosized sensor would defeat the purpose of the minuscule sensor. However, attaching a nanosized electricity generator to the sensor would make the sensor more attractive. Nanogenerators are generators that generate electricity on the nanoscale and then deliver the electricity to an external device. This is a new field of research that is attracting a lot of attention throughout the scientific community [89, 90, 91].

The physical operation of the nanogenerator will be discussed in the section that follows. Accordingly, the exact working of a single nanowire, when bent, is discussed. The generation of a piezoelectric voltage from the strain induced in the nanowire to the conversion to a measurable output voltage is also discussed. Subsequently, a mathematical model is developed to show what parameters influence the output voltage of a single nanowire. This mathematical model is used to op-

timise the output voltage by optimising specific parameters. Lastly, the influence of carrier concentration and resistance on the output voltage is discussed. Neither of these parameter is included in the mathematical model, but they are discussed separately.

2.6.1 The physical description of the operation of the nanogenerator

A nanogenerator, in its simplest form, consists of a single ZnO nanowire that is bent by an electrode. The physical principle for creating the piezoelectric discharge arises from the coupled semiconducting and piezoelectric properties of ZnO. A straight vertical nanowire, as depicted in Figure 2.7 (a), is bent by an electrode. The bending causes a strain field to develop in the nanowire. When the outer surface is stretched, positive strain occurs and when the inner surface is compressed, negative strain occurs, as shown in Figure 2.7 (b). An electric field is created inside the nanowire, in the z-direction, as illustrated in Figure 2.7 (c). The electric field, E_z, is equal to $E_z = \frac{\epsilon_z}{d}$, where d is the piezoelectric coefficient and ϵ_z is the strain of the nanowire. By simplification, the electric potential varies from V_s^+ at the stretched side to V_s^- at the compressed side, as shown if Figure 2.7 (d). The substrate on which the nanowire is grown is at ground potential. V_s^+ and V_s^- are voltages produced by the piezoelectric effect and can be a few tenths of a volt in magnitude [8, 90].

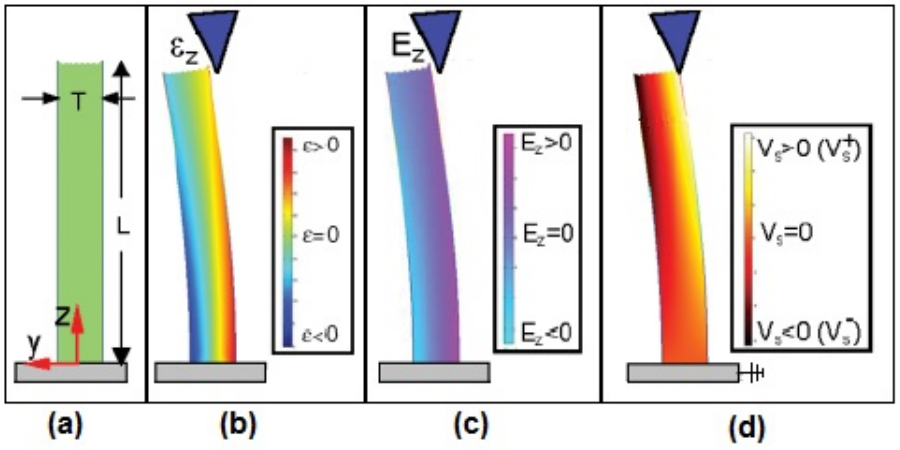

Figure 2.7: (a) Schematic representation of a straight vertical nanowire in specific coordinate system, (b) an electrode bends the nanowire and a strain field is created throughout the nanowire, (c) the strain field causes an electric field throughout the nanowire due to the piezoelectric effect, (d) by simplification, the electric field is converted to a potential difference across the nanowire [8].

The potential is created by the relative displacement of the Zn^{2+} cations with respect to the O^{2-} anions. These ionic charges cannot move freely through the nanowire and cannot recombine without releasing the strain. The potential difference is maintained as long as the nanowire is deformed and no foreign free charges, such as metal contacts or impurities within the nanowire, are present [8, 90, 92].

When the top electrode bends, the nanowire is in contact with the stretched side of the nanowire and has a positive potential of V_s^+. No external voltage is applied to the top electrode, which means the electrode has a potential of zero, $V_m = 0$. The electrode nanowire interface, ΔV, is negatively biased for $\Delta V = V_m - V_s^+ = 0 - V_s^+ < 0$, as shown in Figure 2.8 (a). The nanowires are n-type semiconductors and the electrode is a metal which leads to the formation of a Schottky contact. The metal semiconductor is negatively biased, which means the Schottky contact is a reverse-biased Schottky diode. The result is a little current flow across the metal semiconductor interface, as shown in Figure 2.8 (c). The piezoelectric static charges, Zn^{2+} and O^{2-} ions, are accumulated and preserved at the metal-semiconductor interface. The accumulation of charges prevents leakage of the current during the deformation of the nanowire [8, 89, 90].

The electrode moves across the nanowire until it is in contact with the compressed side of the nanowire. The electrode, still with no external voltage applied, may have acquired a small voltage during the first contact with the nanowire and is no longer zero. However, the electrode nanowire interface will be positively biased for $\Delta V = V_m - V_s^- > 0$, because V_s^- will be larger than V_m, as shown in Figure 2.8 (b). The metal-semiconductor interface is now positively-biased and a positive biased Schottky diode forms. A sudden increase in electric current is observed, as shown in Figure 2.8 (c). The increase in current is due to the flow of free electrons through the nanowire to the electrode, in order to neutralise the piezoelectric ionic charges distributed in the volume of the nanowire. The magnitudes of the piezoelectric potentials, V_s^+ and V_s^-, will drop due to the flow of the free electrons, because this neutralises the ionic charges. The voltage across the resistor, V_L, will drop in accordance with V_s^+ and V_s^- to zero after all the ionic charges have been neutralised [8, 89, 90].

The observed voltage of the piezoelectric nanowire is lower than the theoretical and simulated values, owing to the finite conductivity of the ZnO nanowires. The resistance of the nanowires ranges between 16 kΩ and 16 MΩ, depending on the contact resistance. This resistance is due to the concentration of oxygen vacancies throughout the nanowire volume [8, 59]. The piezoelectric potential is created by the polarisation of ions in the nanowire. The piezoelectric charges are rigid and affixed to the atoms; thus, they cannot move freely. These charges can be screened by

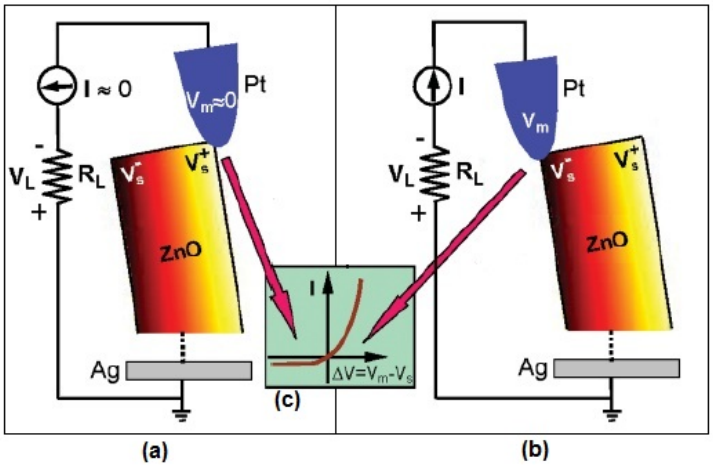

Figure 2.8: (a) Electrode touches stretched side of nanowire, charge accumulation takes place and no voltage is measured. (b) The electrode touches the compressed side of the nanowire, free electrons flow through the nanowire to the electrode and a voltage is measured. (c) During the first stage a reversed-biased Schottky diode is formed and litte current flows through the metal semiconductor interface. During the second stage a positvely-biased Schottky diode is formed and current can flow across the interface [8].

free carriers, like oxygen vacancies and other impurities present in the nanowire. This reduces the number of piezoelectric charges, but cannot completely neutralise them throughout the volume of the nanowire. The screening of the piezoelectric charges can reduce the piezoelectric voltage to half the original value. This screening is a result of the finite conductivity of the ZnO nanowire resulting from the oxygen vacancies and other impurities [59, 93].

The main reason for the lower practical voltage values is that the contact resistance between the nanowire and the electrode can be very large as a result of the small contact area. The contact resistance arises from to the small contact area between the nanowire and the electrode. This small contact area is the only area where current flow can occur [94]. Annealing nanowires lower the contact resistance, because fewer oxygen layers are present on the surface of the nanowires, which decreases the contact resistance [95, 96]. Ensuring a better contact between the nanowire and the electrode will lead to a higher voltage and current output, and is one of the main investigations of this project.

The formation of a Schottky contact is crucial for the operation of the nanogenerator. When an ohmic contact forms between the nanowire and the electrode, no output voltage is observed, as the Schottky contact must be present for the nanogenerator to work. Although the contact between the nanowire and the electrode is responsible for most of the loss of voltage, it plays an important role in the working of the nanogenerator [59].

2.6.2 Mathematical model

In the literature there are two methods for deriving a mathematical model that describes the output voltage of a single ZnO nanowire [97, 98].

In [97] the author starts from the two constitutive equations for piezoelectricity

$$\begin{aligned} \sigma_p &= c_{pq}\epsilon_q - e_{kp}E_k, \text{ and} \\ D_i &= e_{iq}\epsilon_q + \kappa_{ik}E_k. \end{aligned} \tag{2.6.1}$$

These two equations are solved with the aid of complicated mathematical tricks. Accordingly, perturbation theory is used, combined with the simplification of certain parameters to give a final equation as [97]

$$\frac{1}{8\kappa_\perp}\frac{f_y}{I_{xx}E}[2(1+v)e_{15}+2ve_{31}-e_{33}][\frac{\kappa_0+3\kappa_\perp}{\kappa_0+\kappa_\perp}\frac{r}{a}-\frac{r^3}{a^3}]a^3\sin\theta, \tag{2.6.2}$$

where f_y is the magnitude of the applied force (in Newton), κ_0 is the permittivity in vacuum, $\kappa_\perp$ is the material permittivity, $I_{xx} = \frac{\pi}{4}a^4$, θ is the angle between the bent nanowire and the y-axis and e_{xy} is the linear piezoelectric coefficient.

The derivation of the solution is difficult to follow and the answer is also rather difficult to interpret. The second method starts at the polarisation that occurs inside the ZnO nanowire due to the applied force [98]. This is the same as (2.3.10), the direct form of the piezoelectric effect is rewritten for the summation over all polarized particles

$$P_m = \sum_j d_{mj}\sigma_j, \tag{2.6.3}$$

where P_m ($m = 1, 2, 3$) are the piezoelectric polarisation vector components, σ_j (j = 1 to 6) are the stress tensor components and d_{mj} are the piezoelectric constant components. As mentioned, for wurtzite ZnO crystals, d_{mj} is given by (2.4.2). The stress tensor, σ_j, for a ZnO nanowire with diameter $2a$, length l, isotropic elastic modulus with Young's modules E and Poisson ratio v, by applying the Saint-Venant's principle of pure bending [99] is then given by

$$\begin{bmatrix} 0 \\ 0 \\ -\frac{f_y}{I_x}y(l-z) \\ \frac{f_y}{I_x}\frac{3+2\nu}{8(1+\nu)}[a^2-y^2-\frac{1-2\nu}{3+2\nu}x^2] \\ -\frac{f_y}{I_x}\frac{1+2\nu}{4(1+4\nu)}xy \\ 0 \end{bmatrix}, \tag{2.6.4}$$

where $I_x = \frac{\pi}{4}a^4$ is the cross-sectional moment of inertia for the ZnO nanowire and f_y is the applied force on the positive y-axis. Substituting the above two equations back into the original equation gives

$$\vec{P} = \begin{bmatrix} -\frac{f_y}{I_x}\frac{1+2\nu}{4(1+\nu)}d_{15}xy \\ \frac{f_y}{I_x}\frac{3+2\nu}{8(1+\nu)}d_{15}[a^2 - y^2 - \frac{1-2\nu}{3+2\nu}x^2] \\ -\frac{f_y}{I_x}d_{33}y(l-z) \end{bmatrix}, \tag{2.6.5}$$

where the three components of $\vec{P}$ are derived from the shear stress σ_5 on the xy-plane, shear stress σ_4 on the yz-plane and lastly shear stress σ_z along the z-axis.

The charges inside the nanowire, which are polarised, due to the piezoelectric effect, are bound charges instead of free charges. The surface charge density, ρ_s, is zero, because the charges are bound inside the nanowire. The volume charge density, ρ_v, is derived from Gauss's Law as

$$\begin{aligned} \rho_v &= \nabla \cdot \epsilon_0 \vec{E} \\ &= \nabla \cdot \vec{P} \\ &= \frac{f_y}{I_x}\frac{1+2\nu}{4(1+\nu)}d_{15}y - \frac{f_y}{I_x}\frac{3+2\nu}{8(1+\nu)}d_{15}(-2y) - \frac{f_y}{I_x}d_{33}(-1)y \\ &= \frac{f_y}{I_x}(d_{15} - d_{33})y \\ &\triangleq A_y. \end{aligned} \tag{2.6.6}$$

The volume charge density, or polarised charge distribution within the nanowire, is independent on x and z, or only dependent on the direction of the applied force. Using Poisson's equation, the piezoelectric potential φ and volume charge density is related by

$$\nabla^2\varphi = -\frac{\rho_v}{\epsilon}. \tag{2.6.7}$$

As mentioned, the nanowire is simplified as having a cylindrical shape. The above equation is thus expanded using cylindrical coordinates

$$\begin{aligned} \nabla^2\varphi &= \frac{1}{r}\frac{\partial}{\partial r}(r\frac{\partial\varphi}{\partial r}) + \frac{1}{r^2}\frac{\partial^2\varphi}{\partial\theta^2} + \frac{\partial^2\varphi}{\partial z^2}, \\ &= -\frac{A_y}{\epsilon}r\sin\theta. \end{aligned} \tag{2.6.8}$$

But, as also mentioned above, the equation is independent of z, and hence the above

equation simplifies to

$$\frac{1}{r}\frac{\partial}{\partial r}(r\frac{\partial \varphi}{\partial r}) + \frac{1}{r^2}\frac{\partial^2 \varphi}{\partial \theta^2}. \tag{2.6.9}$$

Equation (2.6.9) is a non-homogeneous differential equation and the easiest solution is found by the series expansion of φ. The solution is periodic (due the the $\sin\theta$), and hence a Fourier series expansion is used, giving

$$\varphi = \varphi_0 + \sum_{m=0}^{\infty}(\varphi_{m1}\cos m\theta + \varphi_{m2}\sin m\theta). \tag{2.6.10}$$

Using proper boundary conditions, where the piezoelectric voltage will be zero at both infinity and at zero ($\varphi|_{r=0} = 0 = \varphi|_{r=\infty}$) the solution is obtained as

$$\begin{aligned} &\frac{1}{r}\frac{\partial}{\partial r}(r\frac{\partial}{\partial r}(\varphi_0 + \sum_{m=0}^{\infty}[\varphi_{m1}\cos m\theta + \varphi_{m2}\sin m\theta])) + \\ &\frac{1}{r^2}\frac{\partial^2}{\partial \theta^2}((\varphi_0 + \sum_{m=0}^{\infty}[\varphi_{m1}\cos m\theta + \varphi_{m2}\sin m\theta])) = -\frac{A_y}{\epsilon}r\sin\theta. \end{aligned} \tag{2.6.11}$$

The above equation is multiplied out and then the coefficients are compared, resulting in

$$\begin{aligned} \frac{1}{r}\frac{\partial}{\partial r}(r\frac{\partial \varphi_0}{\partial r}) &= 0, \text{ Boundary conditions,} \\ \frac{1}{r}\frac{\partial}{\partial r}(r\frac{\partial \varphi_{m1}}{\partial r}) - \frac{1}{r^2}m^2\varphi_{m1} &= 0, \text{ m = 1, 2, 3, ... ,} \\ \frac{1}{r}\frac{\partial}{\partial r}(r\frac{\partial \varphi_{m2}}{\partial r}) - \frac{1}{r^2}m^2\varphi_{m2} &= 0, \text{ m = 2, 3, ... and} \\ \frac{1}{r}\frac{\partial}{\partial r}(r\frac{\partial \varphi_{12}}{\partial r}) - \frac{1}{r^2}m^2\varphi_{12} &= -\frac{A}{\epsilon}r. \end{aligned} \tag{2.6.12}$$

The four equations in (2.6.12) are solved

$$\begin{aligned} \frac{1}{r}\frac{\partial}{\partial r}(r\frac{\partial \varphi_0}{\partial r}) &= 0, \\ \Rightarrow r\frac{\partial \varphi_0}{\partial r} &= B_1, \\ \frac{\partial \varphi_0}{\partial r} &= \frac{B_1}{r} \text{ and} \\ \varphi_0 &= B_1\ln r + B_2. \end{aligned} \tag{2.6.13}$$

From the boundary conditions: $B_1 = B_2 = 0 \Rightarrow \varphi_0 = 0$

For the second equation, the substitution $r = e^t$ is used, making it an Euler

differential equation:

$$\begin{aligned}
\frac{\partial \varphi_{m1}}{\partial r} &= \frac{\partial \varphi_{m1}}{\partial t} / \frac{\partial r}{\partial t} \\
&= e^{-t} \frac{\partial \varphi_{m1}}{\partial t} \\
\Rightarrow r \frac{\partial \varphi_{m1}}{\partial r} &= \frac{\partial \varphi_{m1}}{\partial r} \\
\frac{\partial}{\partial r}(r \frac{\partial \varphi m1}{\partial r}) &= \frac{\partial}{\partial t}(r \frac{\partial \varphi_{m1}}{\partial r}) / \frac{\partial r}{\partial t} \\
&= \frac{\partial}{\partial t}(\frac{\partial \varphi_{m1}}{\partial t} / e^{t}) \qquad (2.6.14) \\
\Rightarrow \frac{1}{r} \frac{\partial}{\partial r}(r \frac{\partial \varphi_{m1}}{\partial r}) &= e^{-2t} \frac{\partial^2 \varphi_{m1}}{\partial t^2} \\
e^{-2t}(\frac{\partial^2 \varphi_{m1}}{\partial t^2} - m^2 \varphi_{m1}) &= 0 \\
\Rightarrow \varphi_{m1} &= A_1 e^{mt} + A_2 e^{-mt} \\
&= A_1 r^m + A_2 r^{-m},
\end{aligned}$$

using the boundary conditions, $A_1 = A_2 = 0 \Rightarrow \varphi_{m1} = 0$ for all m.

The third equation is solved in the same manner as the second equation, and the same answer is found, $\varphi_{m2} = 0$ for all m. The last equation is also solved with the substitution $r = e^t$, rendering

$$\begin{aligned}
\frac{\partial^2 \varphi_{12}}{\partial t^2} - \varphi_{12} &= -\frac{A}{\epsilon} e^{3t} \\
\Rightarrow \varphi_{12} &= C_1 e^{-t} + C_2 e^{t} - \frac{A}{8\epsilon} e^{3t} \qquad (2.6.15) \\
&= \frac{C_1}{r} + C_2 r - \frac{A}{8\epsilon} r^3, \qquad (2.6.16)
\end{aligned}$$

with the continuity conditions at the interface between the nanowire and free space, $\varphi|_{r=a-} = \varphi|_{r=a+}$ and $\rho_s = 0$. C_1 and C_2 is calculated as

$$\begin{aligned}
C_1 &= \frac{Aa^4}{4(\epsilon_0 + \epsilon)}, \text{and} \\
C_2 &= \frac{Aa^2(\epsilon_0 + 3\epsilon)}{8\epsilon(\epsilon_0 + \epsilon)}.
\end{aligned}$$

The final answer for the piezoelectric voltage is thus derived as

$$\begin{aligned}
\varphi_{12} &= \frac{f_y}{2\pi\epsilon}(d_{15} - d_{33})(\frac{\epsilon_0 + 3\epsilon}{\epsilon_0 + \epsilon} \frac{r}{a^2} - \frac{r^3}{a^4}) \sin\theta \,, r \leq a \qquad (2.6.17) \\
&= \frac{f_y}{2\pi\epsilon}(d_{15} - d_{33})(\frac{2\epsilon}{\epsilon_0 + \epsilon} \frac{1}{r}) \sin\theta \,, r > a.
\end{aligned}$$

The output voltage is a function of only the diameter of the nanowire. The length of the nanowire does not play any significant role. The other two parameters that are present in the equation are the permittivity and the piezoelectric constants of the ZnO nanowire. In order to optimise the output voltage of the nanowire, the diameter of the nanowire must be made as small as possible while the permittivity and piezoelectric constants need further optimisation. The equations were derived with the aid of [47], [98] and the help of the Mathematics Department at Stellenbosch University.

Substituting actual values into the equation: $E = 126.4$ GPa, $v = 0.417$ [100], $\frac{\epsilon}{\epsilon_0} = 7.77$ [101], $d_{15} = -8.3 \times 10^{-12}$ C/N and $d_{33} = 12.3 \times 10^{-12}$ C/N [100]. The nanowire is 600 nm in length and 50 nm in diameter. A force of 80 nN is applied directly to the tip. The model above gives a maximum piezoelectric potential of 0.271 V, while the other model in [97] gives 0.284 V. A finite element method (FEM) in [102] gives 0.268 V. All three values are very close, showing that all three methods can be used to calculate the generated piezoelectric potential.

The model helps to show where optimisation is necessary in order to increase the generated voltage. From the equations it is clear that, by increasing the applied force, the output voltage will increase. However, in certain applications the applied force is not a controllable parameter and other methods must be used to increase the generated voltage.

The nanowire diameter, a, also influences the generated voltage. A decrease in the nanowire diameter will lead to an increase of the generated voltage. Consequently, the piezoelectric constant of ZnO nanowires can be increased to help increase the generated voltage.

As mentioned previously, the model can provide certain parameters, which, when optimised, lead to a higher generated voltage. In the same sense the model can exclude certain parameters that will have no influence on the output voltage. The one parameter that is excluded is the length of the nanowires, because nanowire length does not influence the generated voltage and hence it is not a crucial parameter for optimisation.

2.6.3 The role of the Schottky contact and carrier density in the nanogenerator

A Schottky contact is formed when a metal and a semiconductor are in contact. There should also be a difference in the work function and electron affinity of the metal and the semiconductor. The conduction across the contact is controlled by thermionic emission of majority carriers over the barrier that is created as a result of the difference in work function and electron affinity. Another important parameter

is the Fermi level, which indicates the energy that is associated with an electron. The Fermi energy will vary with the electron density of the material [103].

When the metal and the semiconductor are not in contact, the Fermi levels will differ. In most cases the electrons in the metal will have less energy than the electrons in the semiconductor. When the metal and the semiconductor are joined, electrons will flow from the semiconductor to the metal to neutralise the difference in Fermi levels. This will lead to the formation of positively charged ions on the semiconductor surface and negatively charged ions on the metal surface. These ions will then generate an electric field which inhibits the further flow of electrons to the metal [103].

When in contact, the ZnO nanowire and the metal electrode form a Schottky barrier with a large resistance (50 to 1000 MΩ). The nanowire forms an ohmic contact with the ground, as illustrated in Figure 2.9 (a). When the electrode pushes the nanowire, the electrode is in contact with the tensile surface which has a positive voltage, V_s^+. Electrons will flow from the metal electrode to the electrode tip, but cannot cross over to the nanowire, because of the presence of a reverse-biased Schottky barrier. The electrons accumulate at the interface and the piezoelectric potential within the nanowire is disturbed due to the screening effect. The piezoelectric charges are screened and thus lowering the piezoelectric potential to V_p^+. The reduction in the piezoelectric potential leads to a reduction of the conduction band and Fermi level at the semiconductor side of the contact, as shown in Figure 2.9 (b) [59, 104, 105].

When the electrode touches the middle of the nanowire, or lifts and breaks contact with the nanowire for a short duration, the piezoelectric potential will drop to zero. The accumulated electrons at the electrode will then flow back through the electrode, restoring the original state when the electrode first touched the nanowire, as depicted in Figure 2.9 (c) [59, 104, 105].

The electrode will eventually make contact with the compressed side of the nanowire, which has a negative voltage, V_q^-. The original voltage, V_s, was screened during the first contact and was reduced to V_p, and when the electrode is in contact with the other side, the piezoelectric charges are screened again, and the potential drops to V_q, so that $V_s > V_p > V_q$. With the tip in contact with the negative potential, the conduction band and Fermi level rise. If this increase is big enough to overcome the Schottky barrier threshold of a positively biased Schottky diode, the electrons can flow from the nanowire to the electrode, creating a circular flow. The electrons flow in order to neutralise the piezoelectric charges [59, 104, 105, 106].

The presence of the Schottky contact at the metal-semiconductor interface is essential for the nanogenerator to work. The Schottky contact accumulates the charge

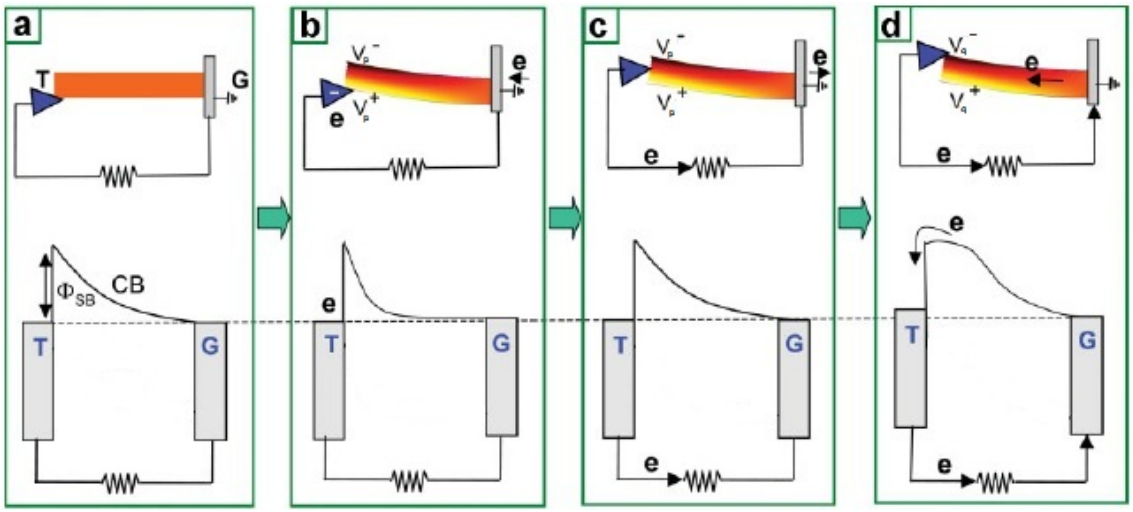

Figure 2.9: Representation of electrode and nanowire with the corresponding conduction band height when (a) electrode first touches the nanowire, (b) the electrode pushes the nanowire and contacts the stretched side of the nanowire, which causes the conduction band at the nanowire to descend, (c) the electrode is in the middle of the nanowire and the conduction band go back to normal and (d) the electrode is in contact with the compressed side of the nanowire, which causes the conduction band to rise at the metal side of the barrier [59].

during the first half of the output cycle. During the second half, the accumulated charge is released and forms a circular flow of electrons which creates a current flow [59].

The piezoelectric voltage that is created when the nanowire is bent is mainly consumed by overcoming the threshold energy at the metal-semiconductor interface. The magnitude of the output voltage is related to the piezoelectric voltage, but is not equal to it. The output voltage is determined by the difference in Fermi levels between the electrode and the substrate. The Fermi level of the electrode is raised due to the flow of electrons to the electrode from the substrate. Although a small amount of charge, Q, is generated (1000 to 10000 electrons), the time, Δt, it takes for the electrons to travel the distance is very short. The voltage output over the resistor R_L is given by $V_L = R_L \frac{Q}{\Delta t}$, with $I = \frac{Q}{\Delta t}$ [59, 106].

The amount of charge that flows is determined by the carrier density of the nanowire. For the n-type ZnO nanowire, the carriers are electrons. The carrier density thus plays a major role in the magnitude of the output voltage. The carrier density also determines the conductivity of the nanowire. For a high carrier density, the piezoelectric charges will be screened, thus reducing the piezoelectric potential. If the piezoelectric potential is too low, the Schottky barrier threshold will not be overcome and no output voltage will be observed. If the carrier density

is too low, the resistance of the nanowire will be much higher, thus limiting the current that can flow through the nanowire [106, 107].

The number of carriers has a big effect on the output of the nanowire. As the carrier density increases, the conductivity also increases. The increase in conductivity reduces the current output of the nanowire, because there are more losses throughout the nanowire. Therfore, an optimal value for the carrier density exists where the conductivity is low enough and the screening of the piezoelectric charges is small enough to ensure maximum power output [107].

2.6.4 The contact resistance between the nanowires and the electrode

When a force is applied to the top electrode, it will move and will start to touch and deform the nanowires. Consequently, an electric contact resistance will be created between the electrode and each nanowire. This contact resistance is responsible for many of the losses that are present in the nanogenerator [96, 108, 109].

The contact resistance is separate from the series resistance of the nanowire itself. The resistance of the nanowire itself can be as high as a few hundred kiloohms. This is due to the presence of oxygen vacancies throughout the nanowire. The resistance can be lowered by annealing the nanowire in argon or nitrogen gas in order to reduce the number of oxygen vacancies in the nanowire. However, the contact resistance between the electrode and nanowire is orders of magnitude bigger than the nanowire resistance [95, 110, 111].

Owing to the small scale of the contact between the electrode and the nanowire, the calculation of the contact resistance differs from large-scale contacts. The contact resistance model for small and large contacts was developed by Holm and Sharvin. For large contacts the resistance is known as the Holm resistance and is given by [96, 112]

$$R_H = \frac{\rho_1 + \rho_2}{4a}, \tag{2.6.18}$$

where ρ_i is the resistivity of the i^{th} material and a is the radius of a circular contact. The Holm resistance will be used when the mean free path of electrons is much smaller than the contact size. The mean free path of electrons is the distance that an electron travel between successive collisions. When the mean free path and the contact size are of the same magnitude, the Sharvin resistance is given by [96, 112]

$$R_S = \frac{p_F}{N\pi e^2 a^2}, \tag{2.6.19}$$

where p_F is the Fermi momentum of an electron, N is the electron density and e is the electron charge [96, 112]. On the nanoscale superposition of the two separate

resistances is necessary and is given by [96]

$$R = \frac{4(\rho_1+\rho_2)\lambda}{9\pi a^2} + \frac{(\rho_1+\rho_2)\lambda}{2\pi a}\int_0^\infty e^{\frac{-\lambda x}{a}}\frac{sin(\pi x)}{\pi x}\mathrm{d}x, \tag{2.6.20}$$

The integral is solved first:

$$\begin{aligned}
\int_0^\infty e^{\frac{-\lambda x}{a}}\frac{sin(\pi x)}{\pi x}\mathrm{d}x &= \int_0^\infty e^{\frac{-\lambda x}{a}}\int_\pi^{-\pi}\frac{1}{2\pi}e^{-j\omega x}\mathrm{d}\omega\mathrm{d}x \\
&= \frac{1}{2\pi}\int_\pi^{-\pi}\int_0^\infty e^{-(\frac{\lambda}{a}+j\omega)x}\mathrm{d}x\mathrm{d}\omega \\
&= \frac{1}{2\pi}\int_\pi^{-\pi}\frac{1}{\frac{\lambda}{a}+j\omega}\mathrm{d}\omega \\
&= \frac{1}{2\pi}[\frac{-j}{2}ln[(\frac{\lambda}{a})^2+\omega^2]+arctan(\frac{\omega a}{\lambda})]_{-\pi}^{\pi} \\
&= \frac{1}{\pi}arctan(\frac{\pi a}{\lambda}).
\end{aligned}$$

Substitution back into (2.6.20) gives

$$R = \frac{4(\rho_1+\rho_2)\lambda}{9\pi a^2} + \frac{(\rho_1+\rho_2)\lambda}{2\pi a}arctan(\frac{\pi x}{\lambda}), \tag{2.6.21}$$

with λ the mean free path of electrons, given by [113] as

$$\lambda = (3\pi^2)^{\frac{1}{3}}(\frac{h}{e^2})\sigma n^{\frac{-2}{3}}, \tag{2.6.22}$$

where h is Planck's constant, e is the electron charge, σ the conductivity and n is the carrier density. From (2.6.21) and (2.6.22) it is clear that the contact resistance depends on the contact size, carrier density and conductivity/resistivity of ZnO. In the literature different values can be found for the inner resistance, ranging from 5.7 GΩ to 19.3 GΩ [109].

Using the conductivity of ZnO nanowires, which is1 $\times 10^{-2}$ Ω·m and for the gold-coated top electrode, the conductivity is about 2×10^{-8} Ω·m. Assuming the contact circle radius is 10 nm and there is a carrier density of 10^{16} cm^{-3}, the mean free path is $\lambda = 17.2 \times 10^{-9}$ m. This gives a contact resistance of $R = 9.15 \times 10^{12}$ Ω. Depending on the measurement setup, different conductivity readings are found for ZnO nanowires and the same applies for the carrier density. This makes it difficult to compute an exact contact resistance.

Reducing the number of oxygen vacancies within the nanowire will not only decrease the inner resistance of the nanowire, but will also decrease the contact resistance. A decrease in the number of oxygen vacancies leads to an increase in carriers (electrons) which will, in turn, screen the piezoelectric charges and thus

reduce the overall piezoelectric potential and eventually the output potential. An optimal value must exist where the resistance of the system is reduced enough and the piezoelectric charges are not screened too much. Reducing the resistance of the system is investigated in this project.

2.7 Conslusion

Energy harvesting is of the utmost importance for wireless sensor networks and small electronic devices, such as pacemakers. These devices can be made to be self-powering by attaching a small energy harvesting module that converts any sort of vibration into an electrical signal. In this project, ZnO nanowires will be used to convert the vibrational force to an electrical signal through the piezoelectric effect. ZnO is a piezoelectric material with a high piezoelectric constant, a measure of the efficiency of converting strain to electricity. Although this field has attracted a lot of attention in the last couple of years, a big gap still exists in the literature on the manufacturing of devices that can convert vibration to electricity. One of the aims of this study is to fill that gap.

Materials on the nanoscale have a larger volume-to-surface ratio compared to their bulk counterparts. This means that surface reactions can occur quicker and are more responsive. The piezoelectric effect, although not a surface effect, is enhanced on the nanoscale, because of the larger number of crystals that are deformed. ZnO nanowires are used, each of which is a single crystal structure. Bending a number of these nanowires will ensure a high piezoelectric voltage.

A physical and mathematical model illustrating the working of the piezoelectric effect on a single nanowire was given in this chapter. The problem is that one single nanowire does not generate enough electricity to be practically useful. Hence, an array of nanowires was used to form a nanogenerator. The nanogenerator was also discussed is detail. The one missing part was the optimisation of the nanogenerator. There are two areas in which the nanogenerator has room for improvement: nanowire growth and the manufacturing of the nanogenerator. Throughout the literature information on the optimisation of both nanowire growth and the nanogenerator manufacturing is very limited. ZnO nanowires are used as described above with few alterations, leading to low output voltages. This study will consequently investigate optimisation techniques that will lead to an increase in the output voltage.

This work is focused mainly on filling the gap in the optimisation of both nanowire growth and nanogenerator manufacturing. Since limited literature is available, all of the techniques used are unique in their application to the ZnO nano-

wires. Certain techniques have been used on either ZnO thin films or other types of nanowire and will be discussed in the chapter that follows.

Chapter 3

Methodology

The focus of this study was the development and optimisation of a ZnO-based nanogenerator. In fulfilling this study the overall quality of the ZnO nanowires was important, as the efficiency and sensitivity of the nanowire devices are dependent on the quality of the grown nanowires. The nanowires were synthesised in the cleanroom facility at the Department of Electrical and Electronic Engineering of Stellenbosch University.

The nanowires were synthesised by two methods, which are discussed below. Both methods were optimised in two ways: One parameter at a time and design of experiments. The growth methods were optimised with respect to the measured output voltage that was generated when the nanowires were bent.

The nanowires were further characterised by using imaging technologies on the nanoscale, scanning electron microscopy (SEM), atomic force microscopy (AFM) , transmission electron microscopy (TEM) and optical light microscopy. Beyond the optical characterisation, different electrical characteristics were examined, including the output voltage, output current, internal resistance and charge carrier concentrations. The main purpose of the measurement of these characteristics was to aid in the optimisation of the nanogenerator.

The different growth methods are discussed in the first part of this chapter as well as the preparation of the different substrates. This is followed by a description of the two optimisation techniques that were used during growth optimisation. The next section discusses all the characterisation techniques and tools. Lastly, the limitations of the methodology of the study are discussed followed by a short conclusion.

3.1 Zinc oxide nanowire growth

Two methods were used to grow the ZnO nanowires: VLS and a chemical bath deposition (aqueous solution method). Both methods have a number of parameters that influence the quality of the nanowires. These methods are widely used and the parameters can easily be found in literature. However, not all equipment is equal and thus the parameters need to be adapted to work on different equipment.

3.1.1 Vapor liquid solid growth

The first method that was used to grow the ZnO nanowires was the VLS method. The exact details on how this method works can be found in Chapter 2. In short, VLS growth takes place in a high temperature furnace loaded with a quartz tube, which is under a vacuum, with the source materials loaded in the centre of the tube and the substrate a fixed distance away. When the desired temperature is reached, a carrier gas is introduced into the system and the growth process starts [71, 79, 80, 81, 82, 83, 84]. Growth takes place in less than 30 minutes, but it takes much longer for the system to reach the high temperature and cool down.

The parameters that influence growth are:

- Growth temperature
- Growth time
- Growth pressure
- Pre-growth pressure
- Amount of source material
- Distance between source material and substrate, and
- Carrier gas flow rate.

During the growth of the nanowires, these parameters were under the direct control of the experimenter and could be changed between successive experiments. Certain parameters were not under the direct control of the experimenter, such as ambient pressure, ambient temperature, humidity and the room airflow, all of which can have an effect on the growth. The parameters that could be controlled needed optimisation for this specific system. The basic growth process is discussed below, without any exact numbers and amounts, which will be discussed in the following section.

The source materials, graphite and ZnO powders, were mixed in a 1:1 weighed ratio. The materials were first weighed separately and then a mortar and pestle was

used to make the powders even finer. The source materials were then transferred to a ceramic crucible, which was then placed in the centre of the quartz tube. The substrate, Si (100) with a thin layer of Au sputtered onto it, was then placed a fixed distance away from the source materials. Aluminium stoppers were fitted to the two ends of the quartz tube and connected to the gas and vacuum pump separately. The vacuum pump and furnace were turned on and the tube was vacuumed while the furnace reached the desired temperature. Once the temperature is reached, the carrier gas was introduced at a specific flow rate. The vacuum inside the tube drops when the gas was introduced, and hence the flow rate and growth pressure were dependent on each other. The system was then left for at least 10 minutes for the growth to take place. After growth, the furnace, gas and vacuum pump were turned off, and the system was left for 12 hours to cool. Once cooled the substrate and the crucible were removed from the quartz tube.

Owing to the high temperature of the VLS method, the choice of substrate was limited to materials that could withstand these extreme temperatures. A different growth method, that operates at lower temperatures, was thus needed to broaden the choice of substrates that could be used for the manufacturing of the nanogenerator.

3.1.2 Chemical bath deposition

The second method that was used for the growth of the nanowires was the chemical bath deposition or aqueous solution method. The exact growth details were discussed in Chapter 2. In short, a solution containing zinc salts and a precursor is prepared and the substrate is suspended on top of this solution for nanowire growth. The solution is placed inside a conventional oven at temperatures below 100°C, for a couple of hours [57, 85, 87, 88]. This method provides the solution to the high temperatures that are needed for the VLS method.

The parameters than influence the growth are:

- Growth temperature
- Growth time
- Amount of solution materials
- Ratio of solution materials
- Closed or open growth, and
- Oven fan on or off.

Consequently, there were fewer parameters to control compared to the VLS method. The same parameters that were not directly controllable during the experiment for the VLS growth were also relevant here. Again, the controllable parameters needed optimisation in order to improve the quality of the nanowires.

The zinc salts that were used were zinc nitrate hexahydrate, $Zn(NO_3)_2$ $6H_2O$ and the precursor that was used was HMTA, $(CH_2)_6N_4$. These materials were mixed in an equimolar solution and dissolved in deionised (DI) water. The substrate, coated in a thin layer of Au followed by a layer of ZnO, was placed on top of the solution, with the layered side in contact with the solution. The solution was then placed inside an oven, at below 100°C for a couple of hours for nanowire growth.

The aqueous solution method solves the problem of the high temperatures needed for VLS growth. However, the compromise was much longer growth time, that was, a couple of hours compared to 30 minutes for the VLS method.

Both methods required certain pretreatment for the substrate that was used. This pretreatment involved cleaning the substrate and the deposition of seed layers to help in the growth process.

3.1.3 Substrate pretreatment

Different substrates were used during the growth of the ZnO nanowires. As mentioned, the VLS method required a substrate that could withstand high temperatures. The substrate that was used is Si (100): doped silicon wafers, 250 to 300 μm thick and 90 mm in diameter, with crystal structure (100). These rigid substrates could easily withstand temperatures of well over 1000°C.

The aqueous solution method did not require a high temperature resistant substrate. For this method, the substrate, was chosen with the manufacturing of the nanogenerator in mind. A flexible nanogenerator was preferred over a rigid one and, hence, the chosen substrate was flexible. Accordingly, Kapton polyimide film, HN500, was chosen. The product specifications could be found in reference [114].

The Si (100) was cut into 10 by 10 mm substrates, using a diamond-like tip cutter. The diamond-like tip was moved over the substrate in straight lines, then rotated 90° and repeated. A weight was then moved around on the wafer, which caused the wafer to break along the lines made by the diamond-like tip. The Kapton film was cut into 15 by 20 mm samples with normal scissors. The substrates were now the desired size and were used for the manufacture of the nanogenerator.

After being cut to the desired size, the samples were cleaned. The samples were then placed inside a glass beaker, which was filled with acetone, ethanol and DI-

water separately. The beaker was placed in a ultrasonic bath that vibrated at more than 20 kHz, thus cleaning the samples. This was repeated for each of the three liquids. The samples were dried by blowing nitrogen gas over the sample. Lastly, the samples were placed on a hotplate at 115°C for 5 minutes to further dry the samples and remove any absorbed moisture.

The growth methods and nanogenerator manufacturing required the deposition of a thin layer of material on the substrates. These thin films have two main functions: to act as a buffer layer during growth and to act as an electrode for the nanogenerator. The buffer layer was necessary, because of the lattice (crystal structure) mismatch between the nanowires and the substrate. The buffer layer bridged this lattice mismatch and ensured good nanowire growth in the desired direction. The nanogenerator required electrodes to function in a certain way and this will be discussed in more detail in Chapter 6. The deposition of these thin films was done using three techniques: thermal evaporation, direct current (DC) sputtering and inverted cylindrical magnetron (ICM) pulsed source sputtering.

Thermal evaporation, the system shown in Figure 3.1, works by thermally evaporating a source material onto a substrate [115]. The system was vacuumed and evaporation was performed at 2×10^{-5} mbar. The source material was then loaded into a tungsten crucible and placed in the centre of the dome. When the desired vacuum was reached, current was directed through the crucible. The current was steadily increased until the source material melts; at this point a divider, that was in place between the source material and substrate, was removed by turning a specific handle. The source material was evaporated and collected on the substrate, which was placed a fixed distance above the source material. A quartz crystal microbalance (QCM) sensor was fixed next to the substrate and measured the thickness of the deposited layer as well as the deposition rate, which was displayed by specially designed software.

The QCM sensor worked by measuring the frequency change of a quartz crystal resonator. Three parameters were used in the setup of each material that was being deposited, namely the density of the material, the tooling factor and a z-factor. The density of the material was easily found in the literature and is self-explanatory. The z-factor is the ratio between sound pressure and particle velocity and can also be found in the literature. The tooling factor was system dependant, and takes into account the distance between the substrate and the source material, the exact position relative to the source material and the quality of the vacuum [115].

After deposition the current was turned down to zero, the vacuum pump was turned off and the system was vented. The thickness of the layer was then measured by the AFM and the value was compared to that of the QCM sensor of the

Figure 3.1: Photograph of the thermal evaporation unit, showing the evaporation dome and control unit in the bottom right-hand corner.

thermal evaporator. If a difference exists, the tooling factor was changed in the software until the QCM and the AFM readings were equal.

DC sputtering was also used to deposit thin films of specific materials onto a substrate. The system is shown in Figure 3.2, where sputtering takes place in the chamber on top. The chamber was placed under a vacuum of 4×10^{-2} mbar. A target material, mostly Au for this system, was fixed to the inside upper part of the chamber. The substrate was then placed at a fixed distance under the source material. A gas valve was opened and a non-reactive gas, argon, was introduced into the system, reducing the vacuum to 2×10^{-1} mbar. The high voltage source was turned on, and a plasma was created between the source material and the anode of the voltage source. This plasma was created as a result of the acceleration of the gas atoms to the source material, because of the strong electric field that exists close to the source materials. These atoms were accelerated to the source material, and collisions occured between the source material and gas atoms, freeing atoms from the source material, which was then deposited onto the substrate below. The deposition rate for Au was 12 nm/min at maximum voltage.

The last process that was used for the deposition of layers onto the substrates was ICM sputtering. The difference between the two sputtering techniques is that ICM can be used for both conducting and non-conducting source materials, whereas DC sputtering is only used for conductive materials.

The ICM system is shown in Figure 3.3. The source material and the substrate were loaded into the chamber on the right. A pulsed high voltage source was then connected to the head of the sputtering chamber, where the source material was

Figure 3.2: Photograph of DC sputtering system. The sputtering takes place in the chamber on top.

located. The system was vacuumed to 1×10^{-4} mbar before the sputtering process was started. Once the desired vacuum was reached, carrier gas was introduced and the vacuum drops to 4×10^{-2} mbar. In this case, the gas acts as both a carrier and a reactant in order to form oxides (for oxygen) or nitrates (for nitrogen), depending on the gas introduced into the system. Once the high voltage was turned on the gas atoms were accelerated to the source material due to both an electric field and a magnetic field that were present inside the head of the chamber. These two fields combine to accelerate the gas atoms and bombard the source material, breaking the bonds between atoms. The source material was deposited onto the substrate located beneath the source material. The entire system was also water cooled to ensure the system does not overheat during deposition. Table 3.1 shows the settings used for the voltage source. The deposition rate for ZnO was 20 nm/min when only oxygen gas used.

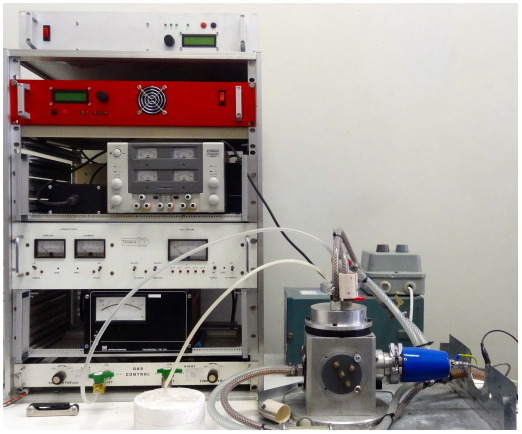

Figure 3.3: Photograph of ICM sputtering system. The sputtering takes place in the chamber on the right.

Table 3.1: Parameters for the high voltage source as used during ICM sputtering of ZnO.

Parameter	Parameter value
Positive voltage	50 V
Negative voltage	-700 V
Power	120 W
Current	0.7 A
Duty Cycle	80%
Frequency	20 kHz

The mentioned substrate preparation was done for all the substrates that were used for nanowire growth. The only difference was the type of material that was deposited by one of the three techniques explained above. Once the substrate was ready for growth, one of the two methods were used to grow the ZnO nanowires. Optimising the growth of the nanowires, with respect to the generated voltage, was a crucial step in the manufacturing of both the nanogenerator.

3.2 Zinc oxide nanowire optimisation

Optimisation techniques are used to optimise a certain experiment with respect to a specific parameter. In the case of the ZnO nanowires optimisation was done with respect to the diameter and length of the grown nanowires [116, 117, 118]. Different techniques were used for optimisation: one parameter at a time [117] and DoE [116, 118].

In this study both of these optimisation techniques were used. The one-parameter at a time approach was used to find minimum and maximum values for each parameter that influenced the growth. DoE was then used, with these minimum and maximum values, further optimising the growth. In contrast to what is found in the literature, the optimisation was done with respect to the measured output voltage of the manufactured nanogenerator and not the diameter or length of the nanowire growth. Both optimisation techniques that were used are discussed below.

3.2.1 One parameter at a time

The one parameter at a time optimisation technique was used to investigate the effect a change in a single parameter had on nanowire growth. Accordingly, a single parameter was changed between consecutive runs and the effect of that change was observed.

Both growth methods were optimised using this approach. Table 3.2 gives the VLS method and Table 3.3 the aqueous solution method. Each table shows the

individual parameters that influenced the growth, the minimum and maximum levels to which each parameter was changed, as well as the increment size that was used between consecutive runs.

Table 3.2: Growth parameters used for VLS growth with minimum and maximum values and incremental size for the one parameter at a time optimisation technique.

Parameter	Minimum value	Maximum value	Increment size
Growth temperature	400°C	1200°C	50°C
Growth time	5 min	60 min	5 min
Growth pressure	0.67 mbar	1010 mbar	N/A
Pre-growth pressure	0.067 mbar	1010 mbar	N/A
Amount of source material	0.5 g	2 g	0.5 g
Distance between source material and substrate	60 mm	560 mm	50 mm
Carrier gas flow rate	0	200 sccm	N/A

The initial and growth pressures were not changed in set increments. Only certain values were possible, due to the vacuum pump and the valve used during growth. The flow rate was also only set to certain values, as this is related to the working pressure.

Table 3.3: Growth parameters used for aqueous solution growth with minimum and maximum values and incremental size for the one parameter at a time optimisation technique.

Parameter	Minimum value	Maximum value	Increment size
Growth temperature	50°C	120°C	10°C
Growth time	1 hour	30 hours	1 hour
Covered growth	No	Yes	N/A
Molar weight of source materials	1mM	100 mM	10 mM
Ratio of source material	0:1	1:0	0.25:0 or 0:0.25

The one parameter at a time technique does not take into account the interaction between parameters; it merely gives an indication of the effect a single parameter has on the output value. In order to see the effect the change in multiple parameters has on the output, another optimisation technique was required.

3.2.2 Design of experiments

Design of experiments (DoE) is the design of all information gathering exercises where variation is present, whether under the full control of the experimenter or not. The experimenter is interested in the effect of some process or the intervention on some objects [119]. In other words, DoE is a guided approach to indentifying what influences a chosen output for a certain experiment. Whenever the experiment is performed, the repeatability of the experiment is critical. In most cases the

results of the experiment will not be precisely the same, but will vary. This is due to external factors not under the full control of the experimenter. Experiments can also have multiple inputs in order to obtain the desired output, and the interaction between these inputs also plays an important role. DoE is the method used to calculate these interactions between inputs and also to take unwanted inputs into the system into account. DoE is based on statistical data about the experiments, which is then used to calculate the most important inputs and also the interaction between inputs.

DoE has a set process that must be followed in order to fulfil its requirements. The process is discussed below.

1. *Recognition and statement of the problem.* Firstly, the recognition and a statement of the specific problem are necessary. The problem must be characterised in detail and all factors must be taken into account. After the problem is fully understood, it should be formulated and written down, so that the experimenter can always refer back to see what exactly the problem is.

   The problem in this study was the optimisation of the output voltage of the nanogenerator. Most of the growth parameters had an influence on the output voltage of the nanowires and this influence was optimised in order to achieve maximum output voltage.

2. *Selection of the response variable.* The response variable is the output variable of the experiment. This variable must be measurable and must also give useful information about the experiment. The response variable will be measured after each experiment to see whether the results of the experiment have improved or not.

   The chosen response variable was the output voltage that the nanowires generated when bent. The output voltage was measured after each experiment to see the change that occured owing to a change in growth parameters.

3. *Choice of factors, levels and range.* All the factors that can influence the response variable within the experiment must be chosen. This is one of the most crucial steps in the DoE method. This includes variables that are not under the direct control of the experimenter. The most important factors are the design factors and for these factors the maximum and minimum levels must also be chosen. It is often not possible to include all the factors that influence the response variable, but as many as possible should be found.

   Table 3.4 shows the parameters that were controllable for the aqueous solution method. The table also includes the minimum and maximum values that

were obtained during the one parameter at a time approach. The values given here differ from the one parameter at a time values in Table 3.3, as only the values that led to high quality nanowires and high output voltage were chosen. Only the aqueous solution growth method was further optimised using the DoE method, because the method yielded higher output voltages for all the experiments during the one parameter at a time optimisation.

Table 3.4: Minimum and maximum values used during the DoE optimisation of the aqueous solution growth method

Parameter	Minimum value	Maximum value
Growth temperature	90 °C	100 °C
Growth time	7 hours	8 hours
Concentration	20 mM	30 mM
Ratio	1:1	1:1.25

These values and parameters were chosen on the back of the one parameter at a time optimisation. The parameters with the biggest effect on the output voltage were chosen. The minimum and maximum values were taken as the range where the largest output voltage was measured during the one parameter at a time optimisation. The parameters not under the experimenter's control were ambient temperature, humidity, room air flow, DI-water quality and external disturbances (power cuts, vibrations, etc.).

4. *Choice of experimental design.* Once all the factors are known, this step is easy. The experimenter should choose how many runs he/she wants to do, how many factors should be varied, and in which order. The experimenter must also know which of the factors are under his/her control and which are not. Not all of the factors will be altered in the experiment, so those factors that will remain constant throughout the experiment must be identified.

   The variables as indicated in Table 3.4 were used, which means it was a 2^4 design, hence with 16 runs. Each run was performed twice to ensure repeatability, resulting in 32 runs in total.

5. *Performing the experiment.* During an experimental run the experiment must be monitored extensively to ensure that no unwanted factors are present, and also to ensure that all the experiments are performed under the same conditions. It is always good to first do a few trial runs to become familiar with the experimentation equipment. This has been done during the one parameter at a time phase. The experiments must also be performed in a random order, in order to minimise external influences.

6. *Statistical analysis of the data.* Statistical methods should be used to analyse the data from the experiment, so that an objective conclusion can be drawn.

   Stat-Ease [120], a DoE software package was used to analyse the data. The experimental setup was entered into the software with the different factors and the two levels. The corresponding output voltages were also entered. The software highlighted the most important factors, as well as the interaction between different factors and the influence it has on the output voltage. The results are given in Chapter 5.

7. *Conclusions and recommendations.* Using the statistical analysis of the data, a conclusion can be reached. This conclusion will be objective, because of the statistical analysis and will give a clear indication of which factors of the experiment are of greater importance, and which are less important. This will also help in determining which parameters to vary in experiments that will follow.

The DoE method continues to build where the one-parameter approach ended. A combination of the two techniques gave an optimal set of growth parameters that led to nanowires with near peak output voltages. Different techniques and equipment were then used to characterise the nanowires after growth.

3.3 Zinc oxide nanowire characterisation

After each run of either optimisation technique, the substrate growth was characterised. The growth was then categorised as having optical and electrical characteristics. Both these categories have a number of techniques and equipment that were used to inspect the nanowires after growth.

3.3.1 Optical characterisation

The first technique that was used to characterise the nanowire growth was a visual inspection of the nanowires. However, due to the small size of the nanowires, conventional methods could not be used. A human with perfect vision can see an object of 0.35 mm in size from 1 m away [121]. The nanowires, however, were much smaller and could not be seen without the aid of specialised equipment.

Therefore, normal light microscopy was used, with maximum zoom capabilities of 800 times. The microscope had a light and a camera attached to a tube and a number of lenses. The substrate was placed beneath the lens and specialised software was used to take images. This magnification was not enough to see individual nanowires, but the overall growth density could be seen. However, this technique

was not used much due to the magnification limitation. Light microscopy works by bombarding the sample with photons and capturing the photons as they bounce off the sample. The problem is that the wavelength of photons in the visible spectrum is larger than the object under inspection, hence, there is a limit to how small an object can be in order to use photons to see it. SEM works on the same principle, except that electrons replace the photons [122].

The SEM has an electron gun, a tungsten filament from where the electrons originate. The electrons are thermionically emitted from the electron gun and are then focused by condenser lenses. The condenser lenses work in the same way as normal glass lenses for light, except that the lenses focus the electrons by means of magnetic fields. The electrons from the electron gun interact with the sample, dislodging secondary electrons from it. Both the primary and the secondary electrons are detected with separate sensors and an image is formed, where contrast originates from the energy of the electrons.

The SEM that was used predominantly in this study was a tabletop SEM from Phenom World [123], shown in Figure 3.4. The electron gun functions at 1.5 kV and only a number of condenser lenses focus the beam. As a result the maximum magnification is only 20 000×.

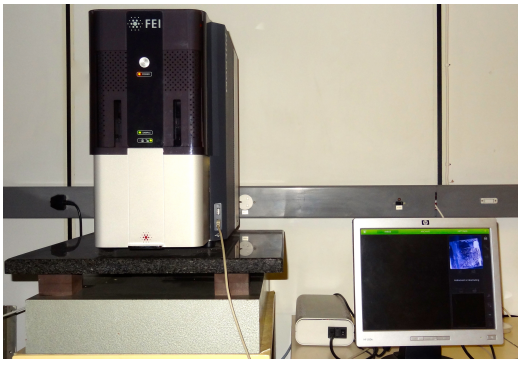

Figure 3.4: Photograph of desktop SEM from Phenom World. The system has a maximum magnification of 20 000×.

The SEM was used to look at nanowire growth. The nanowires were viewed from the top and the overall growth density, at 10 000× magnification, was observed. At this magnification individual nanowires could barely been identified, but the overall density of the growth was visible. At 20 000× magnification individual nanowires could clearly be observed and the growth direction also became apparent. From this view the diameter of the nanowires could be measured. Next, the substrate was loaded at a 90° angle to get a side view of the nanowires. Only

high magnification was used in this setup to see both the length of the nanowires and the growth direction.

After SEM images, with magnification of maximum 20 000× were taken, a TEM was also used. The TEM works on the same principle as the SEM, except that the electrons do not scatter off the sample, but instead move through the sample and are detected beneath. Compared to the SEM many more lenses are required to focus the electron beam. However, TEM cannot be used to view entire substrates like SEM, as only ultra thin objects can be observed.

The TEM required intensive sample preparation for viewing samples. The nanowire growth was scratched off the substrate and mixed into an ethanol solution. A small copper grid was suspended in the liquid for a few seconds, then removed and dried on a hotplate. Single nanowires were now dispersed on the copper grid in random orientation and were ready for TEM viewing. TEM had a magnification of over 100 000×, hence the crystal structure could be observed.

The last piece of equipment used for the optical characterisation was the AFM. The AFM differs from the previous two, as electrons are not used to view the sample. Instead, a small tip, only a few atoms wide, is moved over the sample and the deflection of the tip is recorded [124].

The AFM was used to confirm the length of the nanowires, as measured by the SEM. Furthermore, it was used to scan the substrate after deposition of the thin film to ensure good quality films with low area roughness.

The mentioned optical methods were used to inspect the nanowire samples. The pictures obtained with these methods gave a good indication of the quality, density and size of the growth. TEM imaging was also used to look at the crystal structure. The nanowires were used for the manufacturing of the nanogenerator and, hence, the electrical characteristics were more important than the optical characteristics. Additional techniques were thus necessary to characterise the electrical aspects of the nanowires.

3.3.2 Electrical characterisation

Electrical characterisation of the nanowires was extremely important, as main aim of this project is to optimise the output voltage of the nanogenerator. In order to do this, reliable and repeatable electrical measurements had to be taken. Voltage and current measurements were recorded while bending the nanowires and resistance and carrier concentrations were calculated, using specialised equipment and equations.

Information on how to measure the output voltage of the nanogenerator was not found in the literature. Results from measurements are shown, but either the

measurement setup is never explained or shown, or the information is very limited [93, 125, 126, 127].

To measure the voltage of a single nanowire, expensive and very precise equipment is needed [93, 125]. This is due to the short lifetime of the generated voltage pulse, as well as the magnitude of the signal [93]. The output voltage of a single ZnO nanowire will only be in the order of 10 mV [93]. Accordingly, trying to measure such a small voltage will be difficult due to the presence of environmental noise of the same magnitude [126]. This means that an amplifier stage is required in front of the measurement setup in order to amplify the output voltage to a level where it can easily be measured. A further problem is that the capacitance of the measurement setup must be low enough in order to pick up the voltage peak, because the peak has a very short life time. If the capacitance is too large, the voltage peak will diminish and no output will be displayed. Measurements made by *Wang et al.* showed that the time constant of the system must be less than 0.6 ms, which corresponds to a capacitance of 1.2 pF at a set resistance [93]. The amplifier circuit that is used to amplify the voltage signal must have very low levels for the bias current and bias voltage. A large bias current may lead to a voltage output signal larger than the true signal. To overcome these problems one requires very low noise and low capacitance systems, which are very expensive. *Wang et al.* used a SR560 low noise amplifier and performed all the measurements inside a Faraday cage [125].

A method to overcome these problems was to measure the output voltage of an entire substrate of ZnO nanowires, and not just a single one. Hence, the system capacitance was no longer an important factor, because the output voltage would be much larger, have a longer life time and the small portion that was absorbed by the capacitance, thus ignorable. The influence of environmental noise was also less, because the measured signal would be magnitudes bigger than the noise.

The output voltage and current was recorded by means of an analog to digital converter (ADC) on a computer. The ADC was a LabJack U6 [128] where only one channel was used. The maximum sampling rate of the U6 was 10 samples per second. The silicon nanogenerator was tested by placing a separate gold electrode on top of the nanowire growth. Both the nanogenerator and gold electrode were connected to the amplifier stage by silver paste. The gold electrode was then moved backwards and forwards, with a constant force applied to the electrode. This movement of the electrode caused the nanowires to bend and hence an output voltage was observed. The flexible nanogenerator was bent, as shown if Figure 3.5, from 180° to 90° and then released to return to 180°. The voltage was displayed and recorded on a PC, using software that communicates with the U6. During the

measurements no external voltage was applied to the nanogenerator.

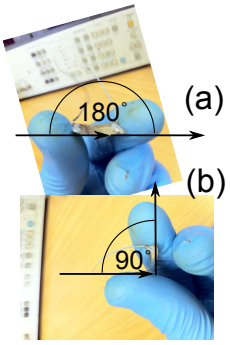

Figure 3.5: The nanogenerator was manually bent from 180° to 90° and then released to return to 180°.

The nanogenerator was manufactured with two electrodes: a bottom and a top electrode. The electrodes were connected to a buffer circuit, which acted as a bridge between the high output nanogenerator and the ADC. The buffer circuit was further used to minimise the noise that was present on the measurements by filtering it out. Figure 3.6 is a schematic of the buffer circuit. The circuit was a non-inverting operational amplifier. The gain of the circuit was given by $1 + \frac{R_2}{R_1}$. The resistors were chosen for unity gain: R_1 was thus orders of magnitude bigger than R_2.

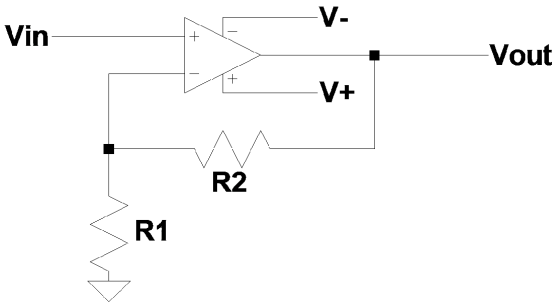

Figure 3.6: Schematic of the buffer circuit that was connected between the nanogenerator and ADC for output voltage measurements.

The operational amplifier used for the buffer circuit was the *LTC2625AC* from Texas Instruments. It is specially designed for low noise and zero offset. The amplifier was limited to input voltages below 7 V, and no amplifier with the same specification was found that allows higher input voltages. Other amplifiers were tested,

like the *LF351*, but the offset and noise added by this amplifier were, at times, of the same magnitude as the generated voltage. Table 3.5 summarises important values of different operational amplifiers. Four different amplifiers were compared with regard to bias current, offset current, noise voltage and offset voltage.

Table 3.5: Comparision of four different amplifiers used for the buffer circuit.

Amplifier	Bias Current	Offset Current	Noise Voltage	Offset Voltage
LF351	200 nA	100 pA	Not specified	3 mV
LTC1049	100 pA	100 pA	3 μV	2 μV
ICL7650	1.5 pA	0.5 pA	Not specified	0.7 μV
TLC2625	4 pA	2 pA	0.003 μV	0.5 μV

From Table 3.5 it is clear that the *TLC2625* is the best option. It had the lowest values for noise and offset voltage and the second lowest values for bias and offset current. The *ICL7650* would also be a viable candidate, depending on the noise voltage.

The last choice for voltage and current measurements was the output resistance over which the measurements were made. Resistors are by definition noisy components and large resistors will add more noise. Resistors as small as a couple of kilo-ohms to resistors of hundreds of mega-ohms were tested to see the effect on the measurements. These tests showed that a 10 MΩ resistor worked best.

The U6 was connected to the PC with the output of the buffer circuit connected to the input of the U6. A resistor was connected between V_{in} and the ground and the nanogenerator was then connected across the resistor.

Different materials were deposited onto the substrate to act as an electrode. As explained in Chapter 2, the work function of the electrode must be higher than the electron affinity of ZnO for a Schottky contact to form and for the output voltage to be observed. When different materials were used, with lower work functions, no output voltage was observed.

To further verify the origin of the measured signal reverse polarity tests were performed. The wires connecting the nanogenerator to the buffer circuit were switched around, reversing the polarity of the nanogenerator. When the nanogenerator was bent in this configuration, the measured voltage was of a different polarity than before.

The tests explained above, with different amplifiers, resistors, electrode materials and reverse polarity, were performed to ensure that the measured voltage signal originates from the nanogenerator and was not environmental or instrument noise.

A peer-reviewed article was accepted for publication based on the measurement setup. The article was published in *Nanotechnology* [129].

Current measurements were recorded with a HP4140B pico ampere meter. The system is over 30 years old and no connectivity to a PC was possible. The values were manually recorded and software was used to plot the graphs. The meter records and displays the current on a LCD screen while the nanogenerator was bent.

The last measurements that were taken are the resistance and carrier concentration. These two values were measured together with the system shown in Figure 3.7. A combination of the Van der Pauw method [130] and the Hall Effect [131] was used to measure these two parameters. Both methods require a magnetic field and hence two magnets were slotted in above and beneath the sample. Contact was made with the sample via a four-point probe technique. Figure 3.8 shows the sample attached to the testboard. The four probes were spring loaded and contact the sample on the four numbered corners, starting in the bottom lefthand corner and moving counter-clockwise, as shown in Figure 3.8.

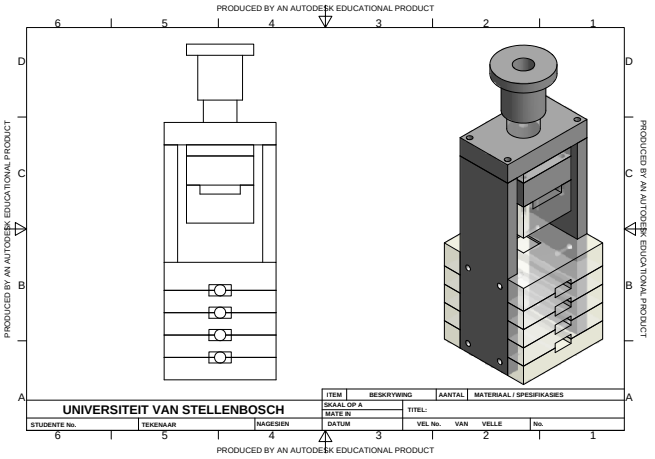

Figure 3.7: Schematic of system used for Hall and Van der Pauw measurements. Magnets were placed above and beneath the sample to create a strong magnetic field. Contact with the sample was made via a four-point probe method.

The Van der Pauw method was used to measure the resistivity of the nanowire substrate. In total, eight different resistance values were calculated by applying current through two terminals and measuring the voltage across the remaining two terminals. Resistances $R_{12,34}$, $R_{34,12}$, $R_{21,43}$, $R_{43,21}$, $R_{23,41}$, $R_{41,23}$, $R_{32,14}$ and $R_{14,32}$ were measured and were generically defined as $R_{ab,cd} = \frac{V_{cd}}{I_{ab}}$, with a, b, c and d integers between 1 and 4. The resistance, R_s, of the nanowire substrate was derived from the Van der Pauw equation [130]

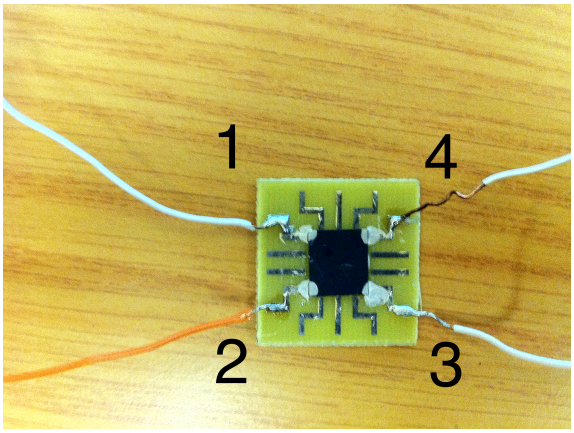

Figure 3.8: Photo of the sample under investigation, attached to the testboard. The probes were placed on the four corners of the substrate and numbered clockwise from the bottom left-hand corner.

$$e^{\pi\frac{R_v}{R_s}} + e^{\pi\frac{R_h}{R_s}} = 1 \text{ , where} \tag{3.3.1}$$

$$R_v = \frac{R_{12,34} + R_{34,12} + R_{21,43} + R_{43,21}}{4}, \text{ and} \tag{3.3.2}$$

$$R_h = \frac{R_{23,41} + R_{41,23} + R_{32,14} + R_{14,32}}{4}. \tag{3.3.3}$$

An exact solution does not exists for the equation. Instead, an iterative approach was taken to solve the equation. The Matlab code is appended. The resulting value of R_s gives the resistance of the entire substrate together with ZnO nanowire growth.

Lastly, carrier concentration was measured by placing the nanowire substrate in a constant magnetic field, and by application of a diagonal constant current, the Hall voltage, V_h, was measured. The currents I_{13}, I_{31}, I_{24} and I_{42} were applied consecutively and the resulting voltages were measured over the open terminals V_{42}, V_{24}, V_{13} and V_{31}, respectively. The magnetic field was then reversed and the same measurements were made again. The voltages measured in the negatively oriented magnetic field were subtracted from the voltages in the positively oriented magnetic field. The carrier concentration was calculated using a modified version of the Hall equation [131] given by

$$n_s = \frac{8 \times 10^{-8} IB}{qd[V_{24} + V_{42} + V_{13} + V_{31}]}\text{ ,} \tag{3.3.4}$$

where I is the constant current in Ampere, B is the magnetic field strength in Gauss, q is the electron charge and d is the depth of the material.

Normally, the Hall and Van der Pauw methods are used for thin films, but the nanowire growth is so dense that it can be modelled as a thin layer. Although the exact values generated from these two methods might not be as accurate, the overall trend of the results will still hold true.

The constant current was applied using the 120B Constant Current source from LakeShore. Voltages were measured using a digital voltmeter.

The resistance measurements were made with a constant current of 10 μA. The Lakeshore current source has a compliance voltage of 11 V and in order to ensure this voltage was never exceeded, all tests were conducted at a low current.

The carrier concentration measurements were performed at a 10 μA constant current, with a constant magnetic field of 1800 Gauss. Measurements were made with the magnetic field applied along the positive z-axis. The field was then reversed and the measurements repeated.

3.4 Limitations

Certain limitations exist within some aspects of this project. Equipment that could measure and probe samples on the nanoscale was extremely expensive. It is only found in very specialised laboratories and was thus not considered for this project.

The vacuum system that was used during the VLS method was a small home-made system, as big systems are expensive. The system had a number of small leaks, which meant that a high vacuum was not possible. The furnace that was used has a very small area where maximum heat was achieved and the temperature controller also lacked certain functions. Hence, the rate of temperature increase could not be set. The increase rate was also rather slow in the higher temperature range. The VLS method was not the best method to grow the nanowires and hence this problem did not limit the study significantly.

The oven used for the aqueous solution growth method was also old. The temperature dial was worn out and made it difficult to set the temperature to an exact value. Accordingly, a small feedback system was implemented to regulate the temperature with moderate success. The DI-water system broke early on in study and upon repair a filter stage was removed, resulting in lower quality DI-water. Most systems can achieve DI-water with resistance of over 18 MΩ-cm, whereas the system in the laboratory only achieved 15 MΩ-cm at best. Throughout the study the water quality was improved by adding new filters. The water quality did improve to the 18 MΩ-cm range and only a slight increase in output voltage was observed (less than 10%).

The overall cleanroom facilities were also an area of concern. Throughout the

substrate pre-treatment, the substrates were moved from one location to another, as the equipment was kept in two separate rooms. Dust and other airborne particles could collect on the surface of the substrate and contaminate the substrate. These airborne particles are orders of magnitude bigger than the nanowires and can have a big influence on the quality of the sensors. The problem of contamination was solved in the manifacturing of the nanogenerator and will be discussed in Chapter 6.

All the techniques used for the deposition of the thin films were prone for contamination. Other students also use the equipment and deposit other materials that could contaminate the substrates. The ICM sputtering machine was a homemade system and lacks certain functions. In-time measurement of the deposition was not available, as with the thermal evaporator. The sputter chamber also has a number of leaks, resulting in lower achievable vacuum. Although none of these limitations had an direct influence on this project it could be detrimental for future projects.

The SEM used was limited to 20 000$\times$ magnification, and at this magnification the resolution was low. A SEM with higher resolution or magnification would have been preferable. Individual nanowires could have been studied with a SEM with higher magnification and resolution, but this SEM was adequate for this study.

Specialised measuring equipment could also have helped to further verify results. The Hall measurements were done with a homemade system and comparison with a commercial product would have added more credibility to the results. Low noise systems could also have been used to measure the output voltage and current, in order to minimise the effect of noise. Although the system that was implemented did function as desired, specialised quipment could help reduce noise even further. The systems and methods implemeted throughout this study did help to prove the thesis. None of the results were comprimised due to the lack of more expensive equipment.

3.5 Conclusion

A number of different methods, in different areas, were used throughout this project. All the methods were adapted to fit the scope of this project and to function as desired in our laboratory.

Two growth methods were used to synthesise the ZnO nanowires. These methods were then optimised using two different techniques. The optimisation gave growth parameters that resulted in nanowire growth that provided high output voltages when bent. All the techniques used were well documented, but certain alterations were necessary for the growth and optimisation to be successful in our

laboratory.

Different characterisation techniques were used to characterise the nanowire growth. Both optical and electrical properties were investigated, using different equipment and techniques. Most of optical techniques are also well documented and easy to implement. The electrical measurements were developed from the ground up. Accordingly, a small system was designed and built to measure the Hall voltage and calculate the resistance and carrier concentration of the nanowire growth. This work was accepted by *Micro-Nano Systems Letters* in 2013 for publication [132]. The measurement of the output voltage was also unique and led to a publication in *Nanotechnology* [129].

The methods used are a good blend of known methods, equipment and new methods that were implemented for this study. With the methods in place, practical results were easily obtained.

Chapter 4

Simulations

Simulations play a big role in scientific research, as they are used to simulate practical problems. Accordingly, specialised software is used and an equivalent model is constructed in the software. Moreover, specific geometry can be specified with boundary conditions and structural properties to best duplicate the real-world problem. After the initial setup the simulation is performed and post-simulation analysis can also be performed.

Comsol Multiphyiscs was used for simulating the piezoelectric effect of the nanowires [133]. Comsol is a finite element simulation package that is best used for situations where different physics models are coupled [134]. Comsol has a number of different modules that focus on one specific type of physics model, including an RF module, MEMS module, plasma module, heat transfer module, fatigue module, pipe flow module, electrodeposition module and many more. Comsol also links to Matlab, Excel and many other programs for additional functionality.

In this work, Comsol was used to simulate the working of the nanogenerator. This was achieved with the MEMS module, that had piezoelectric physics included. The simulations were initiated by building the model, at first consisting of only a single nanowire. A force was then applied to see if an output voltage was created. The influence of various parameters on the output voltage was investigated and compared to the mathematical model derived in Chapter 2. A nanogenerator, consisting of multiple nanowires, was then constructed. Various simulations were performed on the nanogenerator to further verify the physical and mathematical models of Chapter 2. Lastly, a conclusion was drawn on the validity and usefulness of the simulations.

4.1 Single nanowire simulation

The simulations stared by choosing the physics that was applicable to the problem. In this particular case, a force is applied to a nanowire, causing the nanowire to bent and, due to the inherent piezoelectric effect, an electric potential across the nanowire was created. Two different physics branches were used: nanotechnology and piezoelectricity. Both of these are included in Comsol in the MEMS module. No time dependant parameters were included in this simulation and hence a transient analysis was chosen.

The nanowire geometry was specified in the software; a cylinder with a 25 nm radius and a length of 600 nm, as shown in Figure 4.1. ZnO was then specified as the material for the nanowire. Although the ZnO nanowires are not cylindrical, but rather hexagonal, the simulations were performed on cylindrical structures to simplify the simulations.

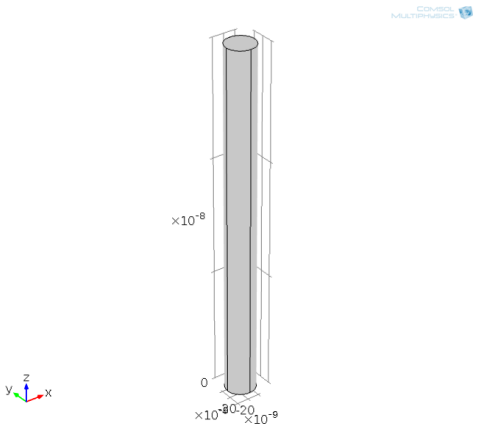

Figure 4.1: The nanowire as constructed in Comsol. The cylindrical nanowire had a length of 600 nm and a radius of 25 nm.

The boundary conditions were set next. The bottom surface of the nanowire was fixed, while the other boundaries remained free to move. The bottom surface was also grounded, while the rest of the structure was not. A force was then applied to the top end of the nanowire in the positive x-direction with a magnitude of 80 nN. The applied force caused the nanowire to bent, as shown in Figure 4.2 (a). The tip displacement of the nanowire was 130 nm at maximum. This created a strain inside the nanowire, as shown in Figure 4.2 (b). This strain in turn created an electric field due to the piezoelectric effect, as shown in Figure 4.2 (c). The simulation showed what was explained in the physical description of the nanogenerator in Chapter 2. Lastly, the created electric field resulted in an electric potential that

was created across the nanowire, as shown in Figure 4.3. The maximum voltage was 0.2885 V. This occurred at the bottom end of the nanowire, where the largest strain on the nanowire was present. As explained in Chapter 2, the nanogenerator was manufactured with an electrode at the top of the nanowire, where the output voltage was slightly less than maximum.

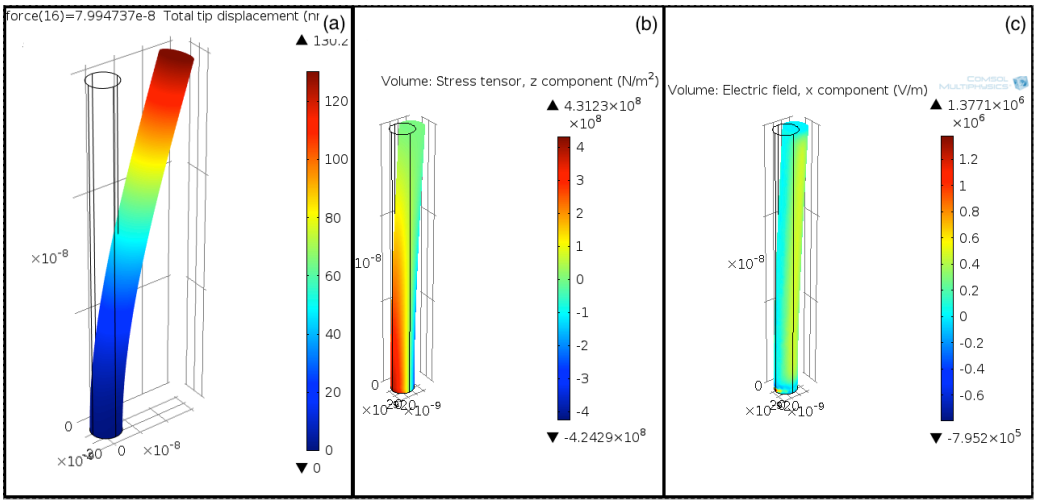

Figure 4.2: The nanowire simulated in Comsol showing (a) the tip displacement, (b) the induced strain and (c) the generated electric field due to an applied force of 80 nN in the x-direction.

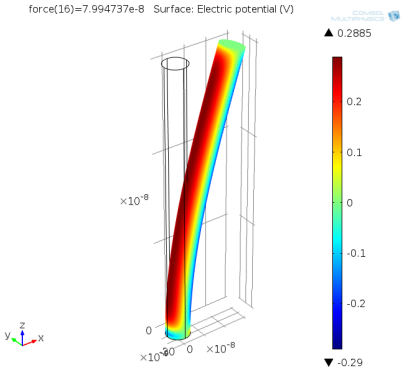

Figure 4.3: Simulated value of the voltage generated in a ZnO nanowire when a 80 nN force was applied in the x-direction.

The magnitude of the voltage produced by the piezoelectric effect was proportional to the applied force, as shown in the mathematics in Chapter 2. As the force increased, the nanowire was bent more, resulting in larger stress on the nanowire,

which led to a higher voltage. Figure 4.4 (a) shows the deflection of the nanowire tip versus applied force, and it was clear that, as the force increased, so did the maximum deflection at the tip. Figure 4.4 (b) shows the generated voltage versus the applied force, and again, as the force increased, the voltage increased, as expected and explained by the mathematics.

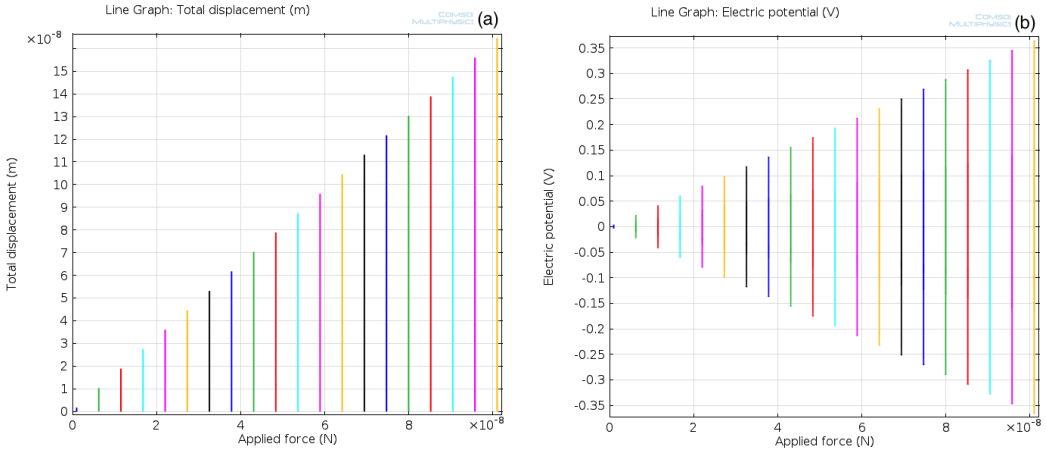

Figure 4.4: Simulated data for (a) nanowire tip displacement and (b) generated voltage with different magnitude force applied to the nanowire tip. Both the displacement and generated voltage increased as the applied force increased.

The final equation derived in the mathematical description of the nanogenerator in Chapter 2, (2.6.17), is given below. It was shown above that the generated voltage was directly proportional to the applied force, as expected. The dimensions of the nanowire were investigated next. The equation

$$\begin{aligned} \varphi_{12} &= \frac{f_y}{2\pi\epsilon}(d_{15}-d_{33})\left(\frac{\epsilon_0+3\epsilon}{\epsilon_0+\epsilon}\frac{r}{a^2}-\frac{r^3}{a^4}\right)\sin\theta\,,\ r\le a \\ &= \frac{f_y}{2\pi\epsilon}(d_{15}-d_{33})\left(\frac{2\epsilon}{\epsilon_0+\epsilon}\frac{1}{r}\right)\sin\theta\,,\ r>a, \end{aligned} \tag{4.1.1}$$

is dependent only on the diameter of the nanowire and not the length.

Figure 4.5 (a) shows the generated voltage versus the nanowire length. As expected, the length did not influence the output voltage. The voltage remained constant and independent of nanowire length. Figure 4.5 (b) shows the generated voltage versus the nanowire diameter. When the diameter of the nanowire increased, the generated voltage decreased and this was verified by the equation above. The voltage dropped quickly as the diameter was increased and this was due to the

quadratic and fourth power diameter expressions that are found in the equation. This means that during the manufacture of the nanogenerator, the grown nanowires should be as thin as possible, while the length does not matter.

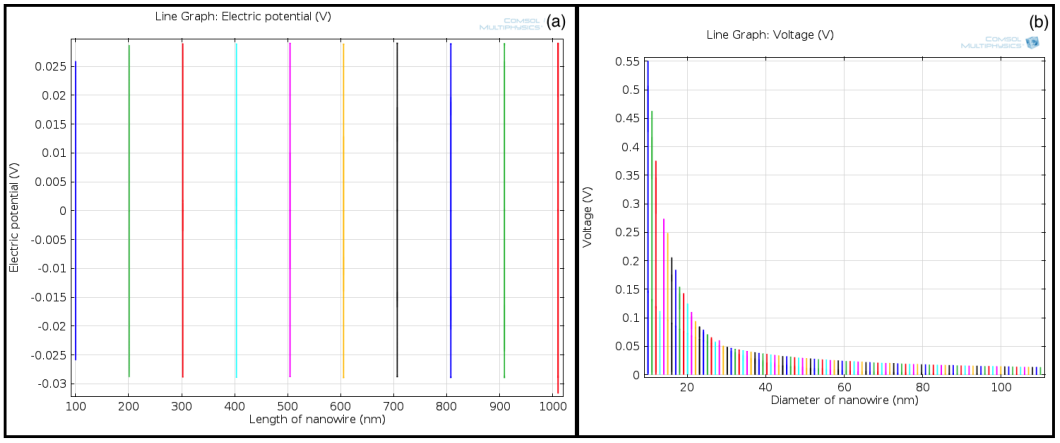

Figure 4.5: Simulation of generated voltage as a function of the nanowire (a) length, which did not influence the magnitude of the output voltage, and (b) diameter which had a considerable effect on the magnitude of the output voltage when a constant force was applied.

The next parameter that was investigated was the piezoelectric coefficient, d_{iJ}, that is given by

$$\begin{bmatrix} 0 & 0 & 0 & 0 & d_{15} & 0 \\ 0 & 0 & 0 & d_{15} & 0 & 0 \\ d_{31} & d_{31} & d_{33} & 0 & 0 & 0 \end{bmatrix} \approx \begin{bmatrix} 0 & 0 & 0 & 0 & -0.48 & 0 \\ 0 & 0 & 0 & -0.48 & 0 & 0 \\ -0.57 & -0.57 & 1.32 & 0 & 0 & 0 \end{bmatrix}. \tag{4.1.2}$$

The piezoelectric coefficient relates the mechanical strain to the produced electrical field. The piezoelectric coefficient, d_{iJ}, applies when the force is applied in direction J and charge is collected on the surface in direction i [46]. That means d_{33} applies when the force is applied in direction 3 and the charge is collected on the same surface. d_{31} applies when the charge is collected on the same surface as above, but the force is applied to surface 1. Lastly, with d_{15}, the charge is collected on surface 1 but the applied force is not applied perpendicular to a surface but rather a shear stress is introduced.

The equation only took d_{15} and d_{33} into account, but this was only due to certain simplifications that were made during the derivation of the equation. All three of the piezoelectric coefficients will influence the generated voltage. Although the ap-

plied force was only in the x-direction, or direction 1, all the elements will influence the generated voltage.

Figure 4.6 shows the generated voltage as a function of d_{15}, d_{31} and d_{33}. The d_{33} coefficient had the biggest influence on the generated voltage, with d_{15} the smallest. Although the equation did not take d_{31} into account, it did have a significant influence on the generated voltage. The polarisation occurred along the z-axis or in direction 3, and hence both d_{33} and d_{31} had a considerable effect on the output voltage. The main problem, however, was that the piezoelectric coefficients are inherent in each material and cannot easily be altered during the synthesis of the nanowires.

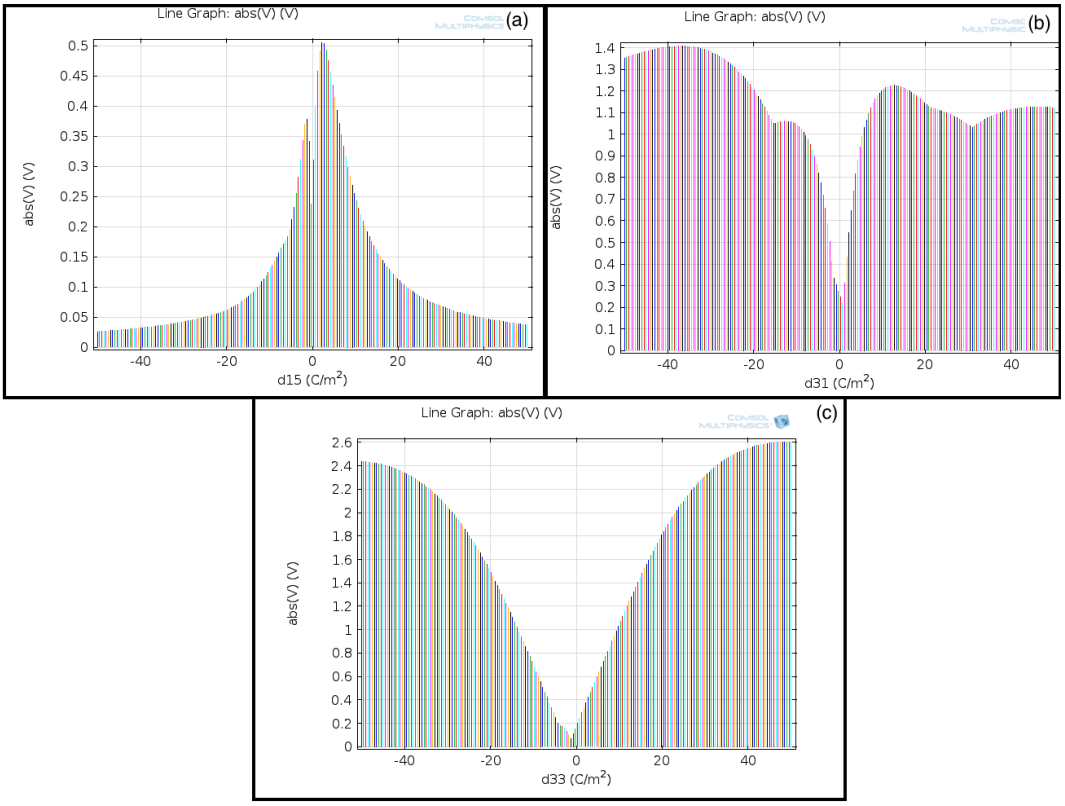

Figure 4.6: Simulation of generated voltage as a function of (a) d_{15}, (b) d_{31} and (c) d_{33}. All three piezoelectric coefficients had an influence on the output voltage.

The last parameter that is present in the equation is ϵ, or the permittivity of the material. The permittivity gives an indication of the resistance of the material when the electric field is formed. It has an inverse relationship with the generated voltage. The lower the permittivity the higher the voltage, as seen in the equation, as well as in Figure 4.7. The generated voltage dropped quickly with an increase

in permittivity. As the permittivity increased, it reduced the induced electric field, which in turn led to a lower generated voltage.

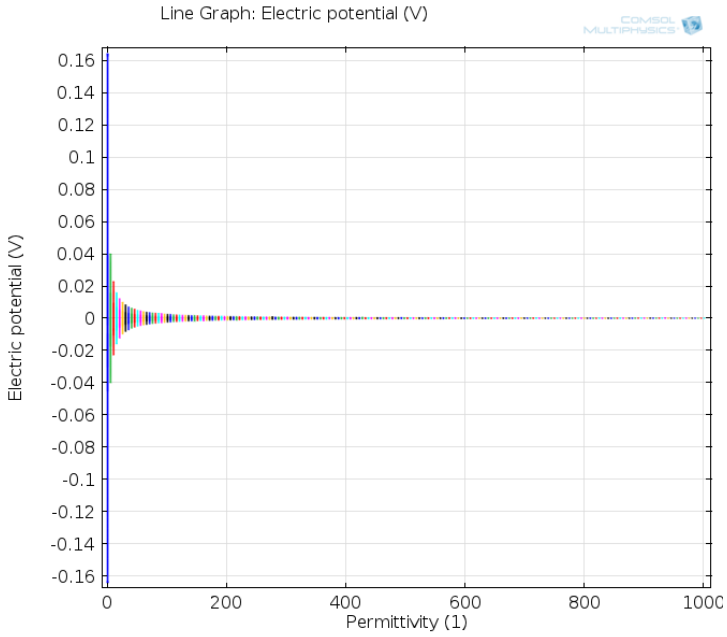

Figure 4.7: Simulation of generated voltage as a function of the permittivity of ZnO.

The current generated by the piezoelectric voltage was also an important parameter. The problem was that the voltage measured up to this point was the open circuit voltage and hence the current will be zero. In order to measure the current, a load must be connected to the nanowire. The piezoelectric physics module did not include this functionality, but the AC/DC module did. The AC/DC module was added to the model and, again, a stationary analysis was performed. As mentioned, the bottom of the nanowire was grounded and with the AC/DC module the top end of the nanowire was labelled *Terminal 1*. A circuit was drawn with the nanowire as a voltage source that was between the ground and node one, and a resistor that was also connected to node one and goes to the ground. When the simulation was performed, the nanowire was bent and a voltage was generated. The AC/DC physics module was then instructed to use the solved voltage as the source for the voltage in the simulation. The current through the resistor was now plotted.

Figure 4.8 shows the current through the nanowire as it flowed through the completed circuit. The nanowire was attached to a 1 MΩ resistor and a 80 nN force was applied. Figure 4.8 shows that the current is uniform throughout the nanowire.

This was a simplification however, as the model did not take the actual resistance into account, and neither the variation in resistance across the nanowire.

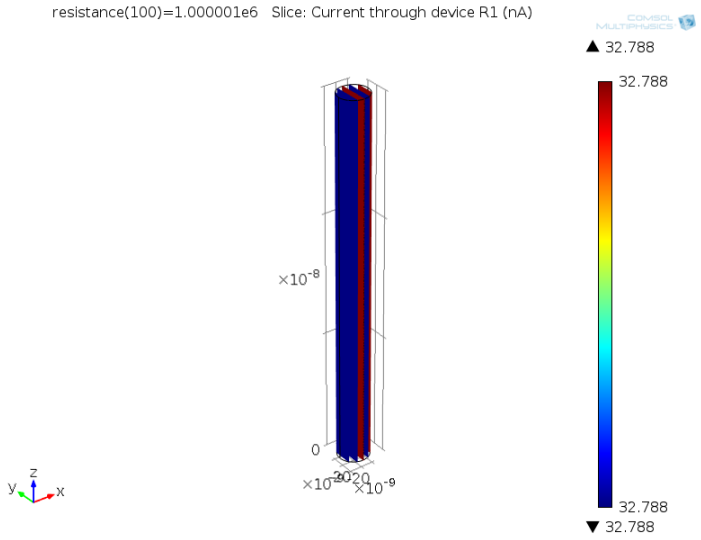

Figure 4.8: Simulation of the current flow through the nanowire when a 1 MΩ resistor was attached as the load and a constant 80 nN force was applied.

The current increased as the applied force increased, in line with the generated voltage, as expected. All the parameters that influenced the voltage also influence the current, as was expected, as current and voltage are linked by Ohm's Law,

$$V = I \times R. \tag{4.1.3}$$

The current was dependant on the load resistance and decreased with an increase in resistance, as expected. Figure 4.9 shows the resulting graph as the load resistance was increased from 1 Ω to 100 MΩ. The current was almost 1 μA when a small load is connected and quickly dropped to below 1 pA as the resistance increased.

As mentioned, the simulation did not take the internal resistance of the nanowire into account. This influenced both the generated voltage and current simulations and the simulated results were expected to be higher than practical measurements.

The simulation of a single nanowire gave a good indication of which parameters were important in increasing the generated voltage. The nanogenerator however, consists of multiple nanowires. Simulating a nanogenerator with millions of nanowires is not practical, as it will require computational power that is beyond

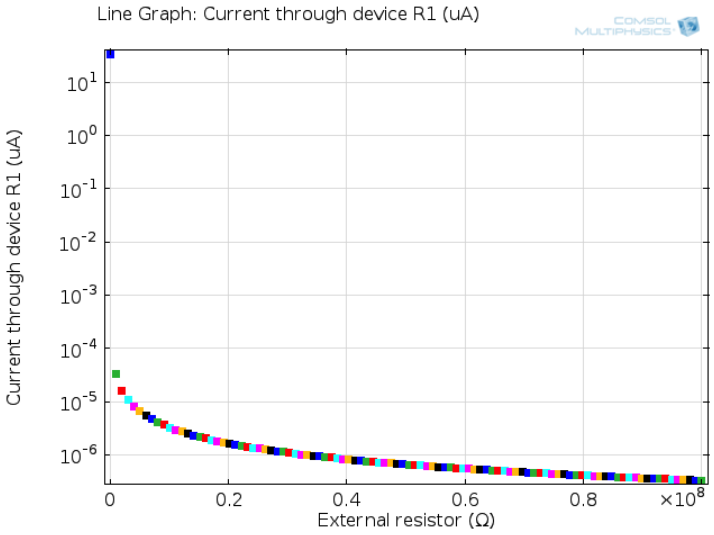

Figure 4.9: Simulation of the current versus load resistance when a constant force was applied to the nanowire.

today's technology. Hence, a simple nanogenerator consisting of only a number of nanowires was simulated to investigate the nanogenerator further.

4.2 Nanogenerator simulation

The nanogenerator was simulated with three separate nanowires connected to a thin plate at the bottom. All three nanowires were of the same dimensions, 50 nm in diameter and 600 nm in length. The nanowires and the bottom plate were all made of ZnO.

Different forces were applied to the three nanowires shown in Figure 4.10. The left nanowire had a force of 20 nN, the middle nanowire 50 nN and the rightmost nanowire a force of 80 nN. The force was applied to the top surface of the nanowire in the positive x-direction.

The current was contained within the nanowire and did not flow through the bottom plate, because the circuit was not complete. In order to get a current flow, the circuit must be completed by connecting a load resistor. This was again done with the AC/DC module. The top ends of all three nanowires were labelled *Terminal 1*, making the entire structure one voltage source.

The voltage with the completed circuit can be seen in Figure 4.11. The load resistor was 1 MΩ and the voltage was measured at 0.2514 V throughout the nanogenerator (it was now modelled as a voltage source, hence one stable voltage throughout). The voltage was slightly less than the maximum voltage of the nano-

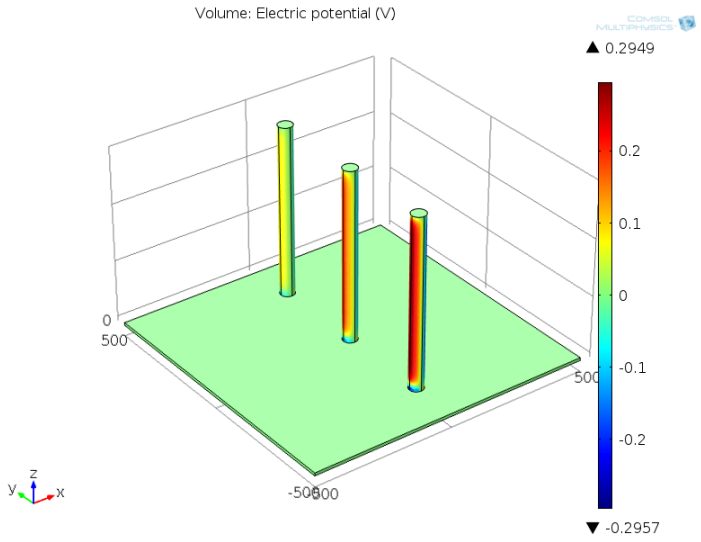

Figure 4.10: Nanogenerator with different forces on each nanowire. The nanowire to the left had a force of 20 nN, the middle nanowire 50 nN and the rightmost nanowire 80 nN.

wire that was bent the most; the voltages did not add up constructively, but were rather equal to the highest voltage. The three nanowires were connected in parallel and, using normal circuit analysis, the voltage over the resistance will be the highest of the three sources.

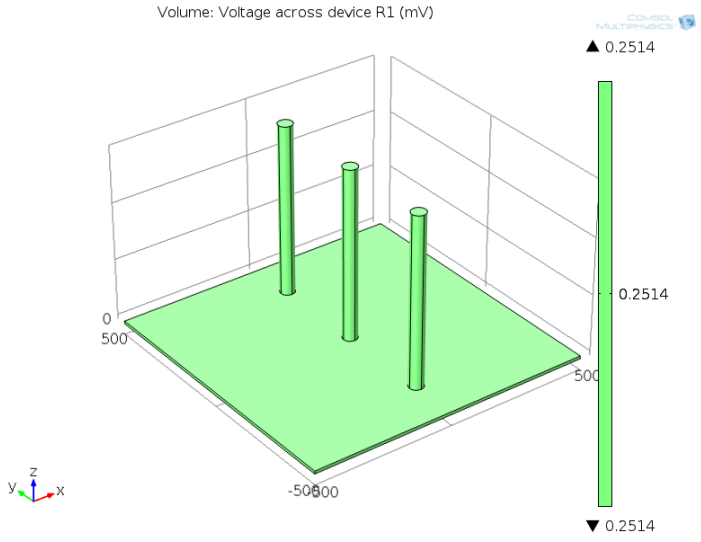

Figure 4.11: Simulation of the voltage when a load resistor was connected to the nanogenerator.

The current, however, added up constructively, giving a larger current com-

pared to the single nanowire case. In the single nanowire case (Figure 4.8), the maximum current was just below 33 nA. Figure 4.12 shows the current that flowed through the load resistance when the three different forces were applied to the nanowires. The maximum current was now over 50 nA when the forces were applied to the three nanowires. The three nanowires were connected in parallel, as mentioned, and the three currents will thus added up to give a larger current flow.

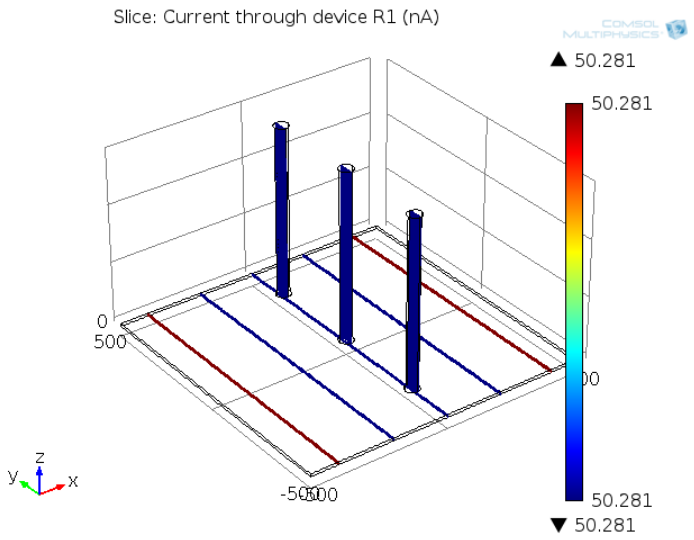

Figure 4.12: Simulation of the current resulting from the connected load resistance. The currents of the three nanowires added up constructively to give a larger current flow through the resistor.

Although only three nanowires were simulated for the nanogenerators, the same characteristics would apply if more nanowires were added. The voltage over the external load will always be equal, or slightly less, than the voltage generated by the nanowire that had the largest applied force. Moreover, the current through the external load would be equal to the generated currents of all the nanowires. This is true if the applied force is in the same direction for all the nanowires. If the force is in the opposite direction, the current will be of the opposite sign and it will be subtracted from the total current flow.

4.3 Conclusion

Simulations were done with the help of Comsol Multiphysics. The MEMS module, and in particular the piezoelectric component of the module was used to simulate the ZnO nanowire. The nanowire was constructed in the software, certain bound-

ary conditions were set and a force was applied to the nanowire. The generated voltage and the influence of certain parameters on the voltage was obsereved.

The generated voltage was dependant on the applied force; the higher the force the higher the output voltage. The simulations, mathematical and physical description all confirmed this. The morphology of the nanowire also affected the output voltage. The mathematics showed that the diameter of the nanowire, as it gets smaller, leads to a larger voltage and this was confirmed with the simulations. It hade been shown that thinner ZnO nanowires showd better properties due to the decrease in free carriers in the nanowire [135] [136]. As mentioned in Chapter 2, the free carriers can screen the piezoelectric charge resulting in a lower voltage. When the nanowire was thinner, fewer free carriers were present and hence the output voltage was higher. The length did not influence the voltage, which seemed strange, as longer nanowires would have more free carriers, hence the same logic applied as for the diameter. The exact reason for why the length has no effect was not clear. Electron transport time increased as length increased, but the simulation was transient, so this would not have had any influence on the generated voltage [137]. It is believed that the increase in the number of polarised charges was equal to the number of free electrons when the length increased and hence no difference in voltage was observed. In contrast, when the diameter increased the number of polarised charges did not increase as they remained in the centre of the nanowire and did not get polarised and, hence, the voltage dropped because the number of free carriers were increased, screening the voltage more.

Other parameters that influenced the voltage were the piezoelectric constants and the permittivity of the material. The piezoelectric constants indicated the efficiency of the material in converting a force applied in a specific direction to a charge built up in a specific direction. As predicated by the mathematics, the piezoelectric coefficients influenced the generated voltage, and the simulations confirm the predictions. The permittivity also greatly influenced the generated voltage, where a lower permittivity resulted in a much larger generated voltage. The permittivity had an inverse relationship with the voltage, as shown in the mathematics and it is also confirmed by the simulations.

The simulation of a single nanowire gave a good indication of where the nanowire could be changed to give a larger voltage. Certain parameters, like the piezoelectric coefficients, were not direclty controllable and other methods are required to increase the generated voltage. The morphology of the nanowires could be controlled during growth and could be optimised for maximum generated voltage. The nanogenerator consists of millions of these nanowires and simulating a few can give a better indication of the working of the nanogenerator.

The simulations showed that the voltage of the nanogenerator would be equal to the voltage generated by the nanowire that was bent the most. The voltages did not add up constructively, because they were effectively connected in parallel. Therefore, the current that flowed through the load resistance did add up and was higher than the highest current from a single nanowire. As mentioned, the nanowires were connected in parallel, and current sources in parallel add up, resulting in a higher current flow through the load resitance. This only occured if the applied force was in the same direction for all the nanowires.

The simulations helped to further explain the working of the nanowire, the piezoelectric effect and the nanogenerator. Together with the physical and mathematical models, a complete description of the piezoelectric effect and nanogenerator had been given. It is clear where improvements could be made to ensure an increase in the generated voltage. The next step is to take this knowledge and apply it to the practical world.

Chapter 5

Zinc oxide nanowire growth and optimisation

The ZnO nanowires are one of the cornerstones of this project. The nanogenerator was manufactured using ZnO nanowires. It was thus necessary to find optimal growth methods and parameters that led to perfect quality nanowires.

The two growth methods, the vapour liquid solid (VLS) and aqueous solution (chemical bath deposition) methods, are well documented and growth parameters could easily be found in the literature [57, 83, 84, 87, 88]. The parameters found in the literature, however, were designed for a specific setup and needed to be adapted in order to work with the equipment available.

After growth parameters were found that resulted in nanowire growth, these parameters could be optimised. These optimised parameters would ensure that optimal nanowire growth occured every time.

In this chapter, the adaptation of growth parameters found in the literature, will be discussed. Accordingly, the influence of different parameters on the resulting growth is discussed. The one parameter at a time optimisation technique is subsequently discussed for both growth techniques. Using the aqueous solution growth method, the growth parameters are then further optimised using design of experiments (DoE). Lastly, the influence of seed layers on the growth is discussed.

5.1 Nanowire growth and one parameter at a time optimisation

As mentioned above, growth parameters found in the literature needed to be adapted to work with the instruments in our laboratory. The VLS method was considered first, after which the aqueous solution method was investigated. The initial stage

of growth and the one parameter at a time optimisation technique were performed simultaneously to see the effect a single parameter has on growth.

5.1.1 Vapour liquid solid

The VLS method had a number of parameters that can influence growth. The parameters that were investigated were:

- Growth time
- Growth temperature
- Amount of source materials
- Initial pressure
- Growth pressure, and
- Gas flow rate.

These six parameters were under the direct control of the experimenter and could be altered between consecutive runs. The growth was done on Si (100) substrates with a 20 nm layer of Au sputtered on.

Initially, in order to simplify the growth process, the vacuum stage was removed. The growth that occured at 900°C for 20 minutes with 3 g of ZnO and 3 g of graphite, was investigated and is shown in Figure 5.1. The nanowires grew in random directions with large areas where no growth was visible. The thickness of the individual nanowires also varied. The growth that occured without the vacuum stage did not look good and, hence, the vacuum stage was added for the ensuing runs.

The addition of a vacuum stage added two extra parameters: the starting and the working pressure. The pressure that was present while the furnace heats to maximum temperature was termed the initial pressure. The working pressure was achieved at maximum temperature when the carrier gas was introduced. To start of with, the working pressure was kept at 1 mbar, and the initial pressure was changed from 260×10^{-3} mbar, the minimum pressure achievable, to 1 mbar. At a working pressure of 260×10^{-3} mbar no growth was observed. When the pressure was increased to 660 mbar small areas of growth were visible, but with random orientation. As the pressure was decreased further, the nanowire growth became denser and more aligned. Figure 5.2 shows the growth of the nanowires at 200 mbar and 1 mbar.

The exact reason why the initial pressure had such a big influence on the growth was not clear. It was argued that from a high pressure, a decrease to 1 mbar was a

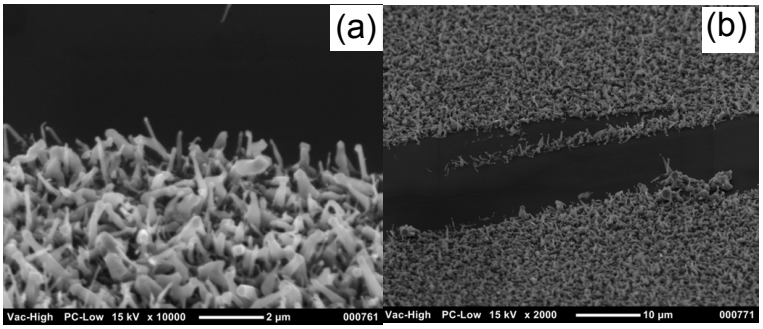

Figure 5.1: SEM image of VLS growth without a vacuum stage. The growth parameters were as follows: 20 min, 900°C with 3 g ZnO and 3 g graphite. (a) The nanowires at 10 000 × magnification, and (b) at 2 000 × magnification. The resulting growth was not optimal and a vacuum stage was added for the ensuing runs.

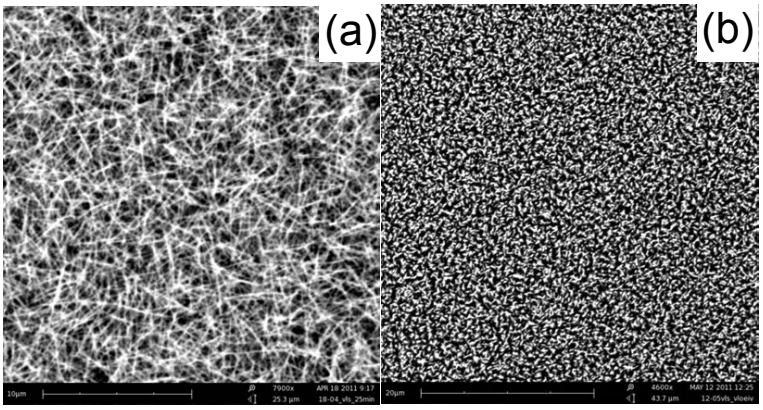

Figure 5.2: SEM image of VLS growth with the initial pressure at (a) 200 mbar, resulting in randomly oriented growth, and (b) 1 mbar, resulting in well-aligned growth. The rest of the growth parameters were as follows: 20 min, 900°C with 3 g ZnO and 3 g graphite and working pressure of 1 mbar.

drastic decrease, meaning the carrier gas flow rate was high. At high flow rate the evaporated source materials were carried beyond the substrate and, consequently, limited to no growth was observed.

Next, the initial pressure was kept at 1 mbar and the working pressure was changed. First the pressure was increased to 2 mbar and, again, no growth was observed. Next, the pressure was decreased to 0.5 mbar, and again no growth was visible. The working pressure thus had a smaller functional range of only 0.9 mbar to 1.5 mbar. Typical nanowire growth within this range is shown in Figure 5.3.

The reason for the change in growth quality was again argued to be the gas flow rate. As the gas flow rate and the pressure were directly related, a flow rate that was too fast resulted in the evaporated materials flowing over the substrate. At

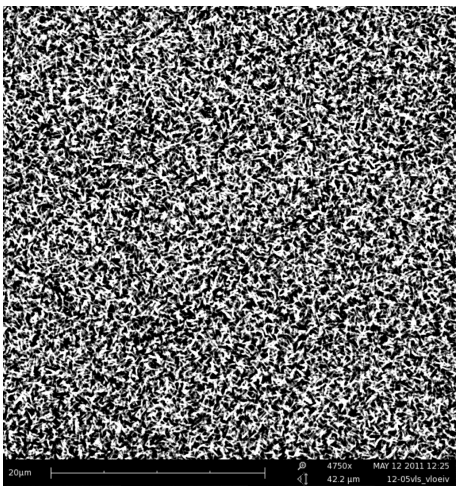

Figure 5.3: Typical SEM image of VLS growth with working pressure in the range of 0.9 to 1.5 mbar. The rest of the growth parameters were as follows: 20 min, 900°C with 3 g ZnO and 3 g graphite and working pressure of 1 mbar.

a too low flow rate, the amount of evaporated material that reached the substrate was too low to led to high growth. Hence, the flow rate and both the initial and the working pressure were closely related. In the optimal pressure range, the flow rate was between 20 and 50 sccm (standard cubic metres per minute).

The next parameter that was investigated was the amount of source powder used during growth. All the previous runs were performed with 3 g each of ZnO and graphite. If less than 1 g of each source material was used, no growth was observed. Between 1 g and 2 g each, some growth was visible, but it was sparse. With more than 2 g of each source material the growth started, but no visible effect was witnessed with an increased amount of source material.

The penultimate parameter was the growth temperature. At low temperatures there was not enough heat to evaporate the source materials and no growth was observed, with the critical point being below 850°C. Between 850°C and 950°C nanowire growth was observed, with no visible change in morphology, density or growth direction. When the temperature was increased further, to beyond 1000°C no growth was observed. At this high temperature the temperature at the substrate was also higher and it was too hot for the evaporated materials to participate in nanowire growth.

Figure 5.4 shows the temperature inside the furnace measured against distance from the centre. As expected, the centre of the furnace was at maximum temperature. The temperature dropped as the distance from the centre increased, but only after 300 mm. The hotzone of the furnace was thus 300 mm in length, after which the temperature dropped sharply, by almost 800°C in only 200 mm. Within this

short 200 mm length there was an optimal area where the evaporated source materials would cool down enough and participate in nanowire growth. Although the distance from the source material and the substrate was not mentioned as one of the growth parameters, it was optimised. However, once a favourable distance was found, it was not changed. The distance was found to be 120 to 150 mm from the hotzone, or between 600 - 400°C. When the temperature was increased, the distance between the source material and the substrate would also need to change, but this was not investigated further.

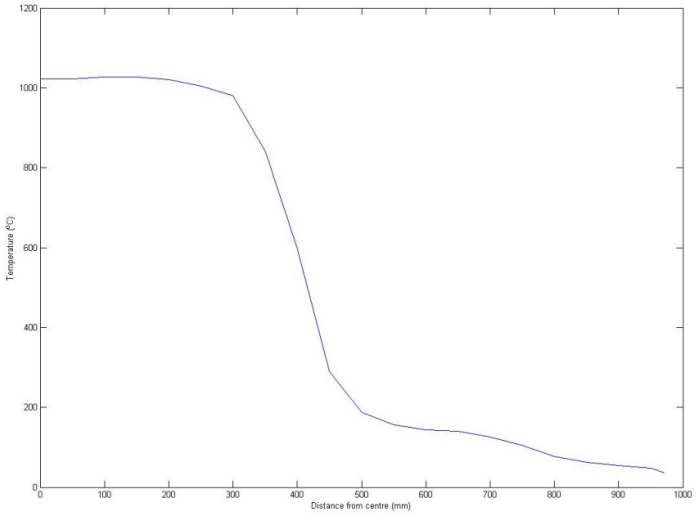

Figure 5.4: Temperature against distance profile of furnace used for the VLS growth of ZnO nanowires. The furnace had a hot zone of 300 mm and beyond this the temperature decreased as the distance increased.

The last parameter than was investigated was the growth time. Figure 5.5 shows the nanowire growth for 5 min, 10 min, 15 min and 30 min respectively. During the first five minutes a seed layer formed on top of the Au layer. Small circular seeds were visible but no growth was visible. After 10 minutes a few nanowires were present on the substrate. The growth had started, originating from the seeds that formed during the first five minutes. The growth was not well aligned at this stage, but as the time increased to 15 minutes the growth became denser and more aligned. As the time increased further to 30 minutes, the growth became even denser and better aligned. If the time was increased further beyond 30 minutes, however, no visible change was observed. The nanowires started to get thicker, but at a slow rate and the growth got longer, but also at a very slow rate.

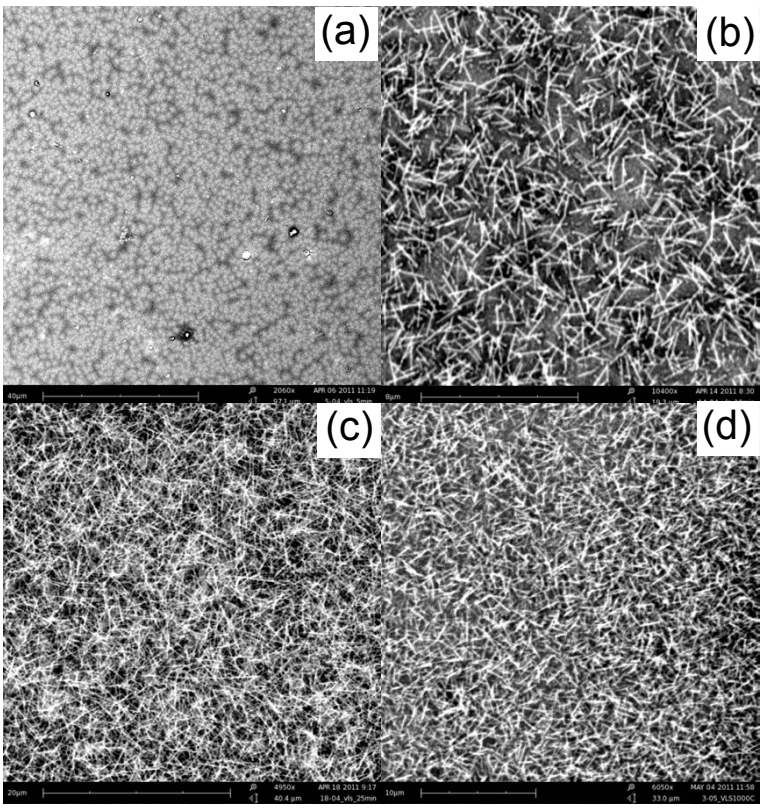

Figure 5.5: SEM image of VLS growth with growth time of (a) 5 min, where a seed layer formed for growth, (b) 10 min, where the growth started but is not aligned or dense, (c) 15 min, where the density increased, but with poor alignment and (d) 30 min, where the growth was dense and aligned. The rest of the growth parameters were as follows: 900°C with 3 g ZnO and 3 g graphite and initial and working pressure of 1 mbar.

The major drawback to the VLS method was repeatability. Consecutive runs with identical parameters resulted in different growth behaviour. The one run yielded perfectly aligned, dense growth, where the other run resulted in low orientation and low-density growth or even no growth at all. This was due to certain parameters that were not under the direct control of the experimenter, such as the atmospheric conditions, the rate of increase in the furnace temperature and the carrier gas pressure. These parameters could influence growth and it was observed that on clear sunny days better growth was achieved than cloudy and rainy days.

A more repeatable method was required to ensure good quality growth every time. Moreover, the growth temperature of the VLS method was very high, limiting the choice of substrate. A low temperature alternative that was more repeatable was thus required.

5.1.2 Aqueous solution method

The aqueous solution growth method was investigated next. As with the VLS method, parameters found in the literature were used and adapted to work in our laboratory. The parameters that were investigated are:

- Growth time
- Growth temperature
- Concentration of source materials, and
- The ratio between the source materials.

These four parameters were investigated and changed one at a time to ascertain the effect an individual parameter had on nanowire growth.

The first parameter that was investigated was the growth temperature. Nanowire growth was observed between 60°C to 120°C. To investigate the effect that temperature had on nanowire growth. The growth period was 5 hours with a 1:1 ratio at 30 mM of source materials. Limited to no growth was observed at the lower temperatures as shown in Figure 5.6 (a). As the temperature was increased, the growth became better aligned and dense nanowires were observed, as seen in Figure 5.6 (b) and (c). When the temperature was too high, no nanowire growth was visible (Figure 5.6 (d)). At low temperatures the energy of the solution was too low to initiate growth, while at temperatures that were too high, there was excess energy and the growth was unstable, resulting in random growth structures.

Next the growth time was investigated by leaving the nanowires to grow for 24 hours at 85°C with a 1:1 ratio of 30 mM solution of source materials. Figure 5.7 shows the growth after 1 hour, 3 hours, 6 hours, 8 hours, 16 hours and 24 hours, respectively. During the first two hours a seed layer was formed. Figure 5.7 (a) shows the small circular seeds that were formed. After three hours small nanoparticles were formed at these seeds. During the first couple of hours, after the initial seed formation, the growth became denser, thicker and longer. After six hours the growth was dense and well aligned and it remained like this until 24 hours have elapsed. After seven to eight hours the thickening and lengthening of the nanowires slows down and no visible change in morphology was observed.

The last two parameters, concentration and ratio of source materials, were investigated together. As mentioned, the source materials were zinc nitrate hexahydrate and HMTA. The zinc nitrate hexahydrate was the source for the Zn, HMTA acted as a pH buffer and added hydrogen to the reaction, and the DI water supplied the oxygen for the formation of ZnO. The concentration of the source materials influenced both the diameter and the length of the nanowires [57]. Figure 5.8 shows

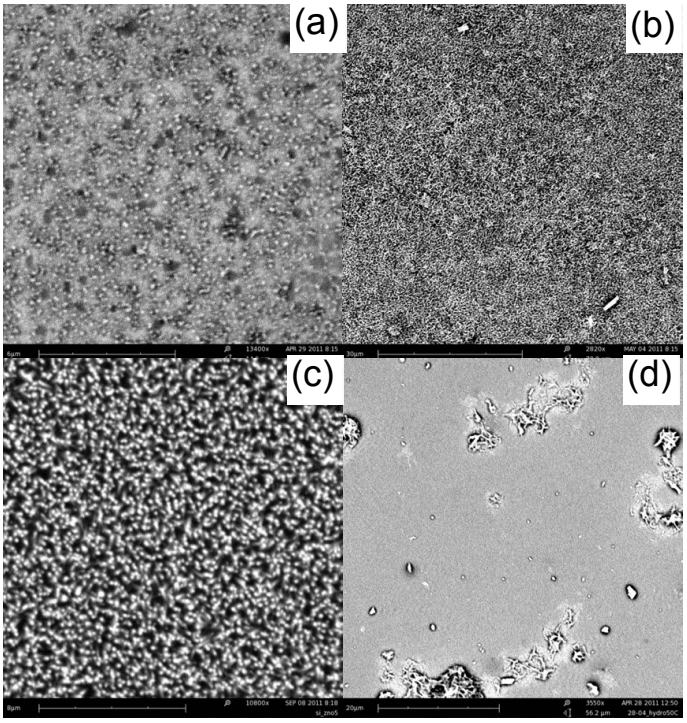

Figure 5.6: SEM image of aqueous solution growth of ZnO nanowires. The growth temperature was (a) 60°C where no growth was visible due to too little energy available to initiate growth, (b) 70°C, (c) 90°C, where good growth was visible, and (d) 120°C, where there was excess energy and random structures are formed. Growth time was five hours with a 1:1 ratio at 30 mM.

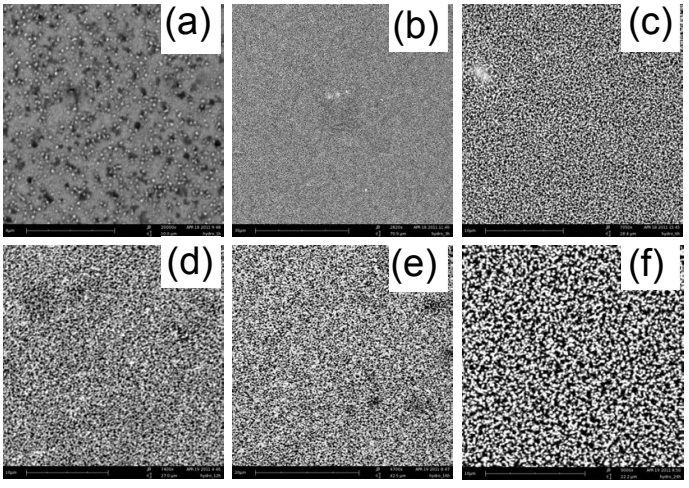

Figure 5.7: SEM image of aqueous solution growth of ZnO nanowires. The growth was left for 24 hours and images at (a) 1 hour, where the seed layer formed, (b) 3 hours, where small nanoparticles were formed on top of the seed layer, (c) 6 hours, (d) 8 hours, (e) 16 hours and (f) 24 hours, when good growth was observed, were shown. The growth temperature was 85°C with a 1:1 ratio at 30 mM concentration.

the growth, with a 1:1 ratio at 85°C for five hours and 20 mM, 50 mM, 70 mM and 100 mM concentration, respectively. As the concentration was increased, the nanowire diameter increased. At 100 mM concentration nanowires were not visible, but larger structures were formed. At concentration values below 20 mM the SEM could not focus on the growth and hence 20 mM was the lowest concentration used.

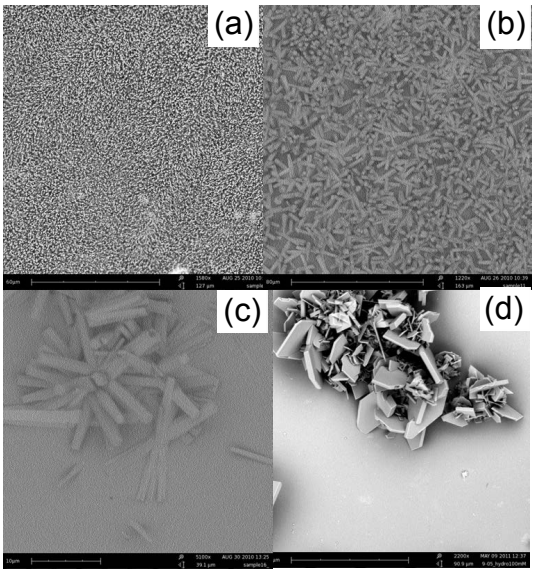

Figure 5.8: SEM image of aqueous solution growth of ZnO nanowires. The growth temperature was 85°C for five hours with a 1:1 ratio at a concentration of(a) 20 mM, where small nanowires formed, (b) 50 mM, where larger wires were grown, (c) 70 mM, where even larger wires were grown and (d) 100 mM, where large, random structures were formed.

The ratio between the two source materials also affected the nanowire growth. With more HMTA than zinc nitrate, more hydrogen ions were present in the solution. This led to limited growth as the solution was overcame by the hydrogen atoms. The extra hydrogen ions bond with the oxygen to form water instead of bonding to zinc. On the other hand, when more zinc nitrate was present there were too many zinc ions. As all the zinc ions could not bond with oxygen and a excess of zinc ions was present, which led to malformation of the nanowires.

The aqueous solution growth method was easier to control and consecutive runs led to nanowire growth that looked identical. The biggest problem was the quality of the DI water. If any other chemicals and materials are present in the water, they actively participate in the nanowire growth and led to imperfections in and contamination of the growth. The biggest advantage was the low temperature at which growth took place, which made it possible for a variety of substrates

to be used. For this reason, the VLS method was not considered any further for this project. Therefore, the aqueous solution method was used for both nanowire growth and the manufacture of the nanogenerator.

As mentioned, growth using the VLS method was done on Si (100) substrates with a 20 nm layer of Au sputtered on. The aqueous solution method was performed with a variety of layers deposited on the substrate. All three of the different deposition techniques (thermal evaporation, DC sputtering and ICM sputtering) were used to deposit a number of different materials onto the substrate for nanowire growth.

5.2 Seed layer influence on nanowire growth

The seed layer that was deposited on the substrate before nanowire growth had two functions: it acted as an electrode for the nanogenerator and as a buffer for the lattice mismatch between the substrate and the nanowires.

As mentioned, the electrode for the nanogenerator required a work function higher than the electron affinity of ZnO. The electron affinity of ZnO nanowires is 4.5 eV, so only materials with a work function higher than 4.5 eV could be used. Table 5.1 shows materials and their corresponding work functions [138]. Table 5.1 shows that only Au and Pt were suitable materials for the electrode.

Table 5.1: Different materials with their corresponding work functions. The work function of the material must be higher than 4.5 eV to work as an electrode in nanogenerator manufacturing. Consequently, only Au and Pt on the list could be used.

Element	Work function (eV)
Ag	4.2
Cu	4.4
Al	4.06
Zn	3.6
Au	5.1
Pt	5.12

The second function of the seed layer was to act as a buffer layer between the nanowire growth and the substrate. The ZnO nanowires are single crystal structures with a definite lattice structure. They prefer to grow in the (0001) direction, which meant that the substrate lattice structure should be closely related to this direction [139]. The aim of the seed layer was to lower the interfacial energy between crystal nuclei and the substrate and thus promote crystal growth [140]. The

substrate also added to the surface roughness, which further promoted nanowire crystal growth [141, 142].

Figure 5.9 shows ZnO nanowires synthesised on different seed layers. Figure 5.9 (a) to (f) shows growth with sputtered ZnO films (30 nm) and (g) to (l) evaporated ZnO films (30 nm). From these images the lattice spacing was measured as 0.28 nm, which corresponded to growth along the (0001) direction. The seed layers resulted in nanowires that developed in the desired growth direction, but ZnO could not be used as an electrode, because the work function is lower than the electron affinity. Hence no Schottky contact would form and the nanogenerator would not work.

Au was investigated as a possible solution for both seed layer and electrode, as the work function is higher than the electron affinity of ZnO. Figure 5.10 shows TEM images of the ZnO nanowires grown with sputtered Au films, 20 nm thick. Again the growth direction was in the preferred (0001) direction. Thus Au could be used as both buffer layer and electrode.

The adhesion between the Au and the substrate, Si (100) or the Kapton polyimide film, was poor. After growth, during the rinsing process, most growth was removed from either substrate. This was due to the poor adhesion mismatch between the Au film and the substrate. In order to solve this problem, a second buffer layer was used to match the Au layer and substrate for better growth. Table 5.2 summarises the results from a number of different materials that were tested.

Table 5.2: Different materials were used as a second buffer layer for better adhesion between the Au layer and the substrate. These materials were tested for the best buffer between the two layers. ZnO was found to be the best material as the adhesion was the best.

Element	**Resulting nanowire growth comment**
Ag	Bad adhesion, growth comes off easily
Al	Limited to no growth
Au	Poor adhesion, growth comes off during cleaning
Cu	Dense growth but in random directions
Cr	No growth
Fe	No growth
Ni	Limited to no growth
Ti	Dense growth but in random directions
Zn	Poor adhesion, growth comes off easily
ZnO	Best result, good growth and adhesion is perfect

From Table 5.2 ZnO was chosen as the best buffer layer. The sputtered ZnO layer had a different crystal structure to the ZnO nanowires and the lattice mis-

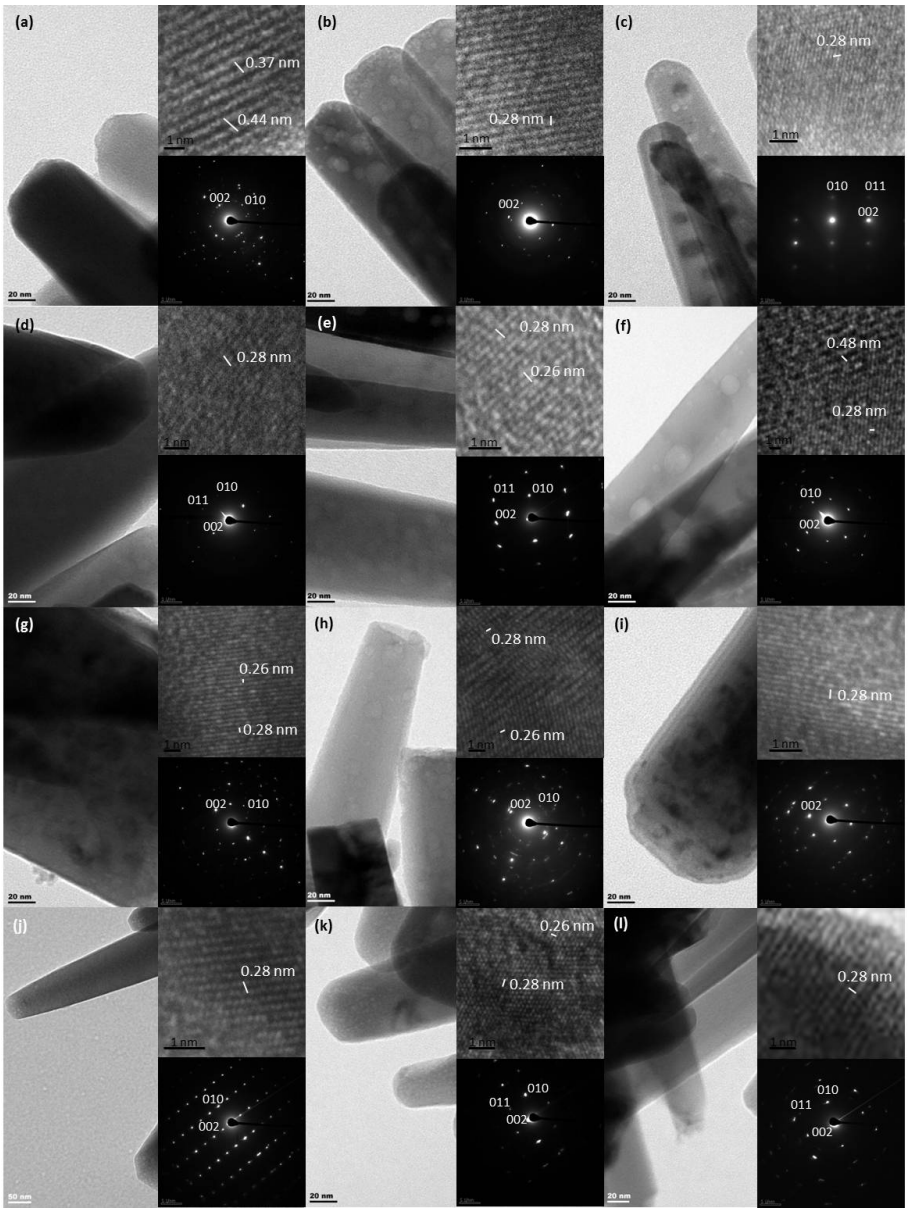

Figure 5.9: TEM images of ZnO nanowires grown on (a—f) sputtered and (g—l) evaporated ZnO films. The inserts show lattice spacing and crystal diffraction that could be used to determine the growth direction of the nanowires. The growth direction was in the preferred (0001) direction.

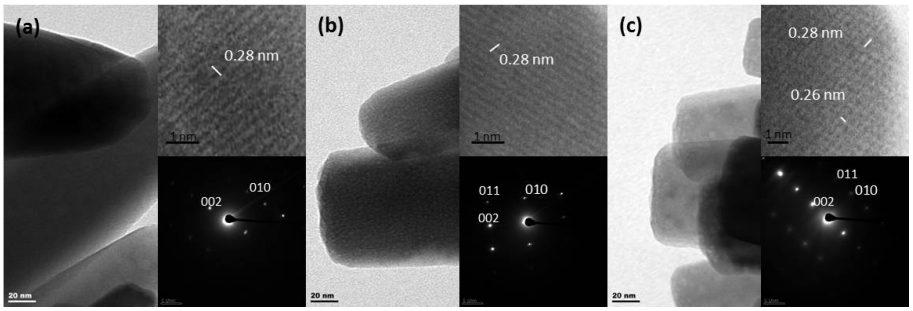

Figure 5.10: TEM images of ZnO nanowires grown on sputtered Au films. The inserts show lattice spacing and crystal diffraction that could be used to determine the growth direction of the nanowires. The growth direction was in the preferred (0001) direction.

match between the two was limited. The adhesion between the ZnO layer and substrate was better and resulted in growth that was near perfect.

With the perfect seed layers found, the growth parameters could be optimised further. At this stage most of the optimisation was done by imaging the nanowires after growth. The optimisation of the output voltage was more important than the optical quality of the growth and, hence, the optimisation was done with respect to the output voltage.

5.3 Optimisation by carrier concentration and resistance

The optical optimisation of the nanowires ensured that nanowire growth took place across the entire sample. The optical quality of the nanowires did not, however, give any indication of the internal properties of the nanowires. The main aim of this project was to increase the generated output voltage of the nanogenerator and it was thus important to optimise the growth for higher output voltage.

The growth was again optimised using the one parameter at a time approach. However, this time the optimisation was done with respect to the output voltage. The substrates, only Si (100), were prepared by sputtering a 20 nm layer of ZnO on top and growth was done by means of both the VLS and the aqueous solution methods. The output voltage was measured as explained in Chapter 3. A separate gold electrode was placed on top of the nanowire growth and was then moved laterally, causing the nanowires to bend. An output voltage was then observed. This measurement was destructive, because the friction between the electrode and the nanowires resulted in both the nanowire and the Au layer being removed over time [129].

Due to the fact that the measurement was destructive, before the output voltage was measured, two other properties were measured, namely carrier concentration

and resistance. These measurements were made to verify the theoretical prediction by Wang et al. that both these quantities have optimal values that will lead to higher output voltage [59, 93]. It is argued that the free carriers that are present in the nanowire can screen the piezoelectric charge that is generated when the nanowires are bent. The problem is that, without these carriers, the resistance of the nanowires would be infinitely large and the generated voltage would be lost internally. On the other end of the scale, if the resistance is too small, the number of carriers is extremely high and hence the voltage is screened completely by these carriers. Somewhere in the middle an optimal situation exists, where these carriers partly screen the generated voltage. At this point the internal resistance is also low enough and only a small portion of the voltage is lost internally.

The carrier concentration and resistance were measured and calculated using the Hall effect and the Van der Pauw method [130, 131]. The output voltage was measured next and the values were plotted to see the effect that both the carrier concentration and resistance had on the voltage.

The growth parameters were within the maximum and minimum range that was obtained during the first round of optimisation. One parameter was changed at a time to ascertain the influence on the output voltage that resulted from the specific change. Over 120 samples were prepared and measured. Just over 30 of these samples were prepared using the VLS method and the rest with the aqueous solution method. The results presented in this section was obtained from both growth methods with various growth parameters. This was done to ensure the resulting growth would have different values for resistance, carrier concentration and output voltage measurements.

Figure 5.11 shows the two different magnetic orientations that were used during the Hall and the Van der Pauw measurements. Although, according to Figure 5.11, the field strength looks identical between the two magnets in (a) or at the same distance from the magnets in (b), practical measurements differ. At first, setup (a) was tried but the magnetic field was not strong enough to gather reliable data. The field was measured at 650 Gauss, which was not enough for these measurements. The two magnets were then both placed above the sample, as in configuration (b), with a measured magnetic field of 1800 Gauss.

Figure 5.12 shows the relationship between resistance and carrier concentration. The fitted graph shows that, at high carrier concentration, the resistance was low. This is to be expected, because high carrier concentration meant the current could flow freely through the material and, hence, the resistance was low. As the carrier concentration reduced, the resistance increased. Fewer carriers were present for the current to flow freely and, hence, the resistance increased.

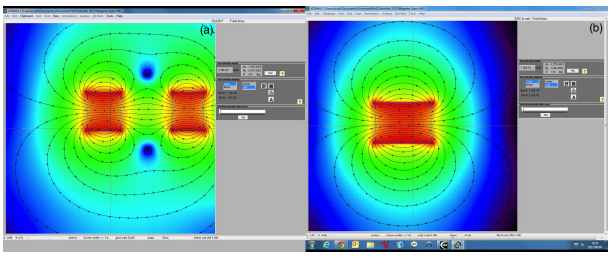

Figure 5.11: Graphical representation of the two different orientations used for the magnets during the Hall and the Van der Pauw methods. The lines represent the magnetic flux. The orientation in (a) results in a practical magnetic field of 650 Gauss, which was too low to use and (b) a field strength of 1800 Gauss, which was used for the practical tests.

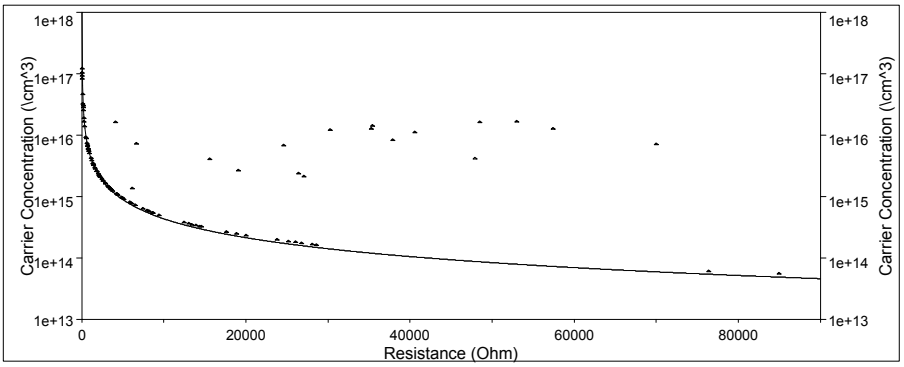

Figure 5.12: Relationship between the resistance and the carrier concentration of grown ZnO nanowire samples. The fitted graph shows that, at low resistance, the carrier concentration was high, and at high resistance, the carrier concentration was low.

The output voltage, as mentioned, would be at a maximum due to the screening of the charge and the resistance of the nanowires. Figure 5.13 shows the output voltage against resistance and a clear peak was visible. Figure 5.14 shows the output voltage against carrier concentration, and again a clear peak was visible. These two graphs show exactly what was predicted by Wang et al. At low resistance there is high carrier concentration, the output voltage is screened too much and a very small voltage is measured. As the resistance increasds and the carrier concentration decreased, the output voltage reached a maximum value. At this point, the balance between the screening of the charge and the loss over the internal resistance was reached. Beyond this point, as the carrier concentration decreased, the resistance increased and the voltage was lost internally.

The morphology and size of the grown ZnO nanowires greatly influenced the output voltage and other parameters of the nanogenerator [143, 144]. The morpho-

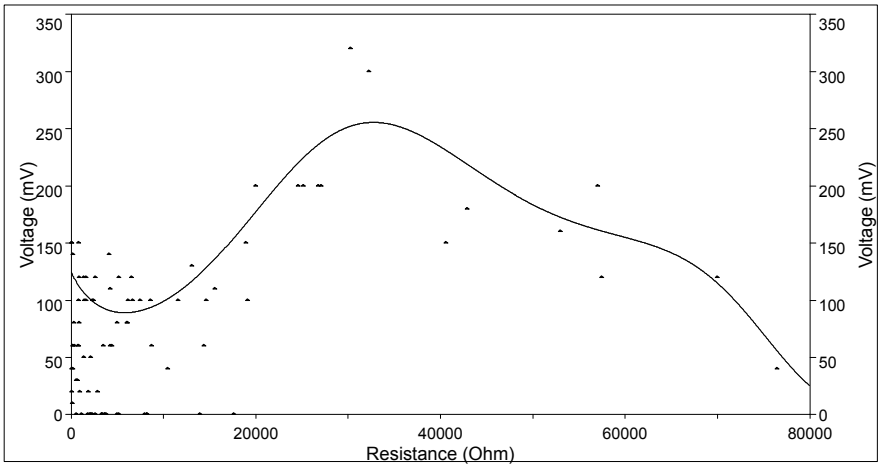

Figure 5.13: Relationship between the resistance and output voltage of grown ZnO nanowire samples. A clear peak in output voltage was observed between 20 kΩ and 40 kΩ, where the piezoelectric voltage was only partially lost internally due to the high resistance.

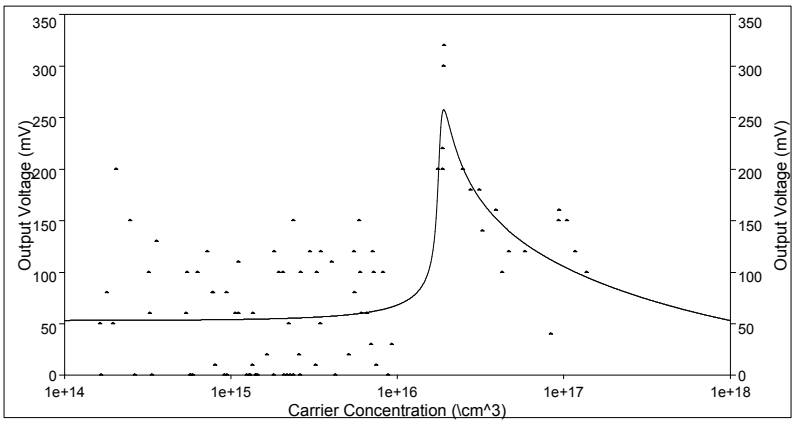

Figure 5.14: Relationship between the carrier concentration and output voltage of grown ZnO nanowire samples. A clear peak was visible between 10^{16} and 10^{17} cm^{-3}where the piezoelectric charges were only partially screened.

logy of the nanowires grown by the two methods was not identical. On average, the output voltage measured for the VLS growth was 50 mV compared to over 100 mV for the aqueous solution growth. Both the resistance and the carrier concentration of the aqueous solution grown nanowires were larger compared to the VLS nanowires. Although the difference in morphology should not influence the resistance and carrier concentration, it would, as mentioned, greatly affect the output voltage. The difference was contributed to the test setup. Both the Hall and the Van der Pauw methods are used for thin films, and although the nanowire growth was dense, it was not a perfect thin film. The output voltage is highly dependant on the c-axis growth of the nanowires [145], and on the c-axis the aqueous solution nanowires were more aligned compared to the VLS method. Thus, the difference in the measured output voltage was attributed to the growth, whereas the difference in resistance and carrier concentration was attributed to the measuring technique.

The above graphs confirm the prediction by Wang et al., that an optimal value for both carrier concentration and resistance exists [59, 93]. The next question was whether it is possible to control these two parameters during growth. If it is possible, the growth can be optimised to fit in the region where the output voltage would be maximum.

The growth of the nanowires could be controlled by changing certain growth parameters, as discussed above. Growth parameters that resulted in nanowires that fall within the golden area, where carrier concentration and resistance led to optimal output voltage, must be found. The problem was that consecutive runs of nanowire growth rarely result in nanowires with identical carrier concentrations, resistance or output voltage. However, certain values of growth parameters did result in better growth, compared to other values.

The aqueous solution method was investigated further, and in particular the growth time. The growth was monitored for 24 hours and measurements were made to determine the carrier concentration, resistance and output voltage.

Figure 5.15 shows the resistance measured for all 24 samples. The resistance was relatively low until the 10-hour mark. Then a sudden increase in resistance was witnessed, reaching a maximum at 17 hours. After the maximum the resistance decreased to the initial low value. From this graph it was clear that the growth time should not fall within the 10 to 24 hour mark, as the resistance was too high. Figure 5.16 shows the carrier concentration during the 24 hour period. The carrier concentration reached a maximum early on, before falling steadily over time. On the fitted graph no clear activity was observed, during the 10 to 17 hour range where the resistance increased. However, upon clearer inspection in that range, the actual measurements did fall under the fitted graph, showing a clear decrease in

carrier concentration and hence an increase in resistance.

The last important graph is shown in Figure 5.17. The output voltage was plotted for the 24 samples. A clear peak was visible in the same range where the carrier concentration peak was witnessed. The sudden increase in carrier concentration, which was not witnessed on the resistance graph, led to an increase in output voltage. The lack of response in the resistance graph was puzzling, as a decrease in resistance was expected. The exact reason for this omission was not clear. From these graphs the optimal growth time would fall in the 5 to 8 hour range.

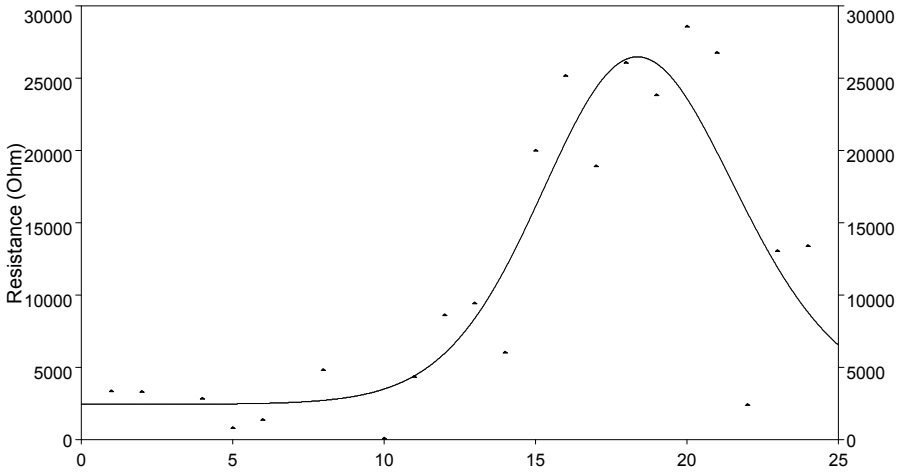

Figure 5.15: Resistance of nanowire samples grown by the aqueous solution method over a 24-hour period. The resistance increases after the 10-hour mark, reaching a maximum at 17 hours before decreasing again.

The graphs show that it was possible to control the carrier concentration and resistance to obtain a higher output voltage. Only the growth time of the aqueous solution was considered. Future work could look into the other parameters to find an area where the output voltage is maximised. This work, was accepted by Micro Nano Systems Letters for publication in 2013 [132].

The above results confirmed that the aqueous solution growth on average resulted in nanowires that generated higher output voltages compared to the VLS method. For this reason, only the aqueous solution method was considered for further optimisation. The one parameter at a time optimisation did not take into account the affect that a combination of the effects had on the nanowire growth. In order to investigate this a different optimisation technique was required.

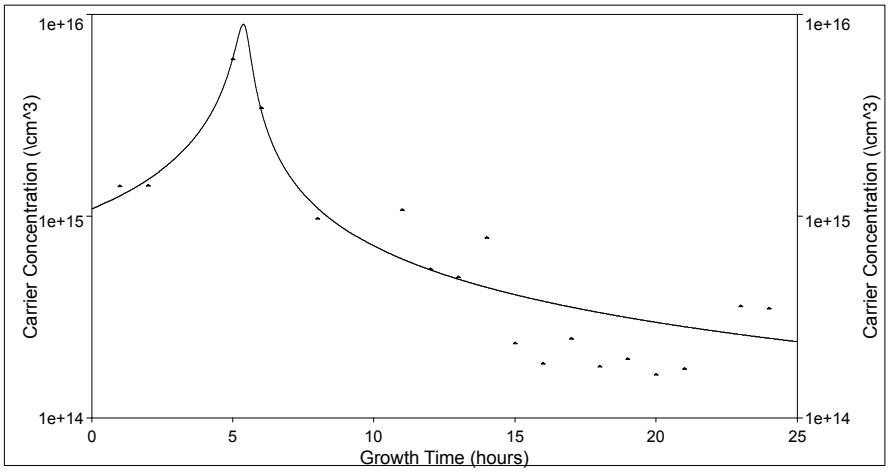

Figure 5.16: Carrier concentration of nanowire samples grown via the aqueous solution method over a 24-hour period. A peak is visible after 5 hours, but no activity is present on the graph where the resistance increased. The actual values do, however, decrease but the fitted graph does not.

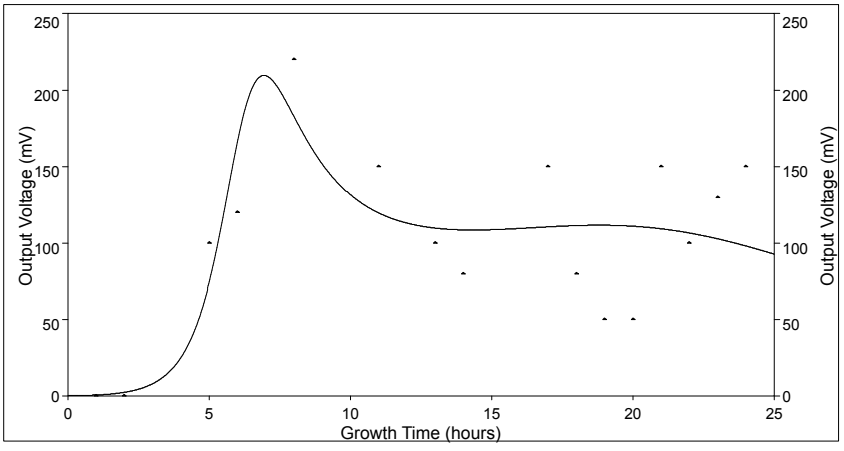

Figure 5.17: Measured output voltage of nanowire samples grown by the aqueous solution method over a 24-hour period. A peak is visible in the carrier concentration at around the 5-hour mark.

5.4 Design of experiments

Design of experiments (DoE) was used to further optimise the aqueous solution growth. It was used to investigate the effect a combination of two or more parameters had on the output parameter.

The DoE was broken down into seven steps. The first four steps were simply the choice of parameters and design, which was discussed in Chapter 3. The fifth step involvesd performing the experiment. Figure 5.18 shows the experimental setup. This table shows all the parameters, with minimum and maximum values, as used during the DoE. The last two columns show the measured output voltage of each run.

Select	Std	Run	Factor 1 A:Temperature C	Factor 2 B:Growth Time h	Factor 3 C:Concentration mM	Factor 4 D:Ratio	Response 1 Output Voltage1 mV	Response 2 Output Voltage2 mV
	13	1	100.00	7.00	30.00	1.25	200	200
	15	2	100.00	8.00	30.00	1.25	120	120
	8	3	110.00	8.00	30.00	1.00	60	80
	14	4	110.00	7.00	30.00	1.25	160	120
	5	5	100.00	7.00	30.00	1.00	40	160
	9	6	100.00	7.00	20.00	1.25	320	160
	16	7	110.00	8.00	30.00	1.25	180	140
	6	8	110.00	7.00	30.00	1.00	100	100
	4	9	110.00	8.00	20.00	1.00	220	120
	1	10	100.00	7.00	20.00	1.00	110	160
	10	11	110.00	7.00	20.00	1.25	100	100
	11	12	100.00	8.00	20.00	1.25	180	100
	3	13	100.00	8.00	20.00	1.00	110	120
	12	14	110.00	8.00	20.00	1.25	100	60
	7	15	100.00	8.00	30.00	1.00	100	150
	2	16	110.00	7.00	20.00	1.00	150	200

Figure 5.18: Design of experiments setup. All the parameters with their minimum and maximum values are shown.

The order in which the nanowires were grown was randomised. This was done to minimise parameters that were not directly controllable by the experimenter. Each run was performed twice to check for repeatability. The growth temperature was higher than previously mentioned, however, because the temperature dial on the oven and the actual temperature differed by about 15°C. The given temperature was the value set on the oven and not the actual, measured temperature of 85 to 95°C.

Each run was performed twice, and the output voltage measured for each run. The output voltage was then loaded into the table. Step six of DoE, statistical analysis of the data, was performed using StatEase [120], a software package designed for DoE data interpretation.

Figure 5.19 gives an overview of the experiment. It gives the minimum and maximum values for the output voltage, the mean and the standard deviation. On average, for the first run the output voltage was 140 mV, and 130 mV for the second run. The standard deviation for the first run was very high at almost 70 mV, compared to 40 mV for the second run. This data already shows that repeatability was a big problem. Each parameter was asigned a number, from A to D for the input parameters, and $Y1$ and $Y2$ for the output parameters.

Design Summary

Study Type	Factorial	**Runs**	16
Design Type	2 Level Factorial	**Blocks**	No Blocks
Center Point	0		
Design Mode	4FI	**Build Time (r**	2.33

Factor	Name	Units	Type	Subtype	Minimum	Maximum	Coded	Values	Mean	Std. Dev.
A	Temperature	C	Numeric	Continuous	100.00	110.00	-1.000=100.00	1.000=110.00	105.00	5.00
B	Growth Time	h	Numeric	Continuous	7.00	8.00	-1.000=7.00	1.000=8.00	7.50	0.50
C	Concentration	mM	Numeric	Continuous	20.00	30.00	-1.000=20.00	1.000=30.00	25.00	5.00
D	Ratio		Numeric	Continuous	1.00	1.25	-1.000=1.00	1.000=1.25	1.13	0.13

Response	Name	Units	Obs	Analysis	Minimum	Maximum	Mean	Std. Dev.	Ratio	Trans	Model
Y1	Output Voltage	mV	16	Factorial	40	320	140.625	68.8446	8	None	Mean
Y2	Output Voltage	mV	16	Factorial	60	200	130.625	39.5759	3.33333	None	R2FI

Figure 5.19: Overview of the results of the design of experiments, including all parameters and results with extra statistical data. The average output voltage for the first run was 140 mV and 130 mV for the second run.

Figure 5.20 shows half normal plots for the two runs. The half normal plot was constructed by estimating the weight of an effect and/or interaction, and also included the relative rank to other effects and interactions (least squares estimation). The plot then shows to what extent each parameter changes the output relative to the mean value [146, 147].

Factors that have a large effect on the output appear in the top right corner of the half-normal plots. As the effect lessened, the parameter moved down to the bottom left corner. Points below the solid line represent points that were part of the model, and points above the line were considered noise, or not relevant. The software selected the parameters and interactions that had the biggest influence on the output as shown in Figure 5.20.

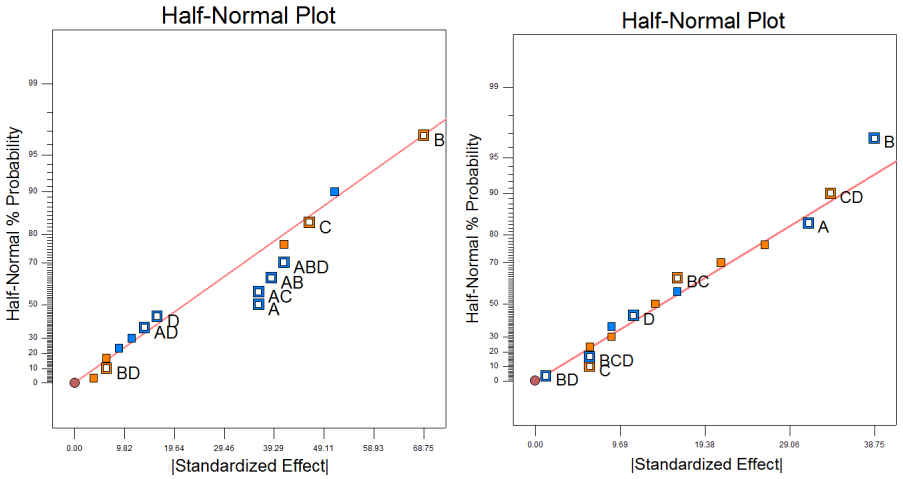

Figure 5.20: Half normal plots of the (a) first run, and (b) second run of the DoE. The points below the graph form part of the model, where points above the graph are considered noise. All the main factors were included in both models with different interactions included in the two graphs.

In the first run, shown in Figure 5.20 (a), six points were not added to the model due to the small effect these factors or interaction between factors had on the output. As expected, the four main factors were present. All the interactions with the temperature were also included in the model, as well as the growth time with concentration interaction.

The second run, shown in Figure 5.20 (b), had a different set of points that form the model. Although exactly the same experiment was performed, certain parameters beyond the control of the experimenter influenced the output. These parameters were not part of the model, but rather interact with factors and influenced the effect these factors had on the output. Again, the main factors were part of the model, but this time none of the temperature interactions were involved in the model. Rather the growth time, concentration and HMTA ratio were involved. Again, this result showed the low repeatability of the experiments.

The software calculated the importance of each factor and/or the interaction between factors by calculating the estimated effect (EE). Each input factor was denoted by an uppercase letter and the interaction of factors was denoted by a string of uppercase letters. Factor A, in this case, was the temperature and AB was the interaction between the temperature and the growth time. Lower case letters represented the high level of the specific factor during a run [148, 149]. For example, ab would mean that temperature and growth time were at a high level, and the concentration and ratio HMTA were at a low level, or run 9 in Figure 5.18. In order to calculate the EE, the contrast or total effect of each factor and interaction between

factors must be calculated with

$$\begin{aligned} Contrast_A &= (a-1)(b+1)(c+1)(d+1) \text{ or} \\ Contrast_{AB} &= (a-1)(b-1)(c+1)(d+1) \text{ or} \\ Contrast_{BCD} &= (a+1)(b-1)(c-1)(d-1). \end{aligned} \tag{5.4.1}$$

When multiplying the brackets out, the end equation will have a ± 1 at the end. This relates to all the factors at their low level. The contrast was calculated by substituting the output value, or the sum of the output values if there was more than one, for each of the given states. It is important to note that ab is not necessarily equal to $a \times b$. In other words, the above equations should be multiplied out and then substituted.

$$\begin{aligned} Contrast_A &= abcd + abc + abd + ab + acd + ac + ad + a - \\ &\quad bcd - bc - bd - b - cd - c - d - 1 \\ &= 320 + 140 + 160 + 340 + 280 + 200 + 200 + 350 - \\ &\quad 240 - 250 - 280 - 230 - 400 - 200 - 480 - 270 \\ &= -360. \end{aligned} \tag{5.4.2}$$

Next, the sum of squares (SS) was calculated. The SS gives an indication of the variance caused in the output due to a change in the input factors

$$\begin{aligned} SS_A &= \frac{Contrast_A^2}{n2^n} \\ &= 16200. \end{aligned} \tag{5.4.3}$$

where n is the number of runs performed. In this case $n = 2$. Lastly, the estimated effect can be calculated as

$$\begin{aligned} EE_A &= \frac{1}{8} \times n \times Contrast_A \\ &= -90. \end{aligned} \tag{5.4.4}$$

These numbers, in themselves, do not tell us a lot about the experiment. On the other hand, calculating the *contrast*, *SS* and *EE* of all the factors and combination of factors would reveal important details regarding the experiment. Software was

used to calculate and interpret the various parameters. The software calculates all the data by using only the important factors, as chosen in the half normal plot. Figure 5.21 shows the results for the first run of the experiment.

Response 1 Output Voltage1

ANOVA for selected factorial model

Analysis of variance table [Partial sum of squares - Type III]

Source	Sum of Squares	df	Mean Square	F Value	p-value Prob > F
Model	49606.25	9	5511.81	1.54	0.3089
A-Temperature	*756.25*	*1*	*756.25*	*0.21*	*0.6620*
B-Growth Time	*756.25*	*1*	*756.25*	*0.21*	*0.6620*
C-Concentration	*6806.25*	*1*	*6806.25*	*1.90*	*0.2172*
D-Ratio	*13806.25*	*1*	*13806.25*	*3.86*	*0.0972*
AB	*2756.25*	*1*	*2756.25*	*0.77*	*0.4141*
AC	*2256.25*	*1*	*2256.25*	*0.63*	*0.4576*
AD	*12656.25*	*1*	*12656.25*	*3.53*	*0.1092*
BD	*5256.25*	*1*	*5256.25*	*1.47*	*0.2713*
ABD	*4556.25*	*1*	*4556.25*	*1.27*	*0.3024*
Residual	21487.50	6	3581.25		
Cor Total	71093.75	15			

Figure 5.21: Resulting data from the first run of the DoE. The calculated data was used to identify the important parameters that influenced growth the most. This was done with the *Prob* > *F* value, where low values indicate important parameters.

The results shown consist of nine factors only and not all 15. This had a noticeable effect on the values which were subsequently calculated. The $Prob > F$ value was the probability of the given response remaining the same with the specific parameter randomised. Thus, if the parameter was changed to some random value, what was the probability that the responseldoudl be the same. The parameter was randomised within the specific minimum and maximum values for that parameter.

From the results, the temperature did not seem to have a significant influence on growth. There was a 66% chance that the response would be the same with the temperature chosen as a random value between the mimimum and maximum values. The same applied for the growth time. The concentration and ratio of materials were more significant, as the response had a small chance of remaining the same if these values were changed. The interaction between the parameters was also more significant than temperature and growth separately. These results clearly

showed that indivdual parameters might have a lesser effect on the response than a combination of two or more parameters.

The results for the second run were very similar to the ones shown for the first run. From these results the important parameters could be summarised. Table 5.3 shows the parameters from most important to least important. As mentioned, the percentage is an indication of the probability that, if the parameter was changed to a random value within the specific range, the output would be identical. The lower the probability, the more significant the parameter.

Table 5.3: Summary of the most important factors than influence the measured output voltage of the nanowires. A lower *Prob > F* indicates a higher importance.

Parameter	***Prob > F***
Ratio	10%
Temperature and ratio	11%
Concentration	22%
Growth time and ratio	27%
Growth temperature, growth time and ratio	30%
Growth temperature and growth time	41%
Growth temperature and concentration	46%
Growth temperature	66%
Growth time	66%

The low repeatability meant that each device had to be tested in order to characterise its performance. A nanogenerator manufactured with identical growth parameters would not necessarily result in similar voltage output measurements. This meant larger amounts of nanowires must be grown, because a certian percentage will have lower performance compared to the rest.

The problem with the results shown in Table 5.3 was that there was no indication as to where the optimal values were. A change in the ratio between the materials would have a big influence on the output voltage, so the big question was where, within the specific range, the optimal value was? Model graphs were used to determine the optimal value for each parameter.

A model graph shows the dependence of two factors at specific values of the other factors. In this experiment, there were only four factors, thus the model graph showed the two factors at specific values of the remaining two factors. In all the model graphs the y-axis was the output factor, or the output voltage in this case. The x-axis was chosen as one of the four growth parameters. Two graphs were plotted, a black line which represented a second parameter at the low level and a

red line at the high level. The remaining two parameters were kept constant for each graph.

In Figure 5.22 the growth temperature was on the x-axis and the two lines represents the growth time. Figure 5.22 (a) was at a concentration of 20 mM and (b) at 30 mM and the ratio was kept at 1:1. At a higher concentration, neither the growth temperature nor growth time had a considerable effect on the output voltage. At a lower concentration and shorter growth time the voltage dropped as the temperature increased. No real effect was observed at a longer growth time.

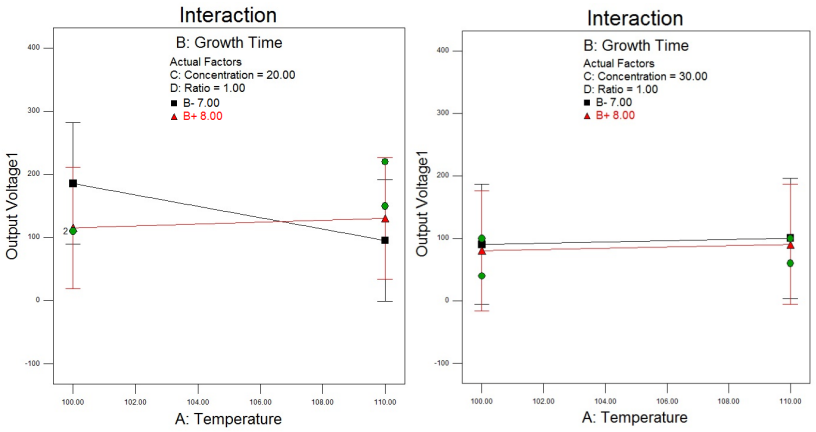

Figure 5.22: Model graph showing temperature and growth time at a concentration of (a) 20 mM and (b) 30 mM at a constant ratio of 1:1. Little or no effect was witnessed at the higher concentration in (b), with the shorter growth time decreasing with an increase in temperature in (a).

Figure 5.23 again shows the temperature on the x-axis, with concentration of 20 mM (black) and 30 mM (red) for 7 hours and 8 hours respectively. The same results were observed as in Figure 5.22, where the higher concentration had a limited response to a change in either temperature or growth time. The only real effect was at a shorter growth time and lower concentration. Again, as the temperature increased, the output voltage decreased.

The last temperature model graph is shown in Figure 5.24. The graph shows the growth time and concentration at 100°C and at 110°C respectively, at a constant ratio of 1:1. Once again, at higher concentration (red lines), limited to no change was observed as the other parameters changed. The lower concentration did however change as the growth time increased. In Figure 5.24 (a), it decreased at the lower temperature and in (b) it increased at a higher temperature, as the growth time increased.

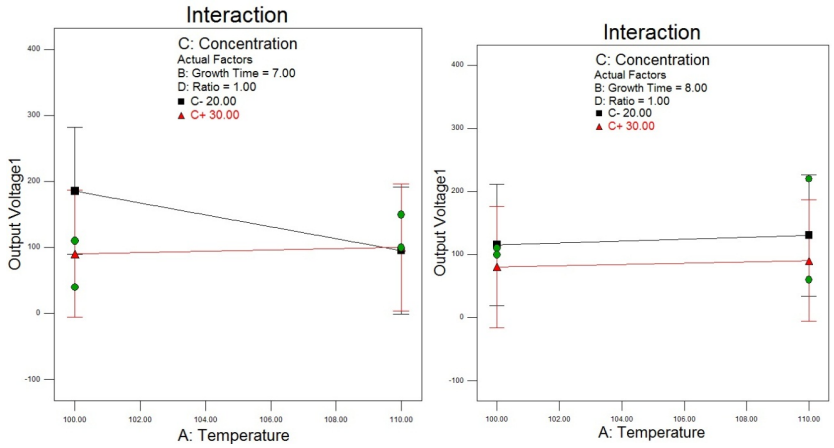

Figure 5.23: Model graph showing temperature and concentration for (a) 7 hours and (b) 8 hours at a constant ratio of 1:1. At a longer growth time in (b) no change was witnessed and in (a), at a lower concentration, the voltage dropped as the temperature increased.

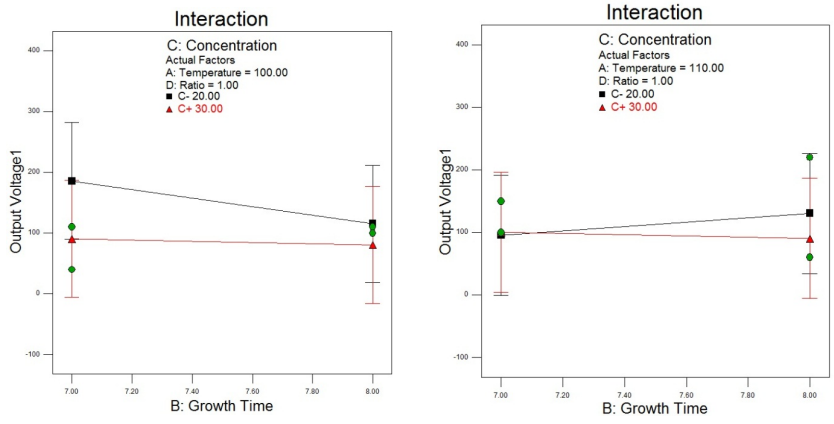

Figure 5.24: Model graph showing growth time and concentration at (a) 100°C, and (b) 110°C hours at a constant ratio of 1:1. In (a) and (b) the higher concentration shows no change. In (a) the voltage decreased with an increase in growth time and in (b) the opposite is witnessed.

From the model graphs the final optimisation of the growth parameters was done. All the graphs showed that the higher concentration solution was less sensitive to changes in the other parameters. For this reason, the higher concentration was used. At a higher growth temperature the output voltage was slightly increased in all the graphs for the higher concentration, and hence the higher growth temperature was used. The growth time had no effect on the output voltage and hence the shorter, seven-hour time was chosen.

Not all the model graphs were shown. The ratio at the higher concentration also had a very small effect and the 1:1 ratio, on average, gave higher output voltage. Table 5.4 shows the final values used for the nanowire growth with the aqueous solution method. This was also the last step in the DoE method, i.e. drawing conclusions about the data and finding the optimal values.

Table 5.4: Final optimised values for the aqueous solution growth as obtained with the DoE method.

Parameter	Importance
Temperature	110°C
Growth time	7 hours
Concentration	30 mM
Ratio	1:1

The DoE method was successfully used to optimise the growth parameters for the aqueous solution method. The parameters were optimised individually and the interactions between the parameters were taken into account. The main problem with the DoE method was that, if the original range for each parameter was not optimal, the results will give optimal values within a non-optimal range. That was why the one parameter at a time approach was used before DoE to ensure an optimal range for all the parameters. Optimal values for all growth parameters were now intact. From this point onwards, all growth will be done with these optimal values.

With optimal growth parameters the nanogenerator could be constructed. This would ensure that the output voltage of the nanogenerator was optimised with regard to the growth parameters.

5.5 Conclusion

ZnO nanowire growth was successfully optimised with respect to output voltage. Two techniques were used to find these optimal values, namely one-parameter at a

time and design of experiments. Moreover, two growth methods were investigated, VLS and aqueous solution. During the one parameter at a time optimisation it was found that the aqueous solution method yielded nanowires that produce, on average, higher output voltages, when compared to the VLS nanowires. For this reason, only the aqueous solution method was further optimised using the DoE method. The aqueous solution growth parameters were optimised further with the DoE. With the aid of the statistical method, optimal growth parameters were found that will ensure good quality nanowires.

Two other important parameters were measured, namely carrier concentration and resistance. Wang et al. predicted an optimal range for these two values, where the output voltage would be at a maximum. This theoretical prediction was tested with the aid of the Hall and Van der Pauw methods. Although both methods were designed for thin film, the results obtained did fall within the range predicted by Wang et al.

With optimal growth parameters, the nanogenerator could be manufactured knowing the nanowires would be of good quality. The aqueous solution method was therefore used exclusively to manufacture the nanogenerator.

Chapter 6

Zinc oxide nanogenerator manufacturing and optimisation

The main part of this study concentrated on the development and optimisation of a ZnO nanowire based nanogenerator. ZnO is a piezoelectric material that converts any mechanical force that is applied to the material to an electrical signal, as discussed in Chapter 2. The working mechanism and a mathematical description of the piezoelectric effect was derived in Chapter 2, with simulations confirming the theory shown in Chapter 4. The nanowires were grown on various substrates, mainly using a wet chemical route. The growth took place at temperatures below 100°C and various types of substrate could thus be used. The growth of the nanowires was also discussed in Chapter 2. The nanowire growth optimisation for maximum voltage output was discussed in Chapter 5. Two different growth methods were used and optimised and the wet chemical growth resulted in nanowire growth with the highest output voltage. The nanowires were then used to manufacture a nanogenerator, a device that generates electricity from a mechanical force.

The manufacturing and optimisation of the nanogenerator is discussed in this chapter. The nanogenerator was first manufactured on silicon (Si) wafers, resulting in a solid nanogenerator. Various manufacturing approaches were taken to optimise the output voltage of the nanogenerator, all of which are discussed in the paragraphs that follow. An improved nanogenerator was then manufactured on a flexible substrate. The flexible nanogenerator can achieve higher output voltages compared to the solid nanogenerator. The influence of the different stages of manufacturing on the output voltage, was investigated and discussed. The two nanogenerators were compared to see why the flexible nanogenerator outperforms the solid nanogenerator. The last step involves optimising the manufacturing of the nanogenerator. Optimisation was done by adding additional steps and addi-

tional materials during the manufacturing process. These optimisation techniques are discussed in detail.

6.1 Silicon nanogenerator

The silicon-based nanogenerator was manufactured on Si (100) wafers. The Si (100) wafers are rigid discs, 90 mm in diameter, with a crystal orientation given by the Miller index of (100). Appendix A gives more details about crystallography and the Miller index. The specific wafers used in this project were 250 to 300 μm thick, doped with phosphor for n-type semiconductor properties and single side polished. Various thicknesses were available, but the wafers were cut into smaller pieces and hence a too thick wafer would be difficult to cut. The doping of the wafer was not important, as the wafer only acts as a substrate and none of the substrate properties were important for this application. The wafers were cut from a larger piece and either both sides or a single side could be polished after the cut. As the nanowires were only be grown on one side, a single polished side was sufficient.

The last important parameter was the crystal orientation of the wafer. The (100) direction was chosen, because the resulting lattice mismatch between the wafer and the nanowires was less [150]. The preferred growth direction of the nanowires was along the (0001) direction and only a small lattice mismatch exists for the nanowires to grow in this direction on the Si (100) wafers [150, 151]. Si wafers with different orientation could be used, but due to large lattice mismatches the growth would not be as good as on Si (100) and might even result in the growth of other nanostructures.

The manufacture of the solid nanogenerator started with the cutting of the Si (100) wafers. The wafers were cut into 10 mm by 10 mm substrates, as described in Chapter 3. Next the substrates were cleaned and the various pretreatment layers were deposited. Although the lattice mismatch was small, a mismatch still existed. This mismatch caused the nanowires to grow in undesired directions and also resulted in the growth of structures other than nanowires. Figure 6.1 shows a SEM image of ZnO nanowires grown on a clean Si (100) substrate. The growth was sparse and the nanowires were bigger than 100 nm and were also not aligned, but rather grew in various directions.

To solve this problem, an additional buffer layer was required to buffer the lattice mismatch between the Si (100) and the ZnO nanowire, as explained in Chapter 5. The best buffer layer was found to be ZnO, as the lattice mismatch between ZnO and the Si (100) was small, and the lattice mismatch between the ZnO layer and

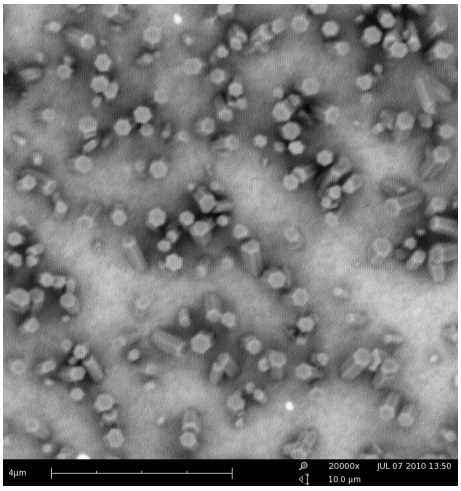

Figure 6.1: SEM images of ZnO nanowires grown on clean Si (100) substrate. Only a few nanowires are visible with diameters larger that 100 nm and random growth direction.

ZnO nanowires was negligible.

The ZnO layer was deposited onto the substrate with ICM sputtering, as explained in Chapter 3. After the sputtering of the seed layer, the substrate was placed in the aqueous solution for nanowire growth. The growth process was discussed in Chapter 2 and the optimisation of the growth parameters in Chapter 5. After growth, the substrate was rinsed and dried, completing the first step of the nanogenerator manufacturing process.

The nanogenerator converts mechanical force to an electrical signal. To do this the nanowires must be bent by an applied force. The manufactured nanogenerator should thus facilitate the bending of the nanowires.

The first solution was to take a gold wire and move it across the substrate surface. The gold wire will then touch and bend the ZnO nanowires resulting in an output voltage. However, the electrode or gold wire needs a work function higher than the electron affinity of ZnO, as explained in Chapters 2 and 5. The substrate was placed on a xy-stage and the gold wire was attached to a z-stage. The gold wire was then lowered until contact was made between the nanowire and the substrate. The stage had a minimum step size of about 1 μm, about the length of the nanowires. This meant that when contact was made, the gold wire touched the tips of the nanowires, and one step down, it was in contact with the sputtered ZnO layer. The xy-stage was then moved around and the output voltage was observed. Figure 6.2 shows the measured output voltage as the xy-stage was moved. The signal was extremely noisy and only three peaks were above 50 mV, which was attributed to the nanogenerator. As the gold wire was moved, it bent the nanowires, and

while still in contact, the piezoelectric field generated an electric potential across the metal-semiconductor interface and an output voltage was observed. The low magnitude was due to the large contact resistance between the gold wire and the nanowires. The gold wire was also moved quickly (the control box does not specify the exact speed) limiting the amount of bending and the contact between the gold wire and the nanowires.

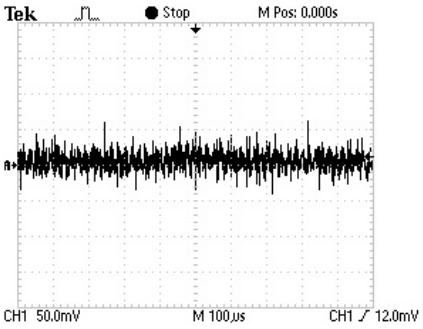

Figure 6.2: Measured output voltage of the solid nanogenerator with a gold wire as electrode. The three peaks above 50 mV were attributed to the nanogenerator. The measured voltage was not sufficient to be used in practical applications.

This method was not practical or very successful as the movement of the gold wire to the exact position limits the application, and the electrode should be put in place without the aid of an expensive stage. The measured output voltage was also very small and could not be used for anything practical. The other problem was that if the gold wire was in contact with the substrate, no voltage was observed. This was due to the short circuit that was created when the nanowires were also in contact with the gold wire. The gold wire touched both the nanowires and the substrate, effectively shorting out the nanowires.

Therefore, a different solution was required that bends more than a few of nanowires at a time. The electrode should also be fixed to the nanogenerator, making it a closed package.

The problem experienced here was the accurate measurement of the nanowire lengths. Tilted scanning electron microscope (SEM) images, or cross-sectional images, did help to measure the lengths, but were not accurate as the maximum magnification was not enough to make small adjustments to the measuring tool. It was thus necessary to accurately determine the average length of the nanowires. Accordingly, atomic force micoroscopy (AFM) was used to measure the length. The nanowires were grown and photoresist was used to cover a small area next to the growth. After the growth the photoresist was removed leaving a clean Si (100) area

exposed. AFM images were then taken, starting from the exposed Si (100) area, and then moving over to the nanowires. Figure 6.3 shows the images resulting from the AFM and SEM measurements. From these figures the average length was found to be 2.6 μm. An AFM scan was done extremely slowly to ensure accurate measurements. A single scan took over five hours to complete, resulting in good, accurate images.

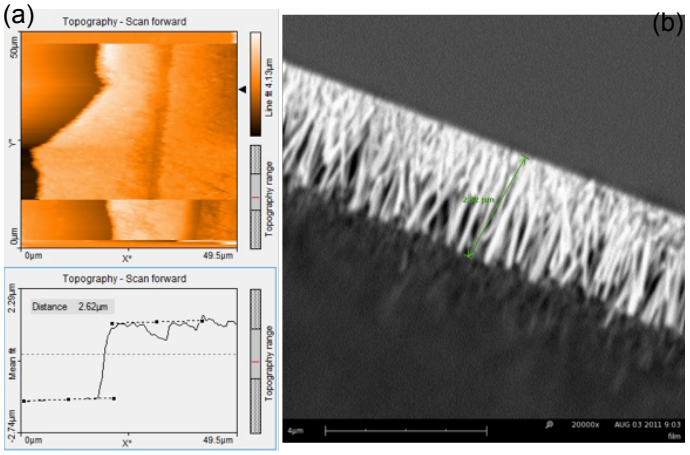

Figure 6.3: Height of the ZnO nanowires (a) measured by the AFM and (b) measured with the SEM. Both images indicate a length of about 2.6 μm.

Ideally, the electrode should be placed about 2.5 μm above the substrate level to ensure good contact between the nanowires and the electrode. The problem was finding a structure that was exactly 2.5 μm in height to place on the substrate before the electrode was put in place.

The easiest solution was to use photoresist. Photoresist is a chemical used during lithography to expose a specific pattern on a material. Photoresist is a liquid that, when backed, gets harder. The photoresist was applied to the substrate by spin coating. Thus, the photoresist was dropped onto the substrate and the substrate was then spun at high speed to distribute the photoresist evenly across the substrate surface. The thickness of the photoresist depended on the speed and time at which the substrate was spun. After baking, a 2.5 μm layer of photoresist, was spun at 1100 rpm for 10 seconds.

Figure 6.4 shows one approach to the manufacturing of the nanogenerator. Photoresist was spun onto two Si (100) substrates, 2.5 μm in height, a few hundred nanometers lower that the nanowire length. The gold electrode was made a bit bigger than the nanowire substrate and placed on top of the two supports, as illus-

trated in Figure 6.4. A heavy weight was placed on top of the gold electrode and silicone-based glue was used to attach the gold electrode to the nanowire substrate. Silicone-based glue allows for movement of either substrate while still holding the entire structure intact.

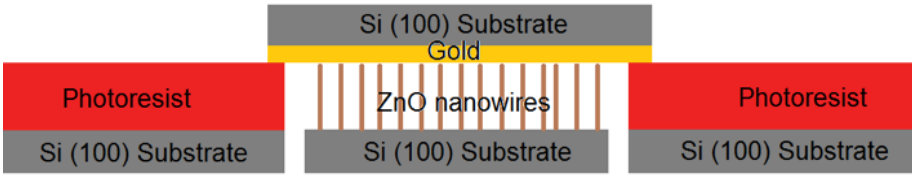

Figure 6.4: Diagram of one method for manufacturing the solid nanogenerator. Two support structures are used to position the gold electrode at the desired height above the nanowire substrate.

Figure 6.5 shows the measured output voltage of a nanogenerator manufactured as described above. The output voltage is extremely small, with maximum peaks at 80 mV and average peaks at less than 50 mV. The output voltage was measured as the force was applied to either of the two substrates. The applied force caused either substrate to move, bending the nanowires against the gold electrode and an output voltage was observed. This method yielded higher output voltages compared to the gold wire method, but the output voltage was still too low for practical applications.

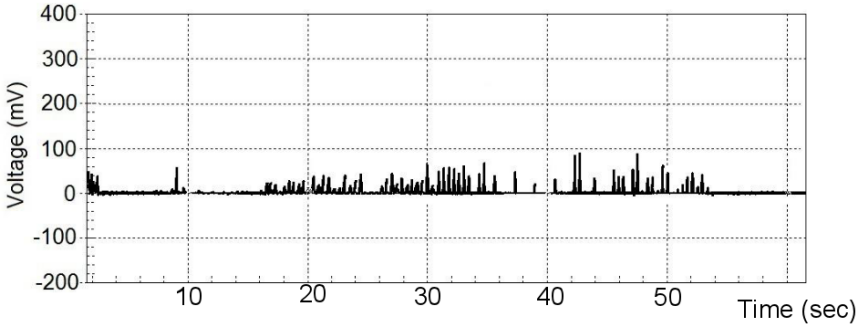

Figure 6.5: Measured output voltage of a nanogenerator manufactured by securing the gold electrode on top of the nanowires. Voltage peaks just below 100 mV are present, but the average voltage output was still too low.

The above method had another big problem, namely repeatability. Over 70 devices were manufactured using this method and fewer than 20 gave an output

voltage when a force was applied. The magnitude of the force did have a considerable influence on the output voltage; the output voltage remained zero until a large force was applied.

The reason for the poor performance was investigated. The finished device was cut in half to see if the nanowires and gold electrode were in contact. Figure 6.6 shows an SEM image of a typical device. A clear gap exists between the nanowires (bottom left) and the gold electrode (top right). This gap, over 40 μm in length, means a considerable force is required to compress the silicone glue to make contact between the two substrates.

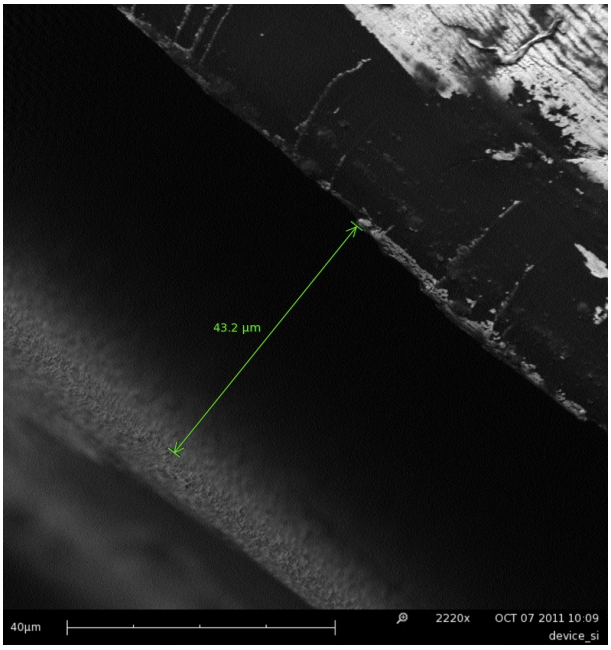

Figure 6.6: SEM image of the solid nanogenerator, cut in half, showing the nanowires on the bottom and gold electrode on top, with a clear gap in between.

The big question is: Why did this gap exist? The photoresist supports were the same height as the nanowires and the gold electrode was placed on top , with a weight placed on the electrode during the glue step to ensure contact. The first possibility was that the glue was too thick and forced the electrode with the weight to lift slightly and break the contact. Different approaches to the glue step were investigated. Different glues were tried, the glue was applied differently, but all with no success.

A closer look at the specifications of the Si (100) wafers provided the answer. The thickness of the wafers are 250 to 300 μm. This 50 μm difference in height was the reason for the lack of contact between the nanowires and the electrode. For

example, if the nanowires were grown on a substrate with a thickness of 250 μm and the photoresist supports were spun onto a substrate with thickness of 280 μm, there will always be a 30 μm difference in height. Even a single wafer can have height differences, which makes this method very unlikely to succeed and explains the low repeatability that was observed.

Prepositioning if the gold electrode was difficult due to the small scale of the nanogenerator. Therefore, a different approach was needed where the electrode was simply placed on top of the nanowires and then secured.

Consequently, the electrode was placed on top of the nanowire substrate, and then the silicone glue applied all around both substrates. A small weight was again placed on one of the substrates to ensure contact, while the glue dried. A second approach was to place the two substrates on top of each other and then secure them by taping them together with sellotape. Both these methods eliminate the problem of the varying thickness of the substrates.

The output voltage of these methods did not improve beyond that of the first method. Figure 6.7 shows the output voltage of a device manufactured using sellotape. The output voltage is slightly higher than the previous case, but not much.

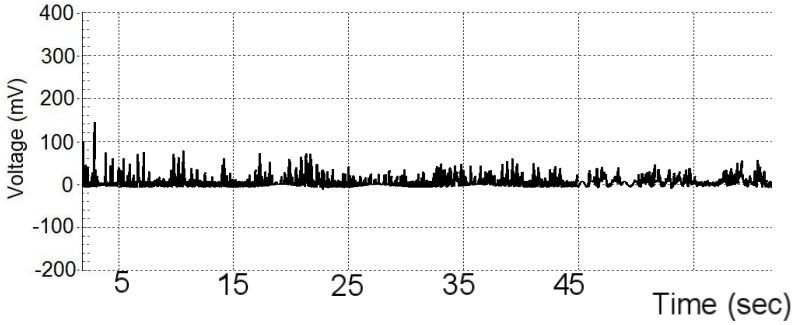

Figure 6.7: Measured output voltage of the solid nanogenerator manufactured by securing the two substrates placed on top of each other with sellotape. The measured output voltage was raised from the previous case, but the average voltage was still too low.

Both manufactured nanogenerators worked and manufacturing was more repeatable, reaching 50%. Although the repeatability was higher, it was still not good enough. The problem with both methods was still the contact between the two electrodes. In the sellotape method, the sellotape glue was not strong enough to ensure proper contact between the two substrates and, after a couple of minutes of applying and removing a force to the nanogenerator, the sellotape would come loose. Another problem affecting all the methods, including the first method, was contamination of the substrates. Figure 6.8 shows the contamination of the

substrate. During the transportation, storage and sputtering of the thin film dust and/or other particles collected on the surface of the substrate. These particles were orders of magnitude bigger than the nanowires, and prevented contact between the electrode and the nanowires. Figure 6.8 (b) shows less contamination, as this substrate was handled with more care and was always stored in special containers, limiting the amount of particles that could gather on the surface.

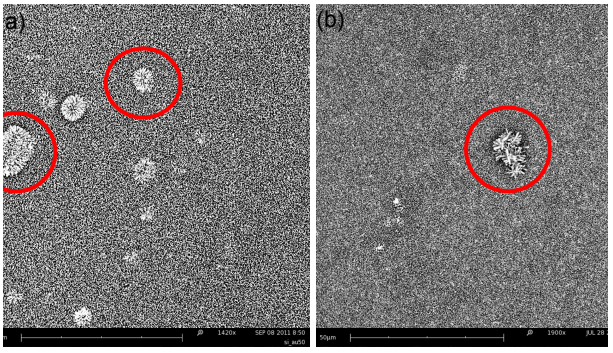

Figure 6.8: SEM images of contamination of substrates where (a) was handeld normally and (b) extra precaution was taken. The contamination was the main reason for the weak contact between the nanowires and electrode.

The main problem still existed however. The contact between the two substrates was difficult to achieve as a result of substrate height variation and contamination of the substrates. The problem was that both substrates were rigid, as illustrated in Figure 6.9. When the substrate was not contaminated, the gold electrode lied perfectly on top of the nanowires, as shown in Figure 6.9 (a). When some sort of contaminant was present however, the substrate did not make contact with all the nanowires, but was rather tilted, and was only in contact with a few nanowires, leading to a lower measured output voltage.

In order to solve this problem a non-flat substrate was used. The Si (100) substrate was again used, but the surface was first scratched to make a number of troughs on the surface before sputtering on the gold layer. A second option was to spin a layer of carbon nanotubes (CNTs) or graphene onto the substrate prior to the sputtering of the gold layer. Figure 6.10 shows the Si (100) substrate where it has been scratched, and in where CNTs have been spin coated on. Both techniques result in a gold electrode surface that was not flat and, hopefully, the contaminants would be less of a problem.

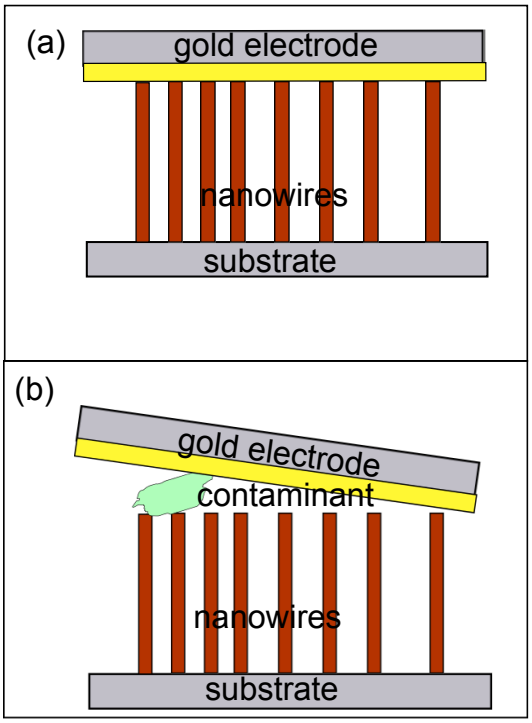

Figure 6.9: Illustration of the solid nanogenerator with (a) no contamination of the substrate and (b) with some sort of contaminant present on the nanowire growth.

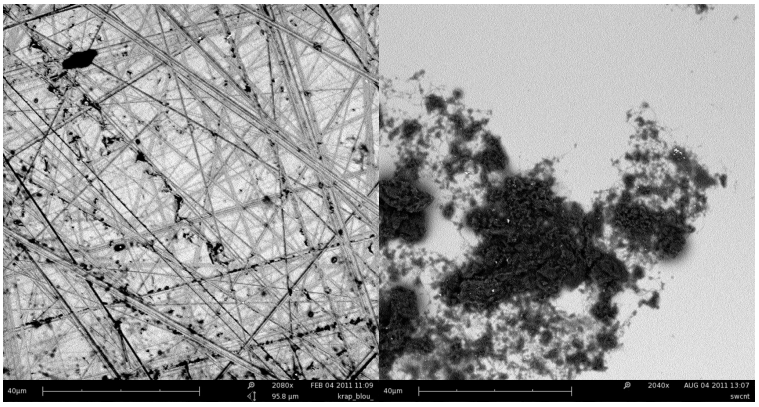

Figure 6.10: SEM images of the Si (100) substrate where (a) the surface has been scratched, and (b) CNTs have been spin coated on before the deposition of the gold layer.

Nevertheless, neither of these methods worked better than any of the previous methods. The measured output voltage was still too low to be practically useful. The main problem was still the connection between the gold electrode and the nanowires.

The best solution that was found was to leave the two substrates separate from one another. Accordingly, the gold electrode was simply placed on top of the nanowires and then moved around backwards and forwards. The moving of the substrate causes the nanowires to bend which, in turn, led to an observable output voltage. The amount of movement that was possible was much larger than any of the previous cases, because there were no restrictions, such as the glue or sellotape, holding the two pieces together.

The output voltage depended largely on the speed of the backwards and forwards movement, as well as the force applied to the gold electrode during the movement. Figure 6.11 shows the measured output voltage when a low force was applied to the electrode during movement. The output voltage has a number of peaks above 100 mV, showing that, even at low forces, this method works better than the previous methods. Figure 6.12 shows the measured output voltage when a larger force was applied during movement of the electrode. Voltage peaks above 200 mV were now observed, with most peaks above 100 mV.

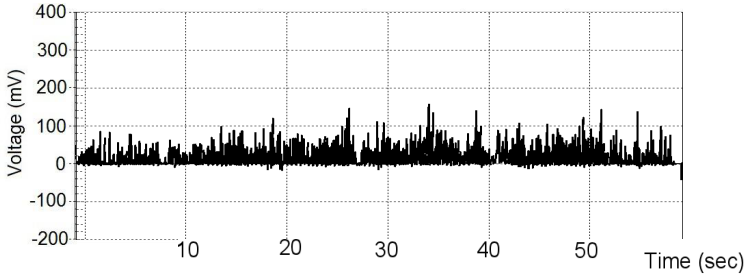

Figure 6.11: Measured output voltage of the solid nanogenerator with a low force (25 g) applied to the gold electrode.

The force was applied by means of different weights. The weight was attached to the gold electrode and then moved forwards and backwards. The weight can then be changed in order to apply a different magnitude force to the nanowires. The first test was performed with a 25 g weight and the second test with a 48 g weight, almost double the force that was applied in the first test. The measured output voltage was also almost double than in the first test, showing a direct relationship between the force applied and the measured output voltage. This direct

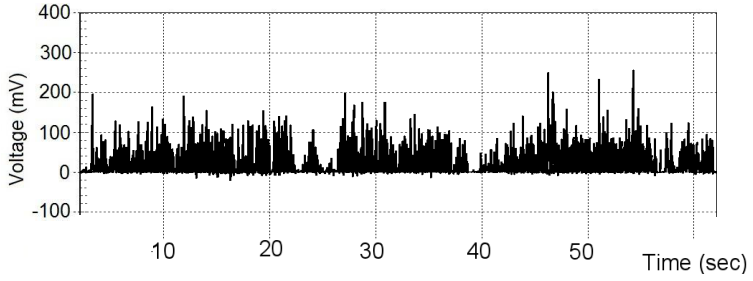

Figure 6.12: Measured output voltage of the solid nanogenerator with a high force (48 g) applied to the gold electrode.

relationship was also shown in Chapters 2 and 4, where the mathematical model and simulations for the nanogenerator respectively, were derived.

The main problem with this method was that the two substrates were separate. Therefore, the two substrates could easily be dislodged and consequently the gold electrode cannot bend the nanowires and no output voltage can be generated. A second problem was that the friction between the two substrates was destructive in that both the gold and the ZnO nanowires were scratched off after a few minutes of movement.

The method above resulted in the highest output voltage from all the methods. However, it was not practically useful as the device was not a complete system, but two separate substrates that move independently. A better solution was still required that would result in even higher output voltages and was a completely integrated device.

6.2 Flexible nanogenerator

The output voltage of the solid nanogenerator was raised from only a couple of millivolts to over 200 mV by using different manufacturing methods. The problem remains, however, that the method that yields the highest output voltage was not an integrated device.

The main problem experienced during the manufacturing was that the two electrodes were usually not in contact. Some contaminants were lodged in between the electrodes, preventing contact or obstructing contact, which led to lower output voltages. Figure 6.9 shows the problem with contamination of either substrate. In order to solve this problem, the gold electrode should be flexible so that it can bend over the contaminant and still make contact with the nanowires.

Figure 6.13 shows a diagram a the nanogenerator manufactured with a flexible electrode. The electrode now bends around the contaminant, losing contact only

over the area where the contaminant lies. This means that a larger percentage of nanowires is in contact with the electrode, which should lead to a higher output voltage.

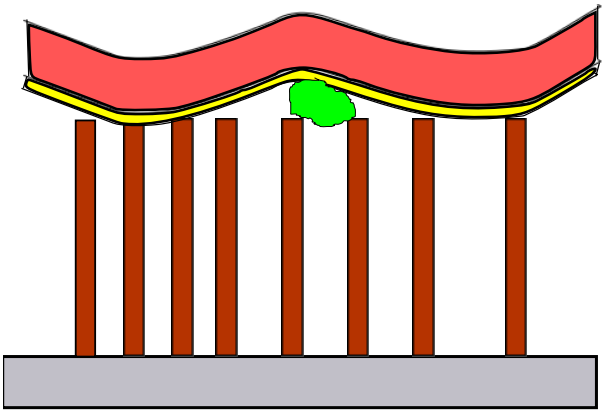

Figure 6.13: Diagram of a nanogenerator manufactured with a flexible electrode. The electrode can bend around the contaminant to ensure better contact.

The solid nanogenerator has another problem: how to bend the nanowires. In order to bend the nanowires the electrode must be moved around. When a solid substrate was used for the electrode, any movement of the electrode caused the nanowires to bent. However, a flexible substrate might just deform a bit and not bend the nanowire enough to generate any output voltage. A second problem is if the force is concentrated on a small area, the flexible electrode might bend too much and only make contact with a small number of nanowires, again leading to a small output voltage. This is illustrated in Figure 6.14.

The problem was that the substrate was solid, and when the force was applied to the substrate and not to the electrode, no output voltage was observed, because nothing was bending the nanowires. A the transition from a solid to a flexible electrode is easy, the substrate for nanowire growth was also replaced with a flexible substrate.

The choice of flexible substrate was considered next. Nanowire growth takes places below 100°C in an aqueous solution. This automatically eliminates any paper-based material, as it will absorb the water and become too fragile. Any thin plastic-based film should be able to withstand the heat and also be flexible enough to be used for both the electrode and the substrate for nanowire growth. After considering various options, Kapton polyimide film was chosen as the best solution [114]. Kapton 500 HN film was chosen largely because it was immediately

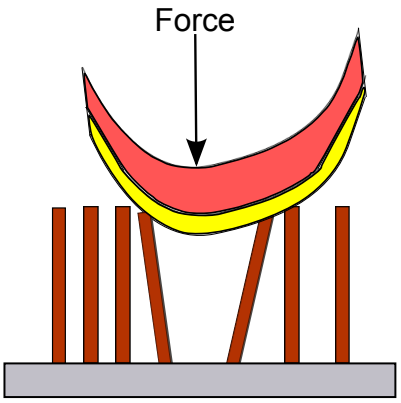

Figure 6.14: Diagram of the nanogenerator manufactured with a flexible electrode when the applied force is concentrated on a small area and the flexible electrode loses contact with the nanowires.

available. Kapton 500 HN film is 125 μm thick, can withstand temperatures of up to 400°C and is extremely flexible [152].

The Kapton film was cut into 15 mm by 20 mm substrates, which were used for both the gold electrode and nanowire growth. The rest of the manufacturing process was the same, from the cleaning of the substrate, to the sputtering of the gold and ZnO layers, to the growth of the nanowires. The nanowire growth looks identical to the growth on the Si (100) substrates. This is due to the same ZnO seed layer being present, which ensures the preferred growth direction is available and no lattice mismatch is present. The polyimide film is not crystalline, hence no lattice mismatch is possible. The adhesion between the layers and the film was a problem, however, and will be discussed later in the chapter. Figure 6.15 (a) - (f) shows typical nanowire growth on the Kapton film. From Figure 6.15 it is clear that the nanowire growth looks identical to that of the Si (100) nanowire growth. However, the nanowires are a bit shorter, at 1.5 μm, compared to over 2 μm for the nanowires on the Si (100).

There was one small difference in the manufacturing process. The solid nanogenerator formed only one Schottky contact, between the nanowires and the gold electrode. This led to voltage peaks in one direction only. The flexible nanogenerator has two gold layers, one on the bottom between the substrate and ZnO layer ,and then the top electrode. This means that two Schottky contacts form on either side of the nanowires and, hence, dual voltage peaks should be observed.

After manufacturing one problem still remained, how to attach the gold electrode on top of the nanowires. The same approaches that were taken for the solid nanogenerator were considered. The electrode was placed on top of the nanowires,

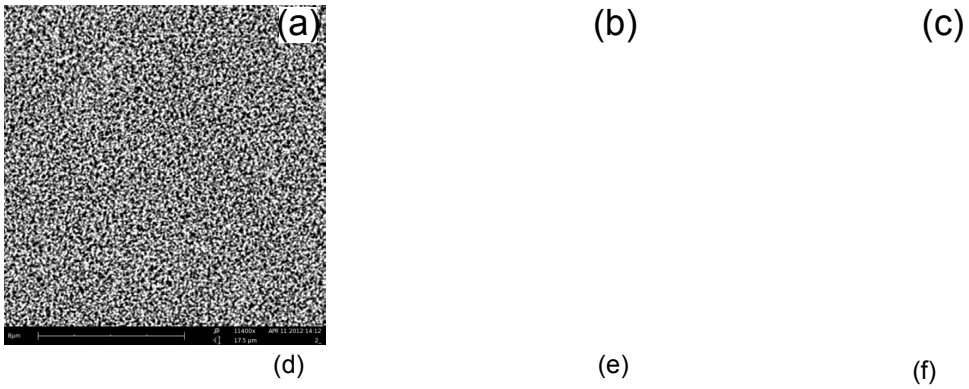

Figure 6.15: SEM images of nanowire growth of the flexible Kapton polyimide film, (a) - (c) top view images at different magnification and (d) -(f) side view images at different magnification.

then silicone glue was used to cover the device and a weight was placed on top while the glue dried, to ensure that contact was not broken. Sellotape was also used agai to secure the two pieces.

As mentioned in Chapter 3, the flexible nanogenerator was tested by bending the film from flat to 90° and releasing it back to flat, as shown in Figure 6.16 (same figure as in Chapter 3). The problem was that the strain exerted on the film causes the silicone glue to tear, thus separating the two substrates, and the same happens to the sellotape. Therefore, neither of these two methods can be used to manufacture the flexible nanogenerator.

One big problem still existed with all the nanogenerators manufactured up to this point, and that is that the contact area between the nanowires and gold electrode was very small. Only the tip of the nanowire is in contact with the electrode, leading to an enormous contact resistance, which was another reason for the small output voltages observed. Ideally, the entire nanowire tip must be covered with gold to ensure proper contact and increase the contact area. This ideal case is illus-

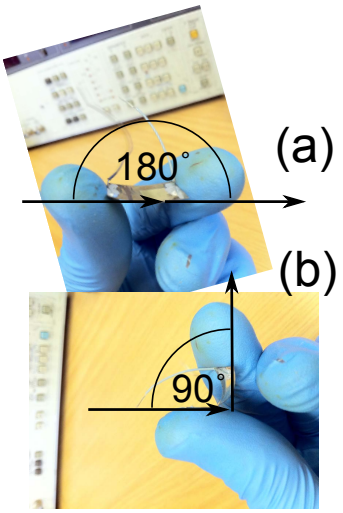

Figure 6.16: The flexible nanogenerator is tested manually by bending it from 180° to 90° and then releasing it back to 180° .

trated in Figure 6.17. In this case, when the film is bent, the nanowires will bend, as the nanowire tips are already in contact with the gold electrode on top, and at the bottom, an output voltage will be observed. The challenge is how to get the gold electrode to float on top, covering just the tips of the nanowires.

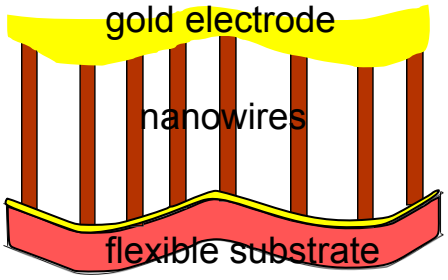

Figure 6.17: Diagram of an ideal nanogenerator manufactured on a flexible substrate with the gold electrode covering the tip of the nanowires.

In order to get the gold electrode to cover the tips of the nanowires, some sort of buffer layer was required. This buffer layer should fill the nanogenerator from the bottom gold electrode all the way to the top, leaving the nanowire tips exposed.

The second gold electrode can then be sputtered onto this buffer layer, covering the nanowire tips and thus completing the nanogenerator manufacturing process.

The buffer layer cannot be conductive, as this will short out all the nanowires and directly connect the two gold electrodes. Moreover, the layer cannot be a solid or a hard material, because the nanogenerator must still be able to bend in order to generate an output voltage. This material should therefore be deformable, flexible and non-conductive.

A perfect candidate is silicone-based glue. The rubbery glue can bend, can be deformed and is not conductive. The only problem is to apply the glue in such a manner that it fills the spaces between the nanowires, exposing only the nanowire tips. Ideally, the buffer material will be applied via sputtering or thermal evaporation. This will ensure that the material fills the spaces between all the nanowires, while the duration of the deposition controls the thickness of the buffer material. When inspecting the substrate with the SEM after the deposition of the buffer layer, the time can be adjusted to deposit just the right amount of buffer material. However, no material exists that can be sputtered or thermally evaporated, which is flexible and non-conductive once deposited.

The only other technique that can be used is to spin the buffer layer on. If the buffer material is in liquid form, it can be spun onto the substrate, and by controlling the speed and duration, the thickness can be controlled. However, the silicon-based glue is not fluid enough to spin onto the substrate. Thus, in order to spin coat the buffer layer onto the substrate, a liquid-based material is required. This material, upon heating should solidify to a degree, but still remain flexible. Photoresist is a liquid that hardens upon heating, but the problem is that it becomes brittle and will not be able to bend without breaking. Therefore, the only solution will be a soft plastic liquid that solidifies when heated.

A suitable solution was PMMA or poly(methyl methacrylate). PMMA is a thermoplastic or polymer that becomes mouldable above a certain temperature [153]. PMMA is a highly viscous liquid and upon heating, it becomes harder. The solidifying temperature for the PMMA used in this study is above 250°C. The PMMA, which was dissolved in water to make it less viscous, was then spun onto the substrate, penetrated between the nanowires and filled the spaces to just leave the tips exposed. The PMMA was then heated, below 250°C, so as not to harden it too much. The absorbed moisture was then removed and the PMMA was transformed to a soft plastic that was bendable and mouldable. This was perfect, as it now added extra stability and protection to the nanogenerator while not affecting its overall performance.

The manufacture of the flexible nanogenerator began by cutting and cleaning

the substrates. Next, the gold layer was sputtered, followed by a ZnO layer. After the deposition of the seed layers the substrate was placed in the aqueous solution for nanowire growth. The growth was explained in detail in Chapter 2, with more details given in Chapter 3, and the optimisation of the growth parameters is discussed in Chapter 5. After the eight hour growth, the substrate was removed and rinsed. PMMA was prepared by using a $\frac{1}{3}$ PMMA and $\frac{2}{3}$ DI-water solution. The PMMA was dripped onto the substrate and was left for 60 seconds to fill the gaps between the nanowires. The substrate was then spun at 6000 rpm for 10 seconds, then placed on a hotplate at 110°C for 50 seconds. While on the hotplate, some of the water evaporated and the PMMA thus hardens a bit. This process was repeated at least five times in order for the PMMA to cover the nanowires but leaving the tips exposed. The second gold layer was then sputtered on top of the PMMA, covering the nanowire tips. Lastly, silverpaste was used to connect wires to the two gold layers, completing the manufacturing process of the flexible nanogenerator. Figure 6.18 shows a diagram of the finished flexible nanogenerator. Figure 6.19 shows the ZnO nanowires after a number of spins of PMMA.

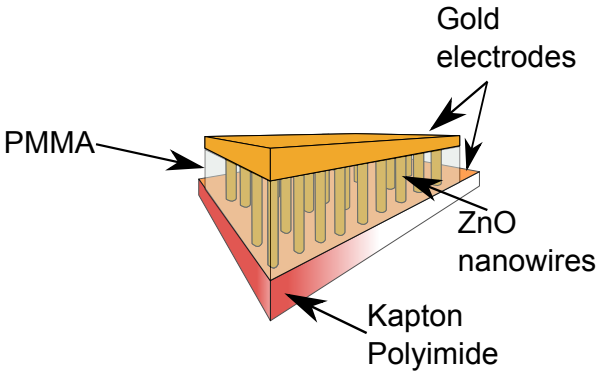

Figure 6.18: Diagram of the manufactured flexible nanogenerator.

Figure 6.20 shows a top-view SEM image of a substrate that has too much PMMA. The lighter areas are exposed nanowire tips and the darker areas the PMMA covering the tips. The gold layer cannot be sputtered onto the PMMA now, as it will only make contact with a few of the nanowire tips. A few nanometres of PMMA have to be removed in order to expose more nanowire tips before the gold layer can be sputtered on.

The removal of PMMA was done by oxygen plasma. Oxygen plasma was created by passing oxygen gas through a high electric field. The ionised oxygen in-

Figure 6.19: SEM image of the ZnO nanowires with PMMA spun onto the substrate. The nanowire tips are still visible, with the PMMA covering the rest.

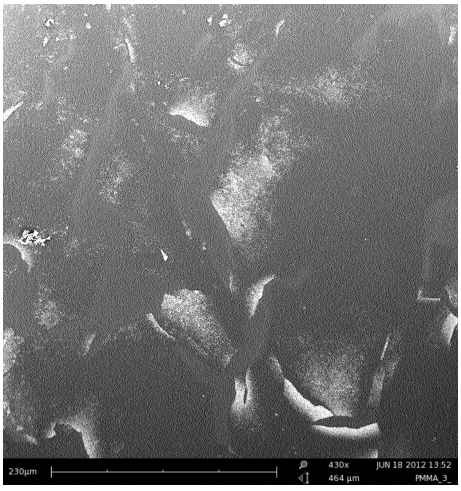

Figure 6.20: SEM image of the ZnO nanowires with PMMA spun onto the substrate and covering the tips in certain areas. A few nanometres of PMMA must be removed before sputtering the second gold layer.

creased the number of electrons, creating a plasma. The ionised oxygen atoms then bombard the PMMA, etching it away. The oxygen plasma can be seen as the inverse of the sputtering process.

The oxygen plasma was created in a vacuum with a DC source set at 4 kV, positive and negative, giving a difference of 8 kV at almost 3 A. Figure 6.21 shows a substrate that has been milled for 30 minutes. More nanowire tips are now exposed and visible on the image, with some darker PMMA areas also still visible.

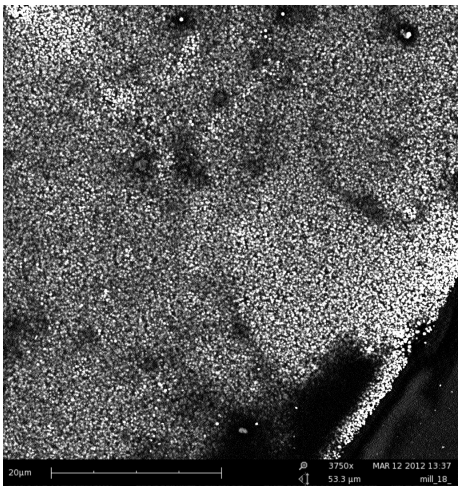

Figure 6.21: SEM image of the ZnO nanowires with PMMA etched with oxygen plasma. More ZnO nanowire tips are exposed.

Each manufactured nanogenerator was viewed in the SEM before deposition of the second gold layer. This was done to ensure that enough nanowire tips were exposed and, if not, the PMMA was etched away further with the oxygen plasma. The second gold layer was then deposited at the same settings, but for five minutes only. This resulted in a 60 nm gold layer, covering the exposed tips of the nanowires.

Figure 6.22 shows the measured output voltage of the flexible nanogenerator. The output voltage was measured in volts and not millivolts as was the case for the solid nanogenerator. The output voltage was recorded as the film was bent, as described in Chapter 3 and earlier in this chapter. The average voltage peak is 1 V with some peaks close to 2 V. The output voltage is 10 times higher compared to the solid nanogenerator. In Figure 6.22 the bending of the film was fast in the beginning and slower for the last couple of bends, showing the dependency on the bending rate.

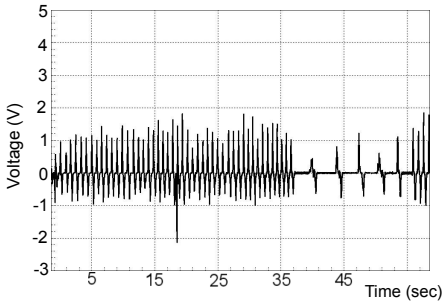

Figure 6.22: Measured output voltage of a typical flexible nanogenerator. The measured output voltage is an order of magnitude larger than the solid nanogenerator.

Figure 6.23 shows the measured output voltage of a flexible nanogenerator that was bent extremely slowly at a rate of two bends every five seconds. This was done to show the behaviour of the flexible nanogenerator. As the nanogenerator was bent, the measured output voltage gradually increased until it reaches a maximum value. This maximum value was reached at maximum bending, or 90°. The voltage keeps increasing until maximum bending was reached and then the voltage starts to decrease. The displacement of the nanowires caused the piezoelectric charges to flow and more charges were generated as the film was bent. At maximum bending the generation of piezoelectric charges stops and the voltage starts to decrease. As the strain in the film was released, piezoelectric charges of opposite polarity were generated, resulting in a negative peak. When no strain was applied to the nanowires, no piezoelectric charges were generated and the output voltage returns to zero.

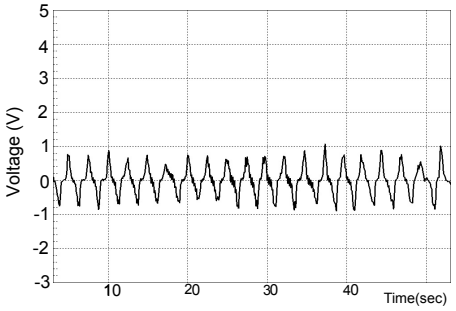

Figure 6.23: Measured output voltage of a flexible nanogenerator bent at a slow rate (2 bends per 5 seconds) to clearly see the voltage behaviour.

The output voltage was proportional to the degree of bending of the film. As mentioned, the bending of the film disturbed the nanowires and when the film was

bent more the nanowires were disturbed more. Figure 6.24 shows the measured output voltage of a flexible nanogenerator that was bent to 120°. The voltage peaks were now above 2 V with most peaks above 1 V, a bit higher than the previous case where the film was only bent to 90°. This shows the clear relationship between the bending degree and the output voltage.

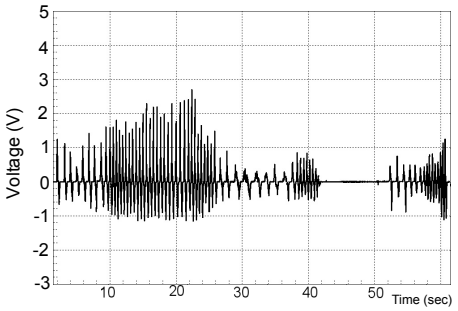

Figure 6.24: Measured output voltage of a flexible nanogenerator bent to 120°, resulting in a higher measured output voltage.

The big question was why the flexible nanogenerator outperforms the solid nanogenerator?. This was argued to be due to two main factors. Firstly, the difference in output voltage was due to the manner in which the external force bends the nanowires. As already mentioned, in the solid nanogenerator the top electrode was moved while it was in contact with only a few nanowires. The movement of the electrode did bent these nanowires until contact was broken between them. The higher the force applied to the electrode, the higher the output voltage. However, the maximum applied force cannot be too high as the silicon is fragile and breaks easily. In the flexible nanogenerator the entire substrate was bent, causing the nanowires to bend due to the force exerted on them by the film. The nanowires can bend a lot more in the flexible nanogenerator, which leads to higher measured output voltage. The higher the bending angle, the higher the output voltage, because the nanowires are under greater strain. It is difficult to compare the two methods directly as, in the first case, the electrode bends the nanowires. The force placed on the electrode was controllable, but the exact force that was transferred to the nanowires is unknown. In the second case, the film was bent, causing the entire structure to bend. This bending disturbs the nanowires and Au electrode, resulting in an output voltage, but again the exact force on the nanowires is not known. If the same force was applied to the nanowires in the two different cases and if all the other properties are equal, the output voltage should be similar. However, it was more difficult to increase the force on the nanowires in the solid nanogenerator as

the silicon is fragile and breaks when the applied force too high. In the flexible nanogenerator the bending angle can be increased and, hence, the forces on the nanowires are increased, leading to a higher output voltage.

The second reason for the superior performance of the flexible nanogenerator is the small contact resistance between the nanowire tips and the Au electrode. In the silicon-based nanogenerator the contact size was very small, with only a small area of the nanowire tip in contact with the electrode. In the flexible nanogenerator the entire tip was covered in Au and thus has a much larger contact size. As predicted by the theory, the losses over the solid nanogenerator will be much higher than the flexible nanogenerator. The small contact area leads to a high contact resistance, which in turn leads to higher losses. The measured resistance of the entire solid nanogenerator was 1.2 MΩ and it was argued that the bulk of the resistance was due to the contact resistance, as predicted by theory. Compared to the flexible nanogenerator the measured resistance was only 80 kΩ, but the contact area was much bigger, and hence the contact resistance was lower. The losses in the nanogenerator are thus reduced, which in turn means that the output voltage was greatly enhanced.

The research on the manufacturing and comparison of the two different nanogenerators led to the publication of a peer-reviewed article in *Microelectronic Engineering* [154].

The output voltage of the nanogenerator has been raised considerably from the solid nanogenerator. Although the output voltage now has peaks above 2 V, it is still not high enough to power most electronic systems. Normal AA batteries supply 1.5 V and in most electronic devices (like TV remotes, wireless mice, etc.) at least two batteries are used. The output voltage of the nanogenerator should thus be increased to supply at least 3 V. In order to do this the manufacturing process needs to be optimised. Additional steps can also be added to optimise the output voltage of the nanogenerator.

6.3 Nanogenerator optimisation

The manufacture and optimisation of the nanogenerator were the main focus of this study. The manufacture of the two different nanogenerators discussed above is entirely new work and little or no information was available on this in the literature. A complete step-by-step description of the manufacturing of both nanogenerators was thus given above. However, optimising the nanogenerator was just as important, because the output voltage at this stage was too small to be practically useful. No information on the optimisation of nanogenerators was available in the

literature.

Nanowires, and ZnO nanowires in particular, are a new field of discovery. Various nanowires were synthesised for the first time in the early part of this century [155, 156]. Over the last ten years researchers have perfected the growth of ZnO nanowires, using various techniques, on various substrates and at various temperatures. Nevertheless, there has not been a lot of research into the optimisation of these nanowires, although ZnO thin films have been around for more than 50 years [157, 158]. Various techniques exist that enhance the quality and functionality of thin films. Hence, a couple of these techniques are used on the nanowires to investigate their effect on the output voltage of the nanogenerator.

6.3.1 Oxygen plasma treatment

The first technique that showed improved quality for ZnO thin films is oxygen plasma treatment. For these tests, the same oxygen plasma that was used to etch away the PMMA was used.

The oxygen plasma affects the binding of the Zn atoms to the O atoms. The Zn atoms will bind to the substrate or to each other, but upon oxygen plasma treatment the Zn atoms will bind to the O atoms [159].

In crystal structures a vacancy is a defect in the crystal, where an atom is missing from a lattice site [160]. For ZnO there are two vacancy defects that can occur, either a Zn atoms or O atoms are missing from a lattice point. Plasma treatment reduces oxygen vacancies. O vacancies donate two electrons to the conduction band, and are mainly responsible for the conductivity characteristics of ZnO thin films. The resistivity of the thin films thus increases as the film is exposed to the oxygen plasma [159].

Figure 6.25 shows the measured output voltage from a nanogenerator that has been plasma treated. After the nanowire growth, before the PMMA was spun onto the substrate, the substrate was plasma treated. The film was then bent to 90°. The measured output voltage was slightly higher compared to the previous cases. The voltage was similar to the nanogenerator that was bent beyond 90°, as there are numerous peaks above 2 V.

The reason for the increase in output voltage is, as explained above, the reduction in O vacancies. This led to a increase in carrier concentration and an decrease in resistivity, and the output voltage was raised. It was argued that the increase in carrier concentration caused the decrease in resistance and less internal loss occured within the nanowires. Consequently, SEM images showed no visible change in the morphology of the ZnO nanowires.

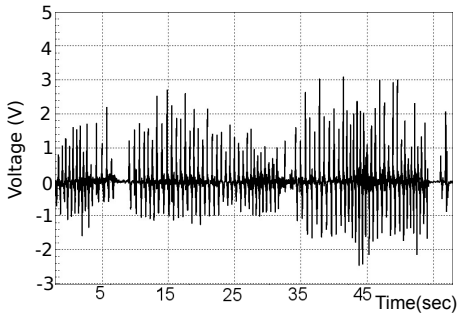

Figure 6.25: Measured output voltage of a flexible nanogenerator that is plasma treated. The measured output voltage is increased compared to the non-plasma treated nanogenerator.

6.3.2 Annealing

The second method that was applied to the thin films was annealing at high temperature in air. The annealing of the films, at temperatures above 500°C, has the same effect as the plasma treatment. The Zn atoms, that are not bound to O atoms before annealing, bind to the O atoms during the annealing phase [161].

Lower annealing temperatures, around 250°C, result in improved crystal structure, again due to the bonding of Zn atoms and O atoms. However, the effect is less at the lower temperature because the thermal energy is not enough to break Zn - Zn bonds [162].

The effect of different gases on the thin films was investigated next. Annealing was done at 250 °C in air, oxygen, nitrogen and argon. Annealing in air, as already mentioned, resulted in the Zn atoms binding to the O atoms, or a reduction in O vacancies. Annealing in the other gases led to increase in either of the two vacancies. Most of the annealing resulted in the bonding of Zn atoms, leading to an increase in the O vacancies [163].

Figure 6.26 shows the measured output voltage of a nanogenerator annealed in air at 250°C for 30 minutes. The output voltage reached 4 V, with a number of peaks above 4 V. This nanogenerator was not plasma treated and was only annealed after nanowire growth.

Table 6.1 shows the measured output voltage of nanogenerators manufactured with nanowires annealed in different gases. From Table 6.1 it is clear that air is best, followed by no annealing. The other three gases, nitrogen, oxygen and argon, led to an increase in O vacancies, reducing the resistivity of the nanowires. This, in turn, led to a larger screening of the piezoelectric potential and, hence, a lower measured output voltage. Annealing in air for 30 minutes gave the right balance between reducing the O vacancies and the screening of the piezoelectric charges.

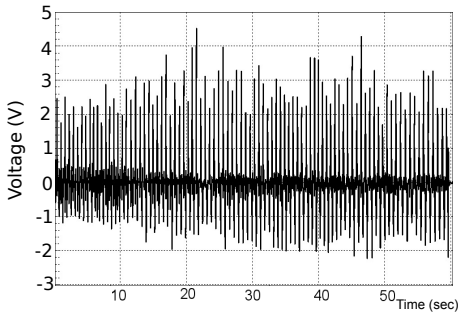

Figure 6.26: Measured output voltage of flexible nanogenerator that was annealed in air at 250°C for 30 minutes. The nanogenerator was not plasma treated.

Annealing for longer periods did not, however, have a considerable effect on the output voltage. SEM images showed no change in morphology after annealing.

Table 6.1: Measured output voltage of nanogenerator annealed in different gases.

Gas	Voltage (mV)
No annealing	1000
Air	3000
Nitrogen	800
Oxygen	900
Argon	400

6.3.3 Adding materials to PMMA

Both methods explained above are additional optimisation of the nanowires, which led to an optimised nanogenerator. Both techniques were adopted from thin films and improved the nanowires as well. The manufacture of the nanogenerator itself was investigated next.

One of the only options for optimisation is in the PMMA step. The deposition thickness of the gold and ZnO layers does not influence the output voltage, neither does the deposition of the second gold layer. The PMMA fills a large portion of the nanogenerator and does not actively contribute to the generation of output voltage. The PMMA adds stability to the nanogenerator, protects the nanowires and acts as a buffer for the second gold layer. Adding active materials to the PMMA before spinning it onto the substrate might help increase the output voltage even further.

Five different materials were added to the PMMA separately: These materials were Au nanoparticles 10 nm in diameter, single-walled CNT (SWCNT) , multi-

walled CNT (MWCNT), graphene, 12 nm flakes and ZnO nanowires. Figure 6.27 shows a diagram of a nanogenerator manufactured with additions to the PMMA. The diagram shows ZnO nanowires that were added to the PMMA, but this can be any of the other materials.

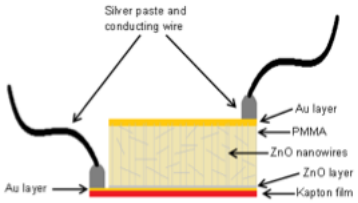

Figure 6.27: Diagram of a nanogenerator manufactured with additional material added to the PMMA.

The additional materials were dispersed in the PMMA by magnetic stirring, as well as ultrasonic stirring. Once the material was distributed evenly throughout the PMMA, it was applied to the substrate. This was done by the same method, whereby the PMMA was dripped onto the substrate and left for 60 seconds, then spun for 10 seconds, and placed on the hotplate for 50 seconds. This process was repeated five times. Before the mixed PMMA was applied, a single layer of PMMA was spun onto the substrate to ensure no short circuit will occur.

Figure 6.28 (a) - (e) show the output voltage of the nanogenerator manufactured with the additional materials added to the PMMA. These nanogenerators were manufactured without annealing or plasma treatment. Furthermore, they were manufactured from ZnO nanowires that did not have optimal growth parameters. The growth time was shortened in order to prepare multiple samples on a single day. Table 6.2 summarises the output voltage of the different nanogenerators. The nanogenerators manufactured with Au nanoparticles, MWCNTs and graphene all had lower output voltages compared to the base model. By contrast, the nanogenerators with SWCNTs and ZnO nanowires had slightly higher output voltages compared to the base model.

The Au nanoparticles are 10 nm in diameter. These nanoparticles can thus easily penetrate between the nanowires and do not agglomerate as in the case of the CNTs or graphene. The nanoparticles will make contact with the top gold electrode, reducing the overall internal resistance of the nanogenerator. This reduction in internal resistance leads to less loss internally and a higher output voltage compared to MWCNTs and graphene. Figure 6.29 shows an equivalent electrical schematic of

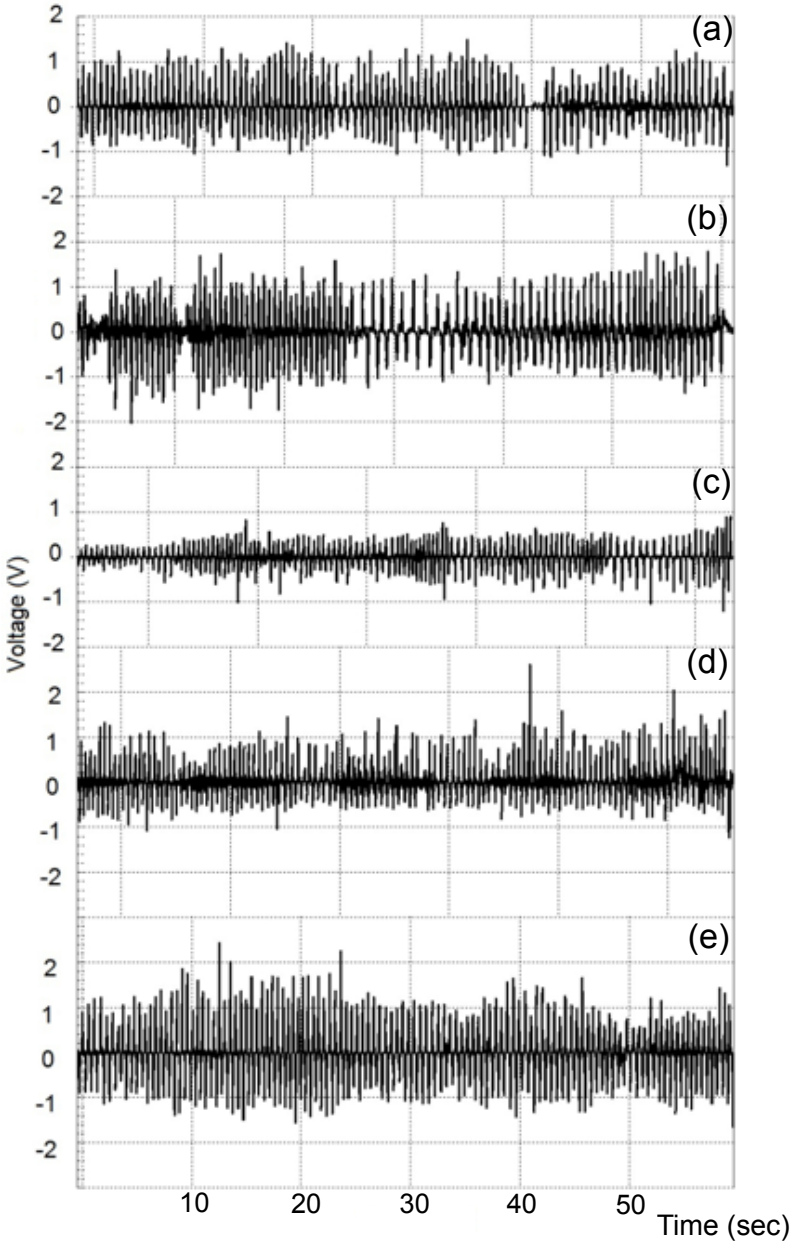

Figure 6.28: Measured output voltage of the nanogenerator manufactured with PMMA and (a) Au nanoparticles, (b) SWCNTs, (c) MWCNTs, (d) graphene and (e) ZnO nanowires.

Table 6.2: Summary of the average output voltage of the nanogenerators manufactured with additional materials added to the PMMA.

Additional material	Voltage (V)
Au nanoparticles	0.8
SWCNTs	1.0
MWCNTs	0.6
Graphene	0.8
ZnO nanowires	1.2

the nanogenerator, where V_i is the voltage generated by the piezoelectric effect, R_s is the internal resistance (the nanowire resistance, the bottom electrode resistance and the top electrode resistance), and C_s is the internal capacitance in the top and bottom electrodes and the capacitance of the nanowire. Resistance R_p is the resistance of all the other nanowires that are not actively contributing to the output voltage and capacitance C_p is the capacitance between the top and bottom electrodes, as well as the capacitance between all the nanowires. The Au nanoparticles affect either R_s or R_p, reducing either resistance value and resulting in a higher output voltage. Furthermore, the ZnO nanowires form local Schottky contacts with the Au nanoparticles, which add to the output voltage. These Schottky contacts are not at the tip of the nanowires, but rather somewhere down the length of the nanowires. The output signal is observed only when there is contact between the nanowire and the Au nanoparticles.

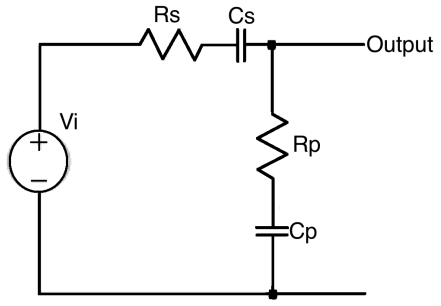

Figure 6.29: Eqivalent circuit diagram of nanogenerator.

The SWCNTs, MWCNTs and graphene all had the same effect. As was the case for the Au nanoparticles, either R_s or R_p were reduced, leading to less internal loss and the production of a larger output voltage. The differences in measured output voltages that were observed were due to the specific attributes of the individual materials. SWCNTs, MWCNTs and graphene are all carbon-based materials, but

they have different levels of conductivity. Graphene is the best conductor of electricity, followed by SWCNTs and then MWCNTs [164, 165, 166, 167]. However, adding SWCNTs to the nanogenerator increased the output voltage more than was the case for graphene. This indicates that the change in internal resistance is not the main factor driving the increase in output voltage.

As mentioned, the magnitude of the generated output voltage is determined by the difference in Fermi level of the top and bottom gold electrodes. When graphene, SCWNTs or MWCNTs are added to the PMMA, contact is made between the ZnO nanowire and the carbon material. A Schottky contact will form when the electron affinity of ZnO (4.5 eV) is smaller than the work function of the other material [168]. The work function for plain carbon is 4.8 eV, but it differs for the nanostructures. Table 6.3 summarises the work functions of the three different carbon structures [169].

Table 6.3: The work functions of the different materials added to the PMMA during nanogenerator manufacturing.

Material	Work function (eV)
SWCNTs	4.8 - 5.05
MWCNTs	4.6 - 4.95
Graphene	4.5 - 4.8

The work function of a material, Φ, is the energy required to move an electron in a solid from its Fermi level to the vacuum level. The Schottky barrier height (E_A) that has to be overcome is the difference between the conduction band of the electrons and the Fermi level at the Schottky interface. These energy levels are shown in the simplified energy band diagram in Figure 6.30, where E_{vac} is the energy at the vacuum level, E_C is the conduction band, E_V is the valence band and E_F is the Fermi level. This means that ZnO and any one of the three carbon structures will form a Schottky contact, due to the individual work functions being larger than the electron affinity of ZnO for all cases. Thus, electrons can flow from the nanowire to the carbon structure, across the Schottky contact interface. A certain amount of energy is required to overcome the Schottky barrier, but once the barrier has been crossed, electrons can move freely across this barrier. The free-moving electrons will flow from the nanowire to the carbon structure, raising the Fermi level and, in turn, raise the generated output voltage. The biggest difference in Fermi levels occurs in the SWCNTs, followed by graphene (and the Au nanoparticles) and, lastly, the MWCNTs, as indicated by the measured output voltages. The data shows that the higher the work function, the higher the output voltage will be. Although gold

has a work function of 5.1 eV, the nanoparticles are so small that the contact resistance increases considerably, and hence the lower measured output voltage. This means that the Fermi level difference for SWCNTs is the biggest, leading to the highest generated output voltage.

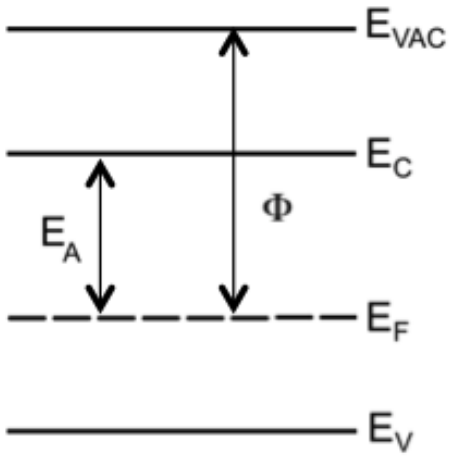

Figure 6.30: Simplified energy band diagram with the Schottky barrier height and work function levels shown.

However, the highest output voltage of all the nanogenerators were observed when ZnO nanowires were added into the PMMA, as is shown in Figure 6.28(e). I believe that this can be attributed to the fact that the additional nanowires in the PMMA are also able to bend, thus contributing to the generated output voltage. It has been shown that laterally oriented nanowires lead to higher generated output voltages, as was observed in our case [56, 170].

Lastly, a combination of the optimising techniques mentioned above was implemented. The nanowires were grown, exposed to oxygen plasma and then annealed at 250°C in air for 30 minutes after growth. PMMA was spun onto the substrate containing a combination of SWCNTs and ZnO nanowires. SWCNTs and ZnO nanowires were chosen, because both individually caused an increase in generated output voltage. The measured output voltage of the optimised device is shown in Figure 6.31. The measured output voltage exhibited peaks as high as 5 V, with an average voltage of above 3 V.

A last optimisation technique was tried, doping of the ZnO nanowires. Doping refers to an action whereby additional elements are added during synthesis to replace either the Zn atoms or O atoms. The aimwais to increase the piezoelectric voltage that is generated during the bending of the nanowires.

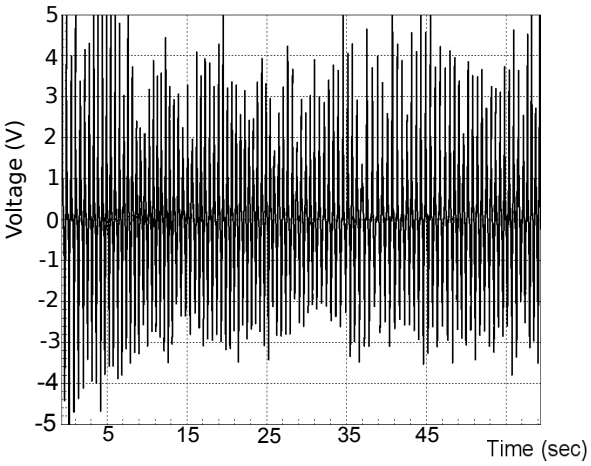

Figure 6.31: Measured output voltage of nanogenerator manufactured with nanowires that were annealed and plasma treated, and with ZnO nanowires and SWCNTs is added to the PMMA.

The doping was done by adding 10 mM of the different materials to the solution during growth. The materials used were selenium, cupric oxide, indium, silver nitrate, boron and yttrium. These materials were chosen, because they were available in the laboratory at the time of experimentation. Doping of ZnO nanowires in the literature is done with arsenic [171], aluminium [172] and copper [173].

As mentioned, the doping was done during the growth of the ZnO nanowires. 10 mM of each material was added to the solution and the nanowires were grown as normal. The nanogenerators were then manufactured and the output voltages measured. However, none of the doped nanogenerators led to higher output voltages. Figure 6.32 shows the output voltage of a nanogenerator manufactured with nanowires doped with silver nitrate, which gave the highest output voltage of all the doped nanowires. The nanowires were plasma treated after growth and then annealed, and SWCNTs and ZnO nanowires were added to the PMMA. Nevertheless, the output voltage was no higher than Figure 6.31, and hence the doping of nanowires was not investigated further.

6.3.4 Current measurements

The optimisation techniques worked well in improving the output voltage of the nanogenerator. The output voltage was increased from a few millivolts to over 5 V. However, it is also importnat to inverstigate the current amplification of the optimised nanogenerator. Specialised equipment is required to measure the output current, because it is extremely small.

The HP4140B pico-ampere current meter was used to measure the output cur-

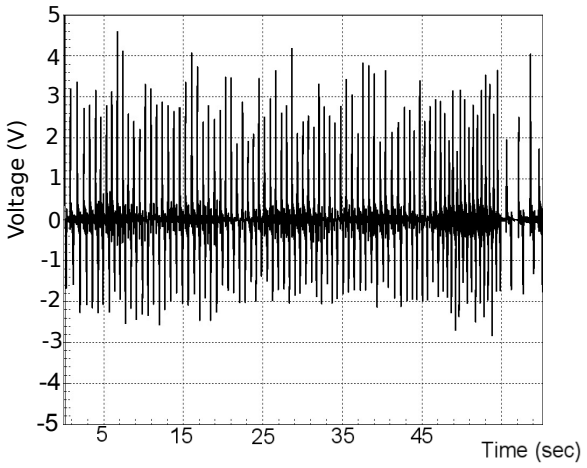

Figure 6.32: Measured output voltage of a nanogenerator manufactured with nanowires doped with silver nitrate. The nanowires were plasma treated and annealed after growth, and SWCNTs and ZnO nanowires were added to the PMMA.

rent of the nanogenerator. This device has an analogue display for the current measurement. The problem is that the sampling rate of the device is one sample every two seconds. The current waveform will be identical to that of the output voltage, which has a very sharp peak. Therefore, taking a sample every two seconds is not good enough and will not result in the peak output current being detected. Unfortunately, this was the only available instrument to measure the current with reliable accuracy.

The output current was measured in exactly the same way as the output voltage. The only difference was that the HP4140B meter replaced the buffer circuit and the analog to digital converter (ADC). The output current was displayed on the analogue screen and the maximum current over a 10 second interval was used as the peak output current. All the current measurements were made with a 10 kΩ resistor connected as the load.

The solid nanogenerator, which was manufactured using the first technique, has extremely low current. The peak current over a 10 second interval was recorded as 5.7 nA. As the working area for all the nanogenerators was 10 mm^2, or 1 cm^2, this means that the current density for this nanogenerator was 5.7 nA/cm^2. The maximum measured output voltage of this nanogenerator was 80 mV, resulting in power generation of 0.46 nW/cm^2. The output power was thus too small to be of any practical use.

The nanogenerators adhere to the superposition principle: When two nanogenerators are coupled in series the voltages adds up, and when two nanogenerators are connected in parallel, the current adds up. However, the output of two

nanogenerators will only add up if both are connected in the right way, otherwise the voltages or currents will be subtracted, leading to lower or no output voltage [104, 174].

The solid nanogenerator with the separate gold electrode measured a maximum output voltage of 250 mV at a peak current of 16 nA/cm^2 over the 10 kΩ load. This was a big increase from the previous nanogenerator; almost double the current and a threefold increase in output voltage. The output power of the nanogenerator was at maximum 4 nW/cm^2, an almost tenfold increase.

Although the substrate of the flexible nanogenerator is bigger, it still only has a 1 cm^2 working area. The non-optimised nanogenerator has a peak output voltage of 1.8 V, at 90° bending. The output current was measured at 45.9 nA/cm^2 through a 10 kΩ load, a massive increase in both current and voltage over the solid nanogenerator. The maximum output power was 82.62 nW/cm^2, a twentyfold increase over the solid nanogenerator.

Lastly, the optimised nanogenerator had a maximum output voltage of 5 V. The maximum output current is measured at 1.25 μA/cm^2 through a 10 kΩ load, giving a maximum output power of 6.25 μW/cm^2. The output power was raised from less than 1 nW/cm^2 to more than 6 μW/cm^2, by changing the nanogenerator substrate and optimising the nanogenerator manufacturing process. At the time of these experiments, the measured output power was the highest achieved throughout the literature.

The nanogenerators can now be stacked on top of each other, connecting them in series or parallel to give more current or more voltage respectively. The entire structure is about 250 μm in height, thus 40 nanogenerators stacked will be 1 centimetre in height. One cubic centimetre of nanogenerators will thus be able to produce 250 μW of clean energy. If the area is increased to 1 m^2 over 25 W can be generated.

6.4 Conclusion

The manufacturing and optimisation of a ZnO nanowire nanogenerator was discussed. The manufacturing of the nanogenerator started by using a gold wire to bend the nanowires. The output voltage was measured as the gold wire was moved around, bending the nanowires. The measured output voltage was only a couple of millivolts in magnitude and hence not practically useful. The nanogenerator was then improved by replacing the gold wire with a solid gold electrode. The output voltage and current were consequently raised to generate output power of 0.46 nW/cm^2. However, this was still not enough power to be used in practical applica-

tions, but it was an improvement over the previous design. The solid gold electrode was then changed in order to improve the contact between the nanowires and the electrode, but even so the output voltage was not raised sufficiently. Contamination of the substrate led to weak contact between the nanowires and the electrode, resulting in low output voltages. The final solution was to have the electrode and the nanowires separate from one another. The gold electrode was then moved in the same way as the gold wire in the first design. This approach improved the output power to 4 nW/cm^2, which was a big improvement, but still not practically useful. Over 700 samples were prepared during this study, with each iteration improving on the previous design. Nevertheless, the solid nanogenerator was never able to achieve output voltages above 1 V.

The solution to the low output voltages was found to be a flexible nanogenerator. The nanowires were grown on a flexible polyimide film and PMMA was used to add stability to the nanogenerator as well as to act as a buffer for the top gold electrode. The nanogenerator was now a single integrated device, that when bent, generated an output voltage. The output power of this device was over 45 nW/cm^2, another tenfold increase over the previous designs. Although the output power was raised from 0.46 nW/cm^2, it was still not high enough to be used in practical applications. In order to increase both the current and the voltage, the manufacturing process of the nanogenerator had to be optimised.

Various approaches were taken to optimise the nanogenerator. Plasma treatment and annealing of the nanowires after growth reduced the oxygen vacancies in the ZnO crystal structure. This also led to an increase in both output voltage and output current. Additional materials were added to the PMMA prior to spinning it onto the substrate, which further helped improve the output parameters of the nanogenerator. ZnO nanowires and SWCNTs led to the biggest increase in output voltage. A nanogenerator manufactured using a combination of these optimisation techniques increased the output power to over 6.25 $\mu W/cm^2$. Over 600 flexible nanogenerators were manufactured over the period of this study.

The work on the optimisation of the nanogenerator led to the publication of a fourth article in *IEEE Transactions on Nanotechnology* [175].

The manufacturing process of the nanogenerator also had to be cheap for the technology to be implemented. Accordingly, the material cost was low as is summarised in Table 6.4. The most expensive materials are the PMMA and the SWCNTs. Overall, the materials that were used amounted to R0.95 in total. Added to the cost are the chemicals used during cleaning, the DI water for growth, and the electricity for the sputtering of the layers, plasma treatment and annealing. These costs amount to less than R1 per nanogenerator as all the instruments work with

multiple samples. This gives an overall cost of less than R2 per nanogenerator that is manufactured on a small scale.

Table 6.4: Material cost for the manufacture of a ZnO nanogenerator.

Material (per nanogenerator)	Cost (R)
Flexible film	R0.05 (R430 for 50 mm by 30 000 mm sheet)
Gold (for electrodes)	R0.10 (R3500 for 1000 μm thick target)
Aqueous solution growth materials	R0.20 (HMTA and zinc nitrate hexahydrate)
PMMA	R0.40
SWCNTs	R0.20
Total	R0.95

These nanogenerators can easily be manufactured on large scale, which will bring the cost down to well below R2 per nanogenerator. The maximum output power for a single nanogenerator is slightly above 6.25 μW, resulting in a cost of about R300 for 1 mW of clean energy. The cost of solar power for 1 mW is around R0.004 per mW [176]. However, the cost was over R1 per mW just 20 years ago [177]. Although the cost is high, it will be reduced as nanogenerators are manufactured on larger scale. Further, optimisation will also lead to improved output voltage and current, thus further reducing the cost per mW of clean power.

The output voltage and current wave from of the nanogenerator is not a direct current, but consists of a number of positive and negative peaks. This is not a useable form of electricity, so it needs to be converted in order to be used with conventional electronics. Simulating circuits that can perform the conversion saves time and helps to design optimal circuits.

Chapter 7

Nanogenerator output circuitry

Scavenging power from the environment to power small electronic devices is of the utmost importance. Remote sensors or similar devices that measure air pollution and seismic activity must harness power from the environment in order to be self-sustaining. Wearable electronics, such as Google glass [178], can also benefit from scavenging power by using nanogenerators incorporated into clothing and shoes. These nanogenerators could even power your cell phone during your morning jog [33].

Numerous devices that use human movement as power source have been shown. Over 1.6 mW can be generated from walking, using smart knee replacements [179]. A 75 kg man can generate up to 675 mW while walking and more than 2 W during a jog with piezoelectric generators incorporated into shoes [180]. Arm movement can also be used. Although less effective, it has been shown that over 40 μW can be generated from a movement of 10 cm [181]. Incorporating these nanogenerators into various areas could lead to enough power being generated to power small electronic devices.

The power generated from these scavenger devices is generally not in a useable form. Although the output voltage of the nanogenerator has been raised to over 5 V, using different optimisation techniques, as discussed in the previous chapters, the output voltage wave consists of a number of peaks of short duration, almost like a number of impulse functions. However, electronic devices need a constant, or DC, current supply to function. This means that a conversion circuit is necessary to convert the generated voltage to a DC voltage.

Various circuits exist that can convert the output voltage of a piezoelectric generator to a useable form. Four different circuits were investigated in this chapter, the full-bridge rectifier, the voltage doubler, the synchronised switch harvesting on inductor (SSHI) and the LTC3588 chip from Linear Technologies. Each circuit was optimised through simulations using LTSpice, an electrical circuit simulation tool

from Linear Technologies [182]. The circuits were then built and tested.

7.1 Simulation of output circuitry

Simulations were used to investigate different aspects of the output circuits before practical tests were conducted. The simulations were used to investigate important circuit components, to optimise the load for each circuit and to find the minimum input each circuit required to function as desired.

7.1.1 Nanogenerator

The first simulation was of the nanogenerator itself. An equivalent model of the nanogenerator was required to simulate the response of each circuit. The two equivalent models for the nanogenerator are shown in Figure 7.1. Figure 7.1 (a) shows the nanogenerator modelled as a voltage source, series resistance R_i and parallel capacitor C_i. The resistance is modelled as the total resistance of the nanogenerator, i.e. the resistance of the nanowires, electrodes and contact resistance. The capacitor includes the capacitance between the two electrodes and between the nanowires. Figure 7.1 (b) shows the Thevenin equivalent model, with a current source and the resistor is parallel [183, 184]. The output voltage of the voltage equivalent circuit is shown in Figure 7.2. The voltage and current sources in Figure 7.1 is equivalent to output shown in Figure 7.2, but bigger in magnitude.

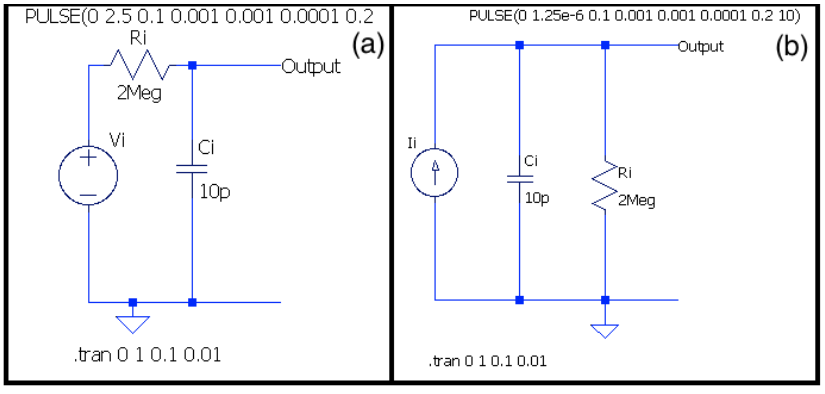

Figure 7.1: Equivalent circuit of the nanogenerator, (a) modelled with a voltage source, and (b) the Thevenin equivalent model with a current source.

The simulated output voltage has only positive peaks with 2.5 V in magnitude. This is different from the actual device, which has positive and negative peaks with magnitudes of 5 V. The magnitude can easily be changed in the simulation

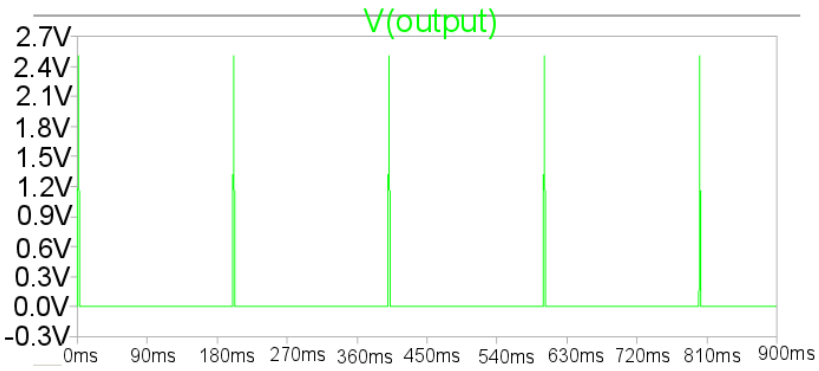

Figure 7.2: Simulated output voltage of the voltage equivalent model of the nanogenerator.

by changing the amplitude of either the voltage or the current source in the model. The current circuit can be improved by having both positive and negative peaks, as shown in Figure 7.3, with output voltage in Figure 7.4.

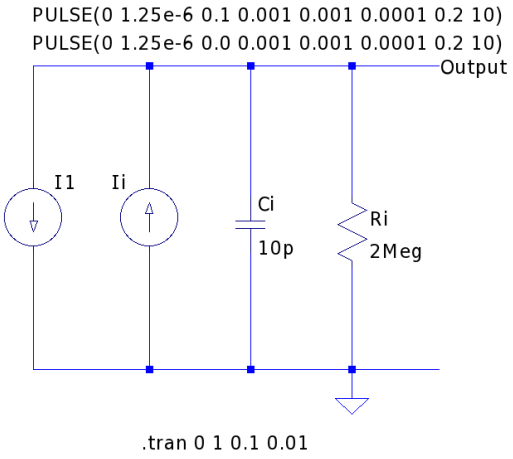

Figure 7.3: Improved circuit model for the nanogenerator.

The simulations were performed using the current source equivalent circuit of the nanogenerator. The current source in Figure 7.1 (b) was replaced by a sinusoidal current source to simplify the simulations. The amplitude was set to 12 μA and the frequency to 10 Hz. After initial simulations the sinusoidal source was replaced by the nanogenerator model for further simulations. After the sinusoidal simulations the model in Figure 7.3 was used for further simulations.

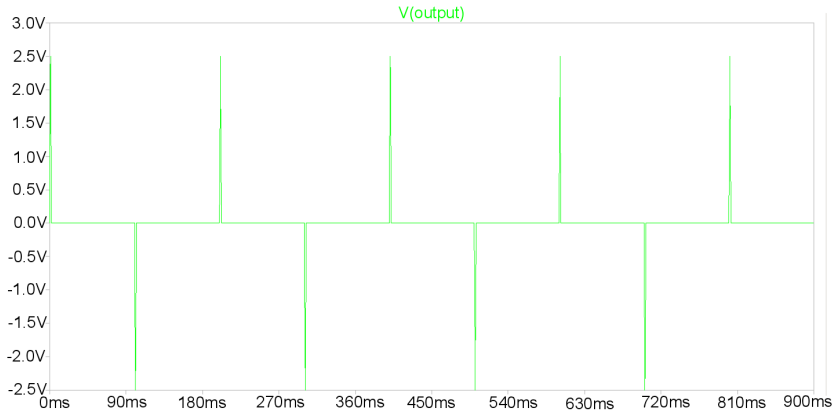

Figure 7.4: Output voltage of improved circuit model for the nanogenerator.

7.1.2 Full-bridge rectifier

The first circuit that was investigated was the full-bridge rectifier, shown in Figure 7.5. For the purpose of these simulations a sine wave was used as source, unless otherwise specified.

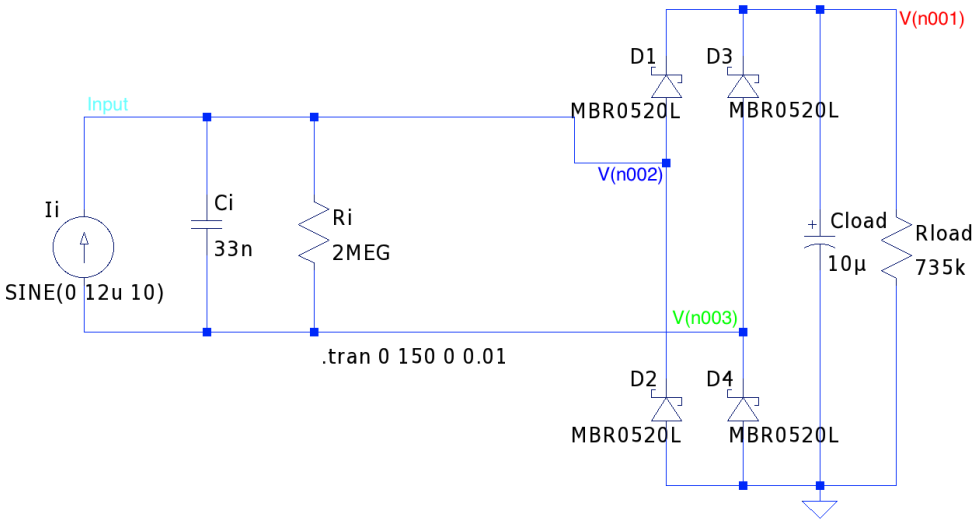

Figure 7.5: Circuit diagram of the full-bridge rectifier circuit.

The full-bridge rectifier operates by conducting the input wave along two paths, depending on the polarity of the input, to the output capacitor and the load resistor. During the positive cycle, diodes $D1$ and $D4$ are conducting, storing the charge in the capacitor. During the negative cycle, diodes $D2$ and $D3$ are conducting, and the

charge is also stored in the capacitor. This means that the capacitor charges during both the positive and the negative cycles of the input.

Different voltages are shown in Figure 7.6. The blue line is the voltage on the node below $D1$, the green line is the voltage on the node above $D4$, the red line is the voltage across the capacitor and the last line is the input voltage, as defined in Figure 7.5. The blue line follows the input for the first part, but is a lot smaller due to the resistance in the circuit. The output remains zero until the voltage is sufficient to forward bias diode $D1$ and $D4$, then the output increases as the capacitor charges. When the voltage decreases below the on voltage of the diode, the capacitor does not charge anymore but rather discharges through the resistor. The negative cycle then commences and the output is raised when the voltage is higher than the on voltage of diodes $D2$ and $D3$, and the output voltage increases again. The output voltage will always be slightly smaller than either the blue or the green line, due to the on voltage of the diodes.

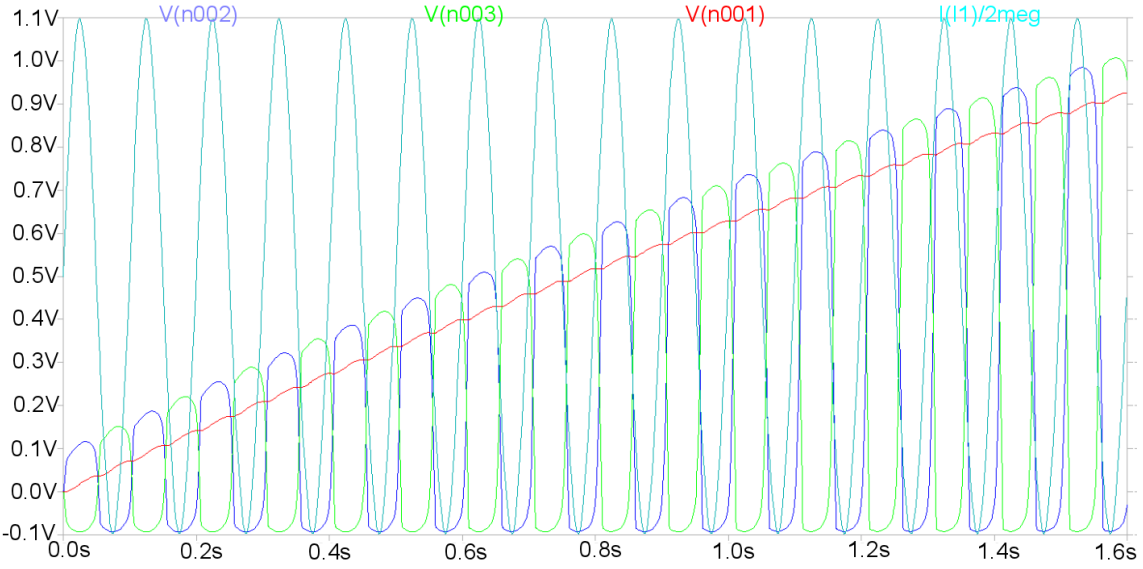

Figure 7.6: Different voltages of the full-bridge rectifier to see the operation of the circuit.

The main problem with the full-bridge rectifier ws that during each cycle, time was spent charging and discharging the internal capacitor, C_i. During this time the diodes were reverse biased and no current flowed to the output capacitor, C_{load}. Once the internal capacitor was charged, one set of diodes were turned on and current flowed to the output. While the output voltage was low, most of the charge was available to flow from the nanogenerator to the load, but as the output voltage

increased the amount of charge available to the load was decreased [185], as shown in Figure 7.7.

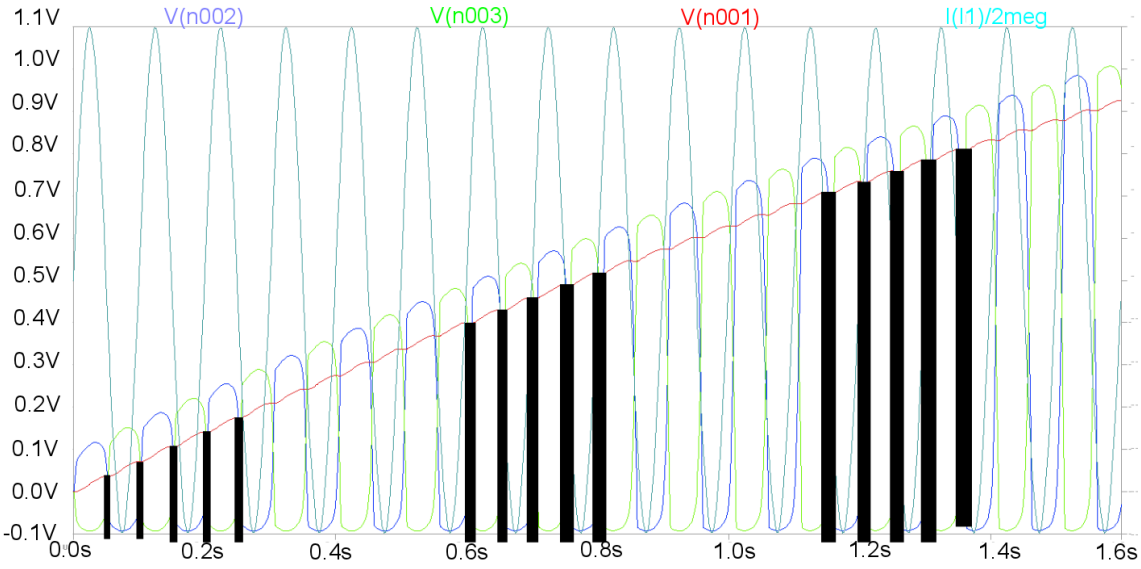

Figure 7.7: The conducting time of the diodes get smaller as the capacitor charges over time.

The main function of the circuit is to convert the signal from the piezoelectric device to a usable form for the load, which can be any electronic device. The circuit thus needs to be optimised for a specific load. Figure 7.8 shows the change in output voltage and power when a variable load is connected. The variable load is changed from a few Ohms to more than 100 MΩ over a specific time frame. Maximum power delivery is of more importance than maximum voltage delivery. At maximum voltage the power is almost half the maximum, and at maximum power the voltage is two-thirds of the maximum. The optimal load is taken as the load that ensures maximum power delivery and is calculated as 735 kΩ. The optimal load in calculated using Figure 7.8.

The influence of the capacitor on the output circuit is investigated next. The capacitor is used to store the charge, which is then used by the load. The capacitor will also influence the amount of time required to reach steady state as well as the ripple on the output voltage. Figure 7.9 shows the output voltage with a 12 μA sinusoidal input, 735 kΩ load resistance and a capacitor value of 1 μF, 10 μF and100 μF. It is clear from Figure 7.9 that the capacitor value is a trade off between ripple and steady state. With the 1 μF capacitor the circuit reaches steady state after about five seconds, but the ripple is more than 100 mV. For the 100 μF capacitor the

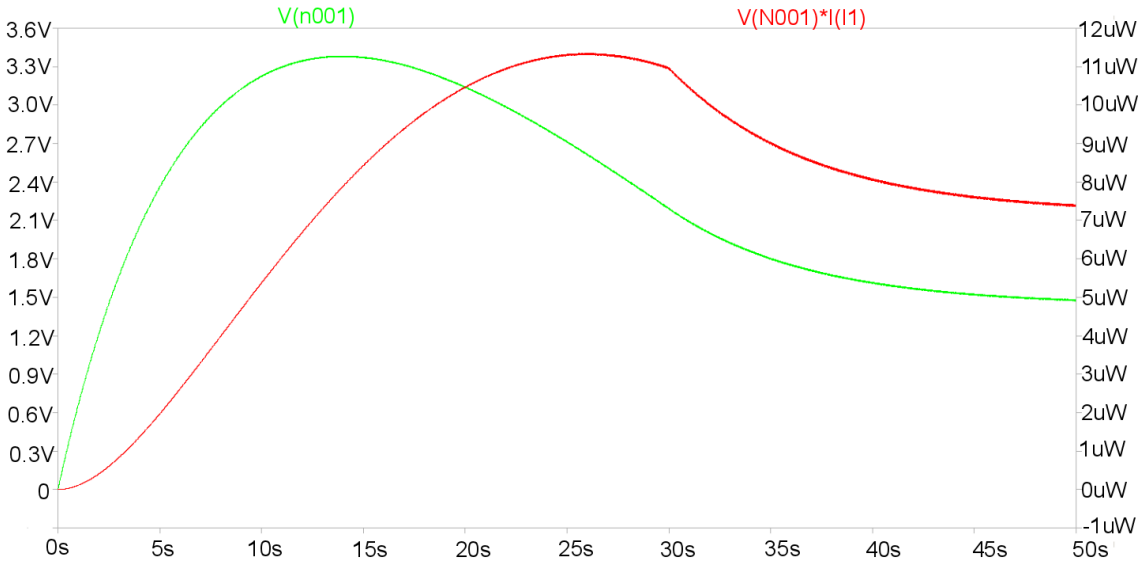

Figure 7.8: Optimal voltage and power delivery to the load in the full-bridge rectifier.

ripple is negligible and steady state is only reached after two minutes. The optimal capacitor value is 10 μF, with a ripple of less than 50 mV and steady state reached after less than 20 seconds.

The last components investigated were the four diodes, $D1$ to $D4$. Different types of diode exist, with silicon and Schottky diodes being the two most commonly used. The output voltages can change from above 3 V to less than 10 μV, depending on the diodes. The most important parameter for the diodes is the reverse current, I_R,normally specified in μA. This is the current that flows when the diode is in the off state; the lower the value, the better. Another important value is the on-voltage, or forward voltage, V_D, of a diode. The forward voltage is specified at a certain current, the higher the current, the higher the voltage. Due to the small nature of the piezoelectric current the forward voltage will be small, but still plays a vital role in the operation of the rectifier. Overall, the best performance was obtained with Schottky diodes, with silicon diodes a close second.

The simulations were performed with various diodes and the output voltages observed. As mentioned, some diode types can lead to almost no observable output voltage being detected. More than 60 diodes were during the simulations and the $MBR0520L$ Schottky diode was found to be the best. A forward voltage drop of less than 0.1 V at the simulating current was observed, with leakage current less than 75 μA. Although certain diodes have less leakage current, the forward voltage drop is higher, leading to less power output at the load. A few of pages of the $MBR0520L$ datasheet are appended in Appendix C.

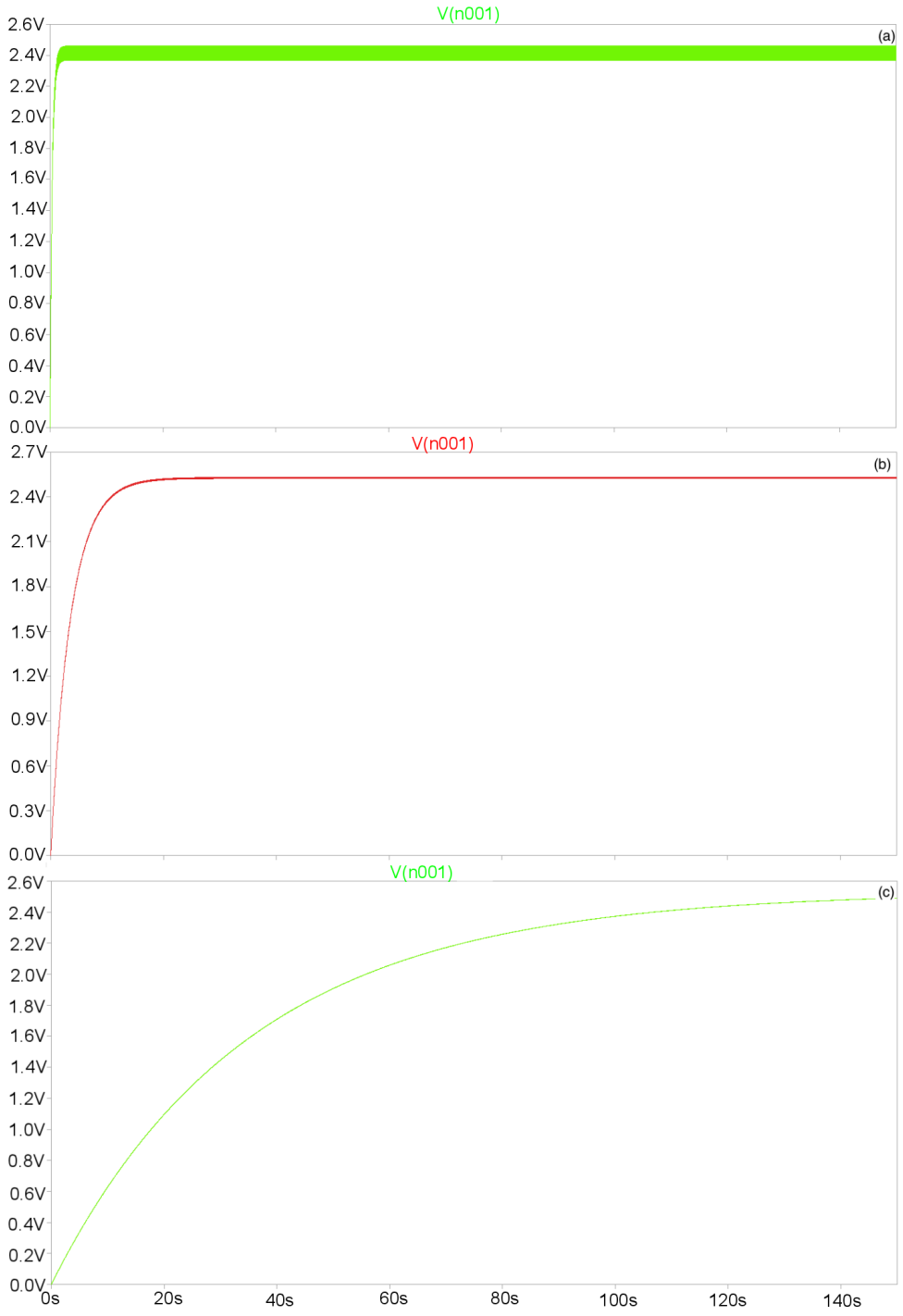

Figure 7.9: Output voltage of the full-bridge rectifier with a 12 μA sinusoidal input, a load of 735 kΩ and a capacitor of (a) 1 μF ,(b) 10 μF and (c) 100 μF.

The efficiency of the circuit was simulated next. At steady state the nanogenerator delivers just below 27 μW of power (after the internal losses over the resistor). The load resistor consumed just more than 7 μW of power, giving an efficiency of just above 25%. Figure 7.10 shows the input power and the output power. The input power was measured after the internal resistor and capacitor and the output power was the power stored in the capacitor (with no load connected). The efficiency is now 91%, showing that only 9% of the generated charge is lost over the diodes and capacitor.

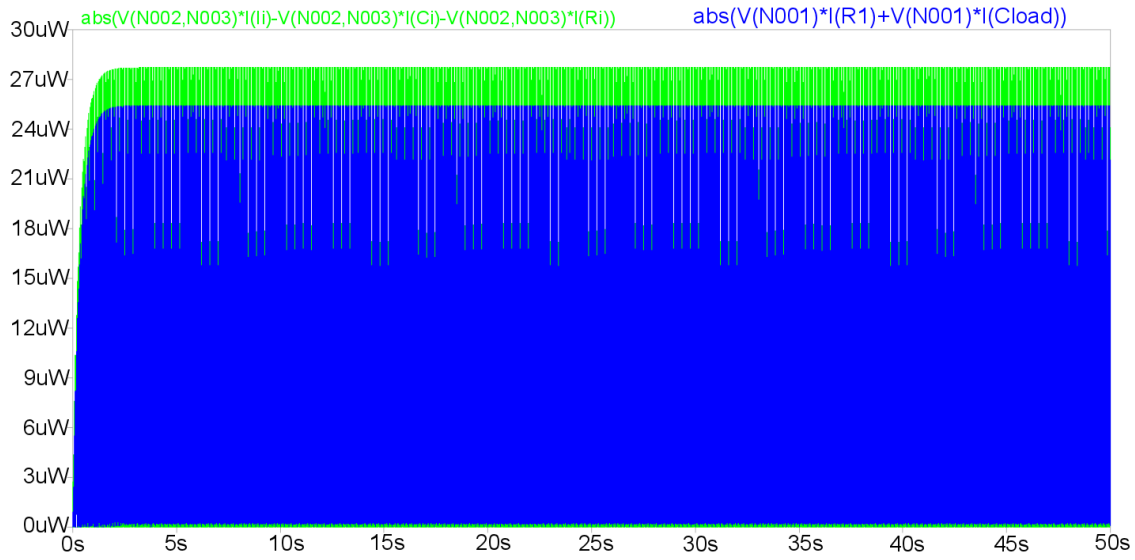

Figure 7.10: Input and output power of the full-bridge rectifier circuit with sinusoidal input.

The pentultimate parameter that was investigated was the minimum input current that will ensure a steady state output voltage of at least 1 V. The input current was reduced until this threshold was reached. For the full-bridge rectifier the minimum input current was 2.8 μA for a 10 MΩ load.

Lastly, the full-bridge rectifier was simulated with a pulse input signal. Figure 7.11 shows the output voltage and power when positive and negative pulses are used as input, with a magnitude of 180 μA. The average power that was delivered to the load over the 50 second interval was 1.1452 μW.

The advantages of the full-bridge rectifier are that it is a simple circuit, with only four diodes, a capacitor and a load. The output voltage consists of both the positive and negative cycles of the input. The circuit also works at low current and can achieve high efficiency at no load, but decreases as the load increases. However, although the piezoelectric device generates voltage continuously, the full-bridge

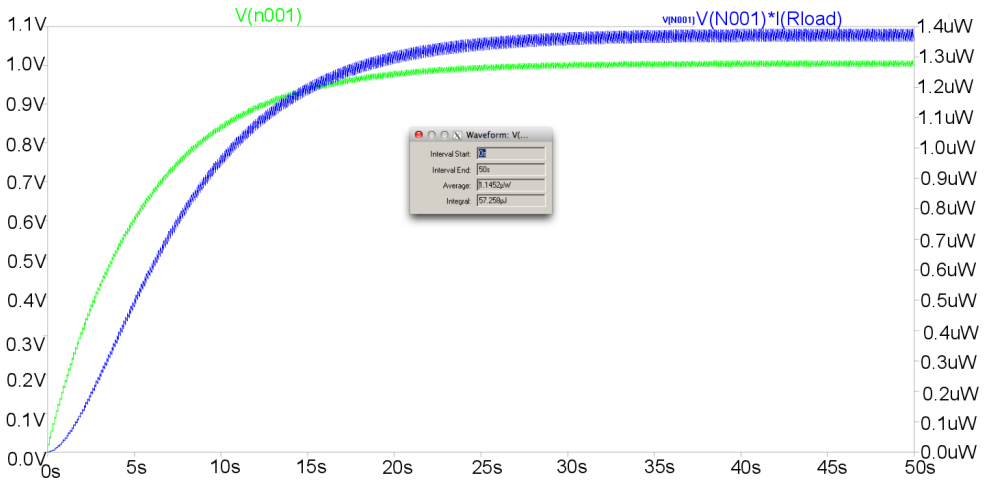

Figure 7.11: Output voltage and power of the full-bridge rectifier when a pulse signal was used as input.

rectifier cannot store all the generated charge. This means that most of the generated piezoelectric voltage will go to waste.

A circuit similar to the full-bridge rectifier might solve some of these problems. The voltage doubler, as the name implies, doubles the input voltage by the charging of capacitors. The voltage doubler was thus investigated next.

7.1.3 Voltage doubler

A voltage doubler circuit is shown in Figure 7.12. The basic operation of the voltage doubler is to charge the capacitors during the positive and negative cycles, and then combine these capacitors over the load, leading to a multiplication of the input voltage.

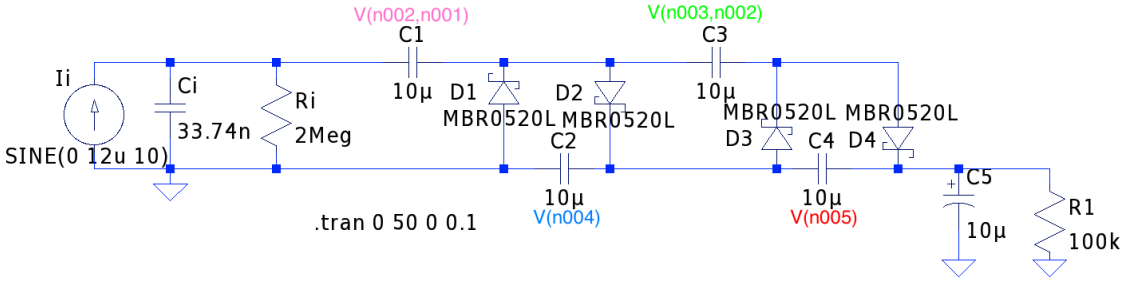

Figure 7.12: Circuit diagram of the voltage doubler.

Figure 7.13 shows four different voltages of the voltage doubler. The voltages shown are the voltage across the capacitors, with the pink line being the voltage over $C1$, green over $C3$, blue over $C2$ and red over $C4$. During the first negative peak, $C1$ is charged through $D1$. During the positive peak $C2$ is charged through $D2$ by the input as well as by $C1$. During the following negative cycle $C1$ is discharged and $C3$ is charged, through $D3$, to the same voltage as $C2$ (almost twice the input voltage). During the following positive cycle $C1$ is charged through the input and $C3$, while $C4$ is charged by the input and $C2$, leading to an output voltage almost four times the original input voltage. From Figure 7.13 the voltage values of capacitors $C2$ and $C3$ are double that of $C1$, and $C4$ is double $C2$ and $C3$, showing perfectly how the capacitors and the input charge the other capacitors during each cycle (the blue and green line are almost equal, and only the blue line is visible). The output capacitor, $C5$, is redundant, as $C4$ is already the output capacitor.

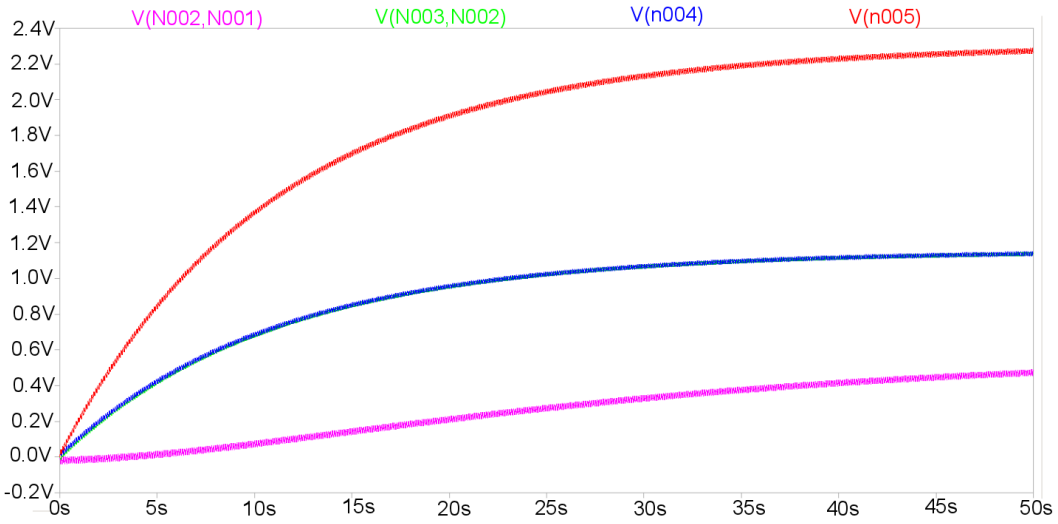

Figure 7.13: Different voltages of the voltage doubler circuit for a better understanding of its operation.

The voltage multiplier also has the problem that it does not conduct the generated charge 100 % of the time, as shown in Figure 7.14. This is illustrated in Figure 7.14, where the black blocks show how the diode blocking time increases. The blocking time is longer at the start, compared to the full-bridge rectifier, and does not increase as rapidly as in the full-bridge rectifier case. The voltage multiplier performs worse compared to the full-bridge rectifier in terms of the generated voltage that is stored in the capacitor [185].

The voltage doubler works best at high load. With a load of 10 MΩ the output voltage is just below 9 V at a current of just below 900 nA. This can be compared to

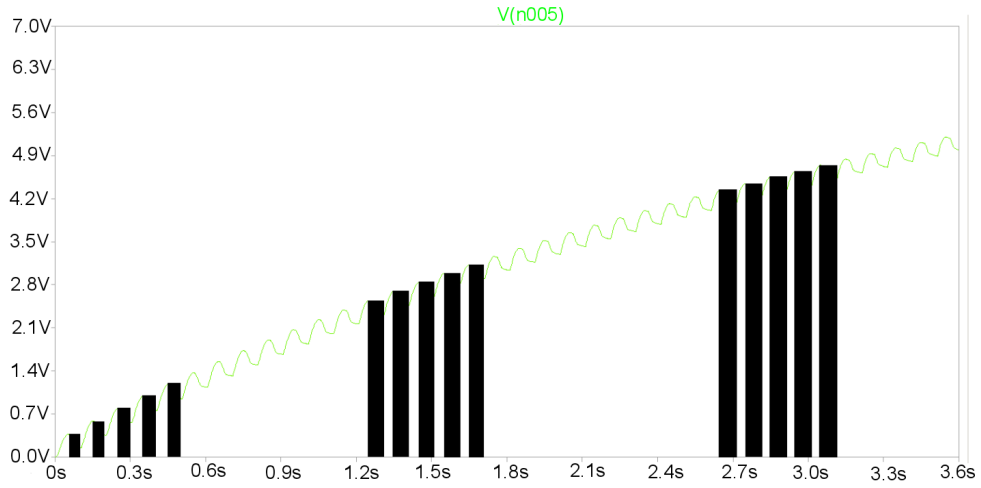

Figure 7.14: The conducting time of the diodes gets smaller as the capacitor charges over time.

the full-bridge rectifier, which has a voltage of just below 5 V and a current of just below 500 nA. Although the voltage doubler gives higher outputs, a load as high as 10 MΩ is not practical. With a load of 100 kΩ the full-bridge recitifier has an output of 600 mV compared to 330 mV for the voltage doubler. The voltage doubler does not function as desired under small load conditions, making the circuit impractical.

The capacitors have the same influence on the circuit as in the full-bridge rectifier case. When the capacitor value increases, the ripple becomes less, but the steady-state time increases. The best capacitor value for this circuit is 1 μF, where a ripple of less than 100 mV is observed and steady state is reached in less than 25 seconds. Larger capacitors increase the steady-state time further. The diodes also have the same influence on the output as was the case for the full-bridge rectifier. Simulations with all the diodes were not repeated as the trend is the same and, hence, the $MBR0520L$ diode was used for the voltage doubler as well.

The power output and input are plotted in Figure 7.15. The input power is again about 27 μW, with the output power just below 8.2 μW, giving an efficiency of 30%, a slight improvement over the full-bridge rectifier.

The minimum input required for a 1 V output, over a 10 MΩ load, is 5.5 μA, which is double the input needed for the full-bridge rectifier. Figure 7.16 shows the output voltage and power when a pulse input current is used. The average output power over 50 seconds is 791 nW, less than the rectifier circuit achieved. This result again shows that the voltage doubler does not function as well under low input current conditions.

The two circuits discussed above work on the same principle. Diodes are used to rectify the input signal and charge capacitors. The full-bridge rectifier and volt-

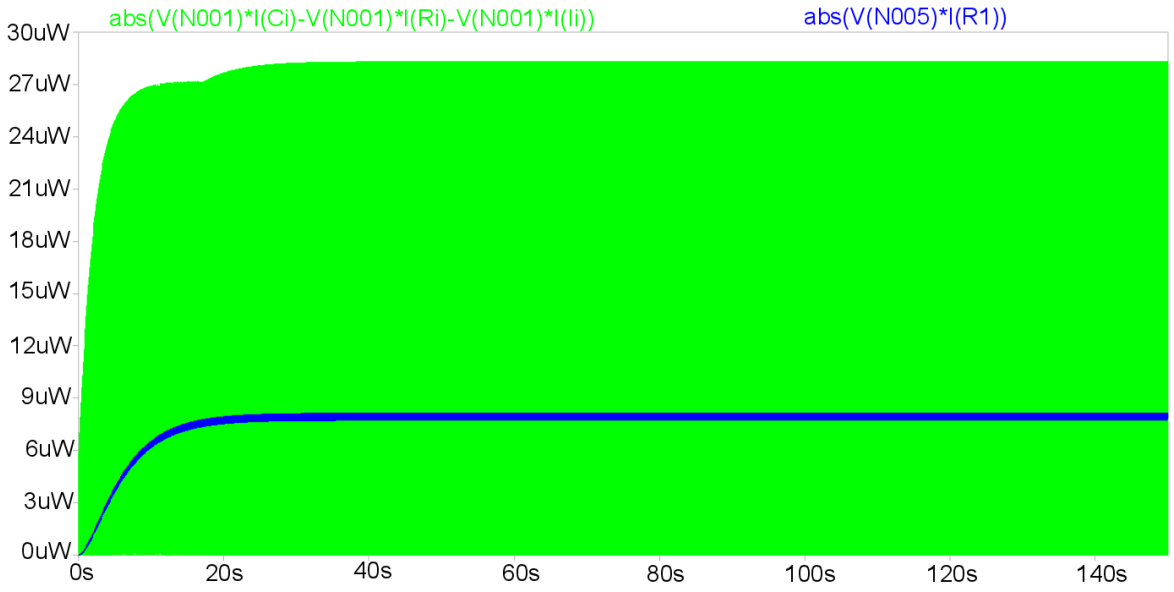

Figure 7.15: Input and output power of the voltage doubler.

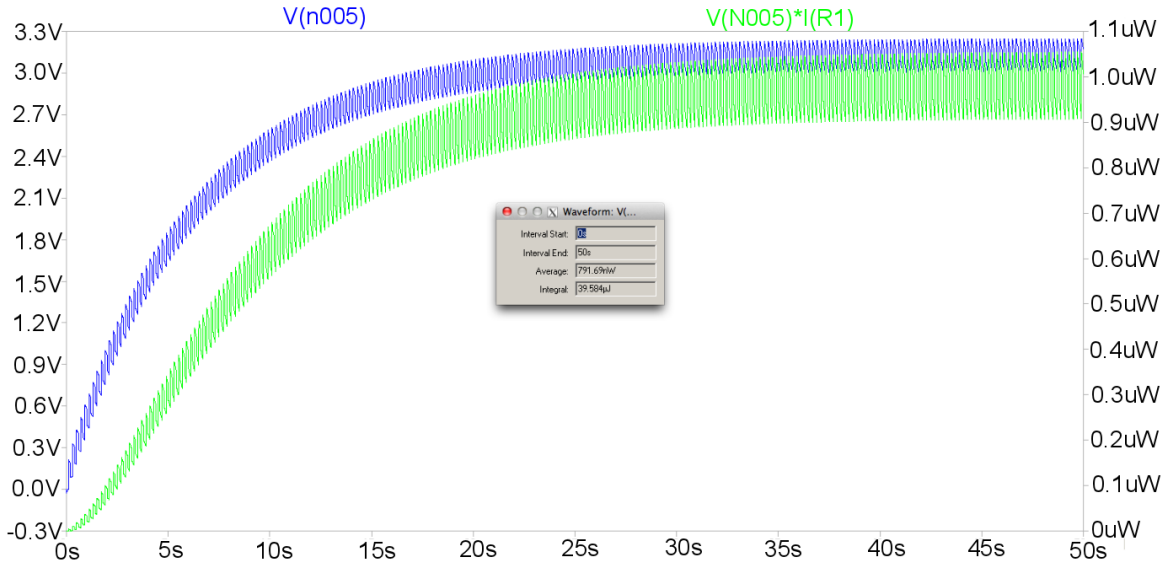

Figure 7.16: Output voltage and power of the voltage doubler when a pulse signal is used as input.

age doubler both have the problem that the diodes block most of the current when the internal capacitor was not charged, meaning that most of the generated voltage was lost. The full-bridge rectifier does, however, function under low current and works well when a pulse input in used. The voltage doubler achieves higher output voltages and power compared to the full-bridge recitifier, but only at high loads. When a smaller load is used, the voltage doubler does not function as desired. At low load the full-bridge rectifier is the better circuit to use, while at high load the voltage doubler outperforms the full-bridge rectifier. A more direct comparison between the two circuits can be found in [185, 186].

A circuit that harnesses all the generated voltage and works with a pulse signal is required. Throughout the literature, the SSHI circuit is used for bulk piezoelectric devices as it gives better performance compared to the other circuits mentioned here.

7.1.4 Synchronised switch harvesting on inductor

Both the full-bridge rectifier and the voltage doubler have the problem that as the internal capacitor charges, the generated voltage is not stored as a result of the diodes not conducting the charge.

The solution to the problem is the synchronised switch harvesting on inductor (SHHI) circuit developed by Guyomar et al. in 2005 [187]. Figure 7.17 shows the basic operation of the SSHI circuit.

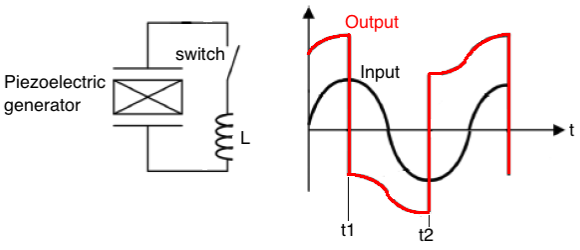

Figure 7.17: Basic operation of the SSHI circuit.

The switch is closed when the input signal reaches a maximum at $t1$, or minimum at $t2$. The inductor and the piezoelectric device form an oscillating circuit. The closing time of the switch is half the period of the oscillating circuit, leading to an inversion of the piezoelectric voltage, as shown in Figure 7.17 [188, 189]. The inversion process is not perfect due to internal losses, as well as further losses over

the load [189, 190]. Guyomar et al. showed that using this technique can result in a 400 to 900% increase in efficiency compared to the full-bridge rectifier and the voltage doubler circuits [187, 188].

Although the basic operation of the circuit is simple, the implementation is more complicated. The switch that opens on the maximum (or minimum) of the piezoelectric voltage is a complicated circuit. The complete SSHI circuit is shown in Figure 7.18.

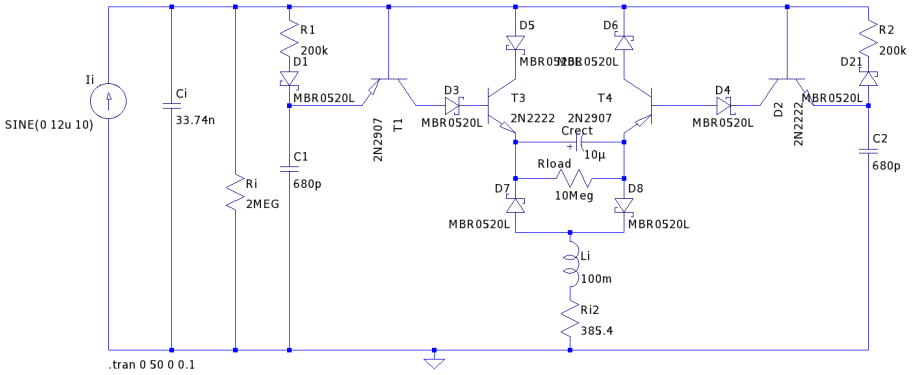

Figure 7.18: Circuit diagram of the SSHI circuit.

The component values were taken from various designs found in the literature [187, 188, 189, 190]. The circuit can be broken into two symmetrical parts. After the current source, the internal capacitor and the internal resistor, the circuit is symmetrical around *Li* and *Ri*2. The left side is for the positive cycle and the right side for the negative cycle. These two circuits represent the switch in Figure 7.17. The circuit works with an electronic breaker that switches on the maximum and minimum peaks. The electronic breaker consists of an envelope detector, a comparator and a switch [191].

The positive cycle is considered first. When maximum input is reached, the envelope detector (*R*1, *D*1 and *C*1) detects this maximum. *T*1 acts as the comparator and *T*3 as the switch. The same applies for the negative cycle, with *R*2, *D*2 and *C*2 acting as the envelope detector, *T*2 the comparator and *T*4 the switch. Before the maximum is detected, the current flow is only through the two envelope detectors, as all the transistors are off. When the input reaches maximum and starts to drop, *T*1 turns on. The capacitor *C*1 discharges through *T*1, *D*3, *T*3, *Crect*, *D*8 and *Li*. Switching on the negative peak follows the identical path for the negative cycle. A more complete description on the operation of the SSHI circuit can be found in [191].

The brief and simplified explanation of the SSHI circuit given above, shows that more parameters and components are present, compared to the full-bridge rectifier and voltage doubler circuits. The circuit has additional diodes, transistors and resistors, compared to the four diodes for the full-bridge rectifier.

Figure 7.19 shows the output from the SSHI circuit when a 60 μA input is used, together with a 347 kΩ load resistor and a 10 μF capacitor. The magnitude of the input is five times larger than the input used for the full-bridge rectifier and voltage doubler, yet the output voltage is lower. When an input current of 12 μA is used, the output voltage is below 400 mV. This is attributed to the additional circuit components. During the positive or negative peak the current flows through four diodes and two transistors, compared to two diodes in both the previous circuits. These additional components require additional input to ensure that they are in the forward active region, a prerequisite for the circuit to function as desired.

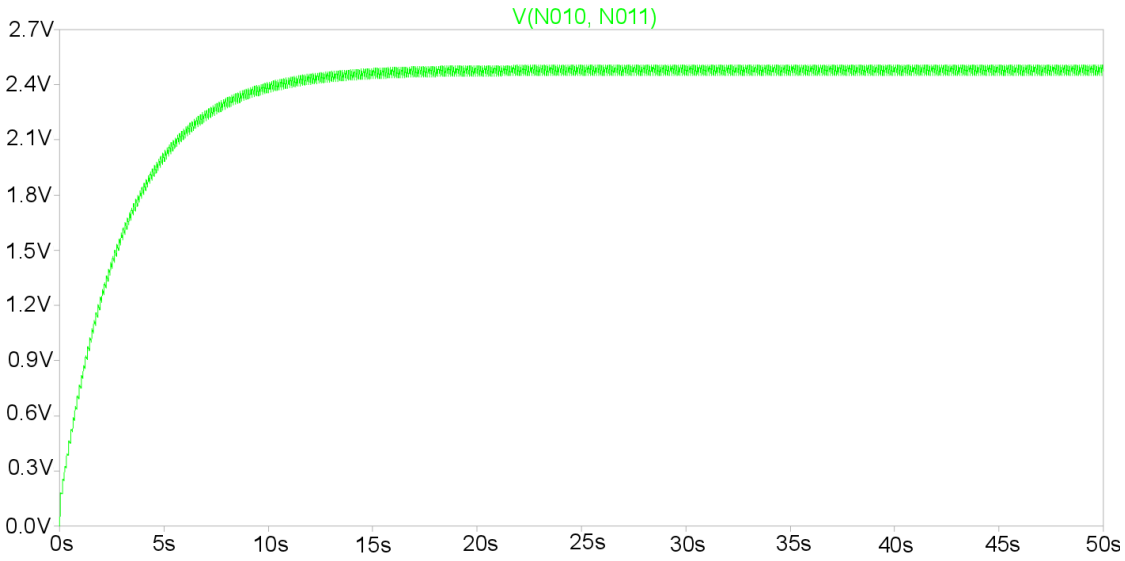

Figure 7.19: Simulated output from the SSHI circuit with a 60 μA input, a 347 kΩ load resistor and a 10 μF capacitor.

The output capacitor, *Crect*, has the same effect as in the previous two circuits, where the value is a compromise between ripple and steady state. The best capacitor value is 10 μF, which leads to steady state in less that than 20 seconds and a ripple of about 100 mV.

The minimum input required to give an output voltage of 1 V is 25 μA, compared to the 2.8 μA for the full-bridge rectifier. Although the SSHI circuit conducts almost 100% of the generated voltage, it does require a larger input current in order to work as desired.

The power efficiency of the SSHI circuit is around 11%, as is shown in Figure 7.20. The input power is just above 200 μW and the output power is just above 22μW. Thus, both of the previous circuits have better power efficiency. However, the circuit has better charge storing efficiency as almost 100% of the charge is stored on the capacitor, compared to the previous circuits where a lot of the charge was lost charging and discharging the intrenal capacitor.

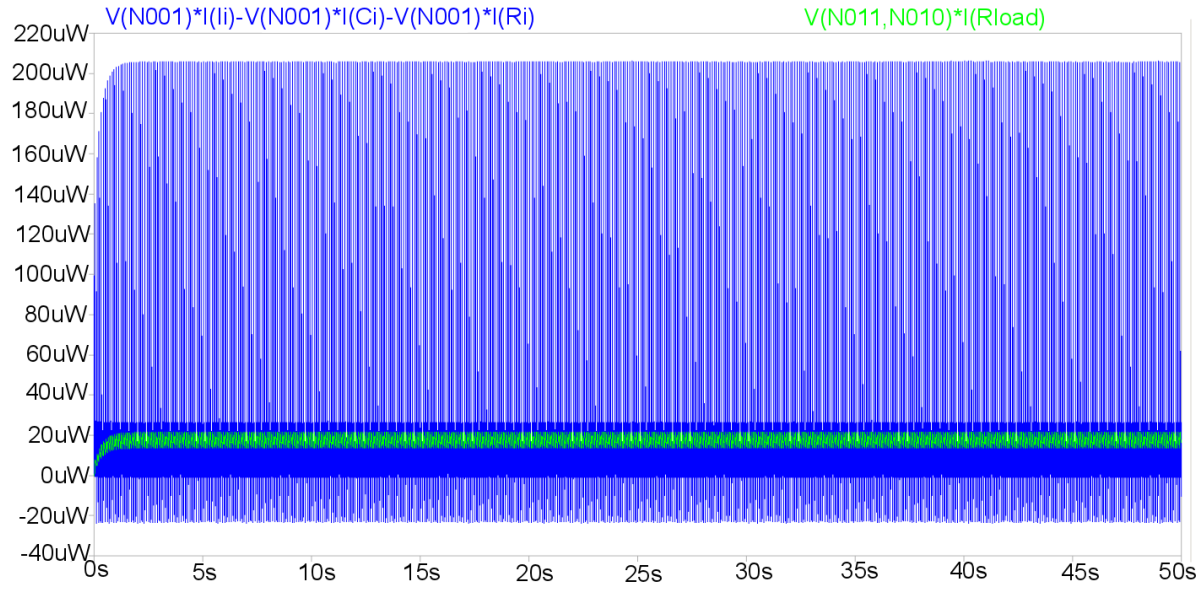

Figure 7.20: Simulated output and input power of the SSHI circuit.

Lastly, the SSHI circuit is simulated with a pulse input signal. The circuit does not work when the input is 180 μA, as is the case with the full-bridge rectifier and voltage doubler. Instead, the required input current is 1.8 mA. Figure 7.21 shows the output voltage and power of the SSHI circuit with a pulse input. The average power is just below 155 μW, compared to just 35 μW when the rectifier circuit has the same input. The SSHI circuit is a lot more efficient compared to the rectifier, but only when the input current is large enough. This is because the SSHI circuit charges the capacitor for the same length of time during each cycle, whereas both the other circuits charge the capacitor less with each cycle, due to the charging and discharging of the internal capacitor.

From the three circuits above it is clear that the SSHI circuit has the best performance. The SSHI circuit conducts the generated voltage almost 100% of the time. This was because the circuit flipped the voltage across the internal capacitor, once charged. The result was that the internal capacitor does not need charging every cycle and, hence, the diodes were conducting almost 100% of the time. The average

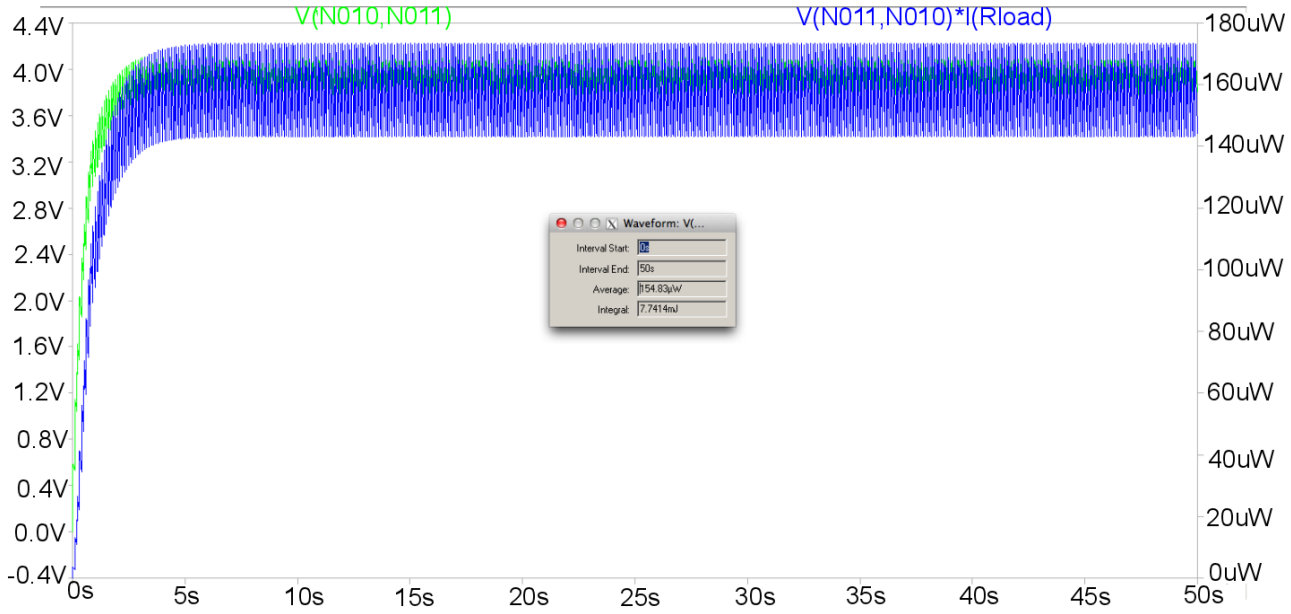

Figure 7.21: Simulated output voltage and power of the SSHI circuit when a pulse input is used with a magnitude of 1.8 mA.

power delivered to the load is also higher when the pulsed signal is used. However, the power efficiency of the SSHI circuit is lower, compared to the rectifier and voltage doubler. The SSHI circuit is, nevertheless, more stable under changes in the magnitude of the load compared to the other two circuits. The main problem with the SSHI circuit is that the minimum current that is necessary for operation is much lot larger compared to the other two circuits. This is due to the extra circuit components that are required to detect the maximum (or minimum).

7.1.5 LTC3588

The last circuit that was investigated is the LTC3588 chip from Linear Technologies [192]. The circuit is not simulated, as no Spice model exists for the integrated circuit (IC) . Figure 7.22 shows the block diagram of the LTC3588 IC [192]. The IC is custom built as an output circuit for a piezoelectric generator.

The LTC3588 has an internal full-wave bridge rectifier that rectifies the piezoelectric input at PZ_1 and PZ_2. The rectified output is then stored in a capacitor at the V_{IN} pin, and is used as an energy reservoir for the buck converter. The full-wave bridge rectifier has a total voltage drop of about 400 mV at 10 μA, which is lower than the diodes used for both the full-bridge rectifier and the voltage doubler. The buck converter is a special type of DC-DC converter and is used to reduce (or

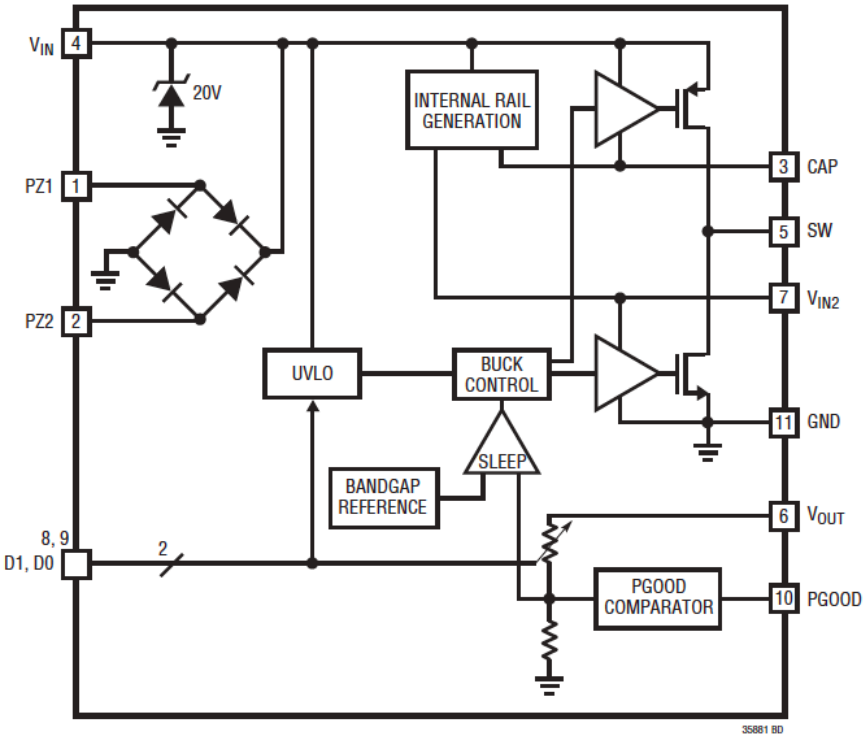

Figure 7.22: Block diagram of the LTC3588 IC [192].

increase) the DC voltage with high efficiency (up to 95%). When the voltage on V_{IN} rises above the undervoltage lockout (UVLO), the buck converter in enabled and the charge is transferred from the input capacitor to the output capacitor. When the input capacitor is below a set voltage, the buck converter is turned off and the input capacitor is charged to the UVLO. Two internal rails are generated from V_{IN}, CAP and V_{IN2}. These internal rails are used to drive the PMOS and NMOS transistors of the buck converter. V_{IN2} also acts as the logic high for the circuit. The buck converter charges the output capacitor through an inductor in order to achieve higher efficiency. The output voltage of the LTC3588 chip can be chosen by select bits $D0$ and $D1$, according to Table 7.1.

Table 7.1: Select bits for the output voltage of the LTC3588 [192].

D1	D2	Output Voltage (V)
0	0	1.8
0	1	2.5
1	0	3.3
1	1	3.6

The power comparator produces a logic high on the P_{GOOD} pin when the output voltage reaches its maximum for the first time. P_{GOOD} remains high until V_{OUT} falls to 92% of the desired output voltage. The input charge can be stored in the input or output capacitors. When the output capacitor is full, excess charge is stored in the input capacitor, making sure none of the generated charge is wasted. The relevant of pages of the datasheet of the IC are appended as Appendix C.

The LTC3588 IC combines all the advantages of the previous circuits. It takes the full-bridge rectifier, which ensures a stable output with low input current, and it charges the input capacitor, which in turn, charges the output capacitor, as a voltage doubler circuit, thus ensuring better efficiency. Lastly, the buck converter almost works as the SSHI circuit, where it turns on at a set value (UVLO) and conducts charge for a while before turning off.

The LTC3588 IC does not supply a constant voltage to a load. Instead, the input and output capacitors are charged to the maximum to ensure the selected output voltage can be achieved. Once the capacitor is charged, the output voltage will be kept constant until the charge in the capacitors drops below a certain point and the output voltage is removed. The capacitors are again charged before the output voltage is turned on again. The LTC3588 will work in bursts and not on a constant basis. This has advantages and disadvantages. It can achieve higher output currents, the output voltage is set at a single voltage without any ripple or change as long as the capacitors are charged, but the output voltage might be off when the load sensor has to sense an important parameter. This limits the application of the LTC3588 IC to a certain extent.

The simulation of three output circuits was discussed above, as was the operation of a fourth IC. Each circuit exhibited a number of advantages making it a better choice than the other circuits, but certain limitations also hampered their operation. The simulations were used to show the behaviour of the circuits and also what is to be expected in practical tests. The rectifier and voltage doubler circuits worked well in low current environments, but were dependant on the magnitude of the load. Both circuits also had the problem that all the generated charge is not transferred to the output capacitor, leading to a decreased in efficiency. The SSHI circuit achieved better efficiency in terms of conducting the generated charge, but did not work under low current situations. The LTC3588 circuit showed great promise, but the output voltage was only available once the capacitors were charged.

However, simulations alone cannot be used to determine the optimal circuit to use for the nanogenerator. As discussed above, all the circuits showed good behaviour under different conditions, but each circuit had certain limitations. Practical experiments are therefore necessary to see which circuit will work best with the

nanogenerator.

7.2 Practical experiments

The simulations of the output circuits helped to optimise the circuits before practical testing. The simulations resulted in diodes that gave high output voltage and capacitor values that ensured fast steady-state conditions with little ripple. Simulations do, however, make certain simplifications and do not take into account component parameter drift or any temperature-dependant factors.

The circuits discussed above were all built with components from RS Electronics [193]. A nanogenerator was connected to each circuit individually and was bent as discussed in Chapters 3 and 6. The voltage across the output load was measured using a 10× probe and an oscilloscope. The current was measured with a HP4140B pico-ampere meter.

7.2.1 Full-bridge rectifier

The full-bridge rectifier was built using the design shown in Figure 7.5. The diodes were surface mount $MBR0520L$ Schottky diodes. Various loads were used, including a 10 kΩ resistor, a 1 MΩ resistor and an LED.

Figure 7.23 shows the measured output voltage of the full-bridge rectifier with a 10 kΩ load and a 10 μF capacitor. The nanogenerator was bent for three minutes before the probe or the load was connected. The measured output voltage fluctuated around 2 V. The high peaks that are visible are attributed to noise, that originated from friction between the nanogenerator and the output circuit, as well as between the load and the output circuit. The nanogenerator was bent while the measurements were taken. The time scale was one second per division and the voltage was 2 V per division. The measured voltage was not stable, with a number of high and low peaks throughout the graph. The circuit does rectify the spiky input from the nanogenerator to a more useable form, but is still not perfect.

The load resistor was changed to 1 MΩ and the resulting measured output is shown in Figure 7.24. The output voltage dropped to about 1 V, contrary to the simulations. During the simulations the output voltage increased when the load was increased, but that was due to the ideal current source that was used to simulate the nanogenerator. The nanogenerator delivers a small amount of current and the bigger load is far from the optimal resistor for the circuit, leading to a smaller measured output voltage. The time scale was now five seconds per interval, showing that the output voltage was a lot more stable, with almost 20 seconds of constant 1 V supply at the beginning of the graph. After the initail stable region, the na-

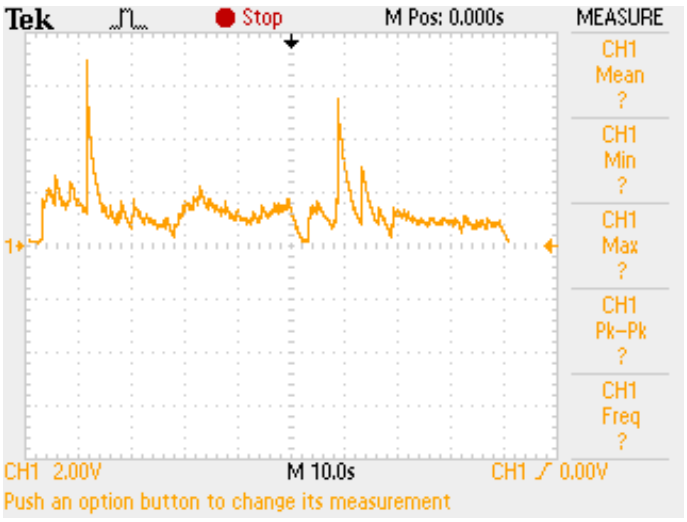

Figure 7.23: Measured output voltage of the full-bridge rectifier with a 10 kΩ load and a 10 μF capacitor. The nanogenerator was bent for two minutes before connecting the load and the probe.

nogenerator is not bent, resulting in a drop in the measured output voltage. Once the nanogenerator was bent again, the graph became eratic while the capacitor charged.

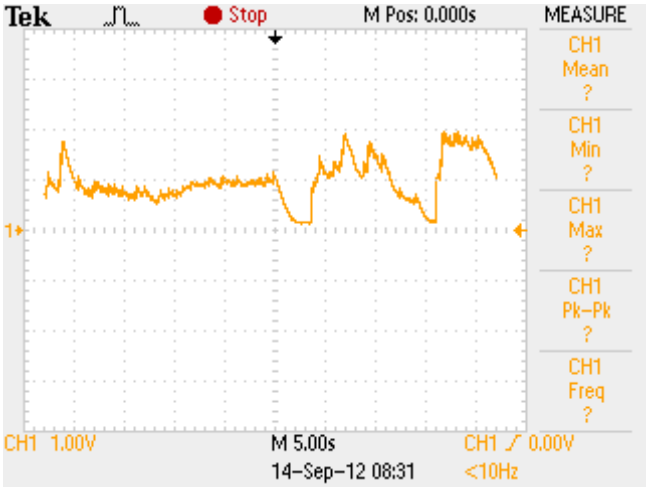

Figure 7.24: Measured output voltage of the full-bridge rectifier with a 1 MΩ load and a 10 μF capacitor. The nanogenerator was bent for 2 minutes before connecting the load and probe.

One important component that could not be investigated during the simulations is the type of capacitor that is used at the output. Different types of capacitor

exist, plastic film capacitors, ceramic capacitors, aluminium capacitors and super capacitors, to name but a few. Each capacitor works best for a different type of application. All the different types of capacitors were tried and plastic film capacitors were found to work the best. This is because the leakage current of these capacitors is the smallest of the capacitors that were tested and, hence, the generated charge could be stored more efficiently.

The mentioned test was carried out with a 10 μF, 4 V plastic film capacitor. A super capacitor was used next for the test, with a capacitance value of 10 mF. The capacitance value is much larger than the previous cases. The super capacitor functionality is different from conventional dielectric capacitors, and the capacitance can be increased an order of magnitude without noticable negative impact on the electronic circuit [194].

Figure 7.25 shows the measured output voltage of the full-bridge rectifier with a 735 kΩ load, using the super capacitor. The load resistance was the optimal value, as calculated during the simulations, and will thus lead to maximum power being delivered to the load.

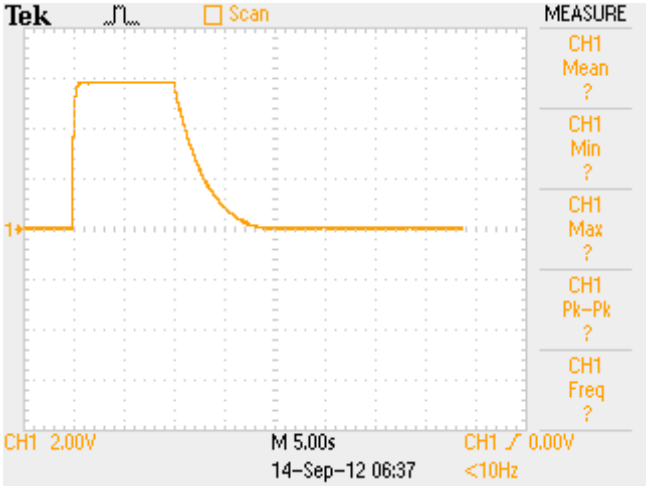

Figure 7.25: Measured output voltage of the full-bridge rectifier with a 735 kΩ load and a 10 mF super capacitor. The nanogenerator was bent for five minutes before connecting the load and the probe.

The output voltage was measured as 5.75 V, much higher than the previous two cases. The optimal load and super capacitor thus enhanced the circuit performance and led to a high output voltage. The nanogenerator was bent for five minutes before connecting the probe. The time scale was five seconds per division, giving a stable voltage for about 10 seconds, while still bending the nanogenerator. Once stopped, the capacitor discharged in 5.5 seconds. At maximum voltage the current

through the load was measured as 20 μA, giving a load power of 0.115 mW. This was achieved after almost five minutes of bending.

The full-bridge rectifier functioned as desired with a maximum output voltage of just below 6 V. This high output voltage was only achieved at optimal load and with a super capacitor. At different load values the output was less than 2 V with a lot of noise at the output. The main problem was that the nanogenerator had to be bent for over five minutes before a high enough voltage was measured. The time scale was large due to the super capacitor that was used.

When a normal capacitor is used the charge time of the capacitor needs to be reduced and the output voltage increased in order for the output circuit to be useful.

7.2.2 Voltage doubler

The voltage doubler was constructed with the same diodes as in the full-bridge rectifier, with 10 μF capacitors connected in between. Figure 7.26 shows the output voltage of the voltage doubler circuit with a 1 MΩ load and a 10 μF capacitor connected. The measured output voltage was above 4 V, and more stable than the measured rectifier circuit output. The time scale was 10 seconds per division, showing how stable the circuit was. The probe was connected to the load after two minutes of bending. The output dropped to zero in 20 seconds and quickly jumped to 2 V and remains steady for a while. After the initial 4 V the nanogenerator was no longer bent and the voltage thus dropped. After 10 seconds the nanogenerator was bent again. It took more than 10 seconds for the graph to increase to 2 V again.

Figure 7.27 shows the measured output voltage of the voltage doubler circuit with a 10 MΩ load and a 10 mF super capacitor connected. The output voltage was measured as 11.8 V, double that of the full-bridge rectifier. The nanogenerator was bent for just over four minutes to achieve this output. The nanogenerator was left undisturbed and the output dropped to zero in 30 seconds, a slight improvement over the full-bridge rectifier. The current measured at maximum voltage was 5.5 μA, a lot lower than the rectifier circuit. The voltage doubler achieved an output power of 64.9 μW, almost half the power achieved by the rectifier circuit.

The charge time for the voltage doubler was slightly shorter and the output voltage double that of the rectifier circuit. The problem is that the output current was much smaller due to the larger load and the basic operation of the circuit. Both the rectifier and the voltage doubler had the problem that they did not transfer all the generated charge to the load due to the diodes that were reversed biased for a large part of the time, due to the effect of the internal capacitor.

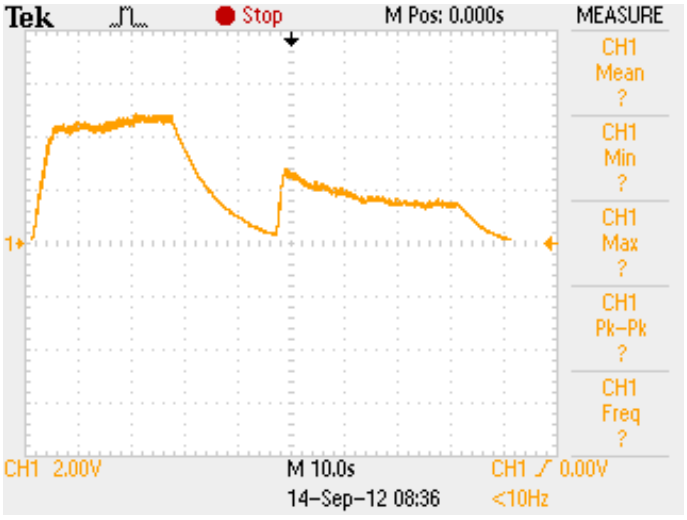

Figure 7.26: Measured output voltage of the voltage doubler with a 1 MΩ load and a 10 μF capacitor. The nanogenerator was bent for two minutes before connecting the load and the probe.

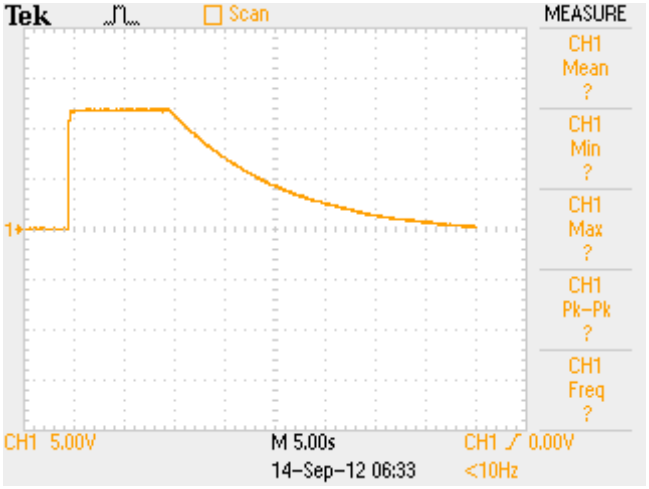

Figure 7.27: Measured output voltage of the voltage doubler with a 10 MΩ load and a 10 mF super capacitor. The nanogenerator was bent for four minutes before connecting the load and the probe.

7.2.3 Synchronised switch harvesting on inductor

The simulations showed that the SSHI circuit can solve the problem of not charging the capacitor 100% of the time, as was the case for the rectifier and voltage doubler circuits. The simulations showed that the SSHI circuit can achieve higher power output, but only at higher input currents, compared to both the rectifier and voltage doubler circuits.

Figure 7.28 shows the measured output voltage of the SSHI circuit. The load resistance was 10 kΩ and a 10 μF capacitor was connected. The output voltage is just above 200 mV, considerably less than the rectifier and the voltage doubler circuits. The output current measured through the load in the rectifier case was only 20 μA and during the simulations 60 μA input was used for the SSHI circuit. When 12 μA input was used in the simulation, the output voltage was 400 mV, showing that the circuit did not function at low currents.

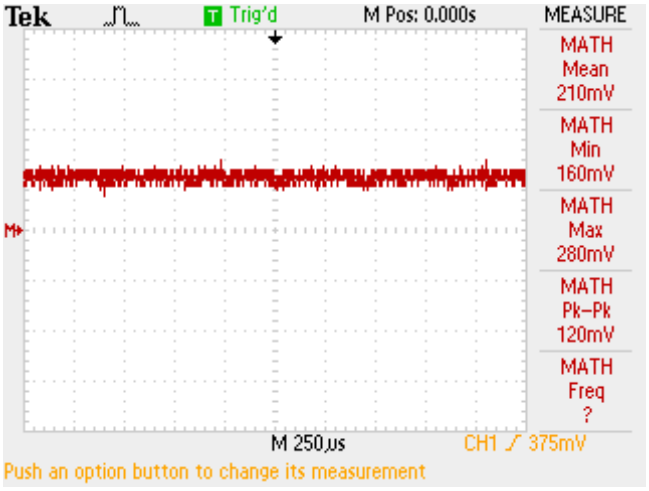

Figure 7.28: Measured output voltage of the SSHI circuit with a 10 kΩ load and a 10 μF capacitor.

Although the simulations showed that the SSHI circuit will be the best choice, practical experiments showed that the nanogenerator current was too small to drive the circuit.

7.2.4 LTC3588

The LTC3588 IC does not have input or output capacitors built into the IC, but instead they are soldered on. Figure 7.29 shows the circuit used with the LTC3588 IC. The circuit was used with the component values obtained from the datasheet

[192]. The output voltage was selected as 1.8 V, through the $D1$ and $D2$ select bits (both are grounded).

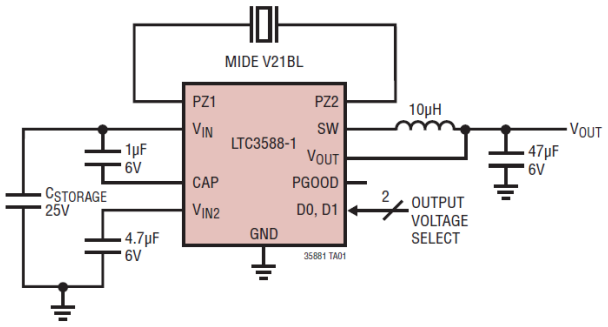

Figure 7.29: LTC3588 circuit with input and ouput capacitors as well as inductor and other circuit components [192].

Figure 7.30 shows the measured output voltage of the LTC3588 circuit. The nanogenerator was bent for six minutes and a constant 1.8 V output was generated. As soon as the voltage was at 1.8 V the bending was stopped. The circuit maintained the output for almost 20 seconds.

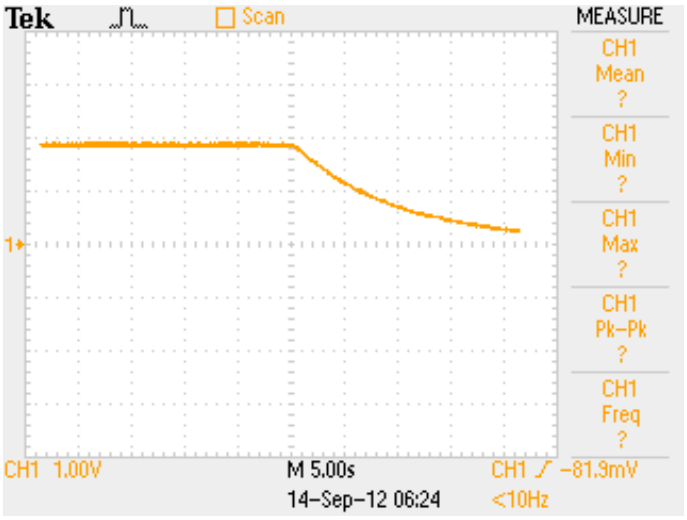

Figure 7.30: Measured output voltage of the LTC3588 circuit after six minutes of bending.

Figure 7.31 shows the measured output voltage of the LTC3588 circuit with the super capacitor. The nanogenerator was now bent for almost 10 minutes to achieve the 1.8 V output. The graph shows only eight seconds of a constant 1.8 V supply, but with the super capacitor and a 10 kΩ load, the voltage was kept constant for close to 20 seconds (only 8 seconds is showed in the graph). The output current at 1.8 V was 0.17 mA, giving an output power of 0.306 mW, more than double that achieved with the full-bridge rectifier.

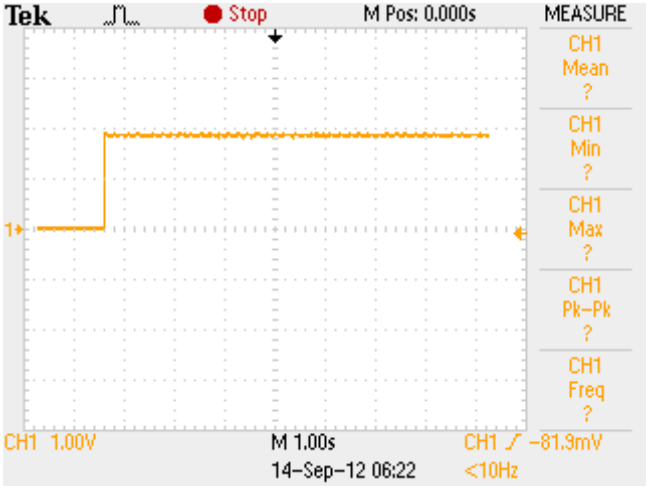

Figure 7.31: Measured output voltage of the LTC3588 circuit with the super capacitor connected as the output capacitor.

The LTC3588 circuit achieves the most constant output voltage of all the circuits. The rectifier and the voltage doubler can both supply a voltage output from the moment the nanogenerator is bent, although the initial voltage is small and increases as the nanogenerator is bent more. In contrast, the LTC3588 circuit can only deliver an output voltage once the capacitor is charged.

7.3 Conclusion

Four different circuits were investigated for use as the output circuit for the nanogenerator. The purpose of the circuits were to convert the spiky signal from the nanogenerator to a DC signal. This is necessary, because most electronic equipment functions on DC and for continuous operation, the spiky input signal will not work.

The four circuits tested were the full-bridge rectifier, the voltage doubler, the SSHI and the LTC3588 IC. The circuits were simulated in LTSpice to optimise the

design and simulate important circuit parameters, including minimum input current, optimal load, output capacitor magnitude and more. The simulations were followed by practical experiments to verify the operation of each circuit and to investigate which circuit operated the best.

The full-bridge rectifier and the voltage doubler circuits both resulted in a DC output during the simulations. Both circuits worked best under high load conditions and also worked with low input currents. In comparison, the SSHI circuit worked with smaller loads, but did not function when the input current is too small. The SSHI circuit solved the problem of the limited conduction time of the rectifier and the voltage doubler circuits. Although the SSHI circuit solved this problem, practical experiments showed that the circuit did not work owing to the small currents generated by the nanogenerator. Therefore, the SSHI circuit was not optimised further.

The rectifier and voltage doubler circuits gave promising results in practical tests as well. The problem was that, due to the unstable input, the output voltage was unstable as well. The output voltage fluctuated a great deal, although stable areas were observed. Both these circuits can be further optimised with additional components added to stabilise the output voltage. The rectifier circuit outperformed the voltage doubler, as the output power of the rectifier was 0.115 mW, compared to the 64.9 μW of the voltage doubler. The simulations also showed that the rectifier outperformed the voltage doubler when the input current was small. The voltage doubler did, however, charge the output capacitor faster than the rectifier. Both circuits, however, still required more than four minutes of continuous bending of the nanogenerator to generate enough charge to supply a decent output voltage.

The last circuit that was investigated was the LTC3588 IC from Linear Technologies. The IC is designed to work with piezoelectric generators. It works by first charging a capacitor and, once fully charged, the output voltage is generated until the capacitor is depleted. The output voltage is then turned off, while the capacitor charges again. This means that continuous operation is not possible with the LTC3588 circuit, whereas with the previous circuits that was possible. The LTC3588 IC can be used to power a device in bursts, but this limits its application. However, the supplied voltage and current will be steady, a more so than the rectifier or the voltage doubler. The output power achieved with the LTC3588 IC was 0.306 mW, double that of the rectifier circuit and almost five times that of the voltage doubler circuit.

The LTC3588 IC also has the advantage that the output voltage does not depend on the load. It supplies a constant voltage, as determined by two select bits, which

are independent of the load magnitude. The load current will, however, vary according to the load magnitude, and the operation time will decrease as the load increases. This makes the LTC3588 circuit the ideal solution for the output circuit, although the burst operation (not working continuously) limits the application.

Most testing was done with the LTC3588 circuit, as it showed the best results in preliminary testing, compared to the rectifier, the voltage doubler and the SSHI circuits. Figure 7.32 shows an LED that lights up for three seconds after the nanogenerator is bent for 10 minutes. The super capacitor was connected to the LTC3588 circuit to store the generated charge. The LED has a forward voltage of 1.8 V and a minimum current of 1 mA.

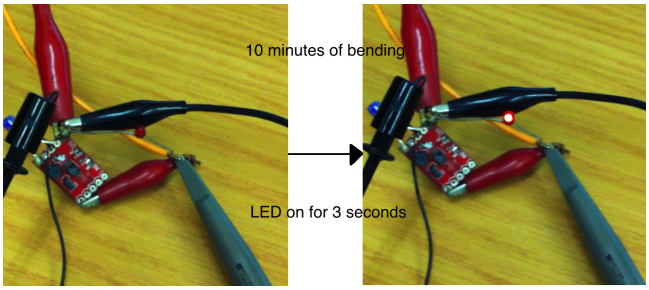

Figure 7.32: Bending a nanogenerator for 10 minutes turns an LED on for three seconds, using the LTC3588 circuit.

The LTC3588 circuit was thus successfully used to power the LED without connecting any voltage source other than the nanogenerator. Although 10 minutes of bending for only three seconds of operation is ineffective, it does show that the nanogenerator can be used to power different loads. When using resistors with varying magnitudes, the output is kept constant for longer periods of time. As mentioned, with a 10 kΩ load the circuit supplies constant voltage and current for 20 seconds. This means that the nanogenerator and the LTC3588 can be used to take measurements every 10 minutes and transmit the data to a different source. Although continuous functioning would be ideal, this is a first step in realising that.

The work presented in this Chapter was published in *Smart Materials and Structures* [195].

Chapter 8

Conclusion

The work presented in this dissertation is based on work done over the course of three years (since 2010). The work is also a continuation of the work done during the author's Master's degree [196]. Over the last five years extensive knowledge in certain areas of nanotechnology has been developed. This knowledge, plus knowledge developed over the four years of undergraduate studies, helped the author to successfully complete this dissertation.

Nanotechnology is a new scientific field, with less than 50 years of extensive research [41]. This means that there is still a lot of room for new innovation and optimisation, but there is also less literature on which to base findings. Throughout this dissertation new methods and techniques were developed to overcome certain obstacles.

This chapter gives an overview of the development and optimisation of a ZnO nanowire-based nanogenerator. Firstly, the aims and the objectives are reviewed, accompanied by remarks if they were met. The main findings of the dissertation are presented again and concluding remarks are made. Next, a brief look is taken at the significance of this work and the contribution it makes to the body of knowledge. Lastly, future research on this topic is discussed.

8.1 Review of aims and objectives

The main objective of this project was to optimise the output voltage of a ZnO nanowire-based nanogenerator. In order to realise the main objective, it is divided into smaller aims.

The literature study in Chapter 2 gave a comprehensive look at the piezoelectric effect of ZnO nanowires. The piezoelectric effect was introduced with a physical and mathematical description of the phenomenon. This was followed by an in-depth discussion of ZnO, and in particular ZnO nanowires. The nanogenerator

was introduced next, followed by a physical and mathematical description of the operation of a nanogenerator. This was done to provide the necessary background for the nanogenerator, in order to identify areas where further optimisation could be achieved. Throughout the literature study, no mention was made of the manufacturing, measuring or optimisation of the nanogenerator. This was because a big gap exists in the literature on these three topics and the aim of this project was to fill that gap. The three aims that were successfully achieved are the development of a physical model, the development of a mathematical model and the identification of the gaps in the optimisation of nanowire growth and nanogenerator manufacturing.

The next objective was to conduct simulations on the nanogenerator. Comsol Multiphysics was used to perform the simulations in both cases [133]. The aims of these simulations were to prove that both the mathematical and the physical models developed during the literature study are correct. The simulations were also used to ensure that ZnO was the best material to use, as well as to identify the areas of optimisation required to increase the output voltage. These aims were successfully achieved.

In order to achieve the main objective, improving the output voltage of the nanogenerator, the growth of ZnO nanowires was of the utmost importance. Different growth methods were investigated. These methods were optimised using two methods, namely one parameter at a time and design of experiments. The main aim was to increase the output voltage by changing specific parameters during growth. This objective was successfully achieved. Using growth optimisation, the output voltage was raised from the base value. The aims achieved for this objective was the identification of the best growth method and optimising the output voltage of the growth methods.

The second main objective was the optimisation of the nanogenerator. This objective was the main focus of this dissertation. Various methods and techniques were used to optimise the output voltage of the manufactured nanogenerator and this objective was achieved with great success. Using the various methods the output voltage was raised considerably. The aims in this section was the successful optimisation of the solid nanogenerator, the manufacturing of a flexible nanogenerator, applying thin film optimisation techniques to the nanowires, using other methods to further increase the output voltage of the nanogenerator and, lastly, the doping of the nanowires. All these aims were successfully achieved.

Figure 8.1 shows the five main objectives of this project, with the amount of time spent on each. The optimisation of the nanogenerator and nanowire growth almost consumed two-thirds of the project. As mentioned, the main objective was

the optimisation of the nanogenerator and this was achieved by optimising nanowire growth and nanogenerator manufacturing. The gas sensor only consumed 10% of the time allocation, as it was only investigated near the end of the project. Various tests were performed on the ZnO nanowires to see what other applications they could be used for. During these tests the influence of gas was seen to be comprehensive and was consequently investigated. The development and optimisation of a ZnO nanowire-based gas sensor will form a project on its own and was hence not comprehensively investigated. The literature study was also a big part of the project as it was used, together with the simulations, to identify areas where both the nanowire growth and the nanogenerator could be optimised to achieve higher output voltage.

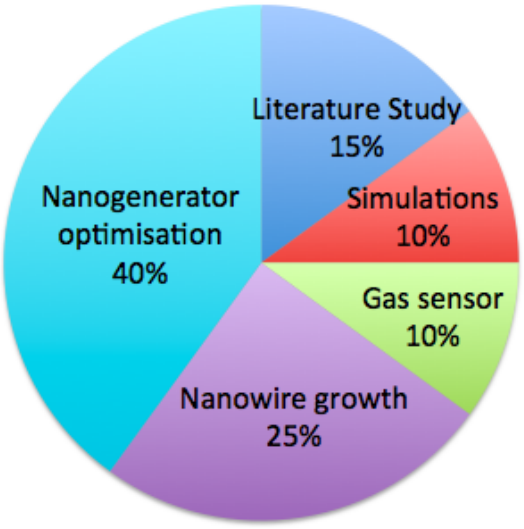

Figure 8.1: Pie chart showing the five main objectives of this project, together with the percentage of time spent on each objective.

Ultimately, the aims was to increase the output voltage of the nanogenerator. For the most part this aim was successfully achieved and the objectives accomplished. These successfully achieved aim and objectives are discussed in more detail in the following section.

8.2 Main findings and significance of work

A number of articles in the literature were found on nanogenerators, but a lack of detail was evident. Very few details were provided on the manufacturing of

the actual device, but the articles tended to focus on specific measurements or applications. The second area where little or no mention was found in the literature was the methodology for measuring the output voltage of the nanogenerator. The voltage generated by the nanogenerator was small in the non-optimised case and certain precautions had to be taken to measure the actual generated voltage. Lastly, throughout the literature many techniques for optimising the manufacturing of ZnO thin film devices are mentioned, but very little is mentioned about the optimisation of ZnO nanowires. These thin film techniques were investigated to see whether they could be applied to the nanowires.

In this section the findings on the three literature omissions mentioned above are discussed in more detail. Firstly, the findings on the method for measuring the output voltage are discussed. This is followed by the findings on the measurement of the carrier concentration and resistance of the nanowires and the significance of this work. Next, the optimisation of the nanowires is discussed. The main findings on the manufacture of two different types of nanogenerator are discussed.

8.2.1 ZnO nanowire electrical measurements

Throughout the literature very limited discussion was found on the measurement of the output voltage of the nanogenerator, and for this reason it was crucial to find a novel method to measure the output voltage of the nanogenerator.

The biggest problem in this regard was that the piezoelectric voltage generated from a single nanowire is very small and is of short duration [91, 93]. Measuring the voltage of a single nanowire was not of importance as the nanogenerator consists of multiple nanowires, all acting together to generate an output voltage. Hence, the focus was on finding a method to measure the output voltage of a nanogenerator which consisted of multiple nanowires. Figure 8.2 shows a block diagram of the setup of the output voltage measurement. The nanogenerator was connected to a buffer circuit, which in turn was connected to an ADC and lastly, this is connected to a PC to display the generated voltage on the screen.

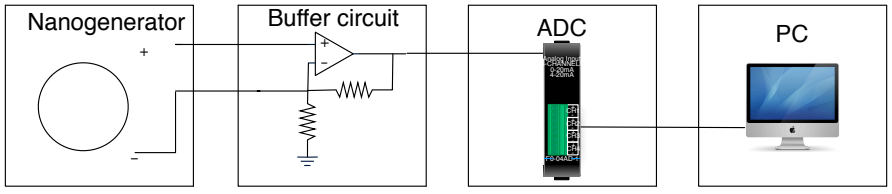

Figure 8.2: Block diagram showing the setup for measuring the output voltage of the nanogenerator.

This method was extremely easy to implement. Once the setup was in place, the output voltage could be measured. The actual measurement was done by placing a gold electrode on top of the solid nanogenerator, or by bending the flexible nanogenerator. Either method caused the nanowires to bend and an output voltage could be measured. Figure 8.3 shows the typical measured output voltage of an optimised nanogenerator.

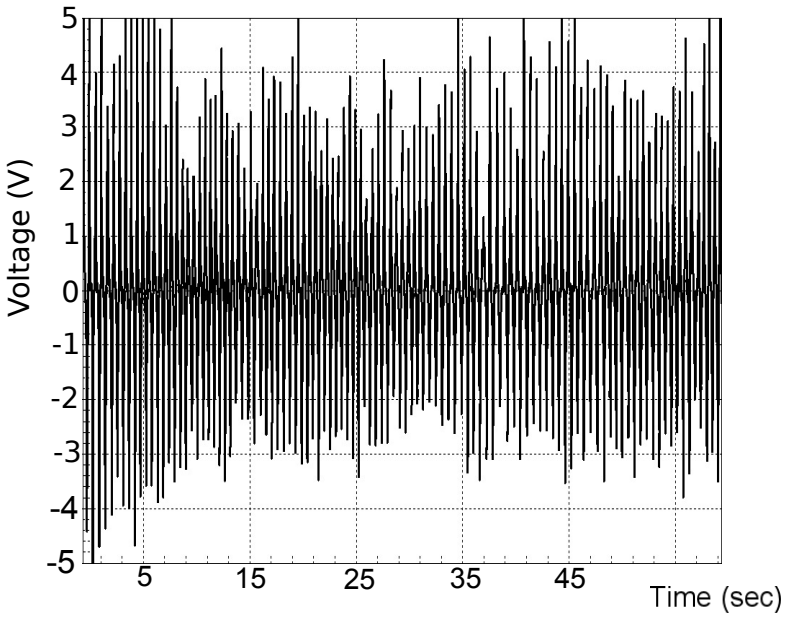

Figure 8.3: Typical measured output voltage of a flexible nanogenerator.

This method can be used to measure and display the output voltage of either type of nanogenerator. It can also be used to inspect the voltage waveform after measurement, depending on the software that is used. The work on the measurement of the output voltage was published in a peer-reviewed journal, *Nanotechnology*, in 2011 [129].

After successful voltage measurements, focus was shifted to other electrical parameters. Two important electrical parameters are carrier concentration and resistance. These two parameters are closely related, as a low carrier concentration means that current will not flow as easily through a material and hence, the resistance is high. These two parameters, resistance and carrier concentration, can be measured using the Van der Pauw [130] and Hall [131] measurement techniques, respectively.

These measurements were made, because Wang et al. [59, 93] predicted that there is an optimal value for both these quantities. At low resistance and high car-

rier concentration, the majority of free electrons screen the piezoelectric charge and the measured output voltage will be much less than expected. At high resistance and low carrier concentration the internal loss in the nanowire will be too large and the output voltage will again be smaller than expected [59, 93]. It was thus argued that an optimal value for both carrier concentration and resistance exists, where the screening of the piezoelectric charges and the internal loss in the nanowire are at such a value that the output voltage is optimal.

Figure 8.4 shows the typical measurement of output voltage versus carrier concentration. A clear peak is visible at a certain carrier concentration, where the measured output voltage is larger than at other carrier concentration values. The theoretical predictions by Wang et al. are shown to be true and an actual optimal range does exist.

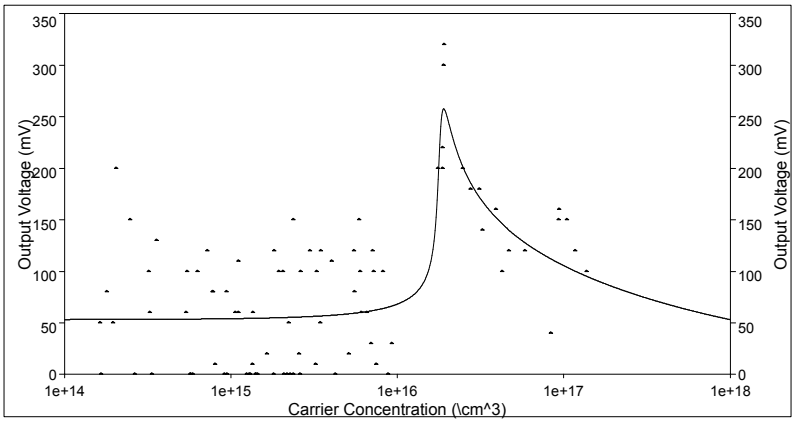

Figure 8.4: Typical measurement showing the output voltage versus the carrier concentration of ZnO nanogenerators.

This work led to the publication of another article in *Micro Nano Systems Letters* [132]. The methods used to measure both the carrier concentration and the resistance were developed for thin films. This means that the values obtained from this work might not be 100% accurate, but are still of importance. The measurements showed that an optimal range exists and, furthermore, it falls within the range predicted by Wang et al. [59, 93]. For more accurate measurements alternative methods will have to be used.

8.2.2 Nanowire growth and optimisation

The output voltage generated by the bending of the nanowires could now easily be measured, and nanowire growth was consequently investigated to optimise the

measured output voltage.

Two growth methods were investigated, the vapour liquid solid (VLS) method and an aqueous solution method. Both methods were discussed in Chapters 2, 3 and 5. The VLS method is a high temperature method, working at temperatures in excess of 900°C, while the aqueous solution method works at below 100°C.

Both methods have a number of parameters that can be changed between growth experiments. For the VLS method these parameters include growth temperature, growth time, initial pressure, growth pressure and amount of source material. For the aqueous solution method the parameters include growth temperature, growth time, concentration solution and ratio of source material. These parameters directly influence the quality of the grown nanowires and were changed between consecutive experiments to investigate the influence. Figure 8.5 (a)—(c) shows nanowire growth using the aqueous solution method, with three different values for the concentration of the solution. The figure shows growth at 90°C for seven hours with a 80 mM solution, 30 mM solution and 40 mM solution. From the three figures it is clear that the concentration of the solution affected the thickness of the nanowires, with Figure 8.5 (a) having the highest concentration and also the thickest nanowires.

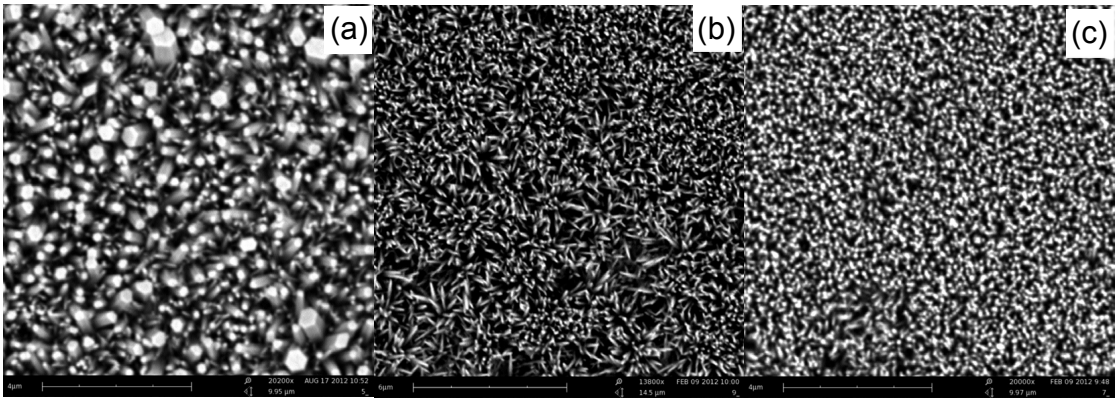

Figure 8.5: ZnO nanowires grown by the aqueous solution method at 90°C for seven hours with a (a) 80 mM, (b) 30 mM and (c) 40 mM solution.

The mathematical model derived in Chapter 2 shows that the output voltage generated by a single nanowire only depends on the diameter of the nanowire and

not the length. According to (2.6.17) the nanowires in Figure 8.5 (b) should thus yield the highest output voltage, because their diameter is the smallest.

The mathematical model and simulations were used to further optimise the nanowires. Both the permittivity and piezoelectric constant plays an important role in the output voltage. It was, however, not as easy to alter these two parameters during the growth, as it was not clear what the influence of the growth parameters would be on these two parameters.

The two growth methods were optimised using two techniques, one parameter at a time and design of experiments. The one parameter at a time optimisation was used to find maximum and minimum values for each parameter mentioned above, for which the nanowire growth was clearly visible, with well-aligned, dense growth. Using this approach, it was also easy to see the influence that a single parameter had on the growth, as is the case in Figure 8.5 with the concentration of the aqueous solution growth. The one parameter at a time optimisation was done for both methods and over 150 samples were grown to find the maximum and minimum values. The output voltage was measured for each sample and it was found that the aqueous solution method outperformed the VLS method. The output voltage for the aqueous solution method was, on average, 150 mV, compared to less than 80 mV for the VLS method.

The maximum and minimum values for the growth parameters of the aqueous solution method are shown in Table 8.1. These values were found during the one parameter at a time optimisation. The parameters were then used for the DoE. During the DoE one parameter was changed at random between consecutive experiments and the output voltage was measured. After all the parameters had been changed to both their low and high values (32 runs in total) the DoE was used to find the optimal values. The DoE technique takes the effect of a combination of two or more growth parameters into account.

Table 8.1: The growth parameters of the aqueous solution method with maximum and minimum values.

Parameter	Minimum value	Maximum value
Growth time	7 h	8 h
Growth temperature	85°C	95°C
Concentration	20 mM	30 mM
Ratio	1 : 1	1 : 1.25

DoE relies on statistical analysis of the growth. Stat-Ease, a DoE software package, was used to analyse the data. From the resulting analysis the optimal growth

parameters are presented in Table 8.2.

Table 8.2: The growth parameters of the aqueous solution method with the optimal values as determined with DoE.

Parameter	Optimal value
Growth time	7 h
Growth temperature	95°C
Concentration	30 mM
Ratio	1 : 1

These optimal values were found after preparing more than 600 samples. The output voltages for all these samples were tested and recorded, together with their corresponding growth parameters.

Throughout the literature optimisation is done with respect to the nanowire growth quality. Accordingly, SEM and TEM are used to investigate the nanowires, as the crystal structure determines whether the growth is good, average or poor. However, the optimal crystal structure might not yield the highest output voltage, as screening of the piezoelectric charge can occur. For this reason it was argued that the optimisation of the output voltage was more important.

Figure 8.6 shows the measured output voltage of nanogenerators manufactured with nanowires grown with the aqueous solution method, where (a) is with non-optimal values and (b) with the optimal values given in Table 8.2. The non-optimal case has small peaks, below 1 V, and the optimal growth has peaks well over 1 V. This shows the importance of optimising the nanowire growth.

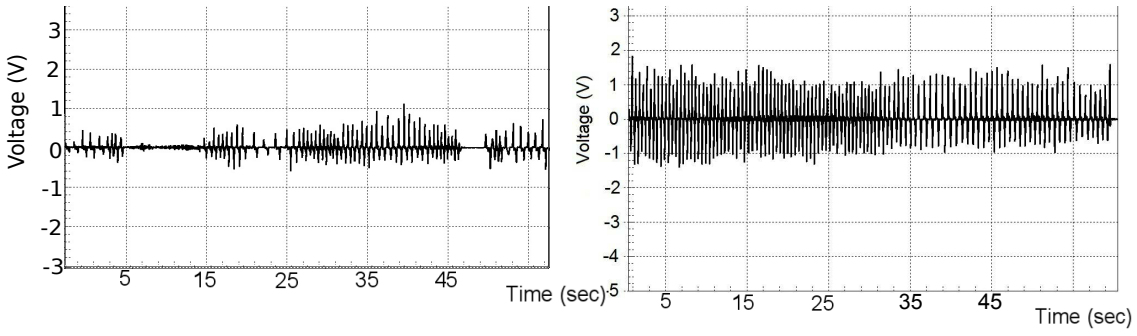

Figure 8.6: Measured output voltage of ZnO nanowires grown by means of the aqueous solution method (a) with non-optimal values and (b) with optimal values. The optimal values lead to a doubling in output voltage.

8.2.3 Nanogenerator optimisation

The optimisation of the nanogenerator was the main focus of this study. The output voltage of the nanogenerator must be raised is order to be of practical use.

The optimisation of the nanogenerator started with the solid nanogenerator, which was manufactured with silicon (100) substrates. The ZnO nanowires were grown on a pre-treated Si substrate. The pre-treatment consisted of the deposition of a layer of ZnO by means of ICM sputtering. The nanowires were grown using the aqueous solution method, with the optimised parameters given in the previous section.

The work function of the chosen electrode must be higher than the electron affinity of ZnO. This is to ensure the formation of an Schottky contact, which is critical for the proper functioning of the ZnO nanogenerator. The only suitable electrode that adheres to this restriction was gold. The gold electrode was manufactured by sputtering a thin layer of gold onto a Si (100) substrate, using DC sputtering.

The construction of the solid nanogenerator was finalised by securing the electrode on top of the nanowires. Various approaches were tried. Firstly, making supports of equal height on both sides of the nanowire and placing the electrode on top of the supports, thus ensuring that the correct height is achieved. Secondly, the electrode was simply placed on top of the nanowires and secured in place. The output voltage of the manufactured nanogenerator was extremely small, only a couple of millivolts. Upon further investigation it was found that contamination of either the growth or the gold electrode prevented proper contact between the two. With little to no contact, the measured output voltage was small.

In order to solve this problem various electrode designs were investigated. The Si (100) substrate was used, but CNTs were added, or the surface was scratched to make an uneven surface. It was hoped that the uneven surface would accommodate the contamination and ensure better contact between the nanowires and the electrode. This was not the case, however. The contact remained poor and a different solution was required.

The solution was to manufacture a flexible nanogenerator. Subsequently, both the electrode and the substrate for nanowire growth were chosen to be flexible. The gold electrode was also put in place on top of the nanowires, thus covering a few nanometres of the nanowire tips. This ensured proper contact between the nanowires and the gold electrode. This method also helped to solve the problem of contamination.

Figure 8.7 shows a diagram of the nanogenerator. The chosen substrate used was a Kapton polyimide film, which is flexible and can withstand temperatures

of up to 400°C. The nanowires were grown on the substrate, which was coated with a layer of gold and ZnO. After nanowire growth, the substrate was filled with PMMA, a transparent liquid that solidifies when heated. The PMMA acted as a buffer between the nanowire base and the gold electrode. It also adds stability and protection to the nanogenerator. The gold electrode was then sputtered onto the PMMA, covering the tips of the nanowires.

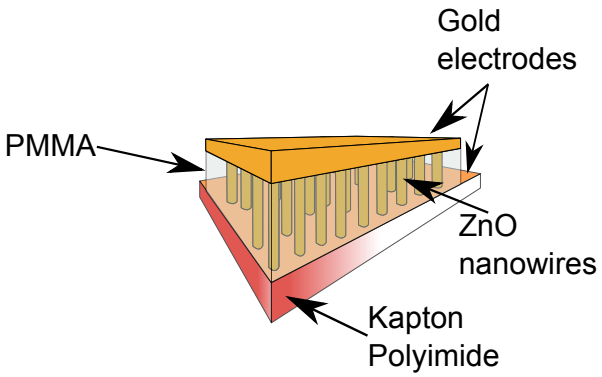

Figure 8.7: Diagram of the nanogenerator manufactured on a flexible substrate.

The new flexible design solved the problem of the low output voltage. Consequently, the output voltage was raised from a few millivolts to over 1 V. The highest measured output voltage for the solid nanogenerator was about 300 mV, with numerous optimisation methods applied to the manufacturing process. The film-based nanogenerator achieved voltages in the range of 1 V, three times higher, without any optimisation.

The higher measured output voltage of the flexible nanogenerator is argued to be due to the method by which the nanowires are bent. In the solid nanogenerator the nanowires were bent by the movement of the electrode. The electrode was placed on top of the nanowires and then moved around. The friction between the nanowire tips and the electrode caused the tips to move and bend, thus generating a piezoelectric voltage. In the film nanogenerator the entire film was bent, and this caused the nanowires to bend. The gold electrode was secured around the tips of the nanowires and, hence, any movement in either the nanowire or the electrode caused a piezoelectric voltage to be generated. The degree of bending in the flexible nanogenerator was higher, compared to the solid nanogenerator case. As shown by both the physical and the mathematical method, and confirmed by the simulations, the degree of bending in the nanowire is directly proportional to the output voltage.

The work on the solid and flexible nanogenerators was published in a peer-reviewed journal, *Microelectronic Engineering*, in 2013 [154].

The flexible nanogenerator is the best design for higher output voltages. However, with no optimisation techniques being applied, the output voltage was still too low. Although the output voltage had been raised to over 1 V, it is still not enough to be practically useful.

In order to increase the output voltage of the nanogenerator, optimisation was required. As already mentioned, throughout literature no mention is made of optimisation techniques for nanowires or the nanogenerator. Only the optimisation of ZnO thin film is mentioned. These techniques were reproduced on the ZnO nanowires to see whether they would help to increase the output voltage of the nanogenerator.

The techniques used were plasma treatment of the grown nanowires, annealing of the nanowires and doping. Both the plasma treatment and the annealing had the same effect, decreasing the vacancies that are present in the nanowires after growth. The vacancies are due to the malformation of the ZnO molecules during the ZnO nanowire growth. Zn vacancies occur when the Zn atom is missing, and O vacancies when the O atom is missing. These vacancies contribute to the unbound electrons, increasing the carrier concentration. A higher carrier concentration leads to a higher screening of the piezoelectric charges and, hence, lower output voltages, was measured.

Plasma treatment works by creating an oxygen plasma. The highly charged oxygen ions are accelerated towards the nanowires and bombard the sample. The oxygen ions are absorbed by the nanowires, leading to a decrease in oxygen vacancies. The annealing was done at 250°C, which resulted in a decrease in both O and Zn vacancies.

The doping of the nanowires did not result in higher output voltages being measured. The output voltagew for all the doped nanowires were less than the undoped case, and hence doping was not investigated further.

The last optimisation technique that was used was the addition of various materials to the PMMA prior to spinning it onto the substrate. The best result was obtained when a mixture of SWCNTs and ZnO nanowires were used. The measured output voltage was increased further by the addition of ZnO nanowires, which were laterally oriented throughout the nanogenerator and could thus achieve higher degrees of bending. Secondly, the measured output voltage was raised, because the SWCNTs acted as a second electrode. The difference in Fermi levels were thus higher, and hence the output voltage was also higher.

Figure 8.8 shows the measured output voltages for two nanogenerators. The

one on the left is the output voltage measured for a nanogenerator manufactured with no optimisation techniques applied. The second nanogenerator was manufactured with all the optimisation techniques applied. Consequently, the output voltage was raised from less than 1 V, to well over 5 V.

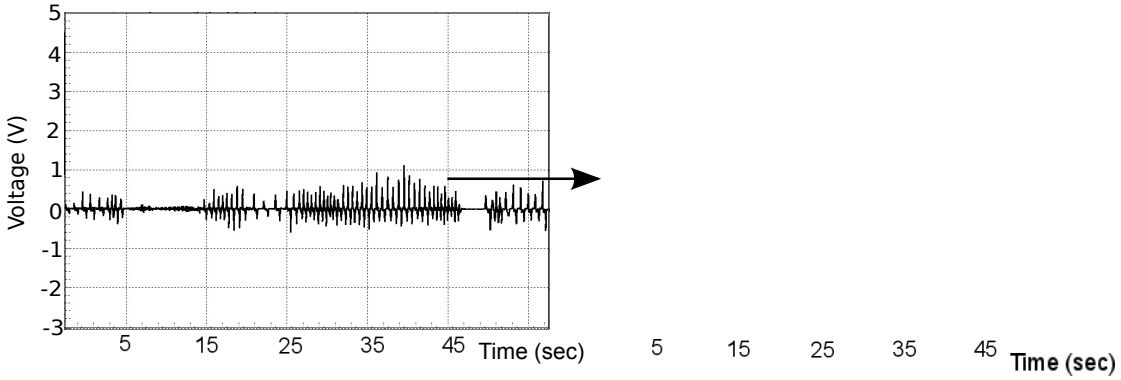

Figure 8.8: Measured output voltage of ZnO nanogenerators with no optimisation compared to one using all the optimisation techniques. This shows how much the measured output voltage had been raised from the beginning of the project.

The final, optimised nanogenerator is the result of three years of work. Over 1200 nanogenerators were manufactured, both solid and flexible. Over 500 voltage measurements were taken over the course of the three years and over 7000 SEM images were taken.

The work done on the optimisation of the nanogenerator has also been published in a peer-review journal, *IEEE Transactions on Nanotechnology*, in 2013 [175].

Articles found in the literature on nanogenerators still report output voltages lower than that achieved by this work [197, 198, 199]. Figure 8.9 shows the progression of achieved output voltages of the nanogenerator over time. In less than 10 years, the output voltage has been raised by a factor of more than 1000. Moreover, the nanogenerator with the 10 V output shown in the graph required expensive additional chemicals and complicated synthesis processes [200]. Even so, the output voltage is less than double that achieved in this project. Furthermore, the process is much more complicated and expensive.

The last part of the project focused on the output circuit of the nanogenerator. Once again,very little information is available in the literature on the subject. However, there is a great deal of literature available on output circuits of bulk piezoelectric devices.

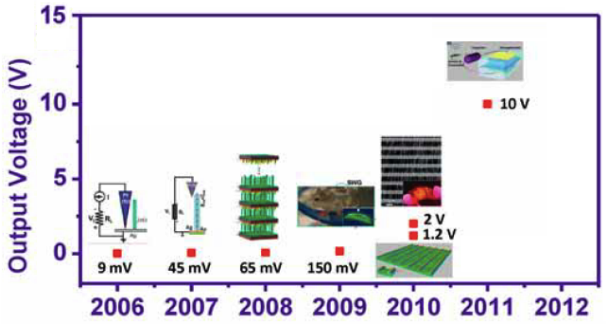

Figure 8.9: Graph showing the output voltage of the nanogenerator over time [201].

Output circuitry was investigated by means of simulations before practical tests were conducted. A full-bridge rectifier was simulated and was shown to work under small input current conditions. The problem with the full-bridge rectifier is that it does not conduct the generated charge all the time. Accordingly, the longer the output capacitor charges, the less charge is stored. In order to solve this problem a second circuit was introduced, the voltage doubler. This circuit, as the name implies, doubles the output voltage compared to the input voltage. The problem is that the circuit relies on diodes and capacitors, as is the case for the full-bridge rectifier, and hence the same problem arises. Moreover, the voltage doubler does not function as well under low input current conditions and only works under high load conditions.

The third circuit, that was taken from bulk piezoelectric devices is the SSHI circuit. The SSHI circuit solves the conduction time problem, almost 100% of the generated charge is now stored in the output capacitor. However, the circuit does not function under low input current, because, of the additional components of the circuit (eight diodes and four transistors compared to four diodes in both the rectifier and the voltage doubler). This added complexity requires more current to switch the components necessary for operation.

The last circuit that was used, was the LTC3588 IC. This IC was specially designed to work with piezoelectric inputs. The IC works under low current conditions and is independent of the load resistor. The problem with this circuit is that it has to charge the capacitor before supplying a load current. In other words, the circuit does not supply a continuous output current, but only supplies the current once the output capacitor is charged. Once the capacitor is charged, the output is triggered and a constant supply is delivered. This can be compared to the previous circuits, where the output voltage and current were not constant, but rather fluctuated too much to be practically useful.

Therefore, the LTC3588 IC was chosen as the best solution. With the nanoge-

nerator connected to the LTC3588, and after 10 minutes of bending, an LED was successfully turned on for a couple of seconds. This circuit could achieve output power of 0.3 mW for close to 10 seconds, after 10 minutes of bending. This work was published in *Smart materials and structures* [195].

Possible applications for the completed device, that is, the nanogenerator integrated with the LTC3588 circuit, are endless. The device can be attached to any environment where vibration or bending is present. The generated voltage can then be used to power a sensor and data can be collected every 10 minutes and transmitted to an offsite location. Another application is to integrate the nanogenerator into clothing for charging electronic devices as one moves around.

8.3 Limitations and future work

The main objective of this project was to optimise the ZnO nanowire-based nanogenerator. After three years of work this objective was successfully achieved. However, as with any big project, more could have been done if everything had gone according to plan and an unlimited budget had been available.

All the work and most of the analysis for this project was performed in the nano-laboratory at the Electrical and Electronic Engineering Department. The laboratory is still in its infancy and will only develop in the years to come. Even though the nano group is still new, many students are actively working in the laboratory. This limits the use of equipment by a single user, as key equipment must be shared among the students. This meant that at certain times, work could not be finished because certain pieces of equipment was being used by someone else. To further complicate matters, most of the equipment is fragile, and improper use can lead to weeks of downtime. Downtime of equipment occurred all too regularly and was a big problem throughout this project.

The second limitation is the access to equipment outside the Electrical and Electronic Engineering Department. The use of equipment is not free of charge, but is charged at an hourly rate. The analysis of nanoscale structures can take time and was not performed on all the samples. In fact, only a few of these tests were performed, where ideally they should be done for all samples. These tests include XRD, TEM and EDX. These tests will help to determine the crystal structure of the nanowires, which can lead to improved understanding of the optimisation techniques.

Various other tests and analyses could be performed on the nanogenerator at various stages of manufacturing and testing. The resistance and carrier concentration test could have been performed if more appropriate equipment had been

available. However, no institution in South Africa could be found that had access to the proper equipment. Further analysis could have been performed on the ZnO and Au layers that are deposited before nanowire growth. The quality, thickness and purity of these layers can be determined by various equipment, but none was freely available at Stellenbosch University.

Lastly, the cleanroom facilities at the Electrical and Electronic Department were not ideal. Most of the laminar flow units are non-operational, meaning dust and other airborn particles could settle on samples during various stages of manufacturing and analysis. This was seen in the construction of the solid nanogenerator, where contamination prevented proper contact between the nanowires and the electrode.

With all these limitations there is a lot of future work that can be done. The resistance and carrier concentration measurements can be made with equipment specially designed for nanowire measurement. As mentioned, the Hall and Van der Pauw techniques are used mainly for thin film measurements and are not perfectly suited for nanowire structures.

Only two ZnO nanowire growth techniques were investigated. However, various other techniques do exist and could be compared with the results of this project.

ZnO was not the only piezoelectric material and other material could be used and compared to ZnO. This was done in the simulations of this project, but practical measurement could be performed to verify the simulations.

The current measurements of the nanogenerator were done using an expensive pico ampere meter. A cheaper method for measuring the small currents needs to be developed to ensure more scientists can work on nanogenerators.

Throughout the project the output voltage of the nanogenerator was increased. A similar approach could be followed to increase the output current of the nanogenerator in order to increase the output power of the device further.

The output circuitry also needs further optimisation. Although the LTC3588 circuit did work, alternatives are required. The SSHI circuit would seem to be the ideal candidate, but it did not function under the low current conditions. Optimising the circuit to function at low currents could thus lead to an improved output circuit that could supply a constant output, unlike the LTC3588 circuit.

A number of improvements can be made to this project. However, the project was very successful and all the original goals were met. The ZnO nanowire based nanogenerator was successfully optimised using various approaches and techniques, all newly developed throughout the course of this project.

Bibliography

[1] A. D. Maynard, "Nanotechnology: The next big thing, or much ado about nothing?" *Annals of Occupational Hygiene*, vol. 51, p. 1, 2007.

[2] J. Youtie, P. Shapira, and A. L. Porter, "Nanotechnology publications and citations by leading coutries and blocs," *Journal of Nanoparticle Research*, vol. 10, p. 981, 2008.

[3] X. Li, Y. Lin, H. Chen, and M. C. Roco, "Worldwide nanotechnology development: A comparative study of USPTO, EPO, and JPO patents," *Journal of Nanoparticle Research*, vol. 9, p. 977, 2007.

[4] E. Hubble, "A relation between distance and radial velocity among extragalactic nebulae," *Proceedings of the National Academy of Sciences*, vol. 15, p. 168, 1929.

[5] R. Allan, June 2006. [Online]. Available: http://electronicdesign.com/energy/little-nano-went-market-eventually

[6] Battery-University, March 2013. [Online]. Available: http://batteryuniversity.com/learn/article/battery_statistics

[7] B. Scrosati and J. Garche, "Lithium batteries: Status, prospects and future," *Journal of Power Sources*, vol. 195, p. 2419, 2010.

[8] Z. L. Wang and J. Song, "Piezoelectric nanogenerators based on zinc oxide nanowire arrays," *Science*, vol. 312, p. 242, 2006.

[9] Energy.gov, August 2012. [Online]. Available: http://energy.gov/energysaver/articles/estimating-appliance-and-home-electronic-energy-use

[10] C. T. Huang, J. Song, C. M. Tsai, W. F. Lee, D. H. Lien, Z. Gao, Y. Hao, L. J. Chen, and Z. L. Wang, "Single InN nanowire nanogenerator with up to 1 V output voltage," *Advanced Materials*, vol. 22, p. 4008, 2010.

[11] K. Uchino, *Piezoelectric actuators and ultrasonic motors*. Springer, 1996.

[12] J. Y. Park and S. S. Kim, "Growth of nanograins in electrospun ZnO nanofibers," *Journal of the American Ceramic Society*, vol. 92, p. 1691, 2009.

[13] A. Rahm, M. Lorenz, T. Nobis, G. Zimmermann, M. Grundmann, B. Fuhrmann, and F. Syrowatka, "Pulsed-laser deposition and characterization of ZnO nanowires with regular lateral arrangement," *Applied Physics A*, vol. 88, p. 31, 2007.

[14] C. Y. Yao, G. J. Chen, and T. Y. Tseng, "Preparation and characterizations of ZnO nanotubes by acidic etching nanowires." *Journal of Nanoscience and Nanotechnology*, vol. 8, p. 4432, 2008.

[15] S. Priya and D. J. Inman, *Energy harvesting technologies*. Springer Science and Business Media, 2009.

[16] F. Yildiz, "Potential ambient energy-harvesting sources and techniques," *The Journal of Technology Studies*, vol. 35, p. 40, 2009.

[17] R. Vijay, K. Aman, H. Jason, F. K. Jonathan, and S. B. Mani, "Design considerations for solar energy harvesting wireless embedded systems," *IEEE International Conference on Information Processing in Sensor Networks*, vol. 1, p. 457, 2005.

[18] Z. L. Wang and J. H. Song, "Piezoelectric nanogenerators based on zinc oxide nanowire arrays." *Science*, vol. 312, p. 242, 2006.

[19] B. Tian, X. Zheng, T. J. Kempa, Y. Fang, N. Yu, G. Yu, J. Huang, and C. M. Lieber, "Coaxial silicon nanowires as solar cells and nanoelectronic power sources," *Nature*, vol. 449, p. 885, 2007.

[20] Z. L. Wang, "Self-powered nanotech-nanosize machines need still tinier power plants," *Scientific American*, vol. 298, p. 82, 2008.

[21] C. Pan, H. Wu, C. Wang, B. Wang, L. Zhang, Z. Cheng, P. Hu, W. Pan, Z. Zhou, X. Yang, and J. Zhu, "Nanowire-based high performance micro fuel cell: One nanowire, one fuel cells," *Advanced Materials*, vol. 20, p. 1644, 2008.

[22] A. W. Correia, C. A. Pope, D. W. Dockery, Y. Wang, M. Ezzati, and F. Dominici, "Effect of air pollution control on the life expectancy in the United States," *Epidemiology*, vol. 24, p. 23, 2013.

[23] R. F. Julian, *Designing indoor solar products: Photovoltaic technologies for AES*. John Wiley, 2005.

[24] P. V. Kamat, "Meeting the clean energy demand: Nanostructure architectures for solar energy conversion," *Journal of Physical Chemistry C*, vol. 111, p. 2834, 2007.

[25] J. M. Woodall and H. J. Hovel, "High-efficiency Ga1-xAlxAs-GaAs solar cells," *Applied Physics Letters*, vol. 21, p. 379, 1972.

[26] M. D. Archer and R. Hill, *Clean electricity from photovoltaics*. Imperial College Press, 2001.

[27] L. Li, M. Wang, F. Zhu, and C. Wang, "Wind power forecasting based on time series and neural networks," *Proceedings of the Second Symposium International Computer Science and Computational Technology*, vol. 26, p. 293, 2009.

[28] C. C. Federspiel and J. Chen, "Air-powered sensor," *IEEE International Conference on Sensors*, vol. 1, p. 22, 2003.

[29] R. Myers, M. Vickers, and H. Kim, "Small scale windmill," *Applied Physics Letters*, vol. 90, p. 054106, 2007.

[30] M. A. Sanz-Bobi and R. Palacios, "Potential use of small waste heat sources based on thermoelectricity: Application to an overhead projector and a battery charger." *15th European Workshop on Thermoelectrics*, vol. 1, p. 58, 1999.

[31] V. Leonov, P. Fiorini, S. Sedky, T. Torfs, and C. V. Hoof, "Thermoelectric MEMS generators as a power supply for a body area network," *13th International Conference on Solid-State Sensors, Actuators and Microsystems*, vol. 1, p. 291, 2005.

[32] A. Lay-Ekuakille and A. Vendramin, "Thermoelectric generator design based on power from body heat for biomedical autonomous devices," *IEEE International Workshop on Medical Measurements and Applications*, vol. 1, p. 1, 2009.

[33] T. Starnet, "Human-powered wearable computing." *IBM Systems Journal*, vol. 35, p. 618, 1996.

[34] S. P. Beeby, R. N. Torah, M. J. Tudor, P. Glynne-Jones, T. O'Donnel, C. R. Saha, and S. Roy, "A micro electromagnetic generator for vibration energy harvesting," *Journal of Micromechanical Microengineering*, vol. 17, p. 1257, 2007.

[35] P. A. Janeway, "Nanotechnology: It's more than size," *American Ceramic Society*, vol. 82, p. 31, 2003.

[36] J. F. Mongillo, *Nanotechnology 101*, G. Press, Ed. Science 101, 2007.

[37] Concana, October 2009. [Online]. Available: http://www.concana.com/Nanotechnology.htm

[38] M. van Zijverden, "Nanotechnology in perspective," National Institute for Public Health and the Environment, Tech. Rep., 2009.

[39] S. A. Edwards, *The Nanotech pioneers: Where are they taking us?*, K. Satz, Ed. Wiley-VCH, 2006.

[40] N. Taniguchi, *Nanotechnology: Integrated processing systems for iltra-precision and iltra-fine products*, T. Kohno, Ed. Oxford Science Publications, 1974.

[41] R. Feynman, "There is plenty of room at the bottom," *Journal of Microelectromechanical Systems*, vol. 1, p. 60, 1992.

[42] J. Tersoff and D. R. Hamann, "Theory of the scanning tunneling microscope," *Physical Review B 31*, vol. 1, p. 805, 1985.

[43] M. Ratner, *Nanotechnology: A gentle introduction to the next big idea*, D. Ratner, Ed. Prentice Hall, 2002.

[44] M. C. Daniel and D. Astruc, "Gold nanoparticles: Assembly, supramolecular chemistry, quantum-size-related properties, and applications toward biology, catalysis, and nanotechnology," *Chemical Reviews*, vol. 104, p. 293, 2004.

[45] W. G. Cady, *Piezoelectricity: an introduction to the theory and applications of electromechanical phenomena in crystals*, H. R. Wenk, Ed. New York: McGraw Hill, 1946.

[46] L. APC International, *Piezoelectric ceramics: Principles and applications*, L. APC International, Ed. APC International, Ltd, 2002.

[47] D. C. Giancoli, *Physics for Scientists and Engineers with Modern Physics*. Addison-Wesley Educational Publishers, 2004.

[48] J. Yang, *An introduction to the theory of piezoelectricity*, D. Y. Gao, Ed. Springer Science and Business Media, 2005.

[49] V. E. Bottom, *Introduction to quartz crystal unit design*, T. A. Skotheim, Ed. Van Nostrand Reinhold Company, 1982.

[50] J. F. Rosenbaum, *Bulk acoustic wave theory and devices*. Artech Print on Demand, 1945.

[51] *IEEE Standard on Piezoelectricity*, The Institute of Electrical and Electronic Engineers Std.

[52] C. Jagadish, *Zinc oxide bulk, thin films and nanostructures*, S. J. Pearton, Ed. Elsevier, 2006.

[53] R. Agrawal, B. Peng, E. E. Gdoutos, and H. D. Espinosa, "Elasticity size effects in ZnO nanowires: A combined experimental-computational approach," *Nano Letters*, vol. 8, p. 3668, 2008.

[54] Z. C. Tu and X. Hu, "Elasticity and piezoelectricity of zinc oxide crystals, single layers, and possible single-walled nanotubes," *Physical Review B*, vol. 74, p. 035434, 2006.

[55] Z. Fan and J. G. Lu, "Zinc oxide nanostructures: Synthesis and properties," *Journal of Nanoscience and Nanotechnology*, vol. 5, p. 1561, 2005.

[56] S. Xu, Y. Qin, C. Xu, Y. Wei, R. Yang, and Z. L. Wang, "Self-powered nanowire devices," *Nature Nanotechnology*, vol. 5, p. 366, 2010.

[57] L. Vayssieres, "Growth of arrayed nanorods and nanowires of ZnO from aqueous solutions," *Advanced Materials*, vol. 15, p. 464, 2003.

[58] Z. Li, R. Yang, M. Yu, F. Bai, C. Li, and Z. L. Wang, "Cellular level biocompatibility and biosafety of ZnO nanowires," *The Journal of Physical Chemistry C*, vol. 112, p. 20114, 2008.

[59] Z. L. Wang, "Towards self powered nanosystems from nanogenerators to nanopiezotronics," *Advanced Functional Materials*, vol. 18, p. 3553, 2008.

[60] C. Kittel, *Introduction to solid state physics*, S. Prakash, Ed. John Wiley and Sons, 1996.

[61] Z. W. Pan, S. M. Mahurin, S. Dai, and D. H. Lowndes, "Nanowire Array Gratings with ZnO Combs," *Nanotechnology Letters*, vol. 5, p. 723, 2005.

[62] Z. L. Wang, "Nanobelts, nanowires, and nanodiskettes of semiconducting oxides: From materials to nanodevices," *Advanced Materials*, vol. 15, p. 432, 2003.

[63] O. Dulub, L. A. Boatnerb, and U. Diebold, "STM study of the geometric and electronic structure of ZnO," *Surface Science*, vol. 519, p. 201, 2002.

[64] J. C. Phillips, *Bonds and bands in semiconductors*, B. Levy, Ed. Academic Press, 1973.

[65] S. O. Kucheyev, J. E. Bradby, J. S. Williams, C. Jagadish, and M. V. Swain, "Mechanical deformation of single-crystal ZnO," *Applied Physics Letters*, vol. 80, p. 956, 2002.

[66] V. A. Coleman, J. E. Bradby, C. Jagadish, P. Munroe, Y. W. Heo, S. J. Pearton, D. P. Norton, M. Inoue, and M. Yano, "Mechanical properties of ZnO epitaxial layers grown on a and c axis sapphire," *Applied Physics Letters*, vol. 86, p. 203105, 2005.

[67] S. S. Lin, J. H. Song, Y. F. Lu, and Z. L. Wang, "Identifying individual n- and p-type ZnO nanowires by the output voltage sign of piezoelectric nanogenerator," *Nanotechnology*, vol. 20, p. 365703, 2009.

[68] R. F. Pierret, *Semiconductor device fundamentals*, K. Harutunian, Ed. Addison-Wesley, 1996.

[69] C. S. Lao, J. Liu, P. Gao, L. Zhang, D. Davidovic, R. Tummala, and Z. L. Wang, "ZnO nanobelt and nanowire Schottky diodes formed by dielectrophoresis alignment across Au electrodes," *Nano Letters*, vol. 6, p. 263, 2006.

[70] S. Reich, C. Thomsen, and J. Maultzsch, *Carbon nanotubes: Basic concepts and physical properties*, R. Forch, Ed. Wiley VCH, 2004.

[71] L. Zhang, X. Fang, and C. Ye, *Controlled growth of nanomaterials*. World Scientific Publishing, 2007.

[72] L. Chen, L. Luo, Z. Chen, M. Zhang, J. A. Zapien, C. S. Lee, and S. T. Lee, "ZnO/Au composite nanoarrays as substrates for surface-enhanced Raman scattering detection," *Journal of Physical Chemistry C*, vol. 114, p. 93, 2010.

[73] Z. Zhang, G. Meng, Q. Xu, Y. Hu, Q. Wu, and Z. Hu, "Aligned ZnO nanorods with tunable size and field emission on native Si substrate achieved via simple electrodeposition," *Journal of Physical Chemistry C*, vol. 114, p. 189, 2010.

[74] X. Wu, L. Gong, H. Chen, F. Qu, and M. An, "Synthesis of vertically aligned dense ZnO nanowires," *Journal of Nanomaterials*, vol. 2011, p. 428172, 2011.

[75] B. Alemán, P. Fernández, and J. Piqueras, "Dense vertical nanoplates arrays and nanobelts of indium doped ZnO grown by thermal treatment of ZnS-In2O3 powders," *Journal of Crystal Growth*, vol. 312, pp. 3117–3121, 2010.

[76] Y. Peng and L. Bao, "Controlled-synthesis of ZnO nanorings," *Frontiers of Chemistry in China*, vol. 3, p. 458, 2008.

[77] X. Wu, W. Cai, and F. Y. Qu, "Spontaneous formation of single crystal ZnO nanohelices," *Chinese Physics B*, vol. 18, p. 1669, 2009.

[78] P. X. Gao and Z. L. Wang, "High-yield synthesis of single-crystal nanosprings of ZnO," *Small*, vol. 1, p. 945, 2005.

[79] W. S. Khan, C. Cao, Z. Chen, and G. Nabi, "Synthesis, growth mechanism, photoluminescence and field emission properties of metal semiconductor Zn-ZnO core shell microcactuses," *Materials Chemistry and Physics*, vol. 124, p. 493, 2010.

[80] D. Suh, C. C. Byeon, and C. L. Lee, "Synthesis and optical characterization of vertically grown ZnO nanowires in high crystallinity through vapor liquid solid growth mechanism," *Applied Surface Science*, vol. 8, p. 4332, 2010.

[81] N. S. Ramgir, K. Subannajui, Y. Yang, R. Grimm, R. Michiels, and M. Zacharias, "Reactive VLS and the reversible switching between VS and VLS growth modes of ZnO nanowire growth," *The Journal of Physical Chemistry C*, vol. 114, p. 10323, 2010.

[82] Y. H. Yang, Y. Feng, and G. W. Yang, "Experimental evidence and physical understanding of ZnO vapor liquid solid nanowire growth," *Applied Physics A*, vol. 339, p. 5944, 2010.

[83] S. Oh, M. Jung, J. Koo, Y. Cho, S. Choi, S. Yi, G. Kil, and J. Chang, "The mechanism of ZnO nanorod growth by vapor phase transportation," *Physica E*, vol. 42, p. 2285, 2010.

[84] A. N. Redkin, Z. I. Makovei, A. N. Gruzintev, E. E. Yakimov, O. V. Kononenko, and A. A. Firsov, "Elemental vapor phase synthesis of nanostructured zinc oxide," *Inorganic Materials*, vol. 45, p. 1246, 2009.

[85] K. Govender, D. S. Boyle, P. B. Kenway, and P. O'Brian, "Understanding the factors that govern the deposition and morphology of thin films of ZnO from aqueous solution," *Journal of Materials Chemistry*, vol. 14, p. 2575, 2004.

[86] M. Willander, L. L. Yang, A. Wadeasa, S. U. Ali, M. H. Asif, Q. X. Zhao, and O. Nur, "Zinc oxide nanowires controlled low temperature growth and some electrochemical and optical nanodevices," *Journal of Materials Chemistry*, vol. 19, p. 1006, 2009.

[87] L. E. Greene, B. D. Yuhas, M. Law, D. Zitoun, and P. Yang, "Solution grown zinc oxide nanowires," *Inorganic Chemistry*, vol. 45, p. 7535, 2006.

[88] L. Vayssieres, K. Keis, S. E. Lindquist, and A. Hagfeldt, "Purpose built anisotropic metal oxide material 3D highly oriented microrod array of ZnO," *Journal of Physical Chemistry B*, vol. 105, p. 3350, 2001.

[89] J. Song, J. Zhou, and Z. L. Zhong, "Piezoelectric and semiconducting coupled power generation process of a single ZnO belt or wire: A technology for harvesting electricity from the environment," *Nano Letters*, vol. 6, p. 1656, 2006.

[90] Z. L. Wang, "Nanopiezotronics," *Advanced Materials*, vol. 19, p. 889, 2007.

[91] Z. L. Wang and Z. L. Wang, "The new field of nanopiezotronics," *Materials Today*, vol. 10, p. 20, 2007.

[92] Z. L. Wang, X. Wang, J. Song, J. Liu, and Y. Gao, "Piezoelectric nanogenerators for self powered nanodevices," *IEEE Pervasive Computing*, vol. 7, p. 49, 2008.

[93] Z. L. Wang, "Energy harvesting using piezoelectric nanowires: A correspondence on Energy harvesting using nanowires? by Alexe et al," *Advanced Materials*, vol. 21, p. 1311, 2009.

[94] W. Tang, M. R. Gomez, Y. Y. Lau, R. M. Gilgenbach, and J. Zier, "Theory and experimental measurements of contact resistance," *IEEE Transactions on Components and Packaging Technologies*, vol. 1 June 2009, p. 1, 2009.

[95] K. Kim, H. Kang, H. Kim, J. S. Lee, S. Kim, W. Kang, and G. T. Kim, "Contact barriers in a single ZnO nanowire device," *Applied Physics A*, vol. 94, p. 253, 2009.

[96] S. S. Baek and R. S. Fearing, "Reducing contact resistance using compliant nickel nanowire arrays," *IEEE Transactions on Components and Packaging Technologies*, vol. 31, p. 859, 2008.

[97] Y. Gao and Z. L. Wang, "Electrostatic potential in a bent piezoelectric nanowire: The fundamental theory of nanogenerator and nanopiezotronics," *Nano Letters*, vol. 7, p. 2499, 2007.

[98] Z. Z. Shao, L. Y. Wen, D. M. Wu, X. F. Wang, X. A. Zhang, and S. L. Chang, "A continuum model of piezoelectric potential generated in a bent ZnO nanorod," *Journal of Physics D: Applied Physics*, vol. 43, p. 245403, 2010.

[99] A. E. Green and W. Zerna, *Theoretical elasticity*. New York: Dover, 2002.

[100] I. B. Kobiakov, "Elastic, piezoelectric and dielectric properties of ZnO and CdS single crystals in a wide range of temperatures," *Solid State Communications*, vol. 35, p. 305, 1980.

[101] N. Ashkenov, B. N. Mbenkum, C. Bundesmann, V. Riede, M. Lorenz, D. Spemann, E. M. Kaidashev, A. Kasic, M. Schubert, M. Grundmann, G. Wagner, H. Neumann, V. Darakchieva, H. Arwin, and B. Monemar, "Infrared dielectric functions and phonon modes of high-quality ZnO films," *Journal of Applied Physics*, vol. 93, p. 126, 2003.

[102] M. A. Schubert, S. Senz, M. Alexe, D. Hesse, and U. Gosele, "Finite element method calculation of ZnO nanowires for nanogenerators," *Applied Physics Letters*, vol. 92, p. 122904, 2008.

[103] I. Wagner, June 2005. [Online]. Available: http://www.hit.ac.il/staff/vagner/Schottky.PDF

[104] Z. L. Wang, R. Yang, J. Zhou, Y. Qin, C. Xu, Y. Hu, and S. Xu, "Lateral nanowire based nanogenerators, piezotronics and piezophototronics," *Materials Science and Engineering R*, vol. 06, p. 15, 2010.

[105] R. Yang, Y. Qin, L. Dai, and Z. L. Wang, "Power generation with laterally packaged piezoelectric fine wires," *Nature Nanotechnology Letters*, vol. 314, p. 1, 2008.

[106] X. Wang, J. Song, F. Zhang, C. He, Z. Hu, and Z. L. Wang, "Electricity generation based on one dimensional group III nitride nanomaterials," *Advanced Materials*, vol. 22, p. 1, 2010.

[107] J. Liu, J. Song, X. Wang, C. Lao, R. Tummala, and Z. L. Wang, "Carrier density and Schottky barrier on the performace of DC nanogenerator," *Nano Letters*, vol. 8, p. 328, 2008.

[108] D. Choi, M. Y. Choi, H. J. Shin, S. M. Yoon, J. S. Seo, J. Y. Choi, S. Y. Lee, J. M. Kim, and S. W. Kim, "Nanoscale networked single walled carbon nanotube electrodes for transparent flexible nanogenerators," *Journal of Physical Chemistry C*, vol. 114, p. 1379, 2010.

[109] Z. Fan and G. Lu, "Electrical properties of ZnO nanowire field effect transistor characterized with scanning probes," *Applied Physics Letters*, vol. 86, p. 032111, 2005.

[110] Y. F. Lin and W. B. Jian, "The impact of nanocontact on nanowire based nanoelectronics," *Nano Letters*, vol. 8, p. 3146, 2008.

[111] Y. F. Lin, W. B. Jian, Z. Y. Wu, F. R. Chen, J. J. Kai, and J. J. Lin, "Determination of contact and intrinsic nanowire resistivity in two-contact ZnO nanowire devices," in *Nanoelectronics Conference, 2008. INEC 2008. 2nd IEEE International*, 2008.

[112] A. Mikrajuddin, F. G. Shi, H. K. Kim, and K. Okuyama, "Size dependent electrical constriction resistance for contact of arbitrary size from Sharvin to Holm limits," *Materials Science in Semiconductor Processing*, vol. 2, p. 321, 1999.

[113] Z. Hu, Q. Chen, Z. Li, Y. Yu, and L. M. Peng, "Large scale and rapid synthesis of ultralong ZnO nanowire films via anodization," *Journal of Physical Chemistry C*, vol. 114, p. 881, 2010.

[114] Du-Pont, December 2012. [Online]. Available: www2.dupont.com/Kapton/en_US/assets/downloads/pdf/Gen_Specs.pdf

[115] [Online]. Available: http://www.betelco.com/sb/phd/ch3/c34.html

[116] S. Shafiei, A. Nourbakhsh, B. Ganjipour, M. Zahedifar, and G. Vakili-Nezhaad, "Diameter optimization of VLS-synthesized ZnO nanowires, using statistical design of experiment," *Nanotechnology*, vol. 18, p. 355708, 2007.

[117] S. Xu, N. Adiga, S. Ba, T. Dasgupta, C. F. Wu, and Z. L. Wang, "Optimizing and improving the growth quality of ZnO nanowire arrays guided by statistical design of experiments," *ACS Nano*, vol. 3, p. 1803, 2009.

[118] N. Gabrielyan, S. Paul, and R. B. Cross, "Optimising the low temperature growth of uniform ZnO nanowires," *Materials Research Society Symposium Proceedings*, vol. 1201, p. 295, 2010.

[119] JMP, "Design of experiments," masters thesis work.

[120] Stat-Ease, July 2011. [Online]. Available: http://www.statease.com/soft_ftp.html

[121] C. D. Klaassen, *Casarett and Doull's toxicology: The basic science of poisons*. McGraw-Hill Professional, 2001.

[122] SEAL-Labs, April 2006. [Online]. Available: http://www.seallabs.com/hiw.htm

[123] PhenomWorld. [Online]. Available: http://www.phenom-world.com/

[124] *Operation Instructions easyScan 2 AFM Version 2.1*.

[125] Y. Qin, X. Wang, and Z. L. Wang, "Microfibre nanowire hybrid structure for energy scavenging," *Nature*, vol. 451, p. 809, 2008.

[126] M. Alexe, S. Senz, M. A. Schubert, D. Hesse, and U. Gosele, "Energy harvesting using nanowires?" *Advanced Materials*, vol. 20, p. 4021, 2008.

[127] J. Liu, P. Fei, J. Zhou, R. Tummala, and Z. L. Wang, "Towards high output power nanogenerator," *Applied Physics Letters*, vol. 92, p. 173105, 2008.

[128] LabJack. [Online]. Available: http://labjack.com/u6

[129] T. S. van den Heever, U. Buttner, and W. J. Perold, "A novel method to measure the generated voltage of a ZnO nanogenerators," *Nanotechnology*, vol. 22, p. 395204, 2011.

[130] L. J. van der Pauw, "A method for measuring the resistivity and Hall coefficient on lamellae of arbitrary shape," *Philips Technical Review*, vol. 59, p. 220, 1958.

[131] E. H. Hall, "On a New Action of the Magnet on Electric Currents," *American Journal of Mathematics*, vol. 2, p. 287, 1879.

[132] T. S. van den Heever and W. J. Perold, "The influence of resistance and carrier concentration on the output voltage of a ZnO nanogenerator." *Micro and Nano Systems Letters*, vol. 1, p. 1, 2013.

[133] Comsol, February 2013. [Online]. Available: www.comsol.com

[134] "Comsol Multiphysics."

[135] Z. Y. Fan, D. W. Wang, P. C. Chang, W. Y. Tseng, and L. G. Jia, "ZnO nanowire field-effect transistor and oxygen sensing property," *Applied Physics Letters*, vol. 85, p. 5932, 2004.

[136] S. H. Jo, J. Y. Lao, Z. F. Ren, R. A. Farrer, T. Baldacchini, and J. T. Fourkas, "Field-emission studies on thin films of zinc oxide nanowires," *Applied Physics Letters*, vol. 83, p. 4821, 2003.

[137] L. Chen and Y. Yin, "The influence of length of one-dimensional photoanode on the performace of dye-sensitized solar cells," *Journal of Material Chemistry*, vol. 22, p. 24591, 2012.

[138] D. R. Lide, *CRC Handbook of Chemistry and Physics*, C. Press, Ed. CRC Press, 2008.

[139] C. Zhang, "High quality oriented ZnO films grown by sol-gel process assisted with ZnO seed layer," *Journal of Physics and Chemistry of Solids*, vol. 71, p. 364, 2010.

[140] S. Bai, "Growth and properties of ZnO nanowires synthesized by a simple hydrothermal method," *Journal of Material Science: Mater Electron*, vol. 23, p. 398, 2012.

[141] H. Li, J. Wang, H. Liu, C. Yang, H. Xu, X. Li, and H. Cui, "Sol-gel preparation of transparent zinc oxidefilms with highly preferential crystal orientation," *Vacuum*, vol. 77, p. 57, 2004.

[142] B. Wen, Y. Huang, and J. J. Boland, "Controllable growth of ZnO nanostructures by a simple solvothermal process," *Journal of Physical Chemistry C*, vol. 112, p. 106, 2008.

[143] C. Q. Chen, Y. Shi, Y. S. Zhang, J. Zhu, and Y. J. Yan, "Size dependence of Young's modulus in ZnO nanowires," *Physical Review Letters*, vol. 96, p. 075505, 2006.

[144] L. Dai, W. C. Cheong, C. H. Sow, C. T. Lim, and V. B. Tan, "Molecular dynamics simulation if ZnO nanowires: Size effects, defects and super ductility," *PubMed*, vol. 26, p. 1165, 2010.

[145] H. Tong, B. L. Wang, and Z. C. Ou-Yang, "Electric potential generated in ZnO nanowire due to piezoelectric effect," *Thin Sold Films*, vol. 516, p. 2708, 2008.

[146] NIST-SemaTech, June 2003. [Online]. Available: http://itl.nist.gov/div898/handbook/pri/section5/pri598.htm

[147] StatSoft, March 2011. [Online]. Available: http://www.statsoft.com/textbook/statistics-glossary/h/

[148] W. G. Cochran and G. M. Cox, *Experimental Designs*, 2, Ed. Wiley Classics Library, 1992.

[149] D. C. Montgomery, *Design and analysis of experiments*, 4, Ed. John Wiley and Sons, 1996.

[150] C. Y. Lee, T. Y. Tseng, S. Y. Li, and P. Lin, "Growth of zinc oxide nanowires on silicon (100)," *Tamakang Journal of Science and Engineering*, vol. 6, p. 127, 2003.

[151] N. K. Hassan, M. R. Hashim, M. A. Mahdi, and N. K. Allam, "A catalyst-free growth of ZnO nanowires on Si (100) substrates: Effect of substrate position

on morphological, strucural and optical properties," *ECS Journal of Solid State Science and Technology*, vol. 1, p. 86, 2012.

[152] *DuPont Kapton polyimide film*.

[153] *Thermosoftening plastics and thermosetting plastics*.

[154] T. S. van den Heever and W. J. Perold, "The performace of nanogenerators fabricated on rigid and flexible substrates," *Microelectronic Engineering*, vol. 112, p. 41, 2013.

[155] C. Guerret-Piecourt, Y. Le Bouar, A. Loiseau, and H. Pascard, "Relation between metal electronic structure and morphology of metal compounds inside carbon nanotubes," *Nature*, vol. 372, p. 761, 1994.

[156] L. Y. Cheng and L. D. Zhang, "Fabrication of highly ordered ZnO nanowire arrays in anodic alumina membranes," *Journal of Materials Research*, vol. 15, p. 2305, 2000.

[157] W. L. Bragg and J. A. Darbyshire, "The structure of thin films of certain metallic oxides," *Transactions of the Faraday Society*, vol. 28, p. 522, 1932.

[158] G. I. Finch and A. G. Quarrell, "Crystal structure and orientation in zinc-oxide films," *Proceedings of the Physical Society*, vol. 46, p. 148, 1934.

[159] S. Lee, S. Bang, J. Park, S. Park, W. Jeong, and H. Jean, "The effect of oxygen remote plasma treatment on ZnO TFTs fabricated by atomic layer deposition," *Physica Status Solidi A*, vol. 207, p. 1845, 2010.

[160] P. Ehrhart, *Properties and interactions of atomic defects in metals and alloys*. Springer Materials, 1991.

[161] Y. Zhang, G. Du, X. Yang, B. Zhao, Y. Ma, T. Yang, H. C. Ong, D. Liu, and S. Yang, "Effect of annealing on ZnO thin films grown on (001) silicon substrate by low-pressure metalorganic chemical vapour deposition," *Semiconductor and Science Technology*, vol. 19, p. 755, 2004.

[162] S. Golshahi, S. M. Rozati, and T. Ghasempoor, "Annealing treatment of ZnO thin films prepared by nonreactive E-beam evaporation techniques," *Digest Journal of Nanomaterials and Biostructures*, vol. 6, p. 445, 2011.

[163] K. H. Tam, C. K. Cheung, Y. H. Leung, A. B. Djurisic, C. C. Ling, C. D. Beling, S. Fung, W. M. Kwok, W. K. Chan, D. L. Phillips, L. Ding, and W. K. Ge, "Defects in ZnO nanorods prepared by a hydrothermal methods," *Journal of Physical Chemistry B*, vol. 110, p. 20865, 2006.

[164] Z. Ounaies, C. Park, K. E. Wise, E. J. Siochi, and J. S. Harrison, "Electrical properties of single wall carbon nanotube reinforced polyimide composites," *Composites Science and Technology*, vol. 63, p. 1637, 2003.

[165] M. Montazer, M. Samin, G. Asghari, and E. Pakdel, "Electrical conductivity of single walled and multiwalled carbon nanotube containing wool fibers," *Journal of Applied Polymer Science*, vol. 121, p. 3353, 2011.

[166] S. Stankovisch, D. A. Dikin, G. B. Dommet, K. M. Kohlhaas, E. J. Zimney, E. A. Stach, D. Piner, S. T. Nguyen, and R. S. Ruoff, "Graphene-based composite materials," *Nature*, vol. 442, p. 282, 2006.

[167] X. Du, I. Skachko, A. Barker, and E. Y. Andrei, "Approaching ballistic transport in suspended graphene," *Nature Nanotechnology*, vol. 3, p. 491, 2008.

[168] Z. L. Wang, "ZnO nanowire and nanobelt platform for nanotechnology," *Materials Science and Engineering: R*, vol. 64, p. 33, 2009.

[169] W. S. Su, T. C. Leung, and C. T. Chan, "Work function of single-walled and multiwalled carbon nanotubes: First-principles study," *Physical Review B*, vol. 76, p. 235413, 2007.

[170] Y. Hu, Y. Zhang, C. Xu, G. Zhu, and Z. L. Wang, "High-output nanogenerator by rational unipolar assembly of conical nanowires and its application for driving a small liquid crystal display," *Nano Letters*, vol. 10, p. 5025, 2010.

[171] W. Lee, M. Jeong, and J. Myoung, "Optical characteristics of arsenic-doped ZnO nanowires," *Applied Physics Letters*, vol. 85, p. 6167, 2004.

[172] L. Schmidt-Mende and J. L. MacManus-Driscoll, "ZnO - nanostructures, defects, and devices," *Materials Today*, vol. 10, p. 40, 2007.

[173] N. Kouklin, M. Omari, and A. Gupta, *Transition metal-doped ZnO nanowires: En-route towards multi-colour light sensing and emission applications*, N. Lupu, Ed. InTech Open, 2010.

[174] S. N. Cha, J. S. Seo, S. M. Kim, H. J. Kim, and Y. J. Park, "Sound driven piezoelectric nanogenerators," *Advanced Materials*, vol. 22, p. 4726, 2010.

[175] T. S. van den Heever and W. J. Perold, "Improving the output voltage of a ZnO nanogenerator by adding CNTs and lateral ZnO nanowires," *IEEE Transactions on Nanotechnology*, 2013.

[176] J. Markoff, December 2007. [Online]. Available: http://www.nytimes.com/2007/12/18/technology/18solar.html?_r=2&ref=technology&

[177] Economist.com, December 2012. [Online]. Available: http://www.economist.com/blogs/graphicdetail/2012/12/daily-chart-19

[178] Google, March 2013. [Online]. Available: http://www.google.com/glass/start/

[179] S. R. Platt, S. Farritor, K. Garvin, and H. Haider, "The use of piezoelectric ceramics for electric power generation within orthopaedic implants," *IEEE-ASME Transactions on Mechatronics*, vol. 10, p. 455, 2005.

[180] J. F. Antaki, G. E. Berocci, E. C. Green, A. Nadeem, T. Rintoul, R. Kormos, and B. P. Griffith, "A gait-powered autologous battery charging system for artificial organs," *ASAIO Journal*, vol. 41, p. M588, 1995.

[181] M. Renaud, T. Sterken, P. Fiorini, R. Puers, K. Baert, and C. van Hoof, "Scavenging energy from the human body: Design of a piezoelectric transducer," *13th International Conference on Solid-State Sensors, Actuators and Microsystems*, vol. 1, p. 784, 2005.

[182] L. Technology, March 2013. [Online]. Available: http://www.linear.com/designtools/software/

[183] Y. Yang and L. Tang, "Equivalent circuit modeling of piezoelectric energy harvesters," *Journal of Intelligent Material Systems and Structures*, vol. 20, p. 2223, 2009.

[184] N. G. Elvin and A. E. Elvin, "A general equivalent circuit model for piezoelectric generators," *Journal of Intelligent Material Systems and Structures*, vol. 20, p. 3, 2009.

[185] Y. K. Ramadass and A. P. Chandrakasan, "An efficient piezoelectric energy harvesting interface circuit using a bias-flip rectifier and shared inductor," *IEEE Journal of Solid-State Circuits*, vol. 45, p. 189, 2010.

[186] Y. K. Ramadass, "Energy processing circuits for low-power applications," Ph.D. dissertation, Massachusetts Institute of Technology, 2009.

[187] D. Guyomar, A. Badel, E. Lefeuvre, and C. Richard, "Toward energy harvesting using active materials and conversion improvement by nonlinear processing," *IEEE Transactions on Ultrasonic, Ferroelectrics and Frequency Control*, vol. 52, p. 584, 2005.

[188] M. Lallart and D. Guyomar, "An optimized self-powered switching circuit for non-linear energy harvesting with low voltage output," *Smart Materials and Structures*, vol. 17, p. 035030, 2008.

[189] A. Badel, D. Guyomar, E. Lefeuvre, and Richard, "Piezoelectric energy harvesting using a synchronized switch techniques," *Journal of Intelligent Material Systems and Structures*, vol. 17, p. 831, 2006.

[190] Y. Ammar and S. Basrour, "Non linear techniques for increasing harvesting energy from piezoelectric and electromagnetic micro power generators," in *Dans Symposium on Design, Test, Integration and Packaging of MEMS*, 2006.

[191] J. Liang and W. H. Liao, "Improved design and analysis of self-powered synchronized switch interface circuit for piezoelectric energy harvesting systems," *IEEE Transactions on Industrial Electronics*, vol. 59, p. 1950, 2012.

[192] *LTC3588-1 Piezoelectric energy harvesting power supply*.

[193] R. Electronics, March 2013. [Online]. Available: http://za.rs-online.com/web/

[194] B. E. Conway, *Electrochemical capacitors*. Chemistry Department, University of Ottawa, 2003.

[195] T. S. van den Heever and W. J. Perold, "Comparing three different energy harvesting ciruits for a ZnO nanowire based nanogenerator," *Smart Materials and Structures*, 2013.

[196] T. S. van den Heever, "A zinc oxide nanowire pressure sensor," Master's thesis, Stellenbosch University, 2010.

[197] V. Gaddam, S. Joshi, M. Parma, K. Rajanna, and M. M. Nayak, "A novel piezoelectric ZnO nanogenerator on flexible metal alloy substrate," in *11th IEEE Sensors 2012 Conference*, 2012.

[198] Z. H. Lin, Y. Yang, J. M. Wu, F. Zhang, and Z. L. Wang, "$BaTiO_3$ nanotubes-based flexible and transparent nanogenerators," *Journal of Physical Chemistry Letters*, vol. 3, p. 3599, 2012.

[199] J. H. Lee, K. Y. Lee, B. Kumar, N. T. Tien, N. E. Lee, and S. W. Kim, "Highly sensitive stretchable transparent piezoelectric nanogenerator," *Energy and Environmental Science*, vol. 6, p. 169, 2013.

[200] Y. Hu, L. Lin, Y. Zhang, and Z. L. Wang, "Replacing a battery by a nanogenerator with 20 V output," *Advanced Materials*, vol. 24, p. 110, 2012.

[201] Z. L. Wang, G. Zhu, S. Wang, and C. Pan, "Progress in nanogenerators for portable electronics," *Materials Today*, vol. 15, p. 531, 2012.

[202] M. De Graef, *Structure of materials: An introduction to crystallography, diffraction and symmetry*, M. McHenry, Ed. Cambridge University Press, 2007.

[203] W. D. Callister, *Materials Science and Engineering: An Introduction*, J. Hayton, Ed. John Wiley and Sons, 2007.

Appendix A: Crystallography

This section presents a brief introduction to crystallography. The section starts with a description of what a crystal structure is and how it is defined. The different two-dimensional and three-dimensional crystal systems are introduced. This is followed by an explanation of the Miller index. Lastly, the hexagonal crystal system is introduced, as this is important for the ZnO nanowires.

A crystal structure is a regular arrangement of atoms or groups of atoms. The regular arrangement repeats in a certain pattern, and this pattern is known as the lattice of the crystal structure. The lattice does not really exist but is a mathematical tool that is used to describe crystal structures. A crystal can now be described by a lattice, with atoms attached to every lattice point that is repeated in space [202]. The smallest unit cell of atoms that is repeated at every lattice point is called a motif. A crystal structure thus can be viewed as a lattice plus a motif at every lattice point, as shown in Figure 1 [60].

A lattice is defined by three translation vectors, a_1, a_2 and a_3, such that the atomic arrangement looks the same in every respect when viewed from the point r as when viewed from the point

$$r' = r + u_1 a_1 + u_2 a_2 + u_3 a_3$$

where u_1, u_2, u_3 are arbitrary integers. The set of points r' defined above for all u_1, u_2, u_3 defines a lattice [60, 202].

Figure 1 (a) shows the lattice with the lattice cells drawn in blue. In two dimensions there are three parameters that define the lattice cell, cell lengths a, b and cell angle γ. The two cells in Figure 1 (a), which each contains four lattice points, are primitive cells and, in two-dimensions, there are four primitive cell types as described in Table 1 [60, 202].

In three-dimensions there are three length parameters: a, b and c and three angle parameters: α (the angle between b and c), β (the angle between a and c) and γ (the angle between a and b). There are seven crystal systems in three-dimensions as described in Table 2 [60, 202]. Figure 2 shows how the lengths and angles are

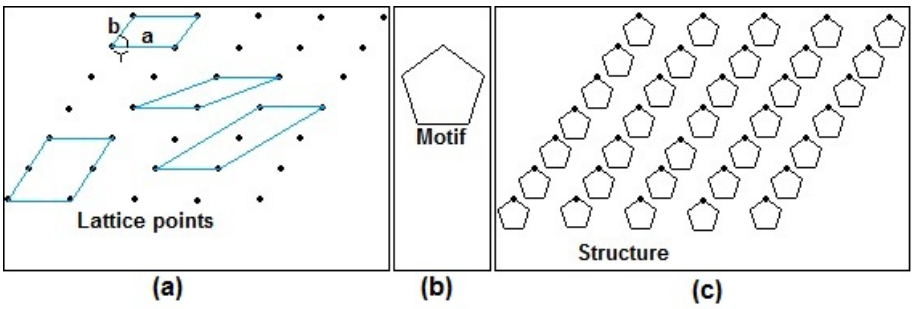

Figure 1: Graphical representation of (a) a lattice point and (b) a motif, which together form the (c) crystal lattice.

Table 1: Four different two-dimensional crystal systems

Length Condition	Angle Conditiion	Crystal System
No condition	No condition	Oblique
No condition	$\gamma = 90°$	Rectangular
$a = b$	$\gamma = 120°$	Hexagonal
$a = b$	$\gamma = 90°$	Square

defined for a three-dimensional system [203].

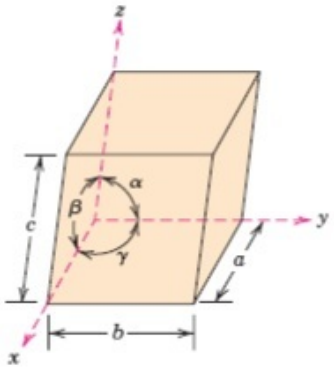

Figure 2: Graphical representation of the definition of lengths and angles of a three-dimensional system [60].

The position of a point located within a crystal system can be specified in terms of coordinates as fractional multiples of the cell lengths. This is illustrated in Figure 3. Point P is an arbitrary point inside the cell. The position of point P is specified by coordinates qrs which are some fractional length of cell lengths a, b and c. The Miller coordinates, as per convention, are not separated by commas or points [203].

Table 2: Seven different three-dimensional crystal systems

Length Condition	Angle Conditiion	Crystal System
No condition	No condition	Triclinic
No condition	$\alpha = \gamma = 90°$	Monoclinic
$a = b$	$\alpha = \beta = 90°; \gamma = 120°$	Hexagonal
$a = b = c$	$\alpha = \beta = \gamma$	Rhombohedral
No condition	$\alpha = \beta = \gamma = 90°$	Orthorhombic
$a = b$	$\alpha = \beta = \gamma$	Tetragonal
$a = b = c$	$\alpha = \beta = \gamma = 90°$	Cubic

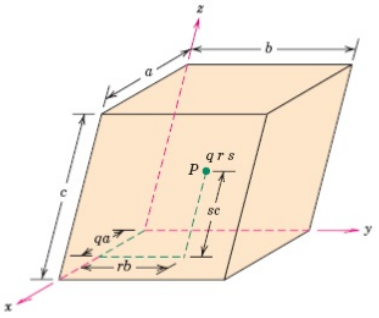

Figure 3: Specifying the posistion of a point in a crystal system by means of lengths or point coordinates [60].

A problem arises when the crystal has a hexagonal crystal system. The problem is that crystallographic equivalent directions will not always have the same set of indices. This is circumvented by using the four axes, Miller Bravais coordinate, system as shown in Figure 4 (b), in the place of the normal Miller coordinate system shown in Figure 4 (a). The three axes, a_1, a_2 and a_3, are contained in a single plane, called the basal plane, and the angles between them are equal. The z axis is perpendicular to the basal plane. The Miller Bravais coordinate system is denoted by four indices $[uvtw]$, whereas the normal coordinates have only three indices $[uvw]$. The first three indices correspond to the directions a_1, a_2 and a_3 and the last index corresponds to the z direction [203].

In a hexagonal system different planes and vectors are defined by the Miller Bravais coordinate system, as shown in Figure 5. The dash on top of a number represents a negative index [203]. The Miller Bravais coordinates, $[uvtw]$, are calculated by converting the Miller coordinates, $[u'v'w']$, using the following equations [203]

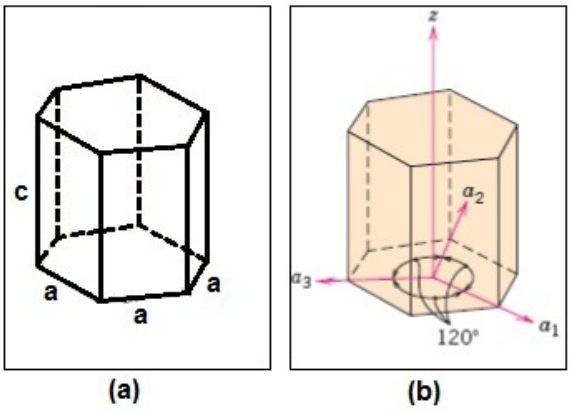

Figure 4: Definition of coordinates for a hexagonal crystal system for the (a) Miller system and (b) Miller Bravais [60].

$$
\begin{aligned}
u &= \frac{1}{3}(2u' - v') \\
v &= \frac{1}{3}(2v' - u') \\
t &= -(u + v) \\
w &= w'.
\end{aligned}
$$

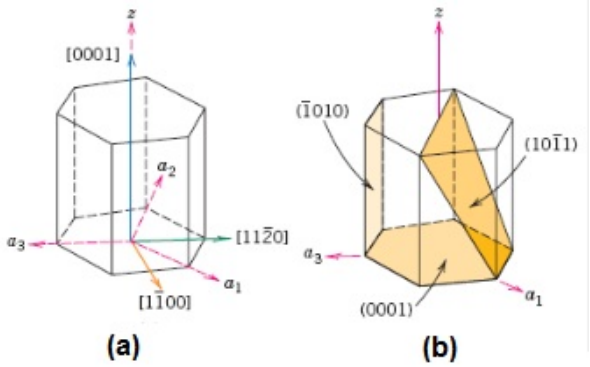

Figure 5: (a) Vectors and (b) planes inside a hexagonal crystal system [60].

Determining the indices of a vector in a three-dimensional system is done by following the following steps [203]:

- The vector must start at the origin of the crystal system.

- The length of the vector is projected on each of the three axes and measured in terms of the unit cell dimensions a, b and c.
- These numbers are then divided by a common factor to reduce the numbers to the smallest integer value.

The indices of a plane are determined in a similar manner to the indices of a vector. The steps for determining the indices (hkl) are [203]:

- One corner of the plane must be at the origin of the crystal system.
- The plane will either intersect or be parallel to each of the three axes and the point of intersection in determined by the cell dimensions a, b and c.
- The reciprocal of these numbers is taken. A parallel plane has an intersect point at infinity, and therefore an index of zero.

Using the above-mentioned conversion equations, the three indices determined by the above-mentioned steps are then converted to the four indices for the hexagonal crystal system. The hexagonal crystal system is of importance because zinc oxide disply thissystem [52].

This brief introduction to crystallography is given so that the crystal structure of ZnO nanowires can be better understood. The crystal structure is important because it influences the nanowire growth and ultimately the output voltage.

Appendix B: Project Planning

The planning of a big project that lasts for a couple of years is of utmost importance. For this project the final submission date for the dissertation marks the end of the study. The planning was therefore done with the submission date in mind. The project was broken down into a number of different parts, each with its own outcome and completion date.

The initial plan for the study is shown in Figure 6. The work starts at the beginning of 2011 with completion in October 2013. The project starts with a literature study and ongoing writing of the thesis. As time progressed more tasks were added and certain tasks were completed. The project did not follow the initial plan however; instead the plan changed over time to accommodate certain limitations and obstacles experienced along the way.

Figure 7 shows the planning as the project unfolded. The Gantt chart in Figure 7 changed constantly over the duration of the project. Due to limited equipment and more than one student, equipment run-time was shared. Equipment failure also led to delays is certain areas. The initial plan to write the thesis as the work progressed also failed in practice and writing commenced during the last quarter of 2012, with completion mid-2013. The project itself started in the fourth quarter of 2010, and not at the beginning of 2011 as planned, as the author finished his MScEng ahead of time.

Additional tasks were added to the plan as the project progressed, and certain tasks were removed. The manufacturing of the electrode was removed as a better nanogenerator manufacturing technique was employed and the separate manufacturing of an electrode was unnecessary. The testing and manufacturing of the gas sensor was also a consequence of work on the nanogenerator. Lastly, the output circuitry was added, as it was not envisaged during the initial planning.

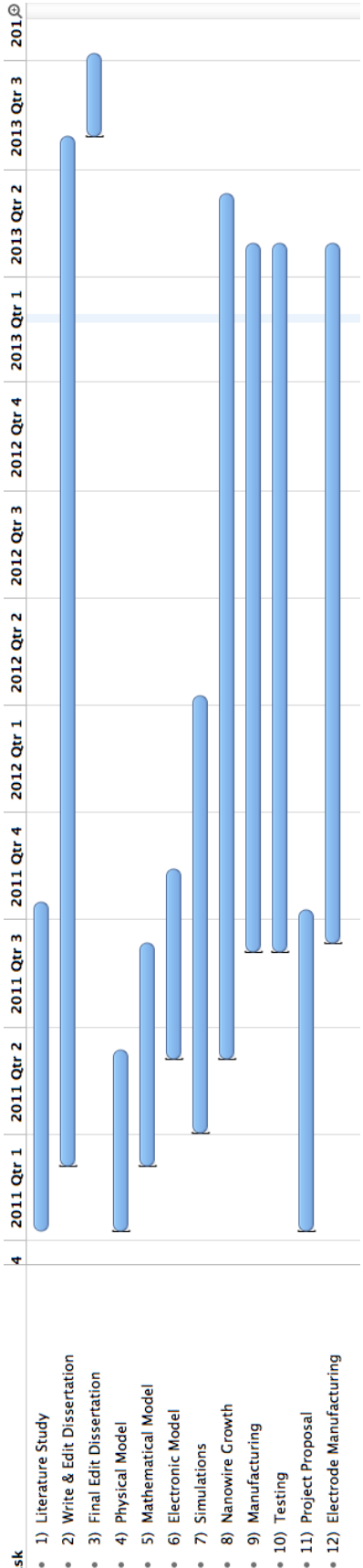

Figure 6: Gantt chart of initial planning for three years of PhD.

Figure 7: Gantt chart of final planning for three years of PhD.

Appendix C: Datasheets

The datasheets for the LTC2625 operational amplifier that was used for the buffer circuit, and the MBR0520L and LTC3588 integrated circuit that was used for the output circuit of the nanogenerator, was shown below. Only a couple of pages are appended for each component.

LTC2605/LTC2615/LTC2625

Octal 16-/14-/12-Bit Rail-to Rail DACs in 16-Lead SSOP

FEATURES

- **Smallest Pin-Compatible Octal DACs:**
  LTC2605: 16 Bits
  LTC2615: 14 Bits
  LTC2625: 12 Bits
- **Guaranteed Monotonic Over Temperature**
- 400kHz I^2C Interface
- Wide 2.7V to 5.5V Supply Range
- Low Power Operation: 250µA per DAC at 3V
- Individual Channel Power-Down to 1µA (Max)
- Ultralow Crosstalk Between DACs (<10µV)
- High Rail-to-Rail Output Drive (±15mA, Min)
- Double-Buffered Digital Inputs
- 27 Selectable Addresses
- LTC2605/LTC2615/LTC2625: Power-On Reset to Zero-Scale
- LTC2605-1/LTC2615-1/LTC2625-1: Power-On Reset to Mid-Scale
- Tiny 16-Lead Narrow SSOP Package

APPLICATIONS

- Mobile Communications
- Process Control and Industrial Automation
- Instrumentation
- Automatic Test Equipment

DESCRIPTION

The LTC®2605/LTC2615/LTC2625 are octal 16-, 14- and 12-bit, 2.7V to 5.5V rail-to-rail voltage-output DACs in 16-lead narrow SSOP packages. They have built-in high performance output buffers and are guaranteed monotonic.

These parts establish new board-density benchmarks for 16-/14-bit DACs and advance performance standards for output drive, crosstalk and load regulation in single supply, voltage-output multiples.

The parts use the 2-wire I^2C compatible serial interface. The LTC2605/LTC2615/LTC2625 operate in both the standard mode (maximum clock rate of 100kHz) and the fast mode (maximum clock rate of 400kHz).

The LTC2605/LTC2615/LTC2625 incorporate a power-on reset circuit. During power-up, the voltage outputs rise less than 10mV above zero-scale; and after power-up, they stay at zero-scale until a valid write and update take place. The power-on reset circuit resets the LTC2605-1/LTC2615-1/LTC2625-1 to mid-scale. The voltage output stays at mid-scale until a valid write and update takes place.

TYPICAL APPLICATION

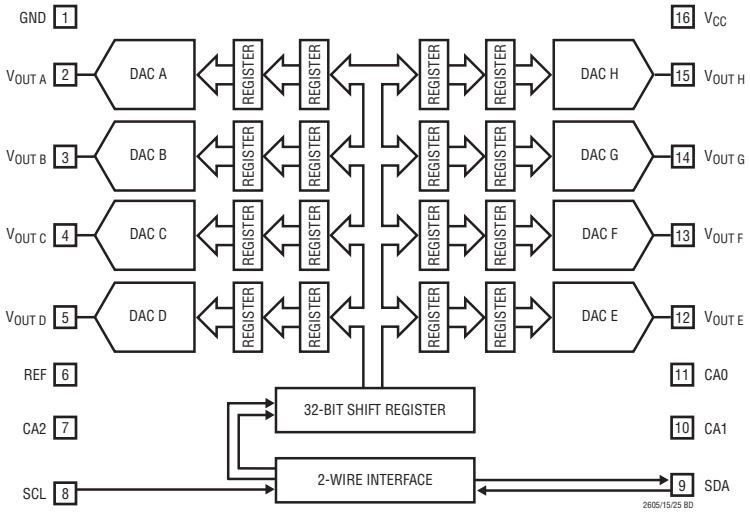

Differential Nonlinearity (LTC2605)

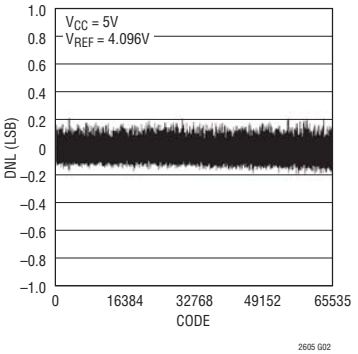

ABSOLUTE MAXIMUM RATINGS

(Note 1)

Any Pin to GND ..... –0.3V to 6V
Any Pin to V_{CC} ..... –6V to 0.3V
Maximum Junction Temperature ..... 125°C
Operating Temperature Range
LTC2605C/LTC2615C/LTC2625C ..... 0°C to 70°C
LTC2605C-1/LTC2615C-1/LTC2625C-1 .... 0°C to 70°C
LTC2605I/LTC2615I/LTC2625I..... –40°C to 85°C
LTC2605I-1/LTC2615I-1/LTC2625I-1 .... –40°C to 85°C
Storage Temperature Range ..... –65°C to 150°C
Lead Temperature (Soldering, 10 sec)..... 300°C

PIN CONFIGURATION

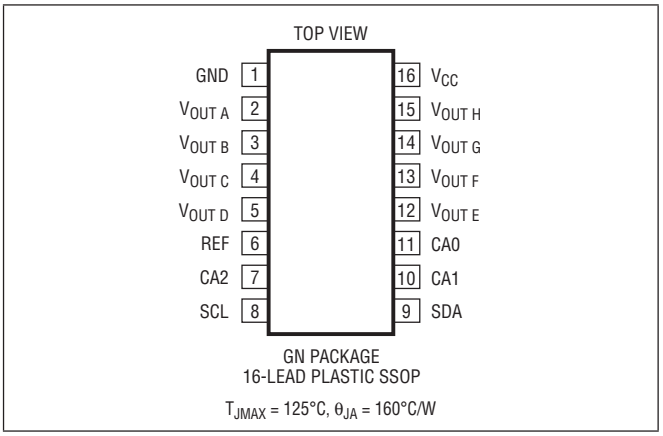

ORDER INFORMATION

LEAD FREE FINISH	TAPE AND REEL	PART MARKING	PACKAGE DESCRIPTION	TEMPERATURE RANGE
LTC2605CGN#PBF	LTC2605CGN#TRPBF	2605	16-Lead Plastic SSOP	0°C to 70°C
LTC2605CGN-1#PBF	LTC2605CGN-1#TRPBF	26051	16-Lead Plastic SSOP	0°C to 70°C
LTC2605IGN#PBF	LTC2605IGN#TRPBF	2605I	16-Lead Plastic SSOP	–40°C to 85°C
LTC2605IGN-1#PBF	LTC2605IGN-1#TRPBF	2605I1	16-Lead Plastic SSOP	–40°C to 85°C
LTC2615CGN#PBF	LTC2615CGN#TRPBF	2615	16-Lead Plastic SSOP	0°C to 70°C
LTC2615CGN-1#PBF	LTC2615CGN-1#TRPBF	26151	16-Lead Plastic SSOP	0°C to 70°C
LTC2615IGN#PBF	LTC2615IGN#TRPBF	2615I	16-Lead Plastic SSOP	–40°C to 85°C
LTC2615IGN-1#PBF	LTC2615IGN-1#TRPBF	2615I1	16-Lead Plastic SSOP	–40°C to 85°C
LTC2625CGN#PBF	LTC2625CGN#TRPBF	2625	16-Lead Plastic SSOP	0°C to 70°C
LTC2625CGN-1#PBF	LTC2625CGN-1#TRPBF	26251	16-Lead Plastic SSOP	0°C to 70°C
LTC2625IGN#PBF	LTC2625IGN#TRPBF	2625I	16-Lead Plastic SSOP	–40°C to 85°C
LTC2625IGN-1#PBF	LTC2625IGN-1#TRPBF	2625I1	16-Lead Plastic SSOP	–40°C to 85°C

Consult LTC Marketing for parts specified with wider operating temperature ranges.
Consult LTC Marketing for information on non-standard lead based finish parts.

For more information on lead free part marking, go to: http://www.linear.com/leadfree/
For more information on tape and reel specifications, go to: http://www.linear.com/tapeandreel/

PIN FUNCTIONS

GND (Pin 1): Analog Ground.

$V_{OUT\,A}$ to $V_{OUT\,H}$ (Pins 2-5 and 12-15): DAC Analog Voltage Output. The output range is 0V to V_{REF}.

REF (Pin 6): Reference Voltage Input. $0V \le V_{REF} \le V_{CC}$.

CA2 (Pin 7): Chip Address Bit 2. Tie this pin to V_{CC}, GND or leave it floating to select an I^2C slave address for the part (Table 2).

SCL (Pin 8): Serial Clock Input Pin. Data is shifted into the SDA pin at the rising edges of the clock. This high impedance pin requires a pull-up resistor or current source to V_{CC}.

SDA (Pin 9): Serial Data Bidirectional Pin. Data is shifted into the SDA pin and acknowledged by the SDA pin. This is a high impedance pin while data is shifted in. It is an open-drain N-channel output during acknowledgment. This pin requires a pull-up resistor or current source to V_{CC}.

CA1 (Pin 10): Chip Address Bit 1. Tie this pin to V_{CC}, GND or leave it floating to select an I^2C slave address for the part (Table 2).

CA0 (Pin 11): Chip Address Bit 0. Tie this pin to V_{CC}, GND or leave it floating to select an I^2C slave address for the part (Table 2).

V_{CC} (Pin 16): Supply Voltage Input. $2.7V \le V_{CC} \le 5.5V$.

BLOCK DIAGRAM

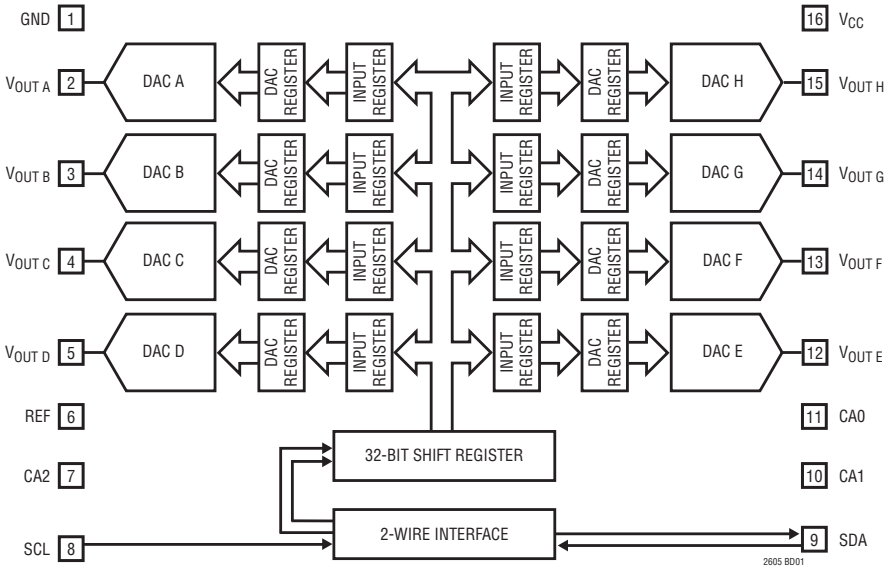

TIMING DIAGRAM

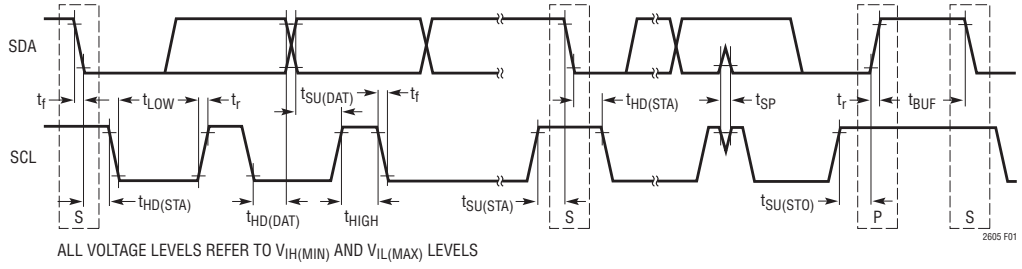

ALL VOLTAGE LEVELS REFER TO $V_{IH(MIN)}$ AND $V_{IL(MAX)}$ LEVELS

Figure 1

LTC3588-1

Piezoelectric Energy Harvesting Power Supply

FEATURES

- **950nA Input Quiescent Current (Output in Regulation – No Load)**
- **450nA Input Quiescent Current in UVLO**
- **2.7V to 20V Input Operating Range**
- **Integrated Low-Loss Full-Wave Bridge Rectifier**
- **Up to 100mA of Output Current**
- **Selectable Output Voltages of 1.8V, 2.5V, 3.3V, 3.6V**
- High Efficiency Integrated Hysteretic Buck DC/DC
- Input Protective Shunt – Up to 25mA Pull-Down at $V_{IN} \geq 20V$
- Wide Input Undervoltage Lockout (UVLO) Range
- Available in 10-Lead MSE and 3mm × 3mm DFN Packages

APPLICATIONS

- Piezoelectric Energy Harvesting
- Electro-Mechanical Energy Harvesting
- Wireless HVAC Sensors
- Mobile Asset Tracking
- Tire Pressure Sensors
- Battery Replacement for Industrial Sensors
- Remote Light Switches
- Standalone Nanopower Buck Regulator

DESCRIPTION

The LTC®3588-1 integrates a low-loss full-wave bridge rectifier with a high efficiency buck converter to form a complete energy harvesting solution optimized for high output impedance energy sources such as piezoelectric transducers. An ultralow quiescent current undervoltage lockout (UVLO) mode with a wide hysteresis window allows charge to accumulate on an input capacitor until the buck converter can efficiently transfer a portion of the stored charge to the output. In regulation, the LTC3588-1 enters a sleep state in which both input and output quiescent currents are minimal. The buck converter turns on and off as needed to maintain regulation.

Four output voltages, 1.8V, 2.5V, 3.3V and 3.6V, are pin selectable with up to 100mA of continuous output current; however, the output capacitor may be sized to service a higher output current burst. An input protective shunt set at 20V enables greater energy storage for a given amount of input capacitance.

TYPICAL APPLICATION

100mA Piezoelectric Energy Harvesting Power Supply

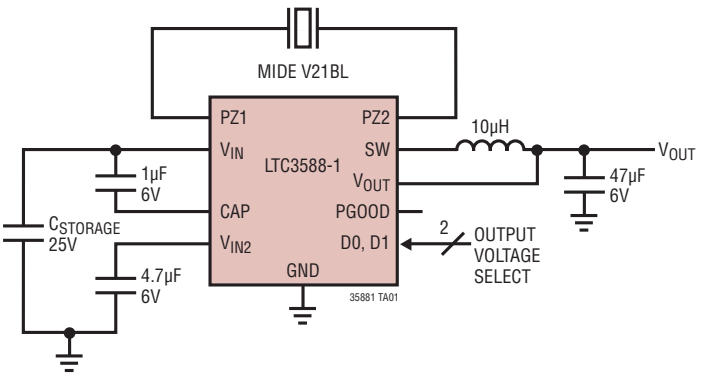

LTC3588-1 3.3V Regulator Start-Up Profile

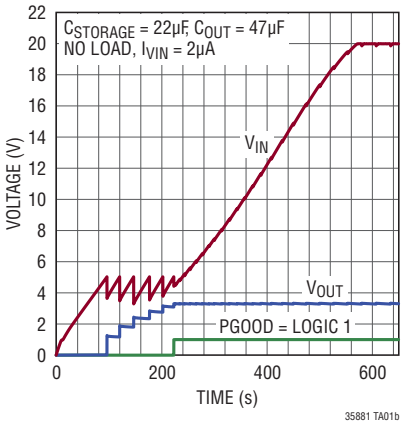

PIN FUNCTIONS

PZ1 (Pin 1): Input connection for piezoelectric element or other AC source (used in conjunction with PZ2).

PZ2 (Pin 2): Input connection for piezoelectric element or other AC source (used in conjunction with PZ1).

CAP (Pin 3): Internal rail referenced to V_{IN} to serve as gate drive for buck PMOS switch. A 1µF capacitor should be connected between CAP and V_{IN}. This pin is not intended for use as an external system rail.

V_{IN} (Pin 4): Rectified Input Voltage. A capacitor on this pin serves as an energy reservoir and input supply for the buck regulator. The V_{IN} voltage is internally clamped to a maximum of 20V (typical).

SW (Pin 5): Switch Pin for the Buck Switching Regulator. A 10µH or larger inductor should be connected from SW to V_{OUT}.

V_{OUT} (Pin 6): Sense pin used to monitor the output voltage and adjust it through internal feedback.

V_{IN2} (Pin 7): Internal low voltage rail to serve as gate drive for buck NMOS switch. Also serves as a logic high rail for output voltage select bits D0 and D1. A 4.7µF capacitor should be connected from V_{IN2} to GND. This pin is not intended for use as an external system rail.

D1 (Pin 8): Output Voltage Select Bit. D1 should be tied high to V_{IN2} or low to GND to select desired V_{OUT} (see Table 1).

D0 (Pin 9): Output Voltage Select Bit. D0 should be tied high to V_{IN2} or low to GND to select desired V_{OUT} (see Table 1).

PGOOD (Pin 10): Power good output is logic high when V_{OUT} is above 92% of the target value. The logic high is referenced to the V_{OUT} rail.

GND (Exposed Pad Pin 11): Ground. The Exposed Pad should be connected to a continuous ground plane on the second layer of the printed circuit board by several vias directly under the LTC3588-1.

BLOCK DIAGRAM

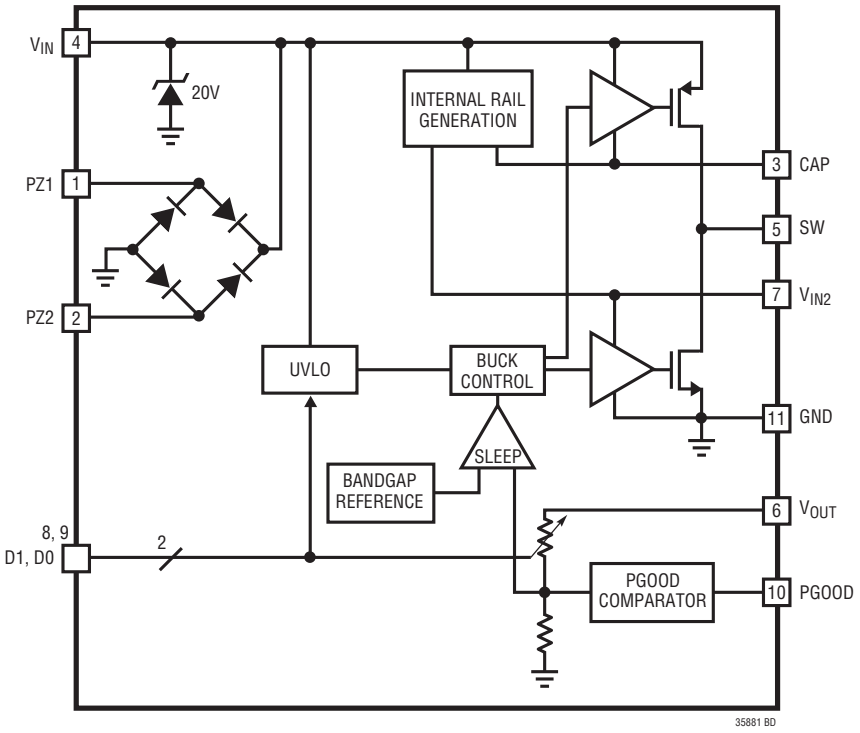

FAIRCHILD SEMICONDUCTOR®

March 2012

MBR0520L
Schottky Rectifier

Features

- 0.5 Ampere, low forward voltage, less than 385mV
- 400 milliwatt Power Dissipation package
- Compact surface mount package with the same footprint as mini-melf

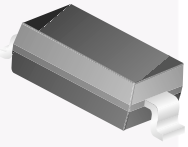

SOD123
Color Band Denotes Cathode
Mark: B2

Absolute Maximum Ratings *

Values are at T_A=25°C unless otherwise noted.

Symbol	Parameter	Value	Unit
V_{RRM}	Maximum Repetitive Reverse Voltage	20	V
$I_{F(AV)}$	Average Rectified Forward Current	500	mA
I_{FSM}	Non Repetitive Peak Forward Current (Surge applied at rated load conditions half wave, single, phase, 60Hz)	5.5	A
T_{STG}	Storage Temperature Range	-65 to +150	°C
T_{Jmax}	Operating Junction Temperature	-65 to +125	°C

* These ratings are limiting values above which the serviceability of any semiconductor device may by impaired.

Thermal Characteristics

Symbol	Parameter	Value	Unit
$R_{\theta JA}$	Thermal Resistance, Junction to Ambient *	340	°C/W
$R_{\theta JL}$	Thermal Resistance, Junction to Lead	150	°C/W

* FR-4 or FR-5 = 3.5 x 1.5 inches using minimum recommended Land Pads.

Electrical Characteristics

Values are at T_A=25°C unless otherwise noted.

Symbol	Parameter		Value	Unit
V_F	Forward Voltage	@ I_F = 100mA	300	mV
		I_F = 100mA, T_a = 100°C	220	mV
		I_F = 500mA	385	mV
		I_F = 500mA, T_a = 100°C	330	mV
I_R	Reverse Current	@ V_R = 10V	75	µA
		V_R = 10V, T_a = 100°C	5.0	mA
		V_R = 20V	250	µA
		V_R = 20V, T_a = 100°C	8.0	mA

Typical Performance Characteristics

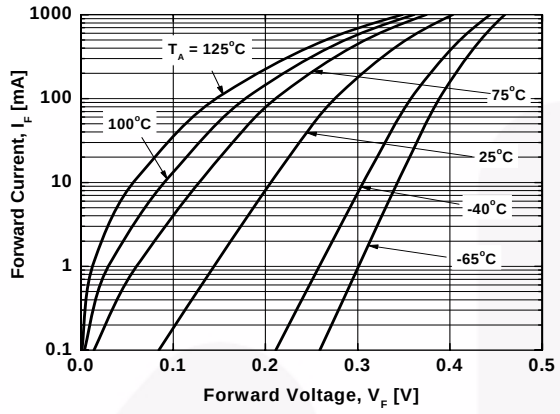

Figure 1. Forward Current vs Forward Voltage

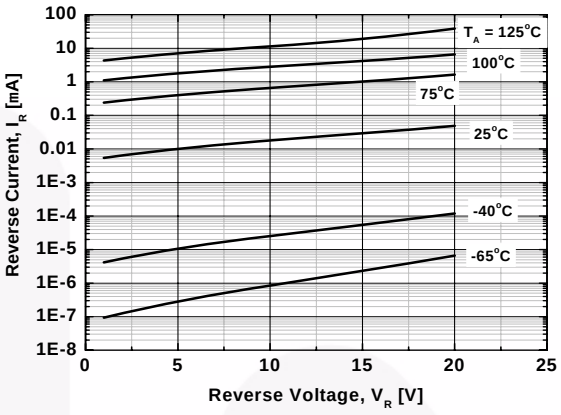

Figure 2. Reverse Current vs Reverse Voltage

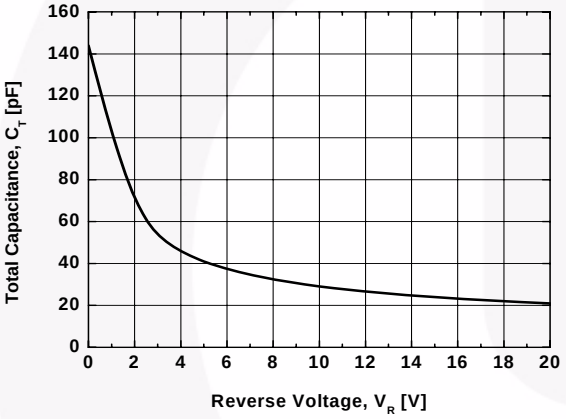

Figure 3. Total Capacitance

Appendix D: Matlab-code

Contact Resistance

Matlab code to calculate the contact resistance between the ZnO nanowire and Au electrode. The calculation was broken into each of the two terms as well as the entire equation.

Van der Pauw and Hall

Matlab code for the calculation of the resistance and carrier concentration of the ZnO nanowires.

```
%Contact Resistance calculation of ZnO nanowire with Gold
clear all;
clc;
const1 = (3*pi*pi)^(1/3);                    %Constant 1 for mean free path calculation
const2 = (6.626*10^-34)/(1.6022*10^-19)^2;   %Constant 2 for mean free path calculation
n = 10^16;                                   %Electron density
p1 = 10^-1;                                  %Conductivity of ZnO nanowire
p2 = 2.44*10^-8;                             %Conductivity of Gold

%lambda = const1*const2*p1*(n^(-2/3))        %Mean free path of electrons calculation

a = 10*10^-9;                                %Radius of contact circle
%term1 = 4*lambda*(p1 + p2)/(9*pi*a*a)       %First term for resistance calculation
%term2 = (p1 +p2)/(4*pi*pi*a)                %Second term for resistance calculation
%trig = atan(pi*a/lambda)                    %Trig part of second term

%R = term1 + term2*trig                      %Contact resistance calculation

for p1 = 0.01:0.01:1,
    lambda = const1*const2*p1*(n^(-2/3));
    term1 = 4*lambda*(p1 + p2)/(9*pi*a*a);
    %term2 = (p1 +p2)/(4*pi*pi*a);
    trig = atan(pi*a/lambda);
    term2 = 0;
    R = term1 + term2*trig;
    hold on
    figure(1)
    plot(p1, lambda)
    %axis([0.001 1 0 2.5*10^9])
    xlabel('Conductivity of ZnO nanowire')
    ylabel('Mean free path of electrons')
    title('Plot of the mean free path of electrons versus conductivity of ZnO')
    hold on
    figure(2)
    plot(p1, term1)
    %axis([0.001 1 0 2.5*10^9])
    xlabel('Conductivity of ZnO nanowire')
    ylabel('First term of contact resistance calculation')
    title('Plot of the first trem of the resistance calculation versus conductivity of ZnO')
    hold on
    figure(3)
    plot(p1, term2*trig)
    %axis([0.001 1 0 2.5*10^9])
    xlabel('Conductivity of ZnO nanowire')
    ylabel('Second term of contact resistance calculation')
    title('Plot of the second trem of the resistance calculation versus conductivity of ZnO')
    hold on
    figure(4)
    plot(p1, R)
    %axis([0.001 1 0 2.5*10^9])
    xlabel('Conductivity of ZnO nanowire')
    ylabel('Contact Resistance')
    title('Plot of the Contact resistance versus conductivity of ZnO')
end
```

Figure 8: Calculation of the contact resistance between the ZnO nanowire and the Au electrode.

```
clc;
close all;
clear all;

Rs_begin=0;
Rv = -30.0326;
Rh = -7.35289;


i=1;
delta=1;
for Rs_begin=0:delta:1000
    d(i) = exp(-pi*Rv/Rs_begin) + exp(-pi*Rh/Rs_begin);
    i=i+1;
end

r=abs(d-1);
[x,y]=min(r);
des=delta*y;

Rs_begin = des

Rs_middel=0;


i=1;
delta=0.0001;
for Rs_middel=(Rs_begin-1):delta:(Rs_begin+1)
    d(i) = exp(-pi*Rv/Rs_middel) + exp(-pi*Rh/Rs_middel);
    i=i+1;
end

r=abs(d-1);
[x,y]=min(r);
des=delta*y;

Rs_middel = (Rs_begin-1)+des

Rs=0;


i=1;
delta=0.000001;
for Rs=(Rs_middel-0.001):delta:(Rs_middel+0.001)
    d(i) = exp(-pi*Rv/Rs) + exp(-pi*Rh/Rs);
    i=i+1;
end

r=abs(d-1);
[x,y]=min(r);
des=delta*y;

Rs = (Rs_middel-0.001)+des

a= exp(-pi*Rv/Rs_middel) + exp(-pi*Rh/Rs_middel)
```

Figure 9: Calculation of the resistance using the Van der Pauw method and the Hall voltage using the Hall-effect.